

Copyright
by
Gregory Linwood Cohen

The Dissertation Committee for Gregory Linwood Cohen certifies that this is the
approved version of the following dissertation:

**Seismic Evaluation and Rehabilitation of Low-Rise Reinforced
Masonry Buildings with Flexible Diaphragms**

Committee:

Richard E. Klingner, Supervisor

Jeffrey K. Bennighof

Michael D. Engelhardt

Dan L. Wheat

Sharon L. Wood

**Seismic Evaluation and Rehabilitation of Low-Rise Reinforced
Masonry Buildings with Flexible Diaphragms**

by

Gregory Linwood Cohen, B.S.; M.S.

Dissertation

Presented to the Faculty of the Graduate School of Engineering

The University of Texas at Austin

in Partial Fulfillment

of the Requirements

for the Degree of

Doctor of Philosophy

The University of Texas at Austin

May 2004

Acknowledgements

The study presented in this dissertation was performed jointly at The University of Texas at Austin and the United States Army Corp Engineer Research and Development Center, Construction Engineering Research Laboratory (CERL). This research was funded by CERL.

Dr. Richard E Klingner, of The University of Texas at Austin, supervised the study; I would like to thank him for his enthusiasm, professionalism, and friendship. His supervision over the past five years encompassed everything from structural dynamics to the strategic placement of conference nametags. I was fortunate to have him as an advisor; I am fortunate to have him as a colleague. Dr. Klingner – thank you.

Steven C. Sweeney and Dr. John R. Hayes Jr., both of CERL, co-supervised this study and are thanked for providing the professional, organizational, and financial framework necessary for success of this research. Steve and Jack are excellent engineers, managers, and colleagues; they have provided critical advice and guidance throughout the study and have made every effort to support the study goals.

Jim Gambill and Bill Gordon, both CERL technical specialists, supported this research with their expertise. Jim contributed through his masterful skills of instrumentation, data collection, and data reduction; Bill contributed through his knowledge of test setups and hydraulic systems.

I would also like to thank the structural engineering faculty at The University of Texas. UT is one of those few schools where doors are truly open and questions are gladly entertained. The school has provided me an excellent education and helped me build a foundation on which to build a career. Dr. Dan Wheat and Dr. Sharon Wood have provided particularly important guidance for this study.

Finally, and most important, I would like to thank my mother and my father, whom have always given me support and motivation in whatever my interest.

Gregory Linwood Cohen

May 2004

Seismic Evaluation and Rehabilitation of Low-Rise Reinforced Masonry Buildings with Flexible Diaphragms

Publication No. _____

Gregory Linwood Cohen, Ph.D.
The University of Texas at Austin, 2004

Supervisor: Richard E. Klingner

In response to Executive Order 12941 (1994), the United States government initiated a coordinated effort to assess and mitigate the seismic hazards of its existing owned and leased facilities. This study was contracted to enhance that effort for low-rise reinforced masonry buildings with flexible diaphragms. The study involved the development of systematic methodologies for the seismic evaluation and rehabilitation of such buildings.

First, the seismic behavior of these types of buildings was characterized. Two, half-scale low-rise reinforced masonry buildings with flexible diaphragms were tested on the US Army Tri-axial Earthquake and Shock Simulator at the US Army Engineer Research and Development Center, Construction Engineering Research Laboratory. This testing provided experimental data for analytical modeling, and provided specific technical substantiation for the generally accepted premise that diaphragm flexibility can significantly affect the seismic

response of low-rise buildings. Following that testing, diaphragms and attached masonry chords were removed from the shaking-table specimens and subjected to reversed cyclic quasi-static displacements.

Observations and conclusions from physical testing were used to develop and validate a simple tool for the analysis of these buildings. The tool was developed in the general case and then analytically bounded for the particular case of low-rise reinforced masonry buildings with flexible diaphragms. It was validated in the linear elastic and nonlinear ranges using data from shaking-table testing, finite-element modeling, and lumped-parameter modeling. Data from previous flexible-diaphragm tests, performed by others, were reevaluated in the context of performance-based engineering and synthesized with the analysis tool into a coherent evaluation methodology intended to supplement the existing methodologies of Federal Emergency Management Agency (FEMA) Documents 310 and 356.

To assess the efficacy of the proposed methodology, four existing buildings were selected from the Ft. Lewis, Washington inventory and evaluated for seismic deficiencies. The buildings were evaluated using procedures of FEMA 310, US Army TI 809-05, and the proposed methodology. Results conclusively demonstrated that the FEMA 310 methodology does not sufficiently characterize the seismic performance of flexible diaphragm systems, and the proposed methodology is simple, effective, and useful. Recommendations are placed in the context of evolutionary updating of the FEMA methodologies, as applied to specific subsets of the national building inventory.

TABLE OF CONTENTS

LIST OF TABLES	xv
LIST OF FIGURES	xvii
1.0 INTRODUCTION	1
<i>1.1 Study Justification, Milestones, and Objectives</i>	1
<i>1.2 Scope of Work</i>	4
<i>1.3 General Outline of Dissertation</i>	5
<i>1.4 Introduction of Diaphragm Drift Ratio</i>	6
2.0 BACKGROUND OF STUDY AND RELEVANT REFERENCE INFORMATION	7
<i>2.1 Seismic Behavior and Design of Low-Rise Reinforced Masonry Buildings with Flexible Diaphragms</i>	7
2.1.1 Design of Flexible Diaphragms	9
2.1.2 Design of Diaphragm Anchorage and the Subdiaphragm Concept	10
2.1.3 Design of In-Plane and Out-of-Plane Masonry Walls	13
<i>2.2 Seismic Performance and the Evolution of Design, Evaluation, and Rehabilitation of Low-Rise Reinforced Masonry Buildings with Flexible Diaphragms</i>	13
2.2.1 Evolution of Seismic Design Requirements for New Construction	15
2.2.2 Evolution of Seismic Evaluation and Rehabilitation Procedures	18
<i>2.3 Previous Research, Further Reading, and Other Resources</i>	20
2.3.1 Flexible Diaphragm Behavior and its Effect on Building Response	20
2.3.2 Masonry Buildings and Assemblies	22
2.3.3 Wood Diaphragms	22
2.3.4 Metal-Deck Diaphragms	24

2.3.5	Shaking-Table Testing	26
2.3.6	Publications for Evaluation and Rehabilitation of Existing Buildings	26
3.0	SHAKING-TABLE TESTING OF LOW-RISE REINFORCED MASONRY BUILDINGS WITH FLEXIBLE DIAPHRAGMS	28
3.1	<i>Specimen Development</i>	28
3.1.1	Remarks on Scaling	31
3.2	<i>Summary of Shaking-Table Testing</i>	34
3.2.1	Testing of Specimen #1 (Lumber Sheathing)	35
3.2.2	Testing of Specimen #2 (Metal Deck)	35
3.3	<i>Summary of Results, Conclusions, and Significance of Testing</i>	38
3.3.1	Summary of Results and Conclusions	38
3.3.2	Significance of Shaking-Table Testing	41
4.0	QUASI-STATIC TESTING OF FLEXIBLE DIAPHRAGMS	43
4.1	<i>Test Setups</i>	43
4.1.1	Diaphragm #1 (Lumber Sheathing)	46
4.1.2	Diaphragm #2 (Metal Deck)	48
4.2	<i>Instrumentation of Test Specimens</i>	50
4.3	<i>Quasi-Static Testing Protocol</i>	51
4.4	<i>Observations During Testing of Diaphragm #1 (Lumber Sheathing)</i>	54
4.4.1	Observed Damage at Low Diaphragm Drift Ratios (Tests #1 - #5)	54
4.4.2	Observed Damage at High Diaphragm Drift Ratios (Tests #6-#9)	57
4.4.3	Observations of Local Damage After Quasi-Static Testing	64
4.5	<i>Observations During Testing of Diaphragm #2 (Metal Deck)</i>	66
4.5.1	Observed Damage at Low Diaphragm Drift Ratios (Tests #1 - #5)	66
4.5.2	Observed Damage at High Diaphragm Drift Ratios (Tests #6-#9)	67

4.5.3	Observations of Local Damage After Quasi-static Testing	71
4.6	<i>Evaluation of Test Data for Diaphragm #1 (Lumber Sheathing)</i>	72
4.6.1	Elastic Moduli of Lumber Sheathing	72
4.6.2	Hysteretic Behavior of Diaphragm #1	74
4.6.3	Internal Forces in Diaphragm #1	82
4.6.4	Hysteretic Energy Dissipation	88
4.7	<i>Evaluation of Test Data for Diaphragm #2 (Metal Deck)</i>	90
4.7.1	Hysteretic Behavior of Diaphragm #2	91
4.8	<i>Summary, Conclusions, and Significance of Quasi-Static Diaphragm Testing</i>	97
4.8.1	Summary of Results and Conclusions	97
4.8.2	Significance of Quasi-Static Testing	98
5.0	LOW-DEGREE-OF-FREEDOM IDEALIZATIONS OF LOW-RISE REINFORCED MASONRY BUILDINGS WITH FLEXIBLE DIAPHRAGMS	99
5.1	<i>General Approach and Mathematical Development</i>	99
5.1.1	First Degree of Freedom, q1	100
5.1.2	Second Degree of Freedom, q2	101
5.1.3	General Expressions for Response	102
5.2	<i>Implementation of Two-Degree-of-Freedom Idealization to Low-Rise Reinforced Masonry Buildings with Flexible Diaphragms</i>	105
5.2.1	Parametric Sensitivity of Response	105
5.2.2	Implications of Parameter Study	114
5.3	<i>Verification of Two-Degree-of-Freedom Idealization for Low Levels of Response (Linear Elastic)</i>	115
5.3.1	Shaking-Table Specimens	115
5.3.2	Hypothetical Prototypical Finite-Element Building Models	116

5.3.3	Comparison With an Existing Period Expression (FEMA 356)	119
5.4	<i>Verification of Two-Degree-of-Freedom Idealization for High Levels of Response (Nonlinear)</i>	120
5.4.1	General Approach and Model Development	121
5.4.2	Modeling of Shaking-Table Specimen #1 (Lumber)	122
5.4.3	Modeling of Shaking-Table Specimen #2 (Metal-Deck)	127
5.5	<i>Summary of Results, Conclusions, and Significance of Idealizations</i>	133
5.5.1	Summary of Results and Conclusions	133
5.5.2	Significance of Idealizations	134
6.0	SEISMIC EVALUATION OF LOW-RISE REINFORCED MASONRY BUILDINGS WITH FLEXIBLE DIAPHRAGMS	135
6.1	<i>FEMA 310: Handbook for the Seismic Evaluation of Buildings – A Prestandard</i>	135
6.2	<i>United States Army Corps Technical Instructions</i>	138
6.3	<i>Potential Gaps in FEMA 310 Methodology</i>	138
6.4	<i>Development of Proposed Supplementary Methodology</i>	139
6.4.1	Previous Diaphragm Tests	140
6.4.2	Interpretation of Diaphragm Test Data	141
6.4.3	Reevaluation of Diaphragm Test Data	145
6.4.4	Significance of Reevaluations and Observed Relationships	148
6.5	<i>Proposed Supplementary Methodology for FEMA 310</i>	150
6.6	<i>Summary of Results, Conclusions, and Significance of Proposed Supplementary Methodology</i>	153
6.6.1	Summary of Results and Conclusions	153
6.6.2	Significance of Proposed Supplementary Methodology	153

7.0 SEISMIC REHABILITATION OF LOW-RISE REINFORCED MASONRY BUILDINGS WITH FLEXIBLE DIAPHRAGMS	154
7.1 <i>FEMA 356: Prestandard and Commentary for the Seismic Rehabilitation of Buildings</i>	154
7.1.1 General Methodology	154
7.1.2 General Provisions and Commentary	156
7.2 <i>United States Army Corps Technical Instructions</i>	159
7.3 <i>Potential Gaps in FEMA 356 Methodology</i>	159
7.3.1 Analysis Procedures	159
7.3.2 Diaphragm Modeling	162
7.3.3 Acceptance Criteria	164
7.4 <i>Proposed Supplementary Methodology</i>	170
7.5 <i>Summary of Results, Conclusions, and Significance of Critical Review and Supplementary Methodology</i>	171
7.5.1 Summary of Results and Conclusions	171
7.5.2 Significance of Critical Review	172
8.0 APPLICATION OF PROPOSED SUPPLEMENTARY SEISMIC EVALUATION METHODOLOGY	173
8.1 <i>Selection of Buildings for Evaluation</i>	173
8.1.1 URS Greiner Inc. Hierarchy of Structural Classifications for Ft. Lewis	173
8.1.2 CERL Screening of Ft. Lewis Inventory	175
8.1.3 Additional Screening of Ft. Lewis Inventory	177
8.1.4 Buildings for Evaluation	178
8.2 <i>Application of Current Seismic Evaluation Methodology</i>	181
8.2.1 URS Greiner Evaluations	182
8.2.2 FEMA 310 Evaluations	184

8.3	<i>Application of Proposed Supplementary Seismic Evaluation</i>	
	<i>Methodology</i>	185
8.4	<i>Summary of Results, Conclusions, and Significance of Evaluations</i>	189
8.4.1	Summary of Results and Conclusions	189
8.4.2	Significance of Evaluations	190
9.0	SUMMARY OF RESULTS AND CONCLUSIONS, SYNTHESIS OF STUDY, AND RECOMMENDATIONS	191
9.1	<i>Summary of Results and Conclusions from Study Phases</i>	191
9.1.1	Summary of Results and Conclusions from Behavior Phase	191
9.1.2	Summary of Results and Conclusions from Analysis Phase	193
9.1.3	Summary of Results and Conclusions from Evaluation and Rehabilitation, and Application and Verification Phases	194
9.2	<i>Synthesis of Study Elements to Meet Study Objectives</i>	196
9.3	<i>Recommendations</i>	197
APPENDIX A : INSTRUMENTATION OF DIAPHRAGM SPECIMENS		200
A.1	<i>Instrumentation of Diaphragm #1 (Lumber Sheathing)</i>	200
A.2	<i>Instrumentation of Diaphragm #2 (Metal-Deck)</i>	204
APPENDIX B : STRUCTURAL AND ARCHITECTURAL DRAWINGS		208
B.1	<i>Building 8</i>	208
B.2	<i>Building 9</i>	215
B.3	<i>Building 6</i>	220
B.4	<i>Building 3</i>	226

APPENDIX C : EXAMPLE SEISMIC EVALUATION	232
<i>C.1 Evaluation Using FEMA 310 Methodology</i>	<i>232</i>
<i>C.2 Evaluation Using Proposed Supplementary Methodology</i>	<i>239</i>
REFERENCES	242
VITA	255

LIST OF TABLES

Table 3-1	Diaphragm design of half-scale specimens	29
Table 3-2	Dynamic properties of half-scale specimens before seismic testing .	34
Table 3-3	11 seismic test motions for Specimen #1.....	37
Table 3-4	12 seismic test motions for Specimen #2.....	37
Table 3-5	Observed diaphragm drift ratio and relationship to damage (Specimen #1)	41
Table 3-6	Observed diaphragm drift ratio and relationship to damage (Specimen #2)	41
Table 4-1	Peak displacements of actuators in loading history (Diaphragm #1) 53	
Table 4-2	Peak displacements of actuators in loading history (Diaphragm #2) 54	
Table 4-3	Key properties of strain-gauged sheathing boards.....	73
Table 4-4	Variation of sheathing axial forces in transverse cross section	88
Table 5-1	Parametric limits of variables affecting response	108
Table 5-2	Calculated and measured peak responses of Specimens #1 and #2 from 2DOF and SDOF idealizations	116
Table 5-3	Finite-element models for verification of 2DOF and SDOF analysis	117
Table 5-4	Comparison of responses from finite-element modeling, 2DOF modeling, and SDOF modeling	118
Table 6-1	Relationships between diaphragm load distribution and diaphragm performance	145
Table 8-1	Numerical assessment of candidate buildings selected by CERL ...	176
Table 8-2	Buildings selected for possible additional seismic evaluation.....	177
Table 8-3	Numerical assessment of candidate buildings for compliance with criteria	178
Table 8-4	Buildings selected for additional seismic evaluation.....	179

Table 8-5	URS Greiner dispositions of selected buildings, evaluated in Ft. Lewis, WA.....	183
Table 8-6	Dispositions of selected buildings, evaluated using FEMA 310	185
Table 8-7	Fundamental periods calculating using FEMA 310 Screening (Tier 1) provisions and proposed supplementary methodology.....	186
Table 8-8	Dispositions of buildings, evaluated using proposed supplementary methodology	187
Table 8-9	Dispositions of selected buildings from evaluations	188

LIST OF FIGURES

Figure 1.1	Synthesis of study elements into a consistent approach to performance of low-rise reinforced masonry buildings with flexible diaphragms	3
Figure 1.2	Characteristic dimension and deflection for definition of the diaphragm drift ratio.....	6
Figure 2.1	Effect of diaphragm flexibility on building response.....	8
Figure 2.2	Deep-beam analogy for the analysis and design of flexible diaphragm systems	9
Figure 2.3	Drag strut (collector element) in diaphragm	10
Figure 2.4	Transverse continuous cross ties in building without subdiaphragm design	11
Figure 2.5	Selection of typical subdiaphragms in building	12
Figure 2.6	Transverse continuous cross ties in building with subdiaphragm design	13
Figure 2.7	Evolutionary relationship of landmark earthquakes and events, landmark documents, and dominant provisions	14
Figure 2.8	Basic organization of a) FEMA 310 and b) FEMA 356 documents for the evaluation and rehabilitation of existing buildings.....	19
Figure 3.1	Schematic of full-scale prototype building	29
Figure 3.2	Schematic of half-scale specimen reinforcement for longitudinal and transverse walls	30
Figure 3.3	Typical details of rafter-to-wall connections for half-scale specimens	30
Figure 3.4	Overall photo of Specimen #1	30

Figure 3.5	Schematic relationship between spectral peaks of input motion and natural frequencies of prototype buildings and scale-model specimens	33
Figure 3.6	Observed yield lines in longitudinal walls	35
Figure 3.7	Characteristic deformations of instrumented diaphragm quarters	38
Figure 3.8	Deformed shape of diaphragms during peak response of Test 9 ..	39
Figure 3.9	Transverse displacements of center of diaphragm and tops of transverse shear walls as measured relative to base of specimen (Test 5, Specimen #1).....	40
Figure 3.10	Transverse accelerations of center of diaphragm and tops of transverse shear walls (Test 5, Specimen #1)	40
Figure 4.1	Plan layout of metal-deck panels in Diaphragm #2	43
Figure 4.2	Box columns support south end of Diaphragm #1	44
Figure 4.3	Low-friction bearing assembly between diaphragm and test frame	44
Figure 4.4	View beneath Diaphragm #1 showing load strut connecting east and west masonry chords at load points (similar for Diaphragm #2)	45
Figure 4.5	Probable vertical eccentricity between shear center of diaphragm and line of action of loading system.....	46
Figure 4.6	Plan of test setup for Diaphragm #1	47
Figure 4.7	Photograph of test setup for Diaphragm #1 (east is to the right) ..	47
Figure 4.8	Typical cross-section of test setup near loading points (Diaphragm #1).....	48
Figure 4.9	Plan drawing of test setup (Diaphragm #2).....	49
Figure 4.10	Plan photograph of test setup (Diaphragm #2, east is to the left) .	49
Figure 4.11	View beneath Diaphragm #2 at south channel showing L-shaped restraining members	50

Figure 4.12	Actual displacement history of actuators for Diaphragm #2 (Diaphragm #1 similar)	52
Figure 4.13	Approximate locations of damage at low diaphragm drift ratios; numbers in boxes are figure numbers	55
Figure 4.14	Longitudinal splitting at point of nailing (DDR = 0.3 %, east side of south quarter)	55
Figure 4.15	Spreading of butt splices under tension (DDR = 0.3 %).....	56
Figure 4.16	Longitudinal splitting of sheathing board at point of nailing and spreading of butt splices (DDR = 0.6 %)	56
Figure 4.17	Nail withdrawal and tear-out at board end (DDR = 0.6 %)	57
Figure 4.18	Approximate location of damage at high diaphragm drift ratios; numbers in boxes are figure numbers	57
Figure 4.19	Sliding-shear failure during displacement to the west along pre- existing cracks in masonry chords (DDR = 1.1 %, northeast corner)	58
Figure 4.20	Withdrawal of nail connecting blocking and nailer member, at diaphragm corner (DDR = 1.1 %, southeast corner).....	59
Figure 4.21	Process causing withdrawal of nails connecting blocking and nailer; shown at northwest corner of diaphragm during displacement to the west	60
Figure 4.22	Severe damage to diaphragm, due to mechanism described in Figure 4.21 (DDR = 2.3 %, northwest corner).....	60
Figure 4.23	Joist splitting at point of nailing (DDR = 1.5 %)	61
Figure 4.24	Butt-splice spreading, nail withdrawal and nail tear-out at sheathing board end (DDR = 1.5 %).....	61
Figure 4.25	Longitudinal splitting of sheathing board at point of nailing (DDR = 1.5 %).....	62

Figure 4.26	Nail withdrawal at maximum diaphragm drift ratio (DDR = 2.3 %)	63
Figure 4.27	Deterioration of masonry chord at maximum diaphragm drift ratio (DDR = 2.3 %, southeast corner)	63
Figure 4.28	Longitudinal splitting of sheathing board at point of nailing at maximum diaphragm drift ratio (DDR = 2.3 %, northwest corner)	64
Figure 4.29	Strain-gauged sheathing boards removed and examined after testing	65
Figure 4.30	Typical deformation of nail and wood at nail hole	65
Figure 4.31	Reference locations and weld-condition symbols for Diaphragm #2	66
Figure 4.32	Example of out-of-plane buckling in north-end quarter panel at high diaphragm drift ratios	68
Figure 4.33	Flaking of Hydrostone® weld coating	68
Figure 4.34	Bearing deformation at side-lap screw	69
Figure 4.35	Locations of failed puddle welds after Test #6 (DDR = 0.61 %)	70
Figure 4.36	Locations of failed puddle welds after Test #7 (DDR = 1.11 %)	70
Figure 4.37	Locations of failed puddle welds after Test #8 (DDR = 1.52 %)	70
Figure 4.38	Locations of failed puddle welds after Test #9 (DDR = 2.27 %)	70
Figure 4.39	Example of weld “tear out” at joist-to-weld interface	71
Figure 4.40	Example of “burn through” at weld perimeter	72
Figure 4.41	Applied load versus diaphragm drift ratio for Major Cycle #2 of Diaphragm #1 (DDR = 0.11 %)	75
Figure 4.42	Idealized force-deformation relationship for a linear-elastic system with Coulomb (linear) damping	75
Figure 4.43	Relationship between applied load and diaphragm drift ratio of Diaphragm #1 for low diaphragm drift ratios (DDR < 0.6 %)	76

Figure 4.44	Relationship between applied load and diaphragm drift ratio of Diaphragm #1 for high diaphragm drift ratios ($DDR > 0.6\%$).....	77
Figure 4.45	Identification of points comprising peak envelopes and intersection envelopes.....	78
Figure 4.46	Hysteresis intersection and peak envelopes for north actuator (Diaphragm #1)	79
Figure 4.47	Hysteresis intersection and peak envelopes for south actuator (Diaphragm #1)	79
Figure 4.48	Comparison of hysteresis intersection and peak envelopes (Diaphragm #1)	80
Figure 4.49	Relationship between total applied load and diaphragm drift ratio of Diaphragm #1 for Major Cycle #9.....	80
Figure 4.50	Illustration of hysteretic pinching due to hole damage in nailed wood assemblies.....	82
Figure 4.51	Decomposition of measured axial forces in sheathing boards	83
Figure 4.52	Comparison of applied in-plane shear and that resisted by lumber sheathing (Test #1, Diaphragm #1).....	84
Figure 4.53	Comparison of applied in-plane shear and that resisted by lumber sheathing (Test #8, Diaphragm #1).....	85
Figure 4.54	Schematic process for normalizing axial forces in sheathing boards	86
Figure 4.55	Normalized axial force distribution in sheathing boards, for a transverse cross-section in the south-end quarter, at peak diaphragm drift ratios (Diaphragm #1, Test #8)	87
Figure 4.56	Contribution of friction to hysteretic energy dissipation	89
Figure 4.57	Relative contributions of friction and inelastic material response to measured hysteretic energy dissipation in Diaphragm #1	90

Figure 4.58	Relationship between applied load and diaphragm drift ratio of Diaphragm #2 for low diaphragm drift ratios ($DDR < 0.6\%$).....	92
Figure 4.59	Comparison of relationships between applied load and diaphragm drift ratio in the north and south actuators for Diaphragm #2 ($DDR < 0.6\%$)	92
Figure 4.60	Relationship between applied load and diaphragm drift ratio of Diaphragm #2 for high diaphragm drift ratios ($DDR > 0.6\%$).....	93
Figure 4.61	Hysteresis peak envelopes for south actuator (Diaphragm #2).....	95
Figure 4.62	Comparison of hysteresis peak envelopes for north and south actuators (Diaphragm #2).....	95
Figure 5.1	Generalized coordinates for 2DOF idealization.....	100
Figure 5.2	Degree-of-freedom mass ratio for four different combinations of maximum and minimum wall mass and diaphragm mass.....	110
Figure 5.3	Degree-of-freedom stiffness ratio over four different combinations of maximum and minimum wall stiffness and diaphragm stiffness	110
Figure 5.4	Fundamental frequency modification factor	112
Figure 5.5	Diaphragm degree of freedom mass participation factor, PF.....	112
Figure 5.6	Diaphragm spectral displacement amplification factor, d	113
Figure 5.7	Two-dimensional slices of Figure 5.4 through Figure 5.6	114
Figure 5.8	Finite-element verification model, VM1 Metal	118
Figure 5.9	Finite-element verification model, VM2 Metal	118
Figure 5.10	Calculated periods of hypothetical prototypical building models	120
Figure 5.11	Schematic of lumped-parameter panel element and 2DOF model	121
Figure 5.12	Hysteresis and backbone stiffness of Specimen #1; Seismic Tests 3, 5, 9 and 10	123

Figure 5.13	Hysteresis of peak response of Specimen #1; Test 9	124
Figure 5.14	Schematic of element hysteresis rules used to model lumber diaphragm.....	124
Figure 5.15	Results of nonlinear modeling of Specimen #1; Test 3	126
Figure 5.16	Results of nonlinear modeling of Specimen #1; Test 5	126
Figure 5.17	Results of nonlinear modeling of Specimen #1; Test 9	126
Figure 5.18	Results of nonlinear modeling of Specimen #1; Test 10	126
Figure 5.19	Hysteresis and backbone stiffness of Specimen #2; Tests 2, 5, 9, 10	129
Figure 5.20	Hysteresis for peak response of Specimen #2; Test 9.....	130
Figure 5.21	Results of nonlinear modeling of Specimen #2; Test 3	131
Figure 5.22	Results of nonlinear modeling of Specimen #2; Test 5	131
Figure 5.23	Results of nonlinear modeling of Specimen #2; Test 9	131
Figure 5.24	Results of nonlinear modeling of Specimen #2; Test 10	131
Figure 5.25	Hysteresis for Test 9 of Specimen #2.....	132
Figure 6.1	Diaphragm under uniformly distributed load.....	141
Figure 6.2	Effective calculation of diaphragm drift ratio for different test configurations.....	144
Figure 6.3	Relationship of applied load and deformation of a metal-deck diaphragm.....	146
Figure 6.4	Relationship between a measure of diaphragm shear stiffness G' and diaphragm drift ratio, at onset of damage, for metal-deck diaphragms	147
Figure 6.5	Relationship between a measure of diaphragm shear stiffness G' and diaphragm drift ratio, at onset of damage, for lumber sheathed diaphragms	148
Figure 6.6	Link between FEMA Performance Levels and proposed methodology.....	149

Figure 6.7	Basic organization of proposed supplementary evaluation methodology for FEMA 310	150
Figure 6.8	Proposed Supplementary Methodology for FEMA 310	152
Figure 7.1	FEMA 356 plausible distribution of lateral and shear forces in a flexible diaphragm.....	162
Figure 7.2	Comparison of FEMA 356 component-specific force-reduction m-factors and FEMA 302/303 and IBC base shear-reduction R-factors	165
Figure 7.3	Relationship between reevaluated diaphragm data and performance levels.....	167
Figure 7.4	Effect of shear eccentricity on resultant connector forces	169
Figure 8.1	Hierarchy of building classification used by URS Greiner for Ft. Lewis, WA	174
Figure 8.2	Building 8.....	179
Figure 8.3	Building 9.....	180
Figure 8.4	Building 6.....	180
Figure 8.5	Building 3.....	181
Figure 8.6	Catalog of building evaluations.....	182
Figure 8.7	Typical joist-to-wall connection in Buildings 9, 6, 3	183
Figure 9.1	Synthesis of study elements into a consistent approach performance of low-rise reinforced masonry buildings with flexible diaphragms	197
Figure A.1	Instrumentation measuring transverse in-plane deflections	200
Figure A.2	Instrumentation measuring relative slip between masonry chords and nailer	200
Figure A.3	Instrumentation measuring relative torsional displacement of end columns	201
Figure A.4	Instrumentation measuring relative in-plane deformations.....	201

Figure A.5	Instrumentation measuring in-plane shear strains	202
Figure A.6	Instrumentation measuring strains in diaphragm rafters and blocking; shaded members are strain-gauged	202
Figure A.7	Instrumentation measuring axial forces in load struts; struts are strain-gauged	203
Figure A.8	Instrumentation measuring transverse in-plane deflections	204
Figure A.9	Instrumentation measuring relative side-lap slip between adjacent panels.....	204
Figure A.10	Instrumentation for measuring end-lap slip at puddle welds	205
Figure A.11	Instrumentation measuring relative torsional displacement of end columns	205
Figure A.12	Instrumentation measuring relative in-plane deformations.....	206
Figure A.13	Locations and labels of welds with thin Hydrostone® coatings.	206
Figure A.14	Instrumentation measuring axial forces in load struts; struts are strain-gauged	207
Figure C.1	FEMA 310 Basic Structural Checklist 3.7.13 (page 1 of 2)	235
Figure C.2	FEMA 310 Basic Structural Checklist 3.7.13 (page 2 of 2)	236
Figure C.3	FEMA 310 Supplemental Structural Checklist 3.7.13S (page 1 of 2).....	237
Figure C.4	FEMA 310 Supplemental Structural Checklist 3.7.13S (page 2 of 2).....	238

1.0 Introduction

This dissertation reports a multi-phased research study performed by The University of Texas at Austin and the United States Army Corp of Engineers, Engineer Research and Development Center, Construction Engineering Research Laboratory (CERL), from September 1999 to May 2004. The study involves the development of supplementary seismic evaluation and rehabilitation methodologies for low-rise reinforced masonry buildings with flexible diaphragms. Some of the information reviewed here has been reported previously (Cohen 2001, Cohen *et al.* 2002a,b,c, 2003a, and 200Xa,b).

1.1 Study Justification, Milestones, and Objectives

In response to Executive Order 12941 (December 1994), the United States government began a large coordinated effort to assess and mitigate the seismic hazards of its existing owned and leased facilities. As part of that effort, the US Army assessed its existing building inventory and preliminarily determined that, in the roughly 4500 seismically vulnerable Army-owned buildings in the continental US, the chief potential seismic deficiency is flexible diaphragms. Furthermore, the 4500 vulnerable buildings comprise mostly low-rise reinforced masonry construction. This study was intended to enhance the accuracy and efficiency of seismic hazard assessment and mitigation for these types of buildings. This was realized in several distinct phases of study: behavior; analysis; evaluation and rehabilitation; and verification and application. Corresponding milestones (key tasks and associated deliverables) accompanied each phase.

First, the seismic behavior of these types of buildings was characterized. From September 1999 to March 2001, two, half-scale low-rise reinforced masonry building specimens with flexible diaphragms were tested on the US

Army Tri-axial Earthquake and Shock Simulator (TESS) at CERL. This testing qualitatively and quantitatively substantiated the generally accepted premise (by the earthquake engineering technical community) that diaphragm flexibility can significantly affect the seismic response of these types of buildings. It also provided experimental data for analytical modeling and other uses. Data from these shaking-table tests were evaluated for internal and external consistency, deformations, and forces.

From March 2001 to August 2001, diaphragms and attached masonry chords from the shaking-table specimens were removed and subjected to reversed cyclic quasi-static displacements. Data from these tests were evaluated for hysteretic characteristics and consistency with shaking-table data. Completion of these tests marked the end of the behavior phase.

From August 2001 to August 2002, observations and conclusions from physical testing were used to develop and validate a simple tool for the analysis of these types of buildings. The tool was developed in the general case and then analytically bounded, through parameter studies, to the particular analysis of low-rise masonry buildings with flexible diaphragms. The tool was validated in the linear elastic and nonlinear ranges using data from shaking-table testing, finite-element modeling, and lumped-parameter modeling. Completion of these validations marked the end of the analysis phase.

From August 2002 to December 2003, the analysis tool was integrated with existing seismic evaluation and rehabilitation methodologies to fill identified gaps in those methodologies. Data from previous flexible-diaphragm tests, performed by others, were reevaluated in the context of performance-based engineering and synthesized with the analysis tool into coherent supplementary seismic evaluation and rehabilitation methodologies. This marked the end of the evaluation and rehabilitation phase.

From December 2002 to September 2003, the integrated tool was applied to the seismic evaluation of several existing military-owned low-rise reinforced masonry buildings with flexible diaphragms. This marked the end of the application phase, and the end of the overall study. The interrelationship of study elements is shown in Figure 1.1.

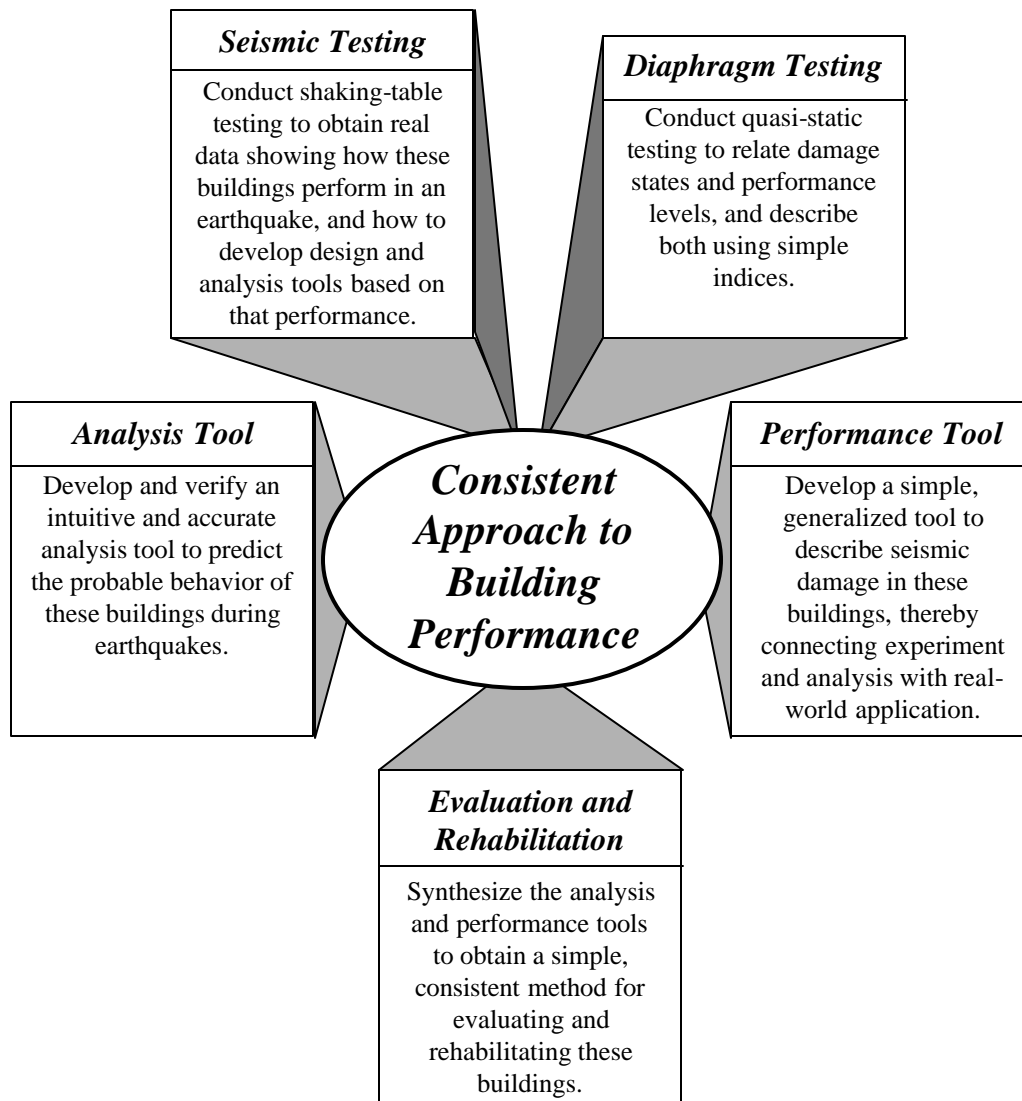


Figure 1.1 Synthesis of study elements into a consistent approach to performance of low-rise reinforced masonry buildings with flexible diaphragms

This dissertation has the objective of reviewing and synthesizing these four phases of study, and thereby achieving the overall objective of the study. Methodologies for the earthquake hazard evaluation and mitigation of these types of buildings were critically assessed and consequently enhanced. In this synthesis an auxiliary and equally significant objective was realized. The conclusions and tools developed in this dissertation were seen to embody a consistent approach for the characterization of seismic performance of these types of buildings. Implications of this are discussed at the end of this dissertation.

1.2 Scope of Work

This study is aimed at the seismic evaluation and rehabilitation of low-rise reinforced masonry buildings with flexible diaphragms. The term *low-rise* implies that only one-story buildings are considered. Although much of this work may be applicable, or at least adaptable, to the evaluation and rehabilitation of two- and possibly three-story structures, those possibilities are not further explored in this dissertation. The term *reinforced masonry* implies that only masonry buildings meeting general minimum prescriptive requirements for reinforcement of the 1973 Uniform Building Code, are considered; conclusions from this study are not applicable to partially reinforced or unreinforced masonry buildings. Finally, the term *flexible diaphragm* implies that only buildings with flexible diaphragms are considered. (Diaphragms classified as “flexible” exhibit in-plane deflections, relative to the tops of their supporting in-plane walls, which are at least twice those of the tops of the walls themselves, relative to their bases.) Moreover, many of the conclusions presented here are applicable only to lumber-sheathed or metal-deck diaphragms.

Further application of the general research methodology presented in this dissertation may demonstrate that the conclusions of this study are indeed

applicable, or least adaptable, to a wide range of structures: multi-story structures, unreinforced and partially reinforced masonry, flexible diaphragms of different construction, and others. Such extension is beyond the scope of this study, however, and is not discussed further.

1.3 General Outline of Dissertation

This dissertation presents the previously described study in the following format:

Chapter 2 presents general background information. This includes a survey of current and past design philosophies; a chronology of the seismic performance, design, evaluation, and rehabilitation of these types of buildings; and a review of applicable existing research and technical literature.

Chapters 3 and 4 summarize the behavior phase of the study. The former outlines the shaking-table testing of two, half-scale low-rise masonry buildings with flexible diaphragms. Detailed reports of this work are provided elsewhere (Cohen 2001, Cohen *et al.* 2002a,c, 2003a, and 200Xa). Salient data and conclusions, however, are reviewed in this dissertation for convenience and reading coherency. Chapter 4 details the quasi-static testing of two, diaphragm-masonry chord assemblies and thoroughly discusses specimen development, testing, and data evaluations.

Based on results and conclusions from Chapters 3 and 4, Chapter 5 presents the analysis phase of the study and outlines the development and verification of a tool for the analysis of these types of buildings.

Chapters 6 and 7 summarize the evaluation and rehabilitation phase of this study. Chapter 6 first identifies potential gaps in the predominant existing seismic evaluation methodology, and then proposes patches for those gaps. The patches integrate the analysis tool developed in Chapter 5 with performance-based

engineering concepts and data to develop a supplementary evaluation methodology for these types of buildings. In Chapter 7, that methodology is related to seismic rehabilitation.

Chapter 8 synthesizes the study elements by applying the proposed supplementary methodology to the seismic evaluation of four existing buildings, and demonstrates that the methodology is needed, rational, and useful.

1.4 Introduction of Diaphragm Drift Ratio

Throughout this dissertation, diaphragm deformations are characterized using the Diaphragm Drift Ratio (DDR). The ratio is related to observed diaphragm damage, in the case of physical testing, and potential for diaphragm damage, in the case of seismic evaluation and rehabilitation. It forms the basis for much of the work presented here, and is defined as:

$$DDR = \frac{2\Delta}{L}, \quad \text{Equation 1-1}$$

where Δ is the in-plane deflection of the diaphragm relative to the tops of its supporting shear walls, and L is the plan length of the diaphragm (Figure 1.2).

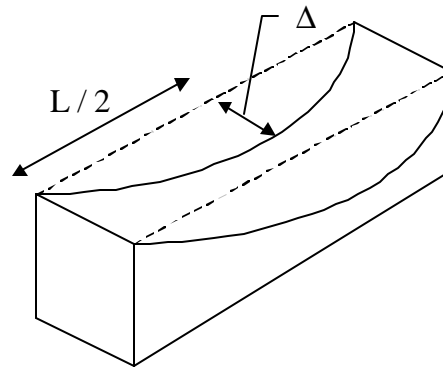


Figure 1.2 Characteristic dimension and deflection for definition of the diaphragm drift ratio

2.0 Background of Study and Relevant Reference Information

To develop a foundation of knowledge, this chapter outlines state-of-the-art philosophies of design, evaluation, and rehabilitation for low-rise reinforced masonry buildings with flexible diaphragms. First, the effect of diaphragm flexibility on building response, as well as current philosophies intended to deal with that effect, are briefly described in terms of diaphragm design, anchorage design, and masonry wall design. Then, the past seismic performance of these types of buildings is outlined and correlated with evolutions in design, evaluation, and rehabilitation requirements. Finally, past and current research applicable to this study is cataloged and briefly described.

2.1 Seismic Behavior and Design of Low-Rise Reinforced Masonry Buildings with Flexible Diaphragms

Low-rise masonry buildings typically have flexible roof diaphragms constructed of wood or metal decking. The in-plane flexibility of those diaphragms can significantly affect the seismic response of such buildings (Figure 2.1). It can increase natural periods; increase in-plane shear forces and deformations in diaphragms and shear walls; increase bending forces and deformations in out-of-plane walls; and increase anchorage forces between diaphragms and walls. Diaphragm flexibility tends to increase the ratio of mass associated with the in-plane response of the roof diaphragm to that of the in-plane shear walls. This flexibility effectively introduces additional (or at least, different) degrees of freedom, associated with in-plane response of the diaphragm (Figure 2.1). These effects are especially pronounced when the building has a high plan aspect ratio (for example, 3:1).

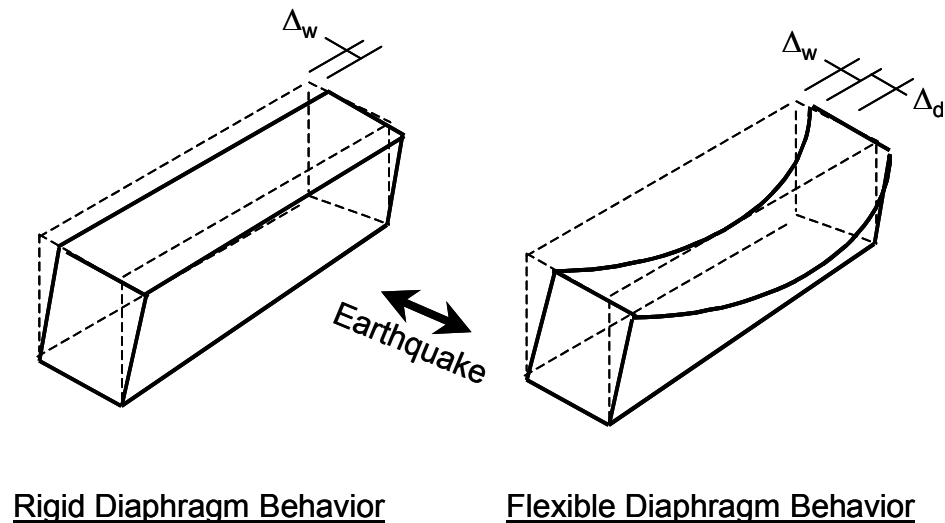


Figure 2.1 Effect of diaphragm flexibility on building response

Seismic response of a flexible diaphragm system is governed, as with any dynamic system, by its mass and stiffness, and by the characteristics of the ground motion exciting it. Mass coupled with the response of the diaphragm derives partially from the mass of the diaphragm itself and partially from that of connected out-of-plane walls. The in-plane stiffness of a diaphragm system derives chiefly from the in-plane stiffness of the diaphragm itself, and to a small degree the out-of-plane stiffness of connected masonry walls.

In the rest of this chapter, current seismic design and analysis methodologies intended to account for this behavior are summarized. General flexible diaphragm behavior and design is discussed, followed by the design of anchorage between in-plane walls and diaphragm and out-of-plane walls and diaphragm. For the latter, the subdiaphragm concept is established. Finally, a comprehensive approach is given for the seismic design and retrofit of masonry walls loaded in-plane and out-of-plane.

2.1.1 Design of Flexible Diaphragms

Flexible-diaphragm systems generally comprise four basic structural components: the diaphragm itself; chord members; drag struts or collector elements; and anchorage components. Breyer (1980 or more recent editions) gives an excellent general discussion of these components and their analysis and design. The following information is not intended to provide for design but rather to describe, in general terms, flexible diaphragm behavior and design.

Design engineers generally analyze diaphragms as deep (shear-critical) beams (Figure 2.2). The web of the deep beam (the main shear-force resisting element) represents the diaphragm itself (for example, the metal-deck or lumber sheathing). The flanges of the deep beam (the main bending-force resisting element) represent the chord members of the diaphragm (for example, the out-of-plane masonry walls or lumber nailers).

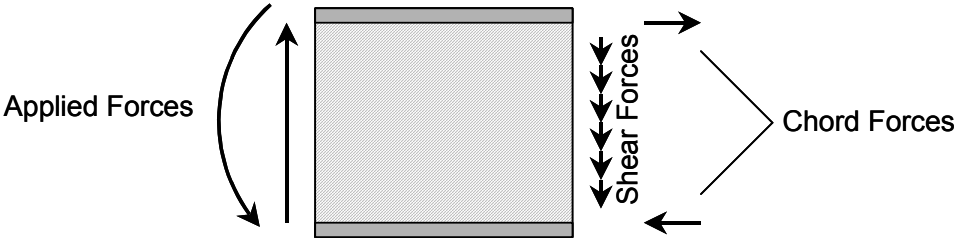


Figure 2.2 Deep-beam analogy for the analysis and design of flexible diaphragm systems

These two diaphragm elements are simply designed to resist the analogous deep-beam forces. The diaphragm itself is designed to resist in-plane shear forces (number, pattern, and size of nails in lumber diaphragms; number, pattern, and size of welds and decking in a metal-deck diaphragm); and chord members are designed to resist chord forces (number and size of reinforcing bars in masonry bond beams and size of nails and nailing patterns for nailers).

Diaphragm design also accounts for openings (stair wells, etc.) and discontinuities in load path (window and door openings at anchorage areas).

Openings can increase local shear and bending forces in a diaphragm; discontinuities can disrupt the load path of a diaphragm. Diaphragms are therefore reinforced around openings to resist the increased forces and special components (drag struts or collectors) are configured to complete any disrupted load paths (Figure 2.3).

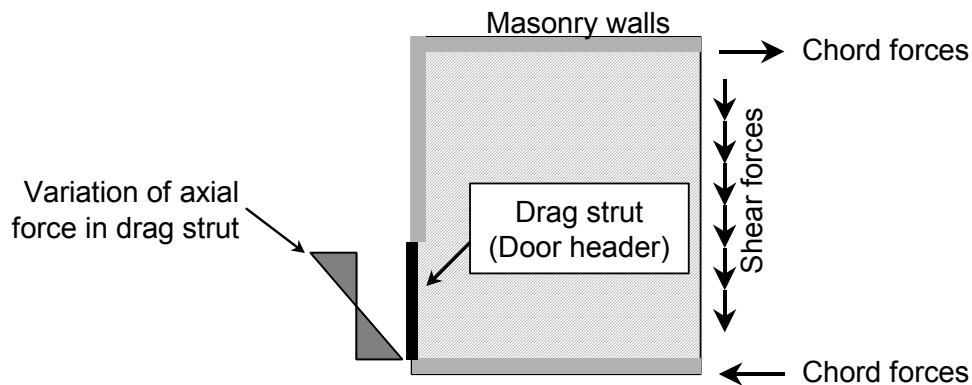


Figure 2.3 Drag strut (collector element) in diaphragm

2.1.2 Design of Diaphragm Anchorage and the Subdiaphragm

Concept

Fundamental to the good seismic performance of a diaphragm is anchorage between it and the connecting walls. Anchorage design depends on whether the anchorage is intended to transfer inertial forces from the diaphragm to the shear walls, or the inertial forces from the out-of-plane walls to the diaphragm. In the former case, the load path extends from diaphragm, to anchorage, to in-plane shear wall. Force originates from response of the diaphragm itself, and anchorage components (anchor bolts, trim angles, and others) are designed to resist expected internal shear forces (Figure 2.2). In the latter case, the load path extends from out-of-plane wall, to anchorage, to diaphragm. Force originates from response of the out-of-plane walls themselves. In this case, anchorage design is more involved, and is now discussed.

Since the 1973 UBC, design requirements for flexible diaphragms have included requirements for continuous cross ties between their chords (Figure 2.4). Cross ties are structural elements, such as beams, that connect parallel diaphragm chords and provide continuous paths for forces oriented perpendicular to those chords (such as out-of-plane wall forces). They are included in design so that anchorage forces fully develop into the diaphragm, preventing anchorage failure and consequent out-of-plane wall failure. The requirement for cross ties can in many cases result in the need for a large number of splices between diaphragm beams (Figure 2.4), which significantly increase building cost and construction time.

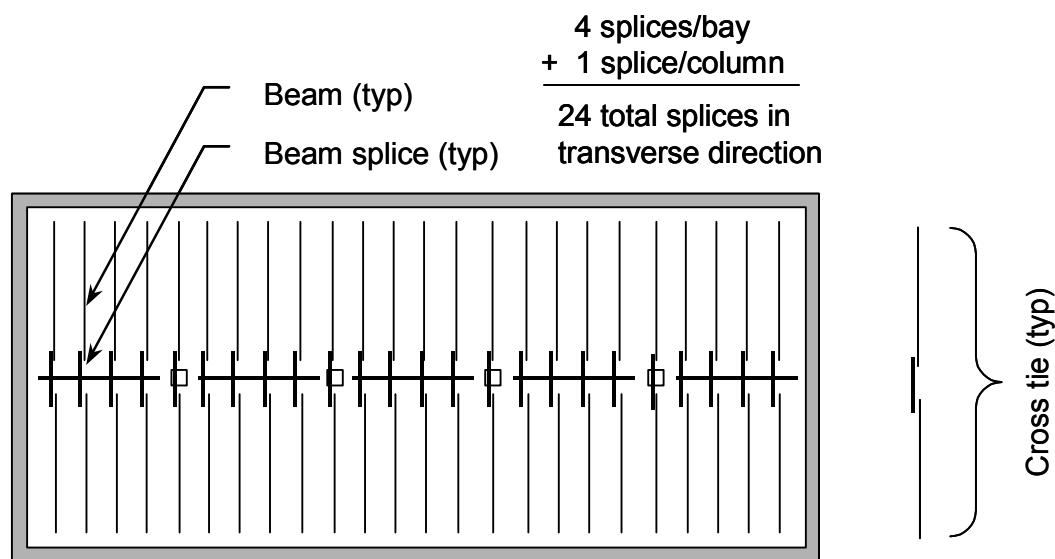


Figure 2.4 Transverse continuous cross ties in building without subdiaphragm design

Alternatively, buildings may be designed using the subdiaphragm concept. The subdiaphragm is a conceptual design tool specifically developed to help engineers satisfy the requirement of continuous cross ties between diaphragm chords, while reducing the total number of beam splices. As suggested by the word, the concept allows engineers to partition a large diaphragm into smaller

“sub-diaphragms.” These smaller subdiaphragms are intelligently selected by the engineer and subsequently designed as independent diaphragms (Figure 2.5). Each subdiaphragm must have cross ties and be connected to adjacent subdiaphragms. Additionally, each subdiaphragm must be designed to maintain sufficient shear and moment capacity to resist tributary wall lateral loads. The subordination of subdiaphragms is not limited. A building may be designed with subdiaphragms within subdiaphragms, each being designed as a fully independent system.

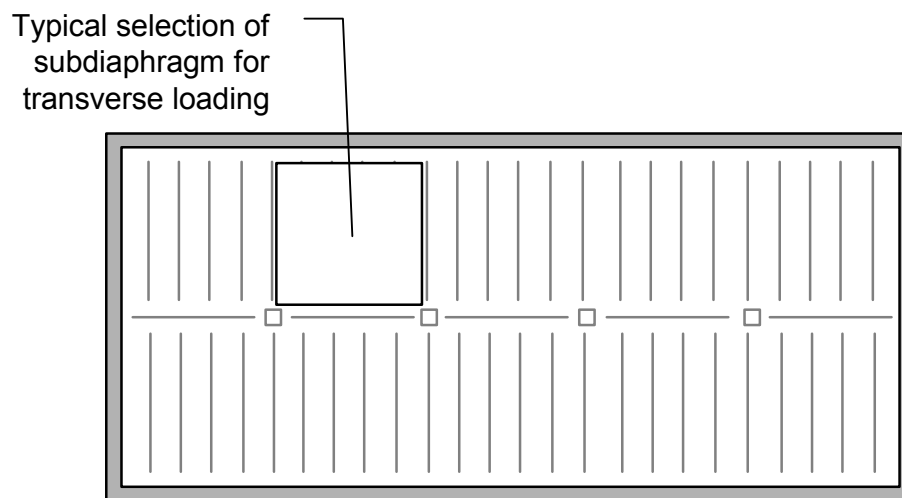


Figure 2.5 Selection of typical subdiaphragms in building

The concept can very effectively reduce the number of required continuous cross ties in a diaphragm (Figure 2.6), without compromising anchorage integrity or out-of-plane wall stability. The arbitrary choice of subdiaphragm size and location results from the fact that subdiaphragms are design tools only; although each subdiaphragm is designed as an independent system, actual independent response is not possible.

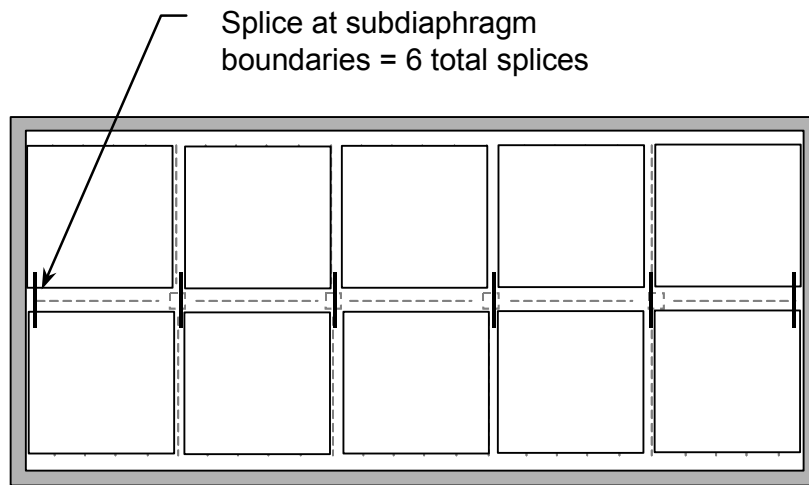


Figure 2.6 Transverse continuous cross ties in building with subdiaphragm design

2.1.3 Design of In-Plane and Out-of-Plane Masonry Walls

The Masonry Designer's Guide 4th Edition (TMS 2003) provides an excellent general discussion of reinforced masonry design. The text devotes large sections to the analysis and design of shear walls, and to the analysis and design of out-of-plane loadbearing and non-loadbearing walls. Also included are special considerations for seismic analysis and design: ductility, detailing, and others.

2.2 Seismic Performance and the Evolution of Design, Evaluation, and Rehabilitation of Low-Rise Reinforced Masonry Buildings with Flexible Diaphragms

The seismic design of low-rise reinforced masonry buildings with flexible diaphragms has evolved over the years. This is primarily due to advances in research and knowledge (for example, base-shear calculations), critical observations of damage following earthquakes (for example, out-of-plane wall anchorage requirements), and also to changes in design and construction practice (for example, allowable-stress and strength design philosophies). In the

following, general observations of damage following major earthquakes are discussed and correlated with consequent changes in major model codes. The following sections of this dissertation describe the relationship between major US earthquakes, the development of landmark documents, and the publication of dominant seismic design provision, as illustrated in Figure 2.7.

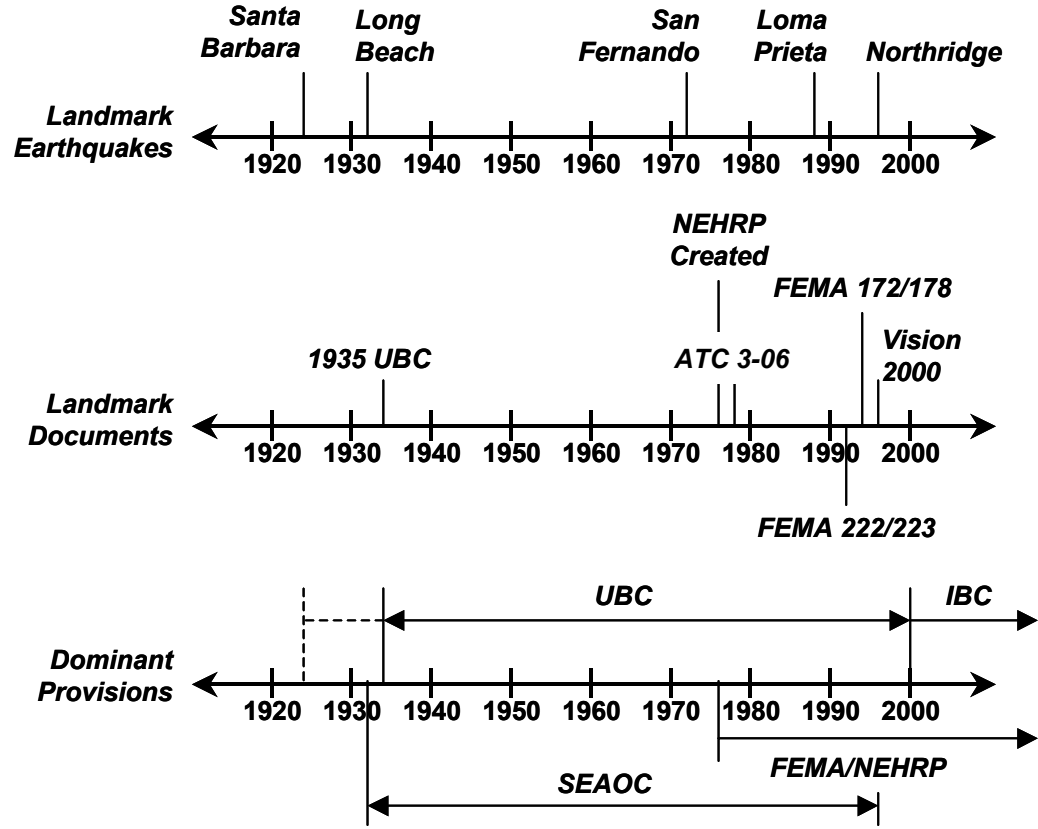


Figure 2.7 Evolutionary relationship of landmark earthquakes and events, landmark documents, and dominant provisions

2.2.1 Evolution of Seismic Design Requirements for New Construction

2.2.1.1 Evolution and Decline of a Major US Model Code for Seismic Design

Model codes containing the seismic design provisions in the US have evolved over the years (TMS 2003). The Uniform Building Code (UBC), published by the International Conference of Building Officials (ICBO), was the dominant model code in the US for seismic design until 1997. Seismic provisions of that document were primarily based on the “Blue Book” of the Structural Engineers Association of California (SEAOC).

Damage to buildings during the 1925 Santa Barbara, California earthquake prompted the development and introduction of the first UBC in 1927. Implementation of those regulations was inconsistent, however, until the 1933 Long Beach, California earthquake. Following that event, most western regions of the United States adopted mandatory seismic design regulations from the 1935 UBC. From 1949 to 1970, the UBC gradually and consistently evolved to account for the growing knowledge of geographic seismicity and seismic zoning, dynamic response of buildings, soil effects, and building usage (importance).

The 1971 San Fernando Valley earthquake caused extensive damage to low-rise masonry buildings; the 1973 UBC addressed those observations with the addition of a number of requirements concerning connectivity between diaphragms and supporting walls. These included: continuous diaphragm cross ties between supporting walls; sufficient out-of-plane wall strength to span between diaphragm anchorage points; prohibition of toe nails connecting wood joists and wood ledgers, and prohibition of nailing configurations causing cross-grain bending in wood ledgers. That edition of the UBC also introduced

minimum prescriptive reinforcement ratios for masonry walls located in zones of high seismic risk.

Under the auspices of the Federal Emergency Management Agency (FEMA), the Applied Technology Council (ATC) published ATC 3-06 in 1978. That document was developed as a resource for future model codes and included national seismic hazard maps, tools for elastic dynamic analysis, drift limits for buildings, provisions for strength design (as opposed to allowable-stress), provisions for soil-structure interaction, provisions for multi-directional excitation effects, and system-specific ductility and response factors (R factors). The UBC adopted these provisions in 1988.

In response to damage caused by the 1989 Loma Prieta Earthquake, the 1991 UBC employed language requiring collector elements and drag struts in diaphragm systems. That document also formally defined a flexible diaphragm using the now-familiar criterion that in-plane deflection of the diaphragm, under lateral loads, be at least twice that of the vertical system supporting it. Furthermore, the subdiaphragm concept was formally recognized for the design of continuous diaphragm cross ties and diaphragm-to-wall anchorage. Simultaneous to this was the emergence of FEMA-funded model-code support efforts, discussed in the next section.

Other than the move in the 1997 UBC to strength design methodologies, with the inclusion of over-strength and horizontal-force factors, there have been no significant changes (to provisions dealing with low-rise masonry buildings) since 1991. Publication of the UBC ceased with its last edition, in 1997. While the 1997 UBC is still enforced in some jurisdictions, its use is expected to disappear.

2.2.1.2 Emergence and Growth of the National Earthquake Hazard Reduction Program and Performance-Based Seismic Design

The National Earthquake Hazard Reduction Program (NEHRP) was established in 1977, following the congressional passing of the Earthquake Hazards Reduction Act (Public Law 95-124), with the stated mission “to reduce the risks of life and property [in the US] from future earthquakes” (www.fema.gov). Four US government agencies partially operate under the auspices of NEHRP: FEMA; the National Institute of Standards and Technology (NIST); the US Geological Survey (USGS); and the National Science Foundation (NSF). NEHRP’s role and influence in the US earthquake engineering community increased significantly in 1990, following passage of the National Earthquake Hazards Reduction Program Act (Public Law 101-614). Acting as the lead NEHRP agency, and to meet the needs of the US structural and earthquake engineering technical communities, FEMA published *Recommended Provisions for the Seismic Regulations of New Buildings* Documents 222 and 223 in 1991, based on ATC 3-06, and updated those documents in 1994 with FEMA 222a and 223a.

A recent trend in structural engineering is the increasing use of performance-based engineering, which can be viewed as an effort to anticipate and improve the overall performance of a structure (damage and post-event occupancy) during a probable earthquake, through coordinated design according to so-called “performance objectives.” Explicit structural performance objectives are assigned to the structure for different levels of earthquakes, and the structure is then designed or evaluated to meet those objectives. For example, should the structure be required simply to not collapse as a result of a strong earthquake, or should it continue to be ready for occupancy? What about a moderate

earthquake? These types of questions are addressed by performance-based engineering.

The philosophy underlying performance-based design was first articulated by the SEAOC Vision 2000 document (1995), which included qualitative definitions of four performance levels: “Fully Operational,” “Operational,” “Life-safe,” and “Near Collapse.” The FEMA documents combined the first two, and defined three performance levels: Immediate Occupancy (IO), Life Safety (LS), and Collapse Prevention (CP). A design earthquake would cause little to no damage for IO; some damage but no immediate threat to human life for LS; and large amounts of damage but continued overall structural stability for CP.

Recent editions of the FEMA design provisions for new construction, Documents 302 and 303 (1997), incorporated these performance-based engineering concepts and formed the framework for the first comprehensive performance-based design methodology in the US. The International Code Commission, a synthesis group created from the major US model-code agencies, adopted those documents into the first edition of the IBC in 2000. FEMA 302 and 303 were updated and reissued in 2000 as FEMA 368 and 369.

2.2.2 Evolution of Seismic Evaluation and Rehabilitation Procedures

Formal dissemination of procedures for the seismic evaluation and rehabilitation of existing buildings began with the creation of NEHRP in 1977, and increased significantly in 1990, following passage of the National Earthquake Hazards Reduction Program Act (Public Law 101-614). That Act, and subsequent development and publication of the FEMA documents that it authorized, significantly increased the guidance available to the design community for the seismic evaluation and rehabilitation of existing buildings.

The first NEHRP document dealing with seismic evaluation of buildings was *Rapid Visual Screening of Buildings for Seismic Hazards: A Handbook* FEMA 154 (1988). That document dealt with the qualitative identification of probable seismic deficiencies in buildings. The first coordinated pair of documents dealing with both seismic evaluation and rehabilitation was published in 1992: *Handbook for the Seismic Evaluation of Existing Buildings* FEMA 178, and *NEHRP Handbook for the Seismic Rehabilitation of Existing Buildings* FEMA 172. FEMA 178 used the first “tiered” seismic evaluation procedure. Simple analysis and evaluation, called “Tier 1” or “Screening,” was first used to quickly identify probable deficiencies. Following that, a more rigorous analysis and evaluation, called “Tier 2” or “Evaluation,” was required on either a deficiency-specific or building-wide basis. This procedure provided practicing engineer with a rapid method for the seismic evaluation of existing buildings.

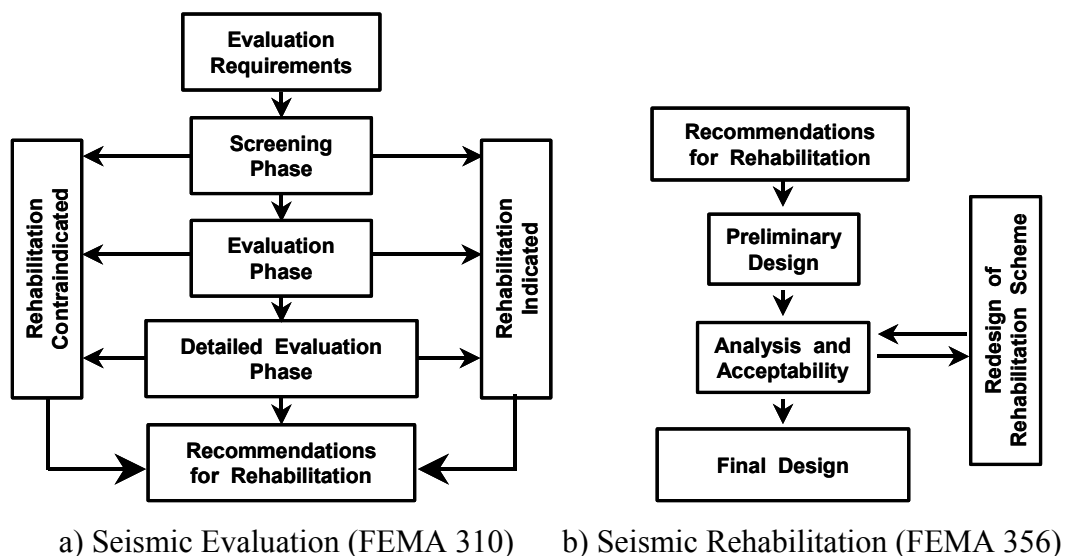


Figure 2.8 Basic organization of a) FEMA 310 and b) FEMA 356 documents for the evaluation and rehabilitation of existing buildings

FEMA 172 and 178 were updated and modified to incorporate performance-based engineering concepts, and were respectively republished in 1997 and 1998 as *NEHRP Guidelines for Seismic Rehabilitation of Buildings*, FEMA 273 and 274, and *Handbook for the Seismic Evaluation of Buildings – A Prestandard*, FEMA 310. In 2000, FEMA 273 and 274 were updated and combined into *Prestandard and Commentary for the Seismic Rehabilitation of Buildings*, FEMA 356. These latter two documents, FEMA 310 and 356, currently comprise the most widely accepted general framework for the systematic seismic evaluation and rehabilitation of existing buildings. Figure 2.8 outlines their basic organization.

2.3 Previous Research, Further Reading, and Other Resources

Previous research exists involving the effect of diaphragm flexibility on overall building response, the behavior, design, and analysis of floor and roof diaphragms, and available techniques for seismic evaluation and rehabilitation. Those resources are now summarized and briefly discussed. Since part of this dissertation describes the shaking-table testing of masonry buildings, general information on shaking tables and previous shaking-table tests of masonry buildings is also provided.

2.3.1 Flexible Diaphragm Behavior and its Effect on Building Response

The consequence of roof and floor diaphragm flexibility on the seismic response of structures has been documented by several research efforts. Agbabian, Barnes and Kariotis present the results of a series of investigations examining the in-plane strength and stiffness of plywood roof diaphragms and their role in the response of low-rise buildings (ABK 1981 a,b,c).

Jain and Jennings (1984) develop rigorous mathematical descriptions for the response of low-rise buildings with flexible diaphragms. That work, however, considered only flexural deformations of the diaphragm. Results of the study are a series of transcendental formulae intended to describe dynamic response.

Funded by the National Science Foundation, the Technical Coordinating Committee for Masonry Research (TCCMAR) directed development of the ABK Lumped Parameter Model, LPM/I (Kariotis *et al.* 1988 a). Application of the model for the non-linear dynamic analysis of low-rise shear-wall buildings with lumber and wood-panel diaphragms is discussed in a companion study (Kariotis *et al.* 1988 b). The results of a six-year research program involving large-scale dynamic testing of wood diaphragms and masonry walls are presented by Kariotis (1995).

Tena-Colunga and Abrams (1995, 1996) compare measured responses of a brick masonry firehouse during the 1989 Loma Prieta earthquake to the responses calculated from lumped-parameter modeling. The studies conclude that the in-plane flexibility of diaphragms can significantly affect the seismic response of masonry structures.

Tremblay and Steimer (1995) discuss the results of an analytical study of low-rise framed buildings with flexible metal-deck diaphragms. The study found that existing design guidelines did not adequately calculate the fundamental period of the structure, maximum drifts, forces and deformations in the roof diaphragm, or ductility demands on the vertical lateral-force resisting system.

Fonseca *et al.* (1996) discusses the strength and deformation capacity of tilt-up structures with plywood roof diaphragms, and Porter *et al.* (1990) discusses the strength and stiffness of concrete plank flexible diaphragms.

Recently, the Mid-America Earthquake Center, based at the University of Illinois, has begun a large research effort that involves several studies of flexible-

diaphragm systems. More information is available at the Internet address <http://mae.ce.uiuc.edu/>.

2.3.2 Masonry Buildings and Assemblies

The TCCMAR effort dealt with the performance of masonry assemblies. Hamid *et al.* (1989) and Blondet *et al.* (1991) studied masonry walls loaded out-of-plane; Leiva *et al.* (1994) and Seible (1994) studied masonry walls loaded in-plane. Button and Mayes (1992) corroborate some of that work by developing analytical models representing walls loaded out-of-plane and comparing the result of that modeling with the observed TCCMAR results. Seible *et al.* (1994) pseudo-dynamically tested a full-scale five-story masonry structure to verify new TCCMAR design guidelines for reinforced masonry buildings in zones of high seismic risk.

A number of experimental studies have been performed involving reduced-scale and full-scale plain and reinforced masonry structures. Abrams and Paulson (1991) and Tomazevic and Weiss (1992) emphasize evaluation of mechanical properties of reduced-scale masonry materials; energy dissipation capacity of reinforced masonry assemblies; and seismic performance of plain and reinforced masonry buildings. These studies note the significant ductility exhibited by reinforced masonry assemblies constructed with proper detailing.

2.3.3 Wood Diaphragms

A significant amount of work has been published on the performance, analysis, and design of wood diaphragms. Peterson (1982) and Carney (1976) provide comprehensive bibliographies of that work. Some of the work specifically referenced for this study is now discussed.

During the 1950's, the Forest Products Laboratory of Madison, Wisconsin performed extensive testing of wood diaphragms: for example, Atherton and

Johnson 1952; Johnson 1952, 1954, 1955a, 1955b; and Stillinger *et al.* 1952, 1954. That work primarily involved the testing of full- and reduced-scale lumber-sheathed diaphragms, and provided force-deflection curves for various diaphragm configurations. The work also proposes preliminary techniques for the strengthening and stiffening of lumber diaphragms. English and Knowlton (1955) performed tests on an existing diagonally sheathed wall building, and provide interesting observations regarding the mechanisms of lumber diaphragm flexibility.

Medearis and Young (1964) provide an early discussion of hysteretic energy-absorptive capacity of plywood shear walls. They performed an experimental program involving the cyclic testing of plywood shear walls and used the results of that program to complement an analytical study. That study investigated the earthquake response of structures.

Foschi (1976) develops a nonlinear finite element for the analysis of wood diaphragms that models the nonlinear behavior of the connecting nails. Finite-element analyses using that element show good agreement with experimental results.

Soltis and Mtenga (1985) present a study involving the dynamic testing of nailed wood subassemblies. The parameters affecting the strength and stiffness of such assemblies, when subjected to dynamic loads, are also discussed.

The Applied Technology Council published document ATC-7, *Guidelines for the design of horizontal wood diaphragms*, in 1981. ATC-7 provides for the basic lateral design of horizontal wood diaphragms and also provides an extensive bibliography on the topic, including a catalog of wood diaphragm tests not listed in this dissertation. The document also notes gaps in the then-current state of the art, and subsequently proposes a series of research needs. Some of the noted research needs are to: develop simplified analytical models for the prediction of

diaphragm deflections; develop analytical models for various types of wall construction; perform dynamic diaphragm tests; and correlate observed responses with analytical studies. The work presented here addresses some of those needs.

The Western Woods Use Book (4th Edition, 1996) is an excellent source of general design information for wood assemblies.

2.3.4 Metal-Deck Diaphragms

Nilson (1960), in the earliest research in the United States on metal-deck diaphragms, performed an extensive experimental program of 46 racking tests on simple metal-deck diaphragms. The American Institute of Steel Construction outlines Nilson's testing procedure in the early design manual, *Design of Light Gage Steel Diaphragms* (1967). Nilson also developed the now-widely-used puddle (arc-spot) welding technique of connecting light-gage metal deck to steel framing members. He discusses various parameters affecting the performance of metal-deck diaphragms.

Many followed Nilson's work. Bryan and El-Dakhkhni (1968) present a rigorous approach to the prediction of diaphragm flexibility. Easley and McFarland (1969) use energy methods and large-deflection theory to develop buckling equations for fairly specific diaphragm configurations. Both efforts conclude that their results of their research correlated well with experiment. Nilson (1969) provides an interesting comparison of Easley's and McFarland's work with other relevant studies.

Ellifritt and Luttrell (1970) performed an extensive experimental program involving the testing of 160 diaphragms. That work develops a series of empirical formulas and design charts for strength and stiffness of metal-deck diaphragms. Following that work, many researchers revisited the challenge of analytically modeling metal-deck diaphragms.

Nilson and Anmar (1974) modeled metal deck diaphragms using a systematic but limited finite-element method with linear elastic orthotropic plate elements. That work correlated well with experiment, in the linear elastic range of response. Easley (1975), continuing his study of buckling, compared and evaluated existing metal-deck buckling solutions, simplified those solutions, and compared those simplifications with experimental results. He observed that the metal-deck panels exhibited significant post-buckling stiffness. Davies (1976) followed with a comprehensive finite-element method for the analysis of metal-deck diaphragms. Following that, Davies (1977) simplified his analysis methods and introduced a method of analyzing diaphragms using then-state-of-the-art frame-analysis software. Easley (1977) provided a contrasting theoretical development of metal-deck strength and stiffness based almost entirely on the force-deflection behavior of the diaphragm fasteners. Easley concluded that the results of the work correlate reasonably well with experimental results, in the working load range. Finally, Kinh *et al.* (1979) presented a simplified method, inspired by Easley's work, for the analysis of metal-deck diaphragms and corroborates that work with finite-element modeling and physical testing.

No work has addressed the performance of metal-deck diaphragms subjected to large reversed cyclic loads, however. Luttrell (1967) and Ellifritt and Luttrell (1970) briefly mention the effect of low-level cycling on a diaphragm's ultimate capacity. The complete hysteretic behavior of metal-deck diaphragms is thus not well understood or modeled.

The Steel Deck Institute *Diaphragm Design Manual* First Edition (1981) and Second Edition (1995) provide general design and analysis information for metal-deck diaphragms.

2.3.5 Shaking-Table Testing

Clark (1992) provides a comprehensive discussion of the characteristics of large multi-degree-of-freedom shaking tables.

A number of research programs involved the shaking-table testing of reduced-scale masonry structures. Manos *et al.* (1984) tested a single-story reduced-scale masonry house. Benedetti *et al.* (1998) tested 24, simple two-story reduced-scale plain masonry buildings. Abrams and Paulson (1991) tested two, three-story reduced-scale reinforced masonry buildings. Tomazevic and Weiss (1992) tested two, three-story reduced-scale plain and reinforced masonry buildings, and Costley and Abrams (1996a,b) tested a reduced-scale brick masonry building.

2.3.6 Publications for Evaluation and Rehabilitation of Existing Buildings

As discussed in Section 2.2.2, NEHRP publishes a series of documents for seismic evaluation and rehabilitation of existing structures, respectively FEMA 310 and 356. Another document, *Evaluation of Earthquake Damaged Concrete and Masonry Buildings* FEMA 306 (1999), provides guidance for the post-earthquake assessment of buildings. While that document does not explicitly consider the in-plane response of diaphragms or the associated out-of-plane response of connecting walls, it does note possible consequences of a diaphragm with inadequate strength, stiffness, or both.

FEMA 172 (1992), *NEHRP Handbook of Techniques for the Seismic Rehabilitation of Existing Buildings*, catalogs typical building deficiencies and discusses, in detail, suggested rehabilitation schemes. Applicable to this study, the document discusses the rehabilitation of wood diaphragms, metal-deck

diaphragms, and diaphragm-to-wall anchorage. The document also includes typical detail drawings and general commentary.

The US Army publishes the *Seismic Evaluation and Rehabilitation for Buildings* document TI 809-05 (1999). That document provides guidance for the systematic seismic evaluation and rehabilitation of structures. Some of the rehabilitation techniques presented there, however, are based on typical practice and engineering judgment, and have not been verified experimentally.

3.0 Shaking-Table Testing of Low-Rise Reinforced Masonry Buildings with Flexible Diaphragms

Two, half-scale low-rise reinforced masonry buildings with flexible diaphragms were tested on the United States Army Triaxial Earthquake and Shock Simulator (TESS) at CERL. The development and results of that testing program are discussed in detail by Cohen (2001) and Cohen *et al.* (2002a, 2003a, 200Xa); salient points and a brief summary are provided here. The compact disc included with this dissertation contains digital videos of the shaking-table tests, in *.avi format.

As discussed earlier, these shaking-table tests were intended first to verify widely held beliefs regarding the effect of diaphragm flexibility on the seismic response of these types of buildings, and second to provide experimental data for use in later phases of this study.

3.1 Specimen Development

This research was directed at the seismic vulnerability of United States Army structures designed and built before 1960 in the United States. For that reason, the prototype masonry structures were designed to be typical of that time period. The structures represent warehouse or storage facilities with large plan aspect ratios and openings on one long side. Such structures are common in the United States Army building inventory, and typically have flexible diaphragms of lumber sheathing, metal deck or precast concrete planks.

A survey of the existing United States Army building inventory provided typical construction details for these types of buildings. Based on that survey, two prototypical building specimens were configured (Figure 3.1), geometrically scaled by one half (Figure 3.2), and then constructed (Figure 3.3 and Figure 3.4).

Half-scale specimen walls used 4-in. CMU grouted vertically at 24 in. with one #3 reinforcing bar per grouted cell and grouted horizontally at bond beams with two #3 reinforcing bars per bond beam (Figure 3.2).

Also based on that survey, two diaphragms were configured. The first half-scale test specimen, Specimen #1, had a diagonally sheathed spruce-pine-fir (SPF) lumber diaphragm. The second half-scale test specimen, Specimen #2, had a metal-deck diaphragm on open-web joists (OWJ). Table 3-1 summarizes specimen designs, and Figure 3.3a and Figure 3.3b show typical diaphragm details for Specimens #1 and #2, respectively. Figure 3.4 shows an overall photo of Specimen #1.

Table 3-1 Diaphragm design of half-scale specimens

Specimen	Prototypical Element	Half-Scale Element
#1 (lumber)	SPF 1-1/2 in. x 11-1/2 in. joists	SPF 3/4 in. x 5-1/2 in. joists
	SPF 3/4 in. x 5-1/2 in. sheathing	SPF 3/8 in. x 3-1/4 in. sheathing
	8d or 10d nails	4d nails
#2 (metal deck)	12 to 24 in. deep OWJ	Vulcraft-8K1, 8 in. deep OWJ
	18 to 22 gauge, wide-rib decking	Vulcraft-1.5B22, wide-rib deck
	One to three #10 side-lap screws per span	One #10 side-lap screw per span
	36 / 3 to 36 / 4 puddle welding	36 / 3 puddle welding

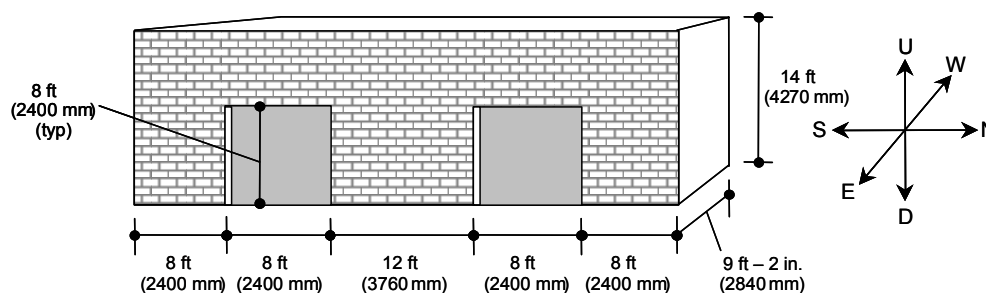


Figure 3.1 Schematic of full-scale prototype building

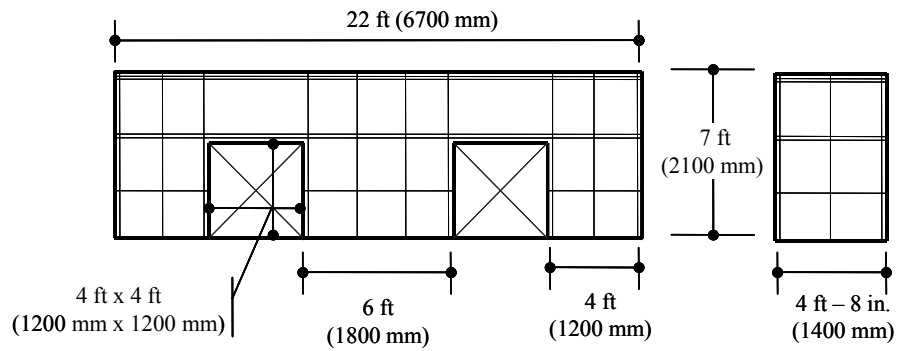
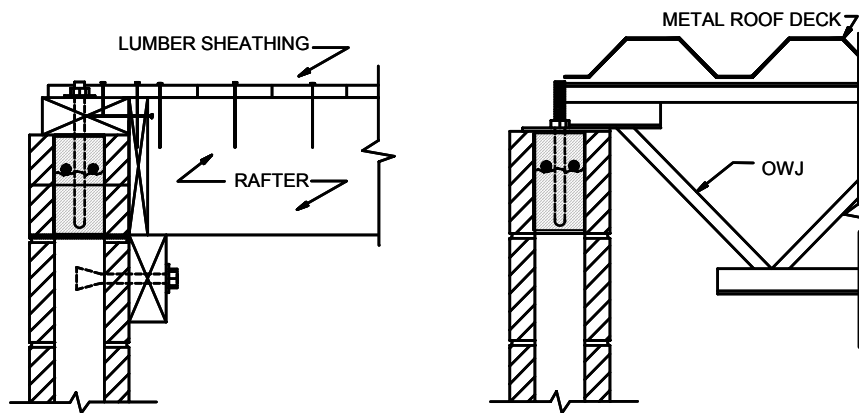


Figure 3.2 Schematic of half-scale specimen reinforcement for longitudinal and transverse walls



(a) Specimen #1

(b) Specimen #2

Figure 3.3 Typical details of rafter-to-wall connections for half-scale specimens



Figure 3.4 Overall photo of Specimen #1

3.1.1 Remarks on Scaling

To arrive at meaningful conclusions and recommendations regarding the behavior, analysis, and design of low-rise reinforced masonry buildings with flexible diaphragms, the implications of dimensional scaling need to be examined. Harris and Sabnis (1999) provide a comprehensive discussion of structural scaling. In this study, however, practical and technological constraints prevented complete dimensional similitude between the half-scale specimens and the full-scale prototype structures.

No supplementary mass was affixed to the half-scale specimens, because attaching supplementary mass in a manner that would permit complete, unrestrained, and compatible response between the specimens and masses was judged to be difficult, time-consuming, and probably not cost-effective. TESS can provide large input accelerations, however, permitting the specimens to be driven to levels of damage comparable to what they might sustain if fitted with supplementary masses.

Similitude between scaled and prototype material mechanical properties generally imposes severe theoretical and practical restrictions on the possible selection of specimen materials. At small scales, a lack of similitude can result in significant distortions between scale and prototype responses. This study scaled by one-half, however. In addition to this relatively large scaling factor, observed behavioral characteristics discussed here, such as the tendency of the diaphragm to respond independently of the transverse shear walls, were quite pronounced and would significantly change only at very small scaling factors.

Prior to considering similitude constraints for the time dimension, it was useful to determine the relationship between the natural frequencies of the half-scale specimens and those of their prototypes. If the natural frequencies are governed by shear deformations, then

$$\frac{\omega_{model}}{\omega_{prototype}} \propto \frac{\sqrt{\frac{K_m}{M_m}}}{\sqrt{\frac{K_p}{M_p}}} = \frac{\sqrt{\frac{G_m A_m / L_m}{M_m}}}{\sqrt{\frac{G_p A_p / L_p}{M_p}}} = \frac{\sqrt{\frac{G_p A_p \alpha^2 / L_p \alpha}{\rho_p L_p^3 \alpha^3}}}{\sqrt{\frac{G_p A_p / L_p}{\rho_p L_p^3}}} = \sqrt{\frac{1}{\alpha^2}} = \frac{1}{\alpha}, \quad \text{Equation 3-1}$$

where,

ω = frequency K = stiffness G = shear modulus α = scaling factor
 M = mass A = unit of area L = unit of length ρ = material density

The relationship of Equation 3-1 also holds if the natural frequencies are governed by flexural deformations.

True similitude between scale specimen and prototype building would have required scaling the time dimension of the ground motions by the square root of the geometric scaling factor. The relaxed similitude constraints discussed here (no supplementary masses, prototype materials, and neglecting gravitational response) were met by scaling the time dimension by the geometric scaling factor – in this case, one-half. This preserved the relationship between spectral peaks of the input records and the lower natural frequencies of the half-scale specimens, as illustrated in Figure 3.5, thus allowing the responses of the half-scale specimens to be consistently related to those of the prototypes.

Shaking-table testing used artificial ground motions developed by Wen and Wu (1999) for Carbondale, IL. The motions selected for transverse and longitudinal excitation were respectively, in the nomenclature of that study, C02_09s and C02_03s (prototype peak ground accelerations (PGA) of 0.67g and 0.55g, respectively). For the reasons discussed above, the input time steps of those motions were changed from 0.010 sec to 0.005 sec (Figure 3.5).

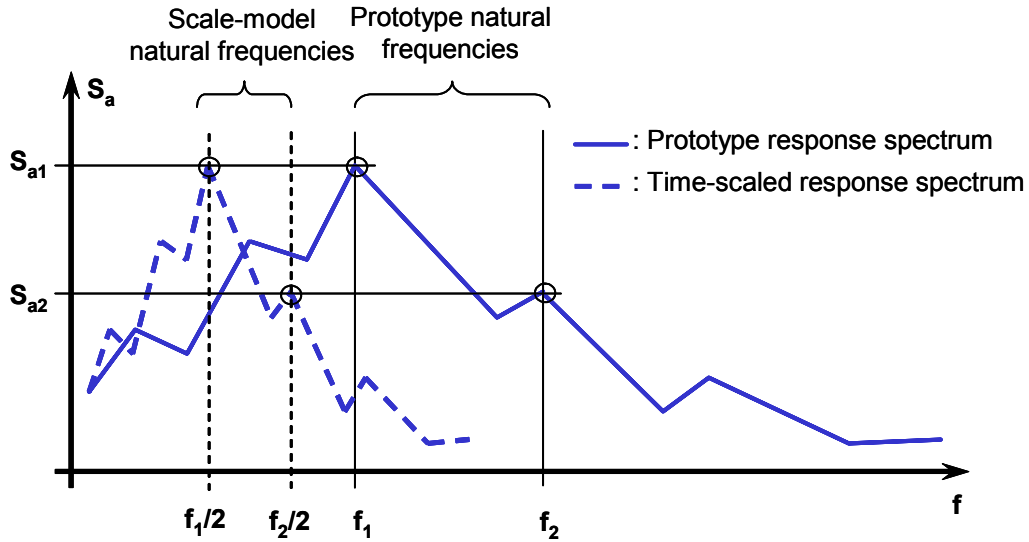


Figure 3.5 Schematic relationship between spectral peaks of input motion and natural frequencies of prototype buildings and scale-model specimens

The scaled input record had ordinates (acceleration values) identical to those of the prototype record. Thus,

$$\frac{S_{a_{model}}}{S_{a_{prototype}}} = 1, \quad \text{Equation 3-2}$$

The relationship between the pseudo-displacement S_d of the specimens and those of the prototypes is therefore,

$$\frac{S_{d_{model}}}{S_{d_{prototype}}} \propto \frac{\frac{S_{a_m}}{\omega_m^2}}{\frac{S_{a_p}}{\omega_p^2}} = \frac{\omega_p^2}{\omega_m^2} = \alpha^2, \quad \text{Equation 3-3}$$

Using dimensional analyses similar to Equation 3-1, Equation 3-2, and Equation 3-3 it can be shown (Cohen 2001) that the prototype structures would have sustained higher levels of damage than the half-scale specimens under the same levels of excitation. For example, for a given ground motion in the appropriate time scale, stresses in the prototype structures would have been twice as large as those in the half-scale specimens. The additional damage would have

likely manifested itself as additional cracking along yield lines, and increased damage to the diaphragms.

The relaxed similitude between scale and prototype mass and scale and prototype material mechanical properties did not adversely affect the results of the study. Indeed, careful scaling of the time dimension allowed responses of the half-scale specimens to be consistently related to those of the prototypes. Conclusions regarding the response of the half-scale specimens are therefore valid for the full-scale prototype structures.

3.2 Summary of Shaking-Table Testing

The half-scale specimens were initially subjected to low-level ($PGA < 0.1g$) dynamic tests intended to evaluate their natural periods and equivalent viscous damping ratios (Table 3-2). White-noise and sine-sweep, or resonant-search, excitations performed prior to seismic testing provided the natural periods of the specimens. Sine-decay testing, performed prior to seismic testing, provided equivalent viscous damping ratios of the half-scale specimens. White-noise tests, following each seismic test, were used to detect test-to-test changes in natural periods of the half-scale specimens.

Table 3-2 Dynamic properties of half-scale specimens before seismic testing

Specimen	Direction	Lowest Natural Period, <i>sec</i>	Equivalent Viscous Damping, %
#1 (lumber)	Transverse	0.071	3
	Longitudinal	0.050	7
	Vertical	0.026	3
#2 (metal deck)	Transverse	0.083	5
	Longitudinal	0.050	5
	Vertical	0.025	N/A (data lost)

3.2.1 Testing of Specimen #1 (Lumber Sheathing)

Specimen #1 was subjected to a sequence of 11 seismic tests of increasing levels of maximum input acceleration (PGA). The 11 input records were the modified Motions C02_09s and C02_03s, scaled to predetermined, and generally increasing, maximum input accelerations. From each uniaxial test to the next, the direction of excitation was alternated between longitudinal and transverse. This was done so that the structure would sustain similar deterioration in both principal plan directions as the test sequence progressed (Table 3-3).

Visible and audible damage to Specimen #1 first occurred during Test 5, at a maximum input acceleration of 0.67g, and increased with increasing maximum excitations. At maximum input accelerations greater than 1.00g (Tests 9, 10, and 11), cracking propagated throughout the structure along what became evident out-of-plane yield lines (Figure 3.6). Also, one of the transverse walls developed bed-joint cracks that were characteristic of wall rocking. Visible damage to the diaphragm finally occurred at a maximum input acceleration of 1.05g in the transverse direction (Test 9). Inspection revealed splitting at nailing points; the end of one piece of sheathing lumber pulled loose; and some sheathing split parallel to the grain. The diaphragm sustained no other visible damage.

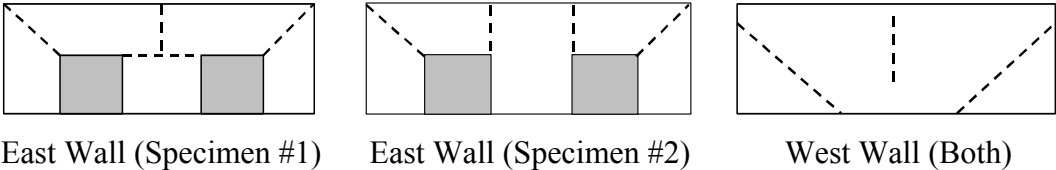


Figure 3.6 Observed yield lines in longitudinal walls

3.2.2 Testing of Specimen #2 (Metal Deck)

Specimen #2 was subjected to a sequence of 12 seismic tests at increasing levels of maximum input acceleration. Like those used for testing of Specimen #1, the 12 input records were the modified Motions C02_09s and C02_03s, scaled

to predetermined and generally increasing maximum input accelerations. In contrast to Specimen #1, the testing sequence was coordinated to minimize the possible influence of prior damage in each of the two principal plan directions of the structure. Several longitudinal tests of increasing levels of maximum input acceleration preceded high-level transverse testing (Table 3-4).

At a peak longitudinal input acceleration of 0.91g (Test 8a), visible and audible damage occurred when two puddle welds connecting the metal deck to the OWJ failed. At a maximum longitudinal input acceleration of 1.56g (Test 8b) diaphragm damage increased when an additional puddle weld fractured and a shear crack formed above the north opening in the perforated wall, though the longitudinal walls were otherwise undamaged. Damage spread quickly and extensively throughout the structure during strong transverse excitation. As with Specimen #1, cracking propagated through the walls along what became evident out-of-plane yield lines (Test 9, Figure 3.6). At a maximum input acceleration of 1.13g (Test 10) in the transverse direction, additional damage occurred to the diaphragm; side-lap screws at the north and south ends of the diaphragm pulled out.

Table 3-3 11 seismic test motions for Specimen #1 (L = Longitudinal, T = Transverse)

Test	Direction	Input PGA Demanded	Longitudinal PGA Provided, g	Transverse PGA Provided, g
1	T	0.15(C02_09s)	-	0.10
2	L	0.15(C02_03s)	0.10	-
3	T	0.75(C02_09s)	-	0.48
4	L	0.75(C02_03s)	0.41	-
5	T	1.00(C02_09s)	-	0.67
6	L	1.00(C02_03s)	0.55	-
7	L + T	0.50(C02_03s) + 0.50(C02_09s)	0.29	0.33
8	L + T	1.00(C02_03s) + 1.00(C02_09s)	0.57	0.67
9	T	1.50(C02_09s)	-	1.05
10	T	2.00(C02_09s)	-	1.49
11	L + T	2.00(C02_03s) + 2.00(C02_09s)	0.99	1.54

Table 3-4 12 seismic test motions for Specimen #2 (L = Longitudinal, T = Transverse)

Test	Direction	Input PGA Demanded	Longitudinal PGA Provided, g	Transverse PGA Provided, g
0	L	0.10(C02_03s)	0.03	-
1	L	0.30(C02_03s)	0.11	-
2	T	0.30(C02_09s)	-	0.16
3	L + T	0.21(C02_03s) + 0.30(C02_09s)	0.07	0.16
4	L	0.60(C02_03s)	0.23	-
5	T	0.60(C02_09s)	-	0.34
6	L + T	0.42(C02_03s) + 0.60(C02_09s)	0.15	0.35
7	L	1.50(C02_03s)	0.55	-
8a	L	2.25(C02_03s)	0.91	-
8b	L	4.00(C02_03s)	1.56	-
9	T	1.50(C02_03s)	-	0.86
10	T	2.00(C02_03s)	-	1.13

3.3 Summary of Results, Conclusions, and Significance of Testing

3.3.1 Summary of Results and Conclusions

Instrumentation of the half-scale specimens measured deformations, displacements, and accelerations. The data presented here are typical examples and were selected to convey a given concept. For instance, Figure 3.8 shows the deformed shape of the diaphragm of Specimen #1 during peak response, of only the ninth seismic test. Similar figures are not provided for the other 10 seismic tests, although identical conclusions could have been drawn from any of those. Detailed evaluations of the seismic test data as well as mechanical properties of the specimen masonry are reported in the references listed at the beginning of this chapter.

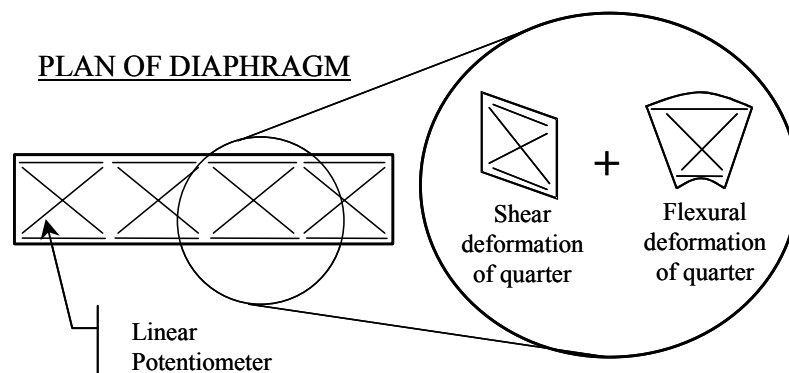


Figure 3.7 Characteristic deformations of instrumented diaphragm quarters

The approximate deformed shape of the diaphragms at any time during a test could be determined by analyzing the diaphragm response data as illustrated in Figure 3.7. Figure 3.8 shows an example of this with the approximate shape of the diaphragms of Specimen #1 and #2, during peak response of the ninth seismic test of each specimen. The figure shows, as expected, that shearing deformations dominated the overall in-plane response of the diaphragms.

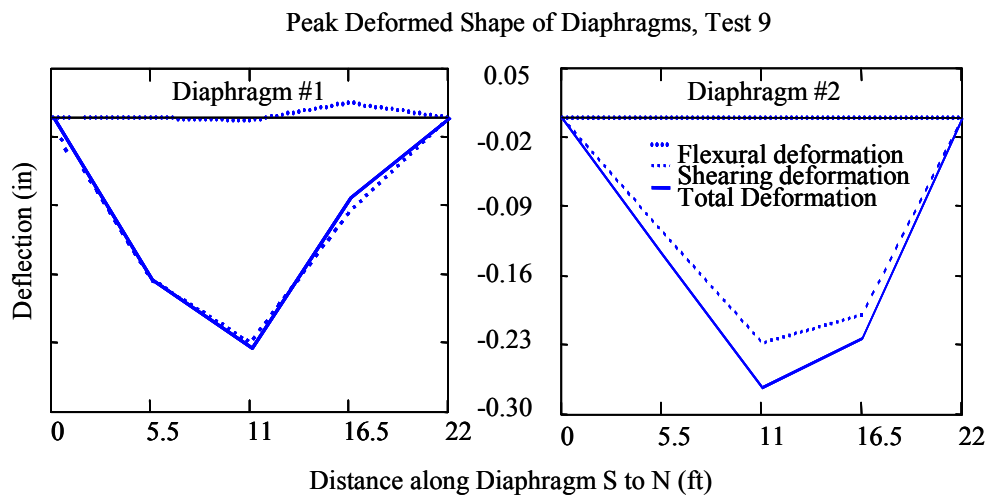


Figure 3.8 Deformed shape of diaphragms during peak response of Test 9

Analytical studies, discussed in the references listed at the beginning of this chapter, calculated a fundamental mode of response controlled by the in-phase in-plane single-curvature response of the diaphragm and the transverse shear walls. Figure 3.8 corroborates this and shows that the diaphragms of both specimens responded in-plane and approximately in single curvature. That figure shows, for Specimen #1, a small positive flexural deformation. This is due to experimental error, contribution of higher dynamic modes to seismic response, or both.

Figure 3.9 shows that the plan center of the diaphragm of Specimen #1 and the tops of the transverse shear walls responded primarily in phase during transverse response. That observation implies that the transverse response of the diaphragm was dominated by the fundamental mode of the specimen. The arrows in Figure 3.10, however, mark several typical regions of amplitude cancellation (“beating”) in the acceleration response of Specimen #1, during Test 5. Figure 3.10 therefore suggests that a higher mode participated in the acceleration response of the specimen at a detectable, but small, level. Specimen #2 exhibited similar behavior as that shown in Figure 3.9 and Figure 3.10.

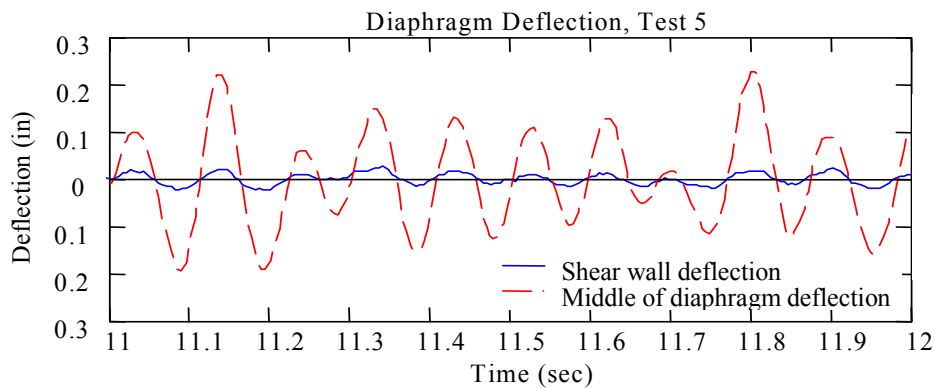


Figure 3.9 Transverse displacements of center of diaphragm and tops of transverse shear walls as measured relative to base of specimen (Test 5, Specimen #1)

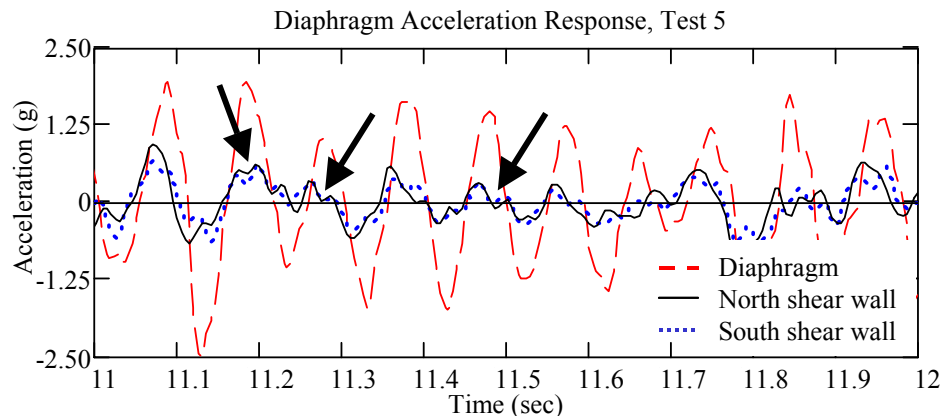


Figure 3.10 Transverse accelerations of center of diaphragm and tops of transverse shear walls (Test 5, Specimen #1)

The transverse shear walls of the specimens remained elastic during low levels of excitation, with no visible cracking or permanent deformation. This observation is substantiated by the fact that even at high input accelerations, wall drift ratios are less than 0.1%. During very strong seismic tests ($PGA > 0.67g$), however, a continuous bed-joint crack developed along the entire plan length of the south shear wall in Specimen #1. This crack was characteristic of rigid-body rotation of the shear wall about that crack (wall rocking). Shear walls of Specimen #2 remained elastic throughout the seismic testing.

Table 3-5 and Table 3-6 summarize the general relationships between level of excitation (PGA), measured response (DDR), and observed damage states for different elements of the shaking-table specimens.

Table 3-5 Observed diaphragm drift ratio and relationship to damage (Specimen #1)

Element	Test	PGA, <i>g</i>	DDR, %	Damage
Longitudinal Walls	5	0.67	0.2	Hair-line cracking of out-of-plane walls
Longitudinal Walls	9	1.05	0.35	Extensive cracking of out-of-plane walls, distinct cracking patterns emerge, yield lines begin to emerge
Longitudinal Walls	10	1.49	0.7	Extensive cracking, hinging about distinct out-of-plane yield lines, slight spalling at crack edges
Diaphragm	10	1.49	0.7	Splitting of sheathing at nailing points, nail withdrawal

Table 3-6 Observed diaphragm drift ratio and relationship to damage (Specimen #2)

Element	Test	PGA, <i>g</i>	DDR, %	Damage
Longitudinal Walls	5	0.34	0.09	Hair-line cracking of out-of-plane walls
Longitudinal Walls	9	0.86	0.40	Extensive cracking of out-of-plane walls, distinct cracking patterns emerge, yield lines begin to emerge
Longitudinal Walls	10	1.13	1.00	Extensive cracking, hinging about distinct out-of-plane yield lines, slight spalling at crack edges
Diaphragm	10	1.13	1.00	Side-lap screw withdrawal and bearing failure

3.3.2 Significance of Shaking-Table Testing

These tests provided important insights and data regarding the seismic response of low-rise reinforced masonry buildings with flexible diaphragms. The tests demonstrated and validated the widely held belief that diaphragm flexibility may significantly affect the seismic response of these types of buildings.

Specifically, these types of buildings rarely behave as single-degree-of-freedom systems, governed by the in-plane response of the shear walls. Rather, they essentially behave as single-degree-of-freedom systems, governed by the in-plane response of the diaphragm.

Evaluation of the test data from the shaking-table tests suggested that an analysis tool specifically developed for these types of buildings is needed; indeed one that explicitly accounts for diaphragm flexibility and accurately describes the seismic response, and hence performance, of the building. Such a tool is developed in this dissertation. First, in Chapter 4, data and conclusions from the shaking-table tests are enhanced with the quasi-static testing of the same diaphragms attached to the half-scale specimens. In Chapter 5, based on observations from shaking-table testing, an analytical tool is developed for the accurate analysis of these types of buildings. The tool is verified in the linear and nonlinear range of response and then applied to seismic evaluation and rehabilitation methodologies in Chapters 6 and 7, respectively. Finally, it is applied to four real structures in Chapter 8 and ultimately shown to be effective, simple, and accurate.

4.0 Quasi-Static Testing of Flexible Diaphragms

Following shaking-table testing, diaphragms and top four courses of attached masonry walls were removed from the half-scale specimens and tested quasi-statically in their own plane. The diaphragm-masonry chord assembly from Specimen #1 is called Diaphragm #1; the diaphragm-masonry chord assembly from Specimen #2 is called Diaphragm #2. Visibly damaged components of the diaphragms were removed, replicated, and replaced in their original configuration. Five pieces of visibly damaged sheathing lumber were replaced in Diaphragm #1 and the metal deck was replaced and re-welded in Diaphragm #2 (Figure 4.1). The compact disc included with this dissertation contains time-lapse digital videos of the quasi-static testing of Diaphragm #1, in *.mp2 format.

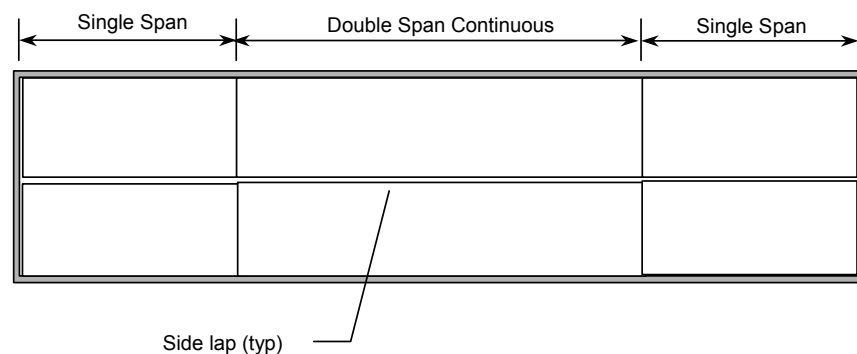


Figure 4.1 Plan layout of metal-deck panels in Diaphragm #2

4.1 Test Setups

During quasi-static testing, the diaphragms were tested in a horizontal orientation, supported by a steel test frame that was bolted to the CERL strong floor. Four, 12 in. built-up box columns supported the diaphragms at their corners

(Figure 4.2 and Figure 4.6) and structural channels supported the diaphragms at their third points. Greased tetrafluoroethylene (Teflon®) pads were placed between the supporting channels and their contact points with the diaphragm assembly to reduce frictional forces at those points (Figure 4.3).



Figure 4.2 Box columns support south end of Diaphragm #1



Figure 4.3 Low-friction bearing assembly between diaphragm and test frame

The diaphragms were loaded at their two outer quarter points using two 50-kip actuators, each with a maximum stroke of ± 3.0 in. The actuators maintained equal displacements throughout the testing. Thus, the outer quarters of the diaphragm had uniform in-plane shear along their lengths, and the middle two quarters had uniform in-plane bending moment and approximately zero in-plane shear.

During seismic excitation, the diaphragm of a low-rise masonry structure is loaded in-plane by the response of the diaphragm itself; by the supporting masonry shear walls oriented in the direction of excitation; and by the supporting masonry shear walls oriented perpendicular to the direction of excitation. To emulate this, two loading struts made of structural tubing connected the east and west masonry chords at the points of load application (Figure 4.4). The loading struts distributed the applied load between the two longitudinal masonry chords.



Figure 4.4 View beneath Diaphragm #1 showing load strut connecting east and west masonry chords at load points (similar for Diaphragm #2)

The diaphragms were subjected to twisting moments about their longitudinal axes as a result of vertical eccentricity between the shear centers of the diaphragms and the lines of action of the loading rams (Figure 4.5). For that reason, the testing frame used for each diaphragm restrained them from rotating out of plane. Each specific test setup is now discussed.

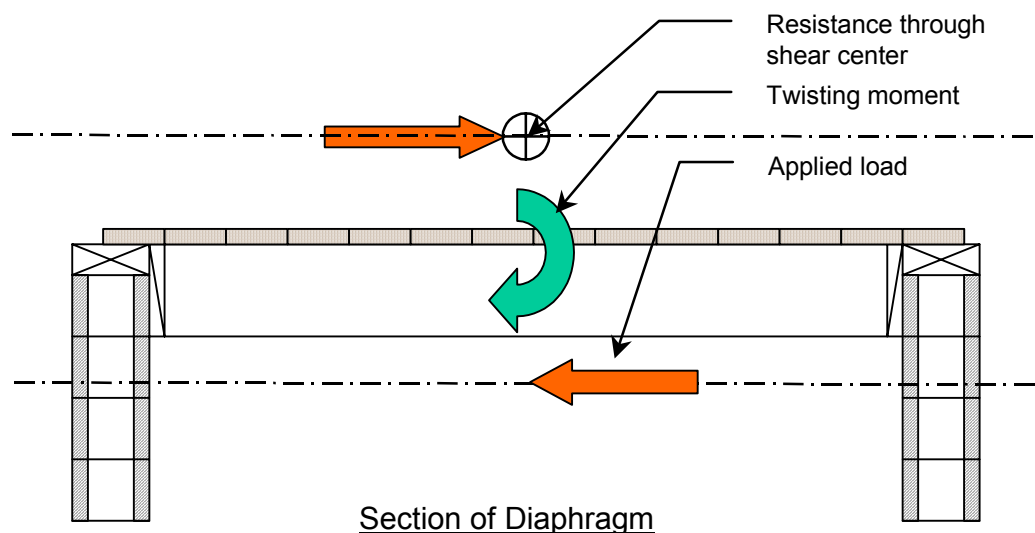


Figure 4.5 Probable vertical eccentricity between shear center of diaphragm and line of action of loading system

4.1.1 Diaphragm #1 (Lumber Sheathing)

Four structural channels supported Diaphragm #1 at its third points during quasi-static testing (Figure 4.6 through Figure 4.8). Two channels supported the masonry chords of the diaphragm (bond beam and three underlying courses) from below, and two channels supported the top of the diaphragm from above. These restrained the diaphragm from twisting about its longitudinal axis.

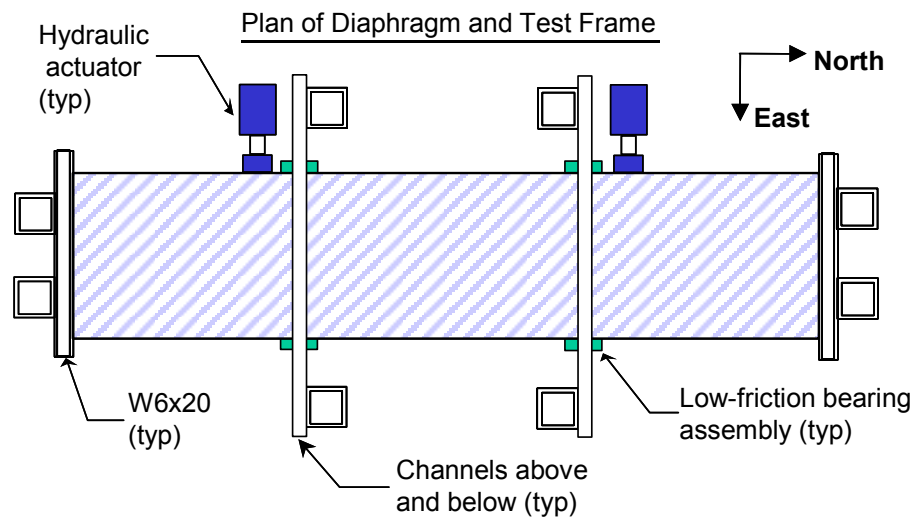


Figure 4.6 Plan of test setup for Diaphragm #1

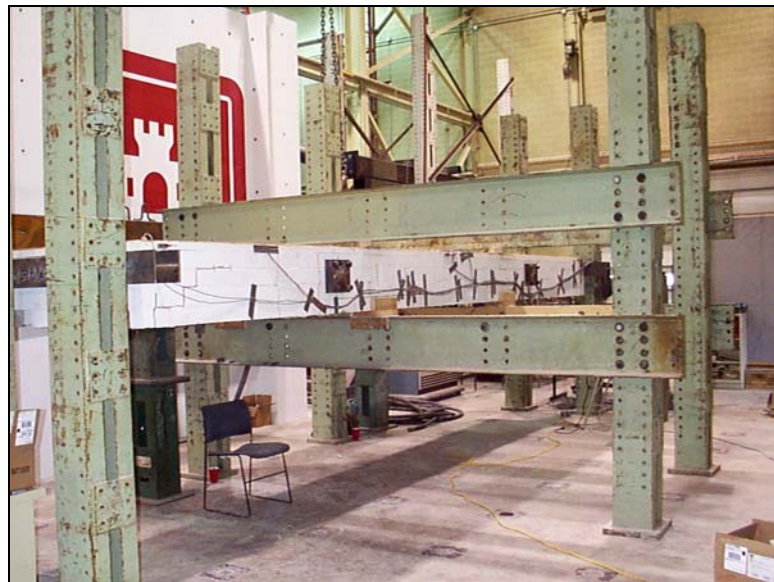


Figure 4.7 Photograph of test setup for Diaphragm #1 (east is to the right)

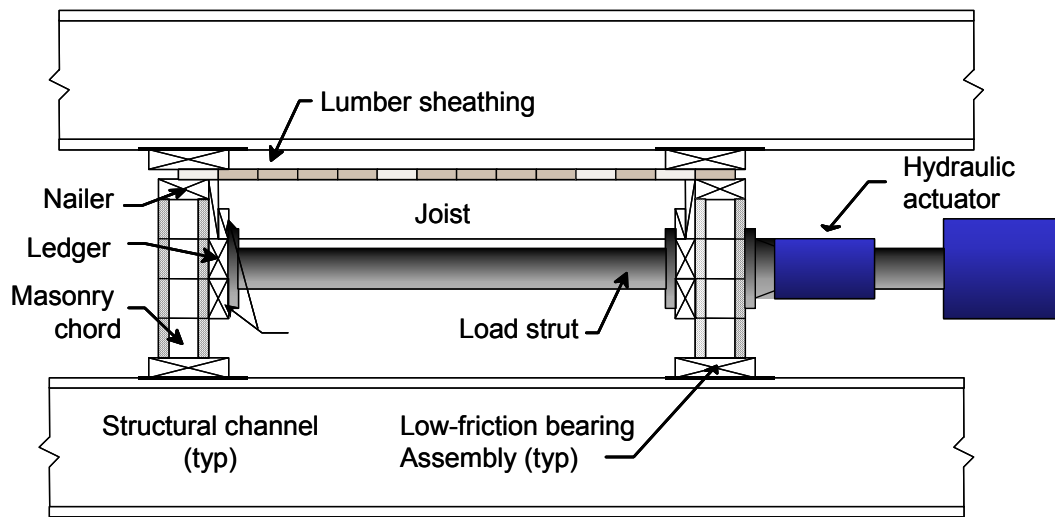


Figure 4.8 Typical cross-section of test setup near loading points (Diaphragm #1)

4.1.2 Diaphragm #2 (Metal Deck)

Two structural channels and four L-shaped structural members supported Diaphragm #2 at its third points during quasi-static testing (Figure 4.9 and Figure 4.10). Two channels supported the masonry chords of the diaphragm (bond beam and three underlying courses) from below, and four L-shaped members (two on each chord) extended from the connection between the load strut and the masonry wall, below the supporting channels, and rested on low-friction bearings attached to those channels (Figure 4.11). These restrained the diaphragm from twisting about its longitudinal axis.

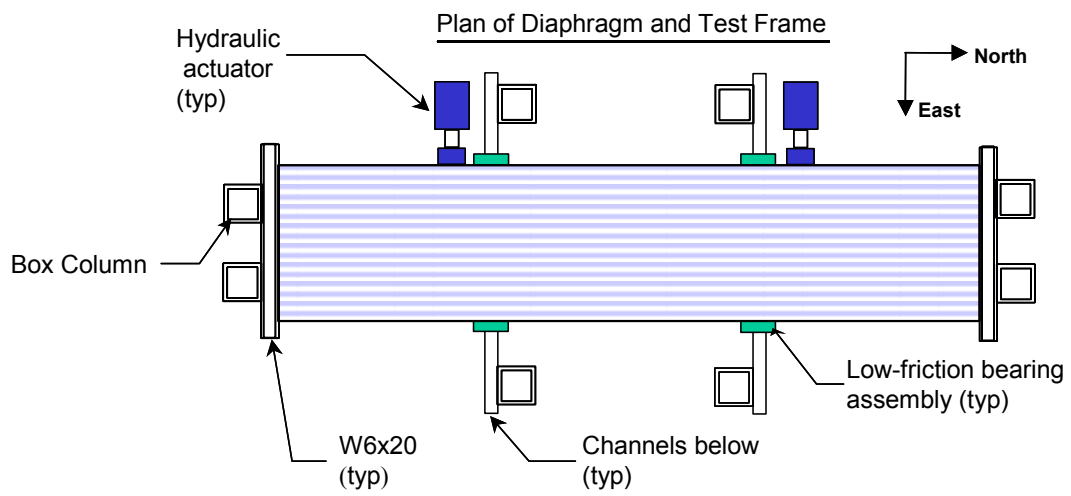


Figure 4.9 Plan drawing of test setup (Diaphragm #2)



Figure 4.10 Plan photograph of test setup (Diaphragm #2, east is to the left)



Figure 4.11 View beneath Diaphragm #2 at south channel showing L-shaped restraining members

4.2 Instrumentation of Test Specimens

The instrumentation scheme for these tests captured deflection and deformation characteristics of the diaphragms, and was similar to that used during previous shaking-table tests of the same diaphragms. Instrumentation common to both Diaphragm #1 and Diaphragm #2 measured:

- transverse in-plane deflection of the diaphragm, relative to a fixed reference independent of the test frame;
- relative torsional deflections of corner box columns;
- in-plane flexural and shearing deformations of the diaphragm;
- axial forces in load struts; and
- forces in actuators.

Instrumentation specific to Diaphragm #1 measured:

- relative slip between masonry chords and nailers;
- in-plane strains in the diaphragm sheathing perpendicular to a transverse cross-section in the south diaphragm panel;
- strains along major axes of selected joists; and
- strains along major axes of selected blocking members.

Instrumentation specific to Diaphragm #2 measured:

- relative side-lap slip between adjacent deck panels;
- relative end-lap slip at puddle welds; and
- yielding of metal deck around welds by coating an area, of about four square inches, around each weld with a thin mixture of Hydrostone® and water.

The load struts were calibrated at the Newmark Structural Engineering Laboratory of the University of Illinois at Champaign. Appendix A illustrates specific instrumentation schemes for Diaphragm #1 and Diaphragm #2.

4.3 Quasi-Static Testing Protocol

The two diaphragm assemblies were tested using an established protocol developed by Krawinkler *et al.* (2000) as part of the Consortium of Universities for Research in Earthquake Engineering (CUREE) and the California Institute of Technology. The protocol dictated that displacement (or load) histories comprise a sequence of large cycles to monotonically increasing maximum displacement (or load), each followed by several smaller-amplitude cycles (Figure 4.12). For example, a large cycle of ± 1.0 in. may be followed by three smaller cycles of ± 0.75 in.; those smaller cycles are then followed by a large cycle of ± 1.5 in.; and so on. The protocol also provided other information, such as suggested ratios

between major and subsequent minor cycles, and suggested numbers of subsequent minor cycles.

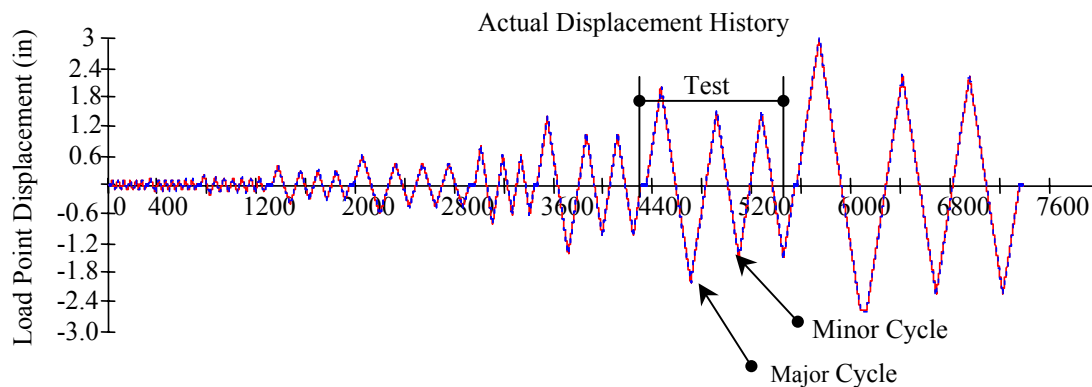


Figure 4.12 Actual displacement history of actuators for Diaphragm #2 (Diaphragm #1 similar)

In this study, large cycles are referred to as Major Cycles and the subsequent smaller cycles are referred to as Minor Cycles. Each Major Cycle and its associated suite of Minor Cycles are collectively referred to as a Test (Figure 4.12). For example, Test #6 of Diaphragm #1 comprised Major Cycle #6 and Minor Cycles #24 and #25. Table 4-1 and Table 4-2 summarize the displacement histories for Diaphragm #1 and #2.

Diaphragm #1 was initially displaced at a rate of about 0.008 in./sec. After Test #7 the displacement rate was increased to about 0.016 in./sec.

Diaphragm #2 was initially displaced at a rate of about 0.008 in./sec. The displacement rate was increased to about 0.016 in./sec after Test #7, and then increased again to 0.033 in./sec after Test #8.

Table 4-1 Peak displacements of actuators in loading history (Diaphragm #1)

Test Number	Major Cycle Index	Major Cycle Displacement	Minor Cycle Index	Minor Cycle Displacement	Diaphragm Drift Ratio, %
1	1	± 0.10 in.			0.08
			1 - 5	5 @ ± 0.10 in.	0.08
2	2	± 0.15 in.			0.11
			6 - 11	6 @ ± 0.10 in.	0.08
3	3	± 0.20 in.			0.15
			12 - 17	6 @ ± 0.15 in.	0.11
4	4	± 0.40 in.			0.30
			18 - 20	3 @ ± 0.30 in.	0.23
5	5	± 0.60 in.			0.45
			21 - 23	3 @ ± 0.45 in.	0.34
6	6	± 0.80 in.			0.61
			24 - 25	2 @ ± 0.60 in.	0.45
7	7	± 1.40 in.			1.11
			26 - 27	2 @ ± 1.00 in.	0.76
8	8	± 2.0 in.			1.52
			28 - 29	2 @ ± 1.50 in.	1.14
9	9	± 3.0 in.			2.27
			30 - 31	2 @ ± 2.25 in.	1.70

Table 4-2 Peak displacements of actuators in loading history (Diaphragm #2)

Test Number	Major Cycle Index	Major Cycle Displacement	Minor Cycle Index	Minor Cycle Displacement	Diaphragm Drift Ratio, %
1	1	± 0.10 in.			0.08
			1 - 6	6 @ ± 0.10 in.	0.08
2	2	± 0.15 in.			0.11
			7 - 12	6 @ ± 0.10 in.	0.08
3	3	± 0.20 in.			0.15
			13 - 18	6 @ ± 0.15 in.	0.11
4	4	± 0.40 in.			0.30
			19 - 21	3 @ ± 0.30 in.	0.23
5	5	± 0.60 in.			0.45
			22 - 24	3 @ ± 0.45 in.	0.34
6	6	± 0.80 in.			0.61
			25 - 26	2 @ ± 0.60 in.	0.45
7	7	± 1.40 in.			1.11
			27 - 28	2 @ ± 1.00 in.	0.76
8	8	± 2.0 in.			1.52
			29 - 30	2 @ ± 1.50 in.	1.14
9	9	± 3.0 in.			2.27
			31 - 32	2 @ ± 2.25 in.	1.70

4.4 Observations During Testing of Diaphragm #1 (Lumber Sheathing)

4.4.1 Observed Damage at Low Diaphragm Drift Ratios (Tests #1 - #5)

Examples of the observed damage are shown in Figure 4.14 through Figure 4.17; Figure 4.13 describes their approximate locations.

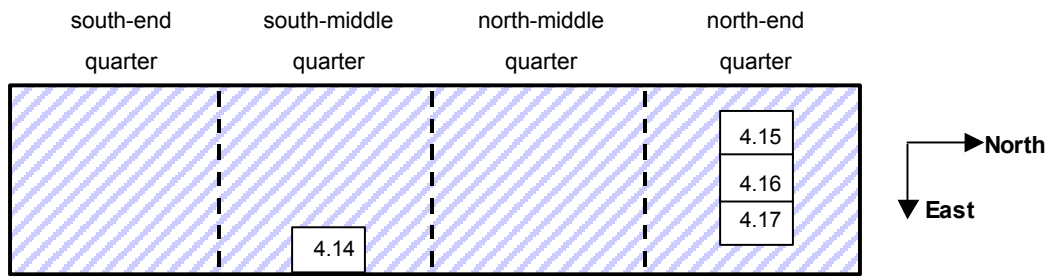


Figure 4.13 Approximate locations of damage at low diaphragm drift ratios; numbers in boxes are figure numbers

Diaphragm #1 sustained visible damage at a DDR of 0.3 % (load-point deflection of 0.4 in.). It occurred in the form of longitudinal splitting at nail holes (Figure 4.14) and visible spreading of butt splices in tension (Figure 4.15). At a DDR of 0.6 % (load-point deflection of 0.8 in.), Diaphragm #1 sustained further longitudinal splitting at nailing points (Figure 4.16) as well as nail withdrawal and nail tear-out at board ends (Figure 4.17).



Figure 4.14 Longitudinal splitting at point of nailing (DDR = 0.3 %, east side of south quarter)



Figure 4.15 Spreading of butt splices under tension (DDR = 0.3 %)



Figure 4.16 Longitudinal splitting of sheathing board at point of nailing and spreading of butt splices (DDR = 0.6 %)



Figure 4.17 Nail withdrawal and tear-out at board end (DDR = 0.6 %)

4.4.2 Observed Damage at High Diaphragm Drift Ratios (Tests #6-#9)

Examples of damage at high diaphragm drift ratios are shown in Figure 4.19 through Figure 4.28; Figure 4.18 describes their approximate locations.

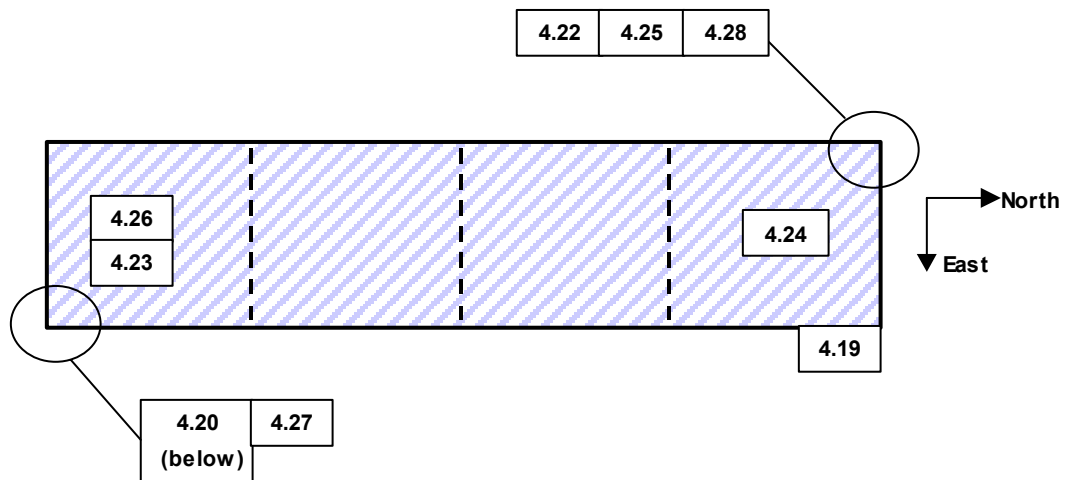


Figure 4.18 Approximate location of damage at high diaphragm drift ratios; numbers in boxes are figure numbers

Damage increased with increasing diaphragm drift ratios. At a DDR of 1.1 % (load-point deflection of 1.4 in.) the masonry chords exhibited out-of-plane sliding-shear failure along pre-existing cracks from the earlier shaking-table tests (Figure 4.19). That behavior was primarily an artifact of the test set-up, and did not indicate additional diaphragm damage. That is, the sliding-shear failure may not have occurred in a different test setup; for example, if the diaphragm had been left attached to the half-scale masonry building and then quasi-statically tested. Also at a DDR of 1.1 %, some nails connecting blockings and nailers partially withdrew in the corners of the diaphragm (Figure 4.20), presumably because in-plane forces from the sheathing caused bending deflections in the nailer perpendicular to the longitudinal walls. Figure 4.21 illustrates this process and Figure 4.22 shows an example of its occurrence during testing.



Figure 4.19 Sliding-shear failure during displacement to the west along pre-existing cracks in masonry chords (DDR = 1.1 %, northeast corner)

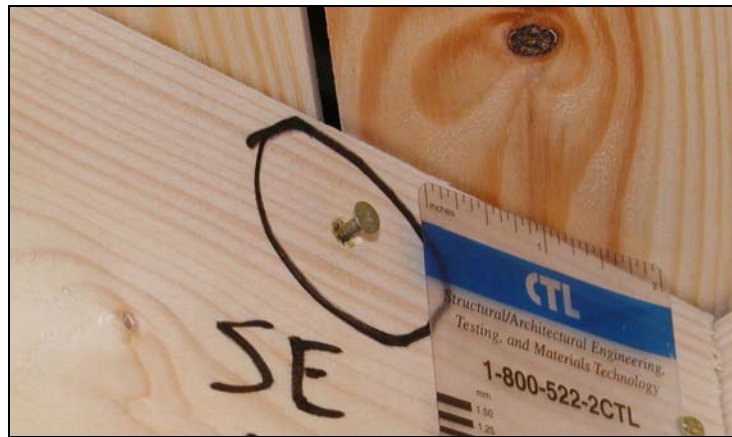


Figure 4.20 Withdrawal of nail connecting blocking and nailer member, at diaphragm corner (DDR = 1.1 %, southeast corner)

Diaphragm #1 sustained significant damage at a DDR of 1.5 % (load-point deflection of 2.0 in.): several joists split at nailing points due to transverse nail forces (Figure 4.23); tension butt splices spread significantly; several nails withdrew from connecting joists; several nails tore through the ends of sheathing boards (Figure 4.24); and several sheathing boards sustained additional longitudinal splitting at points of nailing (Figure 4.25).

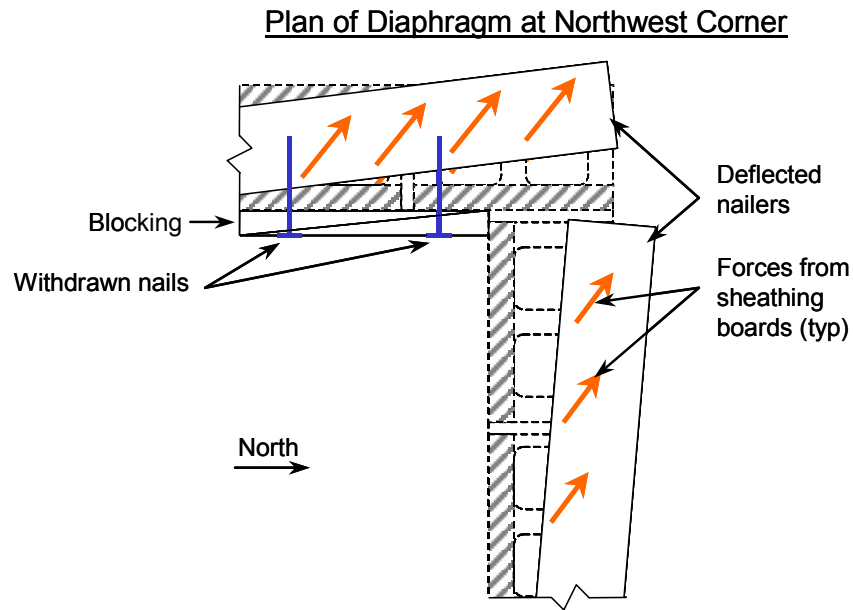


Figure 4.21 Process causing withdrawal of nails connecting blocking and nailer; shown at northwest corner of diaphragm during displacement to the west



Figure 4.22 Severe damage to diaphragm, due to mechanism described in Figure 4.21 (DDR = 2.3 %, northwest corner)



Figure 4.23 Joist splitting at point of nailing (DDR = 1.5 %)



Figure 4.24 Butt-splice spreading, nail withdrawal and nail tear-out at sheathing board end (DDR = 1.5 %)



Figure 4.25 Longitudinal splitting of sheathing board at point of nailing (DDR = 1.5 %)

At the maximum DDR reached during the test (2.3 %), Diaphragm #1 sustained considerable damage: extensive nail withdrawals and nail tear-outs (Figure 4.26); extensive deterioration of masonry chords (Figure 4.27); and extensive splitting of sheathing at nailing points (Figure 4.28). The most severe local damage occurred at the northwest corner of the diaphragm (Figure 4.22).

Nearly all damage sustained by the diaphragm occurred in its two outer quarters, which were loaded in uniform shear. It has been shown in this dissertation and elsewhere (Cohen 2001, Cohen *et al.* 2002a,c) that the prototype diaphragms represented by Diaphragm #1 deform predominantly in shear. Therefore, in-plane deflections of the diaphragm should result almost entirely from shearing deformations of the north-end and south-end quarters, and those two quarters should sustain much more damage than the inner two quarters under transverse loading. The observed damage is consistent with this hypothesis.



Figure 4.26 Nail withdrawal at maximum diaphragm drift ratio (DDR = 2.3 %)



Figure 4.27 Deterioration of masonry chord at maximum diaphragm drift ratio (DDR = 2.3 %, southeast corner)



Figure 4.28 Longitudinal splitting of sheathing board at point of nailing at maximum diaphragm drift ratio (DDR = 2.3 %, northwest corner)

4.4.3 Observations of Local Damage After Quasi-Static Testing

When a diagonally sheathed lumber diaphragm is subjected to reversed cycles of in-plane loading, some damage occurs as bearing failure of the wood matrix at nail holes and plastic deformation of the nails themselves. To examine this in more detail, those sheathing boards to which strain gauges had been attached were removed after the quasi-static testing, and their nails and nail holes were closely examined (Figure 4.29). That examination revealed bearing deformation (ovalling) at nail holes and plastic bending deformation of the nails themselves (Figure 4.30). Transverse bending tests were conducted on those same sheathing boards to determine basic material properties for subsequent data evaluation.



Figure 4.29 Strain-gauged sheathing boards removed and examined after testing



Figure 4.30 Typical deformation of nail and wood at nail hole

4.5 Observations During Testing of Diaphragm #2 (Metal Deck)

Diaphragm #2 sustained damage as a result of the quasi-static testing. Damage to metal-deck diaphragms generally manifests itself as failed deck-to-joist and deck-to-deck connections. In the former case, those connections are puddle welds (arc-spot welds) and the modes of failure are typically tear-out of welds from metal decking or cleavage fracture of welds at deck-to-joist interfaces. In the latter case, those connections are self-drilling sheet-metal screws and the modes of failure are typically bearing into the metal deck and withdrawal from the metal-deck. In the following discussion, locations of damage are described using the schematics of Figure 4.31.

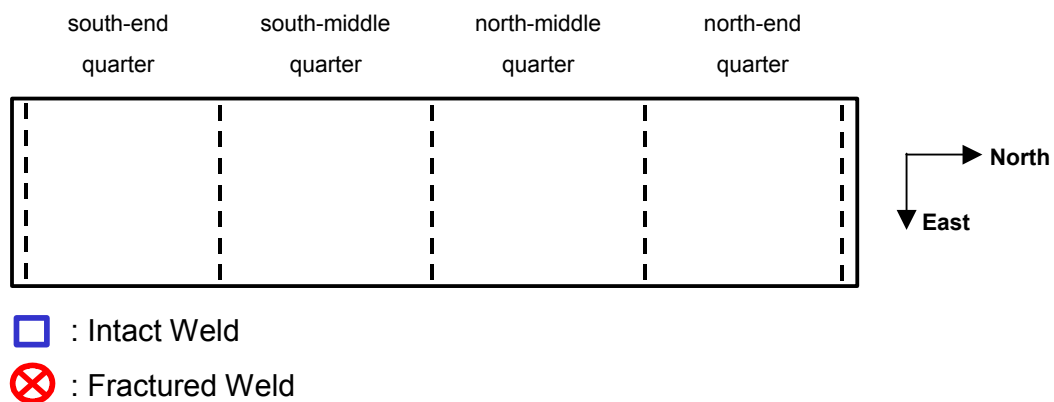


Figure 4.31 Reference locations and weld-condition symbols for Diaphragm #2

4.5.1 Observed Damage at Low Diaphragm Drift Ratios (Tests #1 - #5)

Diaphragm #2 sustained no visible damage at diaphragm drift ratios less than 0.45 % (load-point deflection of 0.6 in.). At a DDR of 0.45 %, many of the Hydrostone® weld coatings in the south-end quarter and north-end quarter flaked slightly, suggesting local yielding of the metal deck around the welds.

4.5.2 Observed Damage at High Diaphragm Drift Ratios (Tests #6-#9)

Damage increased with increasing diaphragm drift ratios. At a DDR of 0.61 % (load-point deflection of 0.8 in.) decking panels in the south-end quarter and north-end quarter buckled out of plane (Figure 4.32) and weld WMS1 failed. (Weld locations and nomenclature are discussed in Appendix A. WMS1, for example, indicates *Weld Middle South number 1*). Decking panels in the outer two quarters of the diaphragm consistently buckled out of plane at diaphragm drift ratios greater than about 0.6 %. Such buckling does not indicate failure, however, provided that sufficient connectivity is maintained between the deck panels and supporting perimeter framing to mobilize tension fields in each diagonal direction. As will be discussed, eventual failure of the panel welds at higher diaphragm drift ratios ultimately destroyed the tension fields and precluded further panel buckling.

At a DDR of 1.11 % (load-point deflection of 1.4 in.) the Hydrostone® coating flaked off most of the welds in the diaphragm's outer two quarters (Figure 4.33), suggesting yielding of the metal deck around the welds, and welds WMS2, WES3 and WES4 failed (Figure 4.36). Also, side-lap screws in the north-end quarter and south-end quarter exhibited visible bearing deformation into the metal deck (Figure 4.34).

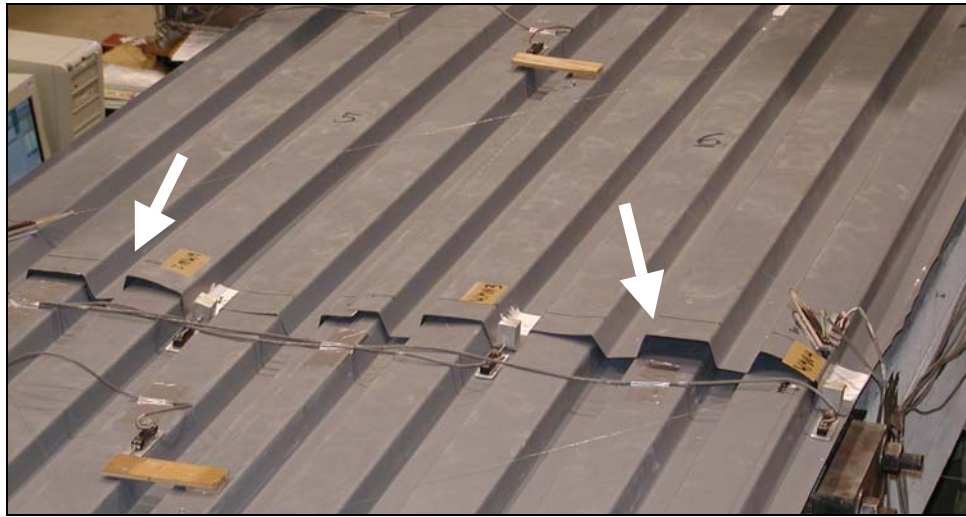


Figure 4.32 Example of out-of-plane buckling in north-end quarter panel at high diaphragm drift ratios



Figure 4.33 Flaking of Hydrostone® weld coating

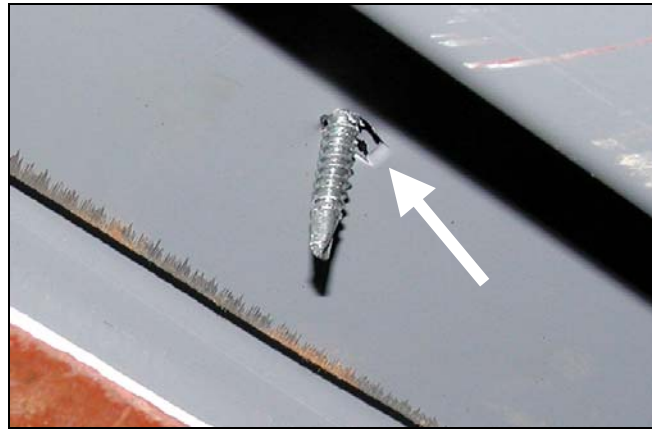


Figure 4.34 Bearing deformation at side-lap screw

At a DDR of 1.52 % (load-point deflection of 2.0 in.) the remainder of the welds (WES1 and WES2) connecting the metal deck to the southernmost joist failed and weld WMN3 in the north-end quarter failed (Figure 4.37). At this point in the testing, the south-end quarter retained only two intact welds out of an original eight and its metal-deck panels no longer significantly contributed to the shear strength or stiffness of the diaphragm.

Welds WMN3, WMN4 and WEN2 in the north-end quarter failed at the maximum DDR achieved during the test, 2.27 % (load-point deflection of 3.0 in.). At this point in the testing, the north-end quarter retained only four intact welds out of an original eight and its metal deck panels no longer significantly contributed to the strength or stiffness of the diaphragm.

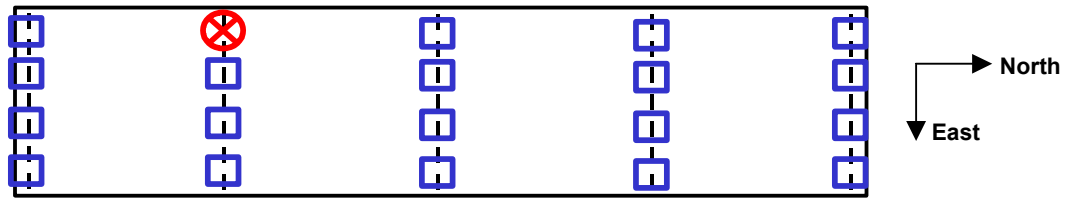


Figure 4.35 Locations of failed puddle welds after Test #6 (DDR = 0.61 %)

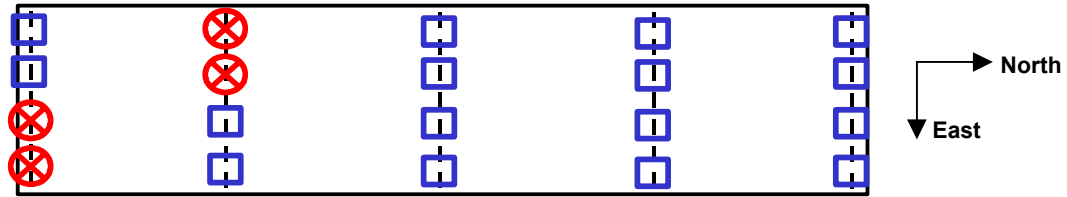


Figure 4.36 Locations of failed puddle welds after Test #7 (DDR = 1.11 %)

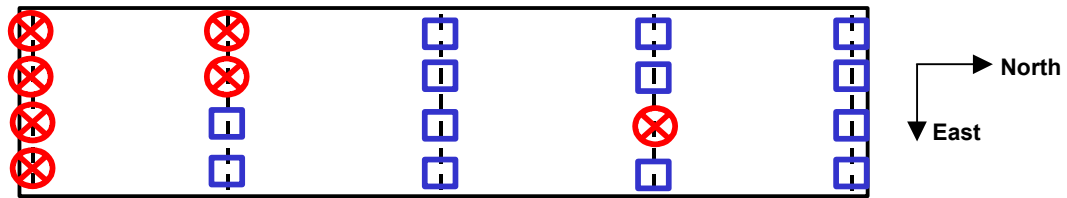


Figure 4.37 Locations of failed puddle welds after Test #8 (DDR = 1.52 %)

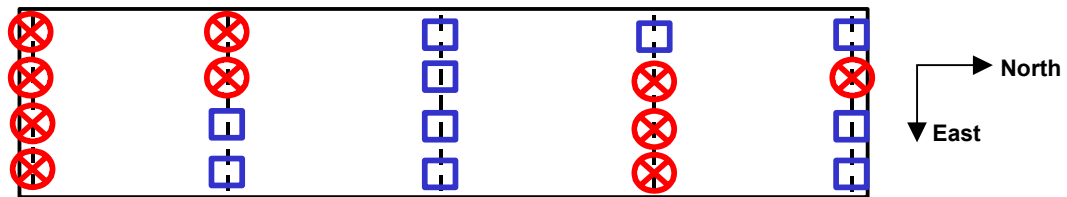


Figure 4.38 Locations of failed puddle welds after Test #9 (DDR = 2.27 %)

Similar to Diaphragm #1, all damage sustained by Diaphragm #2 occurred in its outer two quarters, which were loaded in uniform shear. It has been shown in this dissertation and elsewhere (Cohen 2001, Cohen *et al.* 2002a,c) that the prototype diaphragms represented by Diaphragm #2 deform predominantly in shear. Therefore, as in the case of Diaphragm #1, in-plane deflections should result almost entirely from shearing deformations of the two outer panels, and

those should sustain much more damage than the inner two quarters under transverse loading. The observed damage is consistent with this hypothesis.

4.5.3 Observations of Local Damage After Quasi-static Testing

Examination of the puddle welds following quasi-static testing provided some interesting observations. About half of the welds failed by tearing out of the metal-deck panels, leaving the weld metal connected to the open-web joist (Figure 4.39). This indicated complete fusion between the decking and the joist (AWS D1.3-98 and SDI 1992). The remaining welds failed by cleavage fracture of the metal deck from the open-web joist, at the deck-to-joist interface. This, on the other hand, indicated incomplete fusion between deck and joist. Several of the welds showed pre-existing “burn through,” where the welding arc had consumed some of the deck material at the weld perimeter (Figure 4.40).



Figure 4.39 Example of weld “tear out” at joist-to-weld interface

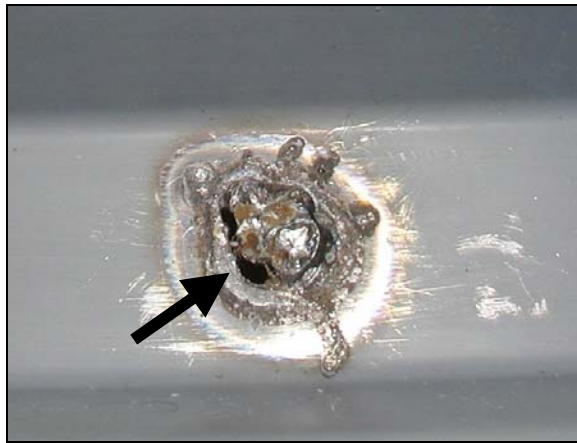


Figure 4.40 Example of “burn through” at weld perimeter

4.6 Evaluation of Test Data for Diaphragm #1 (Lumber Sheathing)

Data from the instrumentation were evaluated for deflections, deformations, and, where appropriate, internal forces. Of particular interest were the hysteretic relationships between applied lateral load and diaphragm drift ratio, which were examined using a variety of evaluation techniques including envelope curves and energy dissipation. Also, elastic moduli for the lumber sheathing were measured. Results of those data evaluations are now presented.

4.6.1 Elastic Moduli of Lumber Sheathing

Instrumentation of Diaphragm #1 measured longitudinal strains in the sheathing boards of a transverse cross-section of the diaphragm, in its south-end quarter (Figure 4.29).

To evaluate the measured longitudinal strains as axial forces, third-point bending tests (ASTM D198-99) were performed on the strain-gauged boards to establish their effective longitudinal elastic moduli. The moduli were evaluated using both measured deflections of the third-point test specimens and their

measured strains. The moisture content (MC) of each board at the time of its test was also measured. Table 4-3 summarizes results of these tests.

Table 4-3 Key properties of strain-gauged sheathing boards

Board	MC	Width	Thickness	Length	E (deflection)	E (strain)
#	%	<i>in.</i>	<i>in.</i>	<i>in.</i>	<i>ksi</i>	<i>ksi</i>
10	< 4	2.642	0.369	12	2126	2487
11	< 4	2.672	0.373	12	1364	1534
12	< 4	2.656	0.378	12	1307	1578
13	< 4	2.610	0.373	12	1846	2981
14	< 4	2.651	0.365	12	1421	1661
15	< 4	2.638	0.383	12	1945	1880
16	< 4	2.601	0.370	12	1804	2334
17	< 4	2.622	0.363	12	1625	1760
18	< 4	2.608	0.368	12	1570	2608
19	< 4	2.625	0.367	12	1316	1317
20	< 4	2.629	0.369	12	1545	1960
Average	< 4	2.632	0.371	12	1624	2009

In that table, sheathing boards are numbered according to their position in the diaphragm. In Figure 4.29 Board 10 is the second board from the right (west) side of the diaphragm; Board 20 is the second board from the left (east) side of the diaphragm. Each technique of determining an effective elastic modulus of the lumber (by measured strain or by measured deflection) has inherent sources of error. For example, the first technique may have errors originating from the electronic equipment, the strain gauge itself, the adhesive attaching the strain gauge to the sheathing board, or the loading equipment, separately or in combination. The second technique may have errors originating from the loading equipment, or the equipment measuring deflection, separately or in combination. The second method was determined to be most reliable, and therefore, moduli

evaluated from deflection (rather than strain) are used in the evaluations discussed in Section 4.6.3.

4.6.2 Hysteretic Behavior of Diaphragm #1

4.6.2.1 Low Diaphragm Drift Ratios (Test #1 - #5)

The diaphragm was supported at its third points by structural channels. At those support points the diaphragm slid on grease-coated tetrafluoroethylene (Teflon®) pads. Unfortunately, some frictional forces still resisted the applied lateral forces and also dissipated energy. This effect is especially pronounced in hysteresis of the diaphragm at very low levels of deflection, when the diaphragm should respond in a linear elastic manner. Figure 4.41 shows the hysteretic loop for applied load versus diaphragm drift ratio for Major Cycle #2, with a maximum DDR of 0.11 % (load-point deflection of 0.15 in.). The loop in that figure is open, implying energy dissipation, and the loading and unloading slopes of that loop are constant, implying linear elastic behavior.

In general, hysteretic loops of the form shown in Figure 4.41 and idealized in Figure 4.42 are characteristic of a Coulomb-damped, or linear-damped, system. In the case of Diaphragm #1, Coulomb damping develops from two mechanisms: frictional forces in the Teflon® bearing pads and frictional forces within the diaphragm itself. Figure 4.41 shows that frictional forces totaled about 0.50 kip and that Diaphragm #1 had an elastic stiffness (Force/DDR) of about 7 kips for each increase of one percentage point in DDR. Or similarly, Diaphragm #1 had an effective elastic shearing rigidity, $A'G$, of about 175 kip.

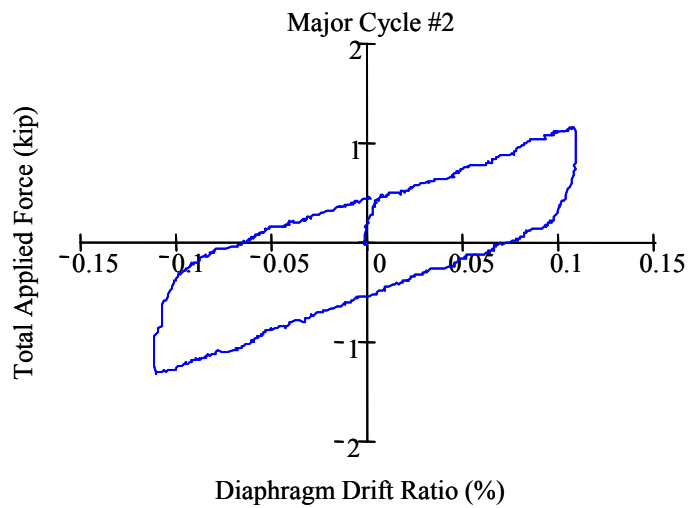


Figure 4.41 Applied load versus diaphragm drift ratio for Major Cycle #2 of Diaphragm #1 (DDR = 0.11 %)

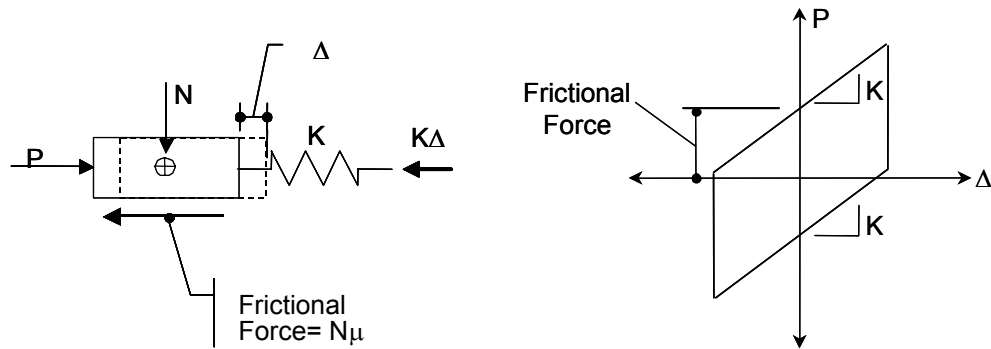


Figure 4.42 Idealized force-deformation relationship for a linear-elastic system with Coulomb (linear) damping

Figure 4.43 shows the hysteretic relationship between the applied load and the diaphragm drift ratio for Diaphragm #1, for Tests #1 - #5. That figure includes both the major and minor cycles of applied lateral force and shows little degradation in stiffness or strength. Diaphragm #1 exhibited stable hysteretic behavior for diaphragm drift ratios less than 0.6 % (Tests #1 - #5).

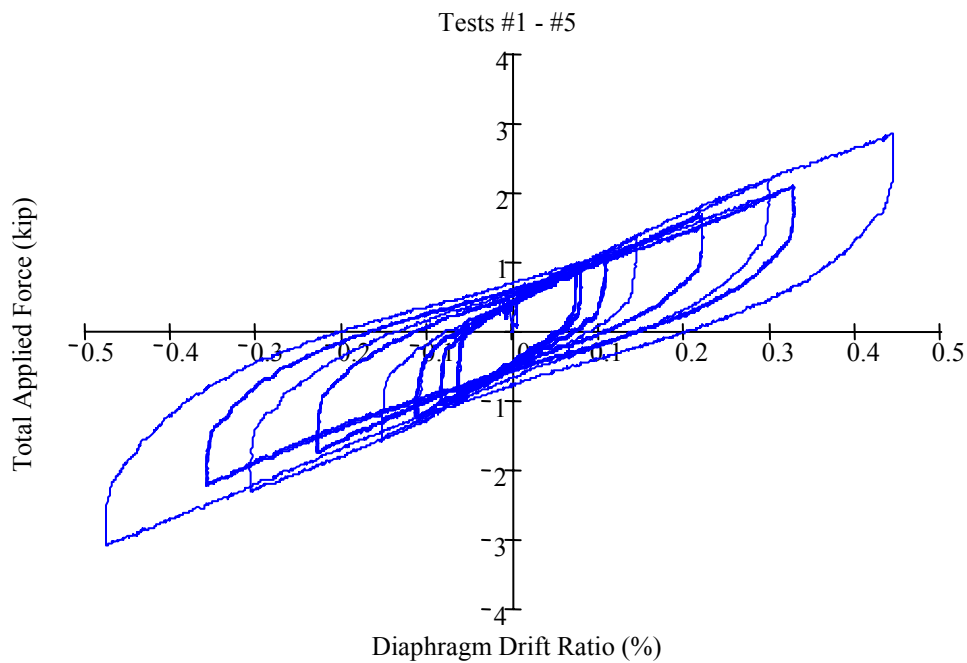


Figure 4.43 Relationship between applied load and diaphragm drift ratio of Diaphragm #1 for low diaphragm drift ratios (DDR < 0.6 %)

4.6.2.2 High Diaphragm Drift Ratios (Test #6 - #9)

Figure 4.44 includes both the major and minor cycles of applied lateral load and shows the hysteretic relationship between applied load and DDR for Diaphragm #1, for Tests #6 - #9. That figure shows that Diaphragm #1 exhibited considerable stiffness degradation, but no strength degradation, as a result of hysteretic cycling. The maximum loads of major cycles consistently increased with increasing diaphragm drift ratios; minor cycles, of equal diaphragm drift ratio, consistently have nearly identical maximum loads, and consistently increase from test to test.

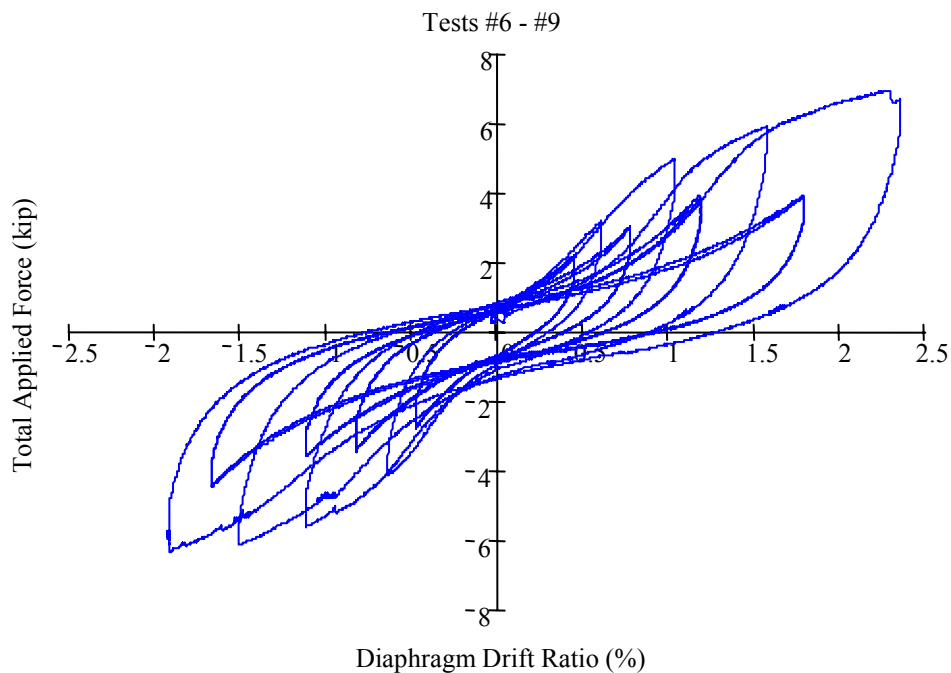


Figure 4.44 Relationship between applied load and diaphragm drift ratio of Diaphragm #1 for high diaphragm drift ratios (DDR > 0.6 %)

To investigate this behavior more thoroughly, it was useful to compute the load-drift envelopes of the diaphragm, using two techniques. The first technique, illustrated in Figure 4.45a, describes the hysteretic loops in terms of “peak envelopes,” defined by the maximum and minimum applied loads in each cycle and the corresponding diaphragm drift ratios. The second technique, illustrated in Figure 4.45b, describes the hysteretic loops in terms of “intersection envelopes” (or “degraded envelopes”) points at which the descending branch of one hysteretic loop intersects the ascending branch of the following loop, and their corresponding diaphragm drift ratios. This type of envelope is also presented in the FEMA 356 document (2000).

Separate peak and intersection envelopes were identified for the major and minor cycles of the loading history. In the case of peak envelopes, the

approximate peak of a suite of minor cycles from a given test was identified. In the case of intersection envelopes, the approximate intersection between a suite of minor cycles from a given test and the suite of minor cycles from the subsequent test was similarly identified.

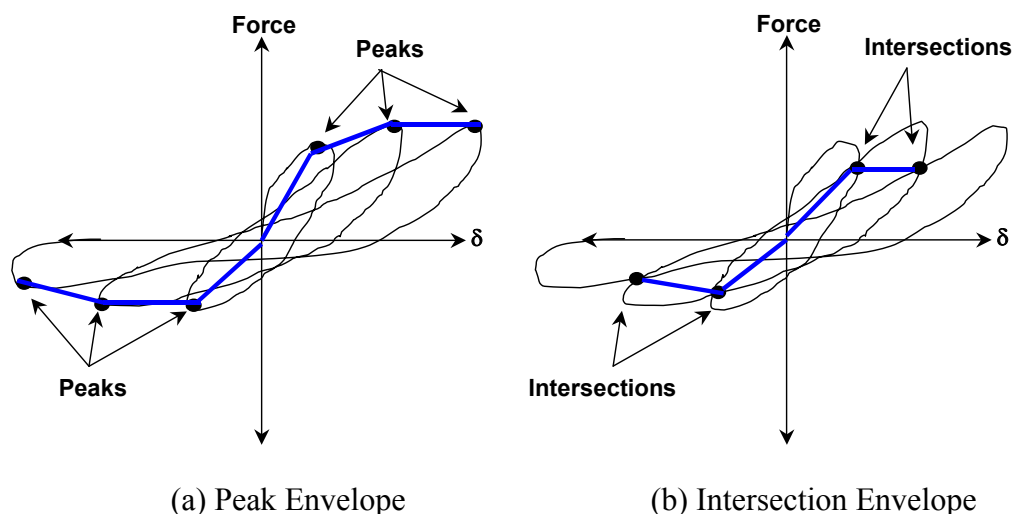


Figure 4.45 Identification of points comprising peak envelopes and intersection envelopes

The envelopes were not developed for the total applied load, but rather for each actuator load. This permitted using the curves to identify differences in load-drift behavior between the two ends of the diaphragm, as possible indicators of unsymmetrical behavior. A diagonally sheathed lumber diaphragm is an orthotropic assembly, for which symmetric actuator displacements do not necessarily imply symmetric actuator loads. The envelopes of Figure 4.46 through Figure 4.48, however, show that the north and south actuators maintained nearly equal loads (within 10 %) throughout the loading history. The non-symmetric orthotropic assembly of Diaphragm #1 therefore behaved symmetrically with respect to transverse displacements. This implies that in spite

of its physical orthotropy, a diagonally sheathed diaphragm can be idealized as isotropic.

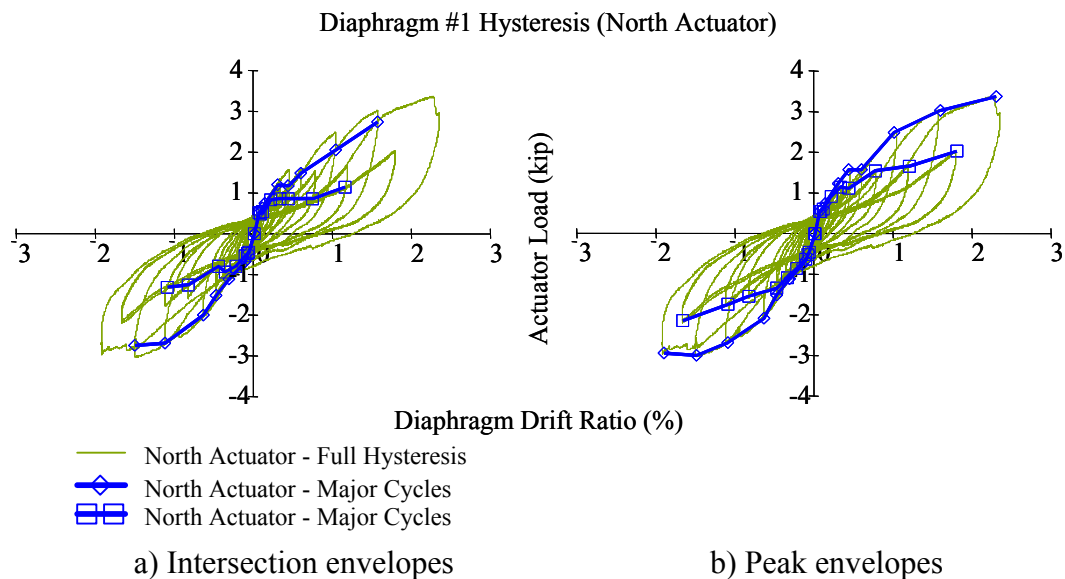


Figure 4.46 Hysteresis intersection and peak envelopes for north actuator (Diaphragm #1)

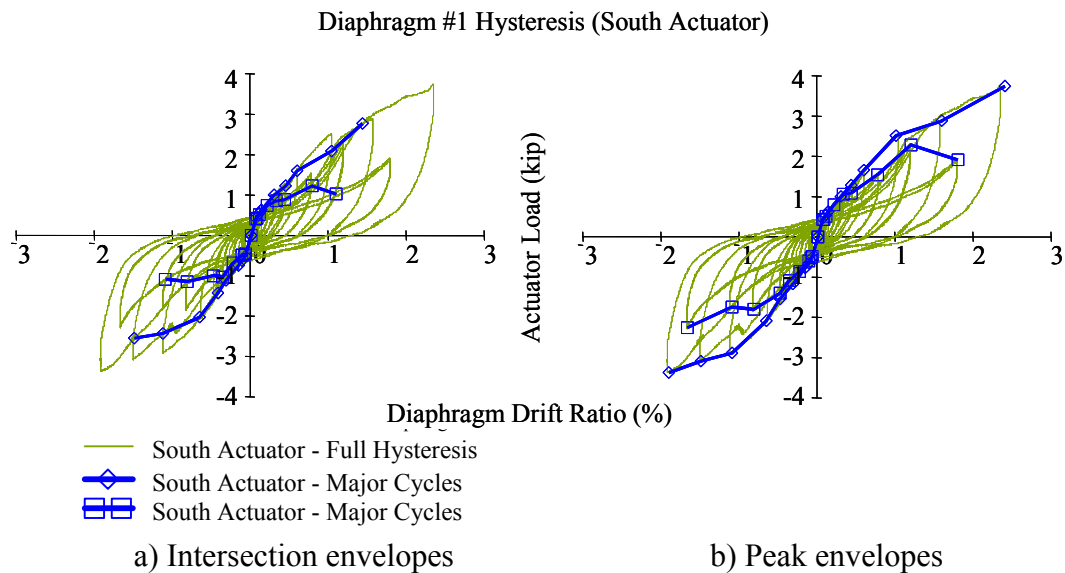
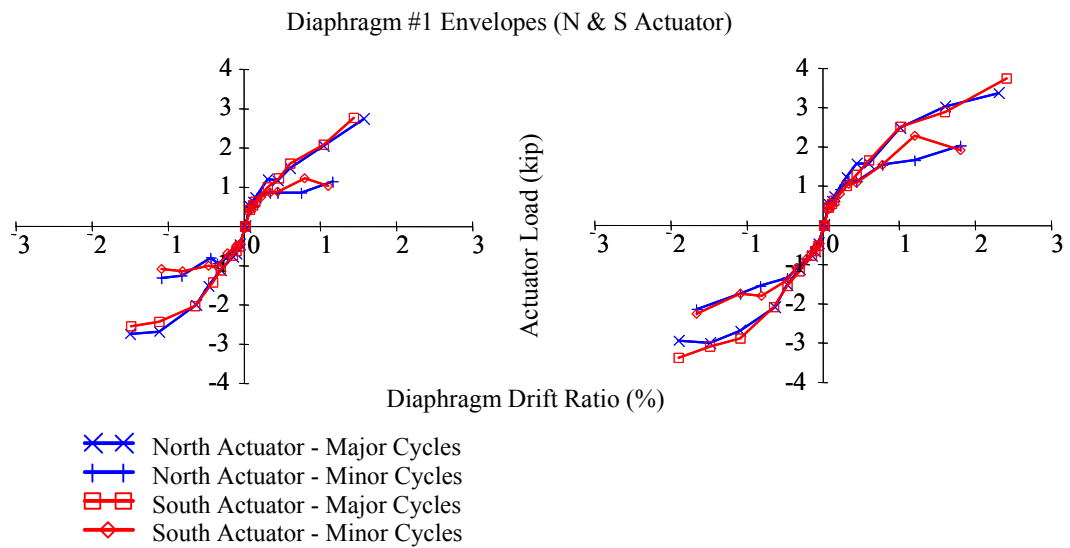


Figure 4.47 Hysteresis intersection and peak envelopes for south actuator (Diaphragm #1)



a) Intersection envelopes

b) Peak envelopes

Figure 4.48 Comparison of hysteresis intersection and peak envelopes (Diaphragm #1)

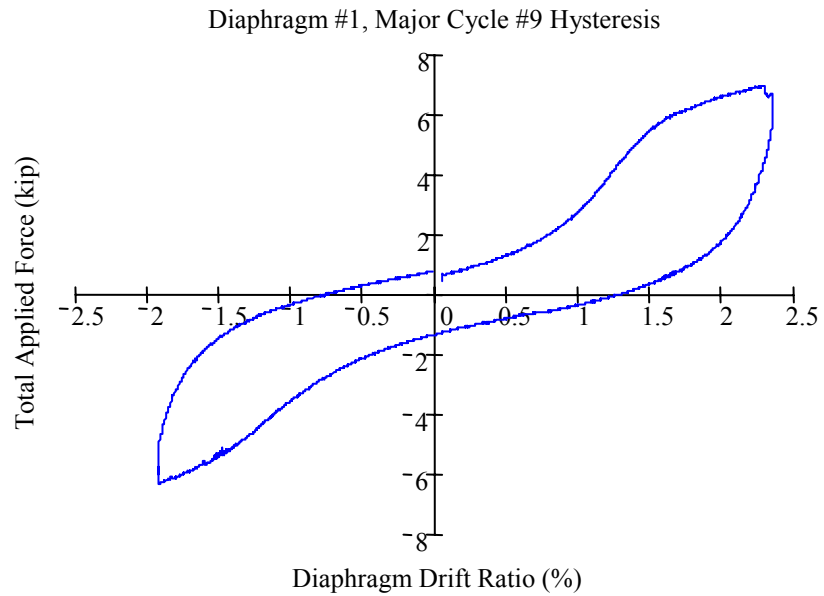


Figure 4.49 Relationship between total applied load and diaphragm drift ratio of Diaphragm #1 for Major Cycle #9 (DDR = 2.3 %)

The two types of envelopes (intersection and peak) suggest similar overall hysteretic behavior. They show that with increasing values of DDR, the diaphragm exhibited a decrease in lateral stiffness. They do not show, however, that the diaphragm exhibited any decrease in its lateral capacity with increasing diaphragm drift ratios. Diaphragm #1 exhibited stable overall hysteretic behavior with a significant degradation of lateral stiffness at high diaphragm drift ratios.

Diaphragm #1 exhibited considerable hysteretic pinching at high levels of diaphragm drift ratio (for example, Figure 4.49). In reinforced concrete and reinforced masonry elements, pinching occurs primarily from opening and closing of existing cracks and sliding shear. In the case of a diagonally sheathed lumber diaphragm, pinching occurs from bearing failure of the wood matrix at nail holes and plastic deformation of the nails themselves. This process, illustrated schematically in Figure 4.50, was observed in these tests (Section 4.4.3), and has been noted elsewhere (for example, Soltis and Mtenga 1985).

The relationships discussed here, between applied lateral load and diaphragm drift ratio for Diaphragm #1, demonstrated that at low diaphragm drift ratios ($DDR < 0.6\%$), the diaphragm did not degrade in stiffness or strength; at high diaphragm drift ratios ($DDR > 0.6\%$), the diaphragm exhibited stable overall hysteretic behavior (no strength degradation) with stiffness degradation and pinching. Furthermore, the diaphragm behaved symmetrically and isotropically, in the context of lateral deflections.

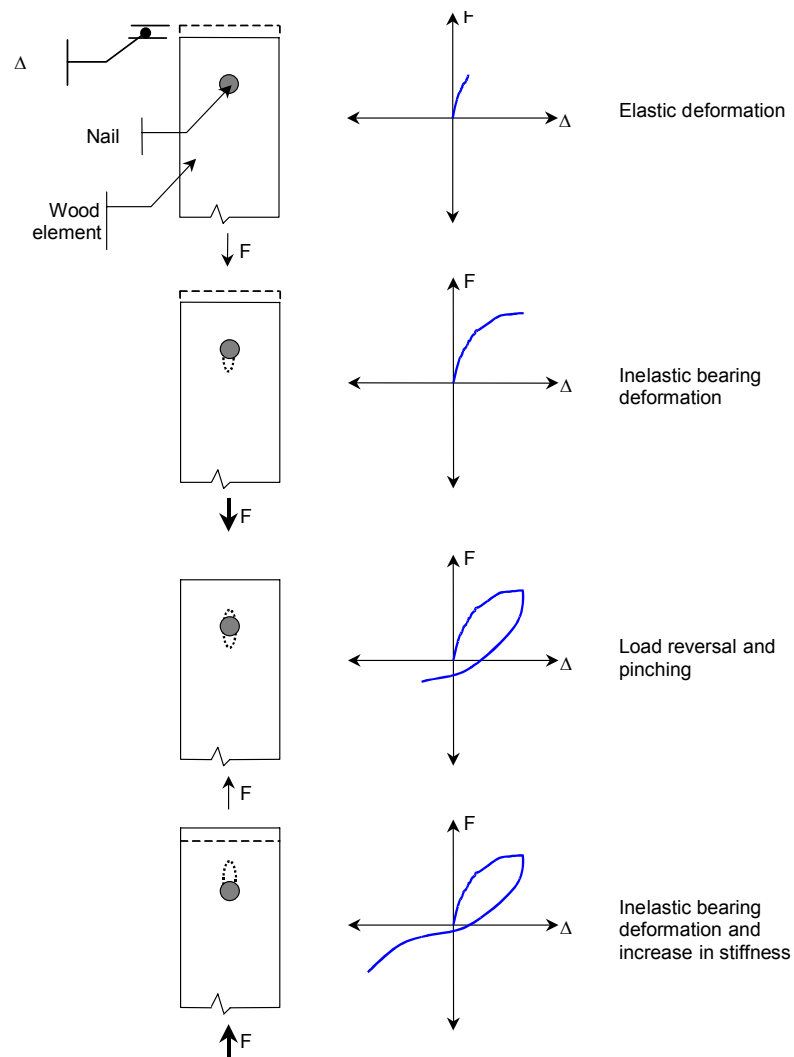


Figure 4.50 Illustration of hysteretic pinching due to hole damage in nailed wood assemblies

4.6.3 Internal Forces in Diaphragm #1

Instrumentation of Diaphragm #1 (Appendix A) provided in-plane longitudinal strains in the diaphragm sheathing, in a transverse cross-section, in the south-end quarter of the diaphragm. The sheathing boards were instrumented

on their top and bottom surfaces to detect out-of-plane bending and their elastic moduli and cross-sectional areas (Table 4-3) permitted interpretation of those strains as axial forces. Those forces, their relationship to the applied lateral load, and their relationship to the observed diaphragm damage are now discussed.

The sheathing board axial forces were decomposed into components aligned with the transverse (W-E) and longitudinal axes (N-S) of Diaphragm #1 (Figure 4.51). Components of force parallel to the transverse axis of the building thus represented in-plane shear force. Figure 4.52 and Figure 4.53 show the measured shear in the sheathing at that particular cross-section in the diaphragm for respectively Tests #1 and #8.

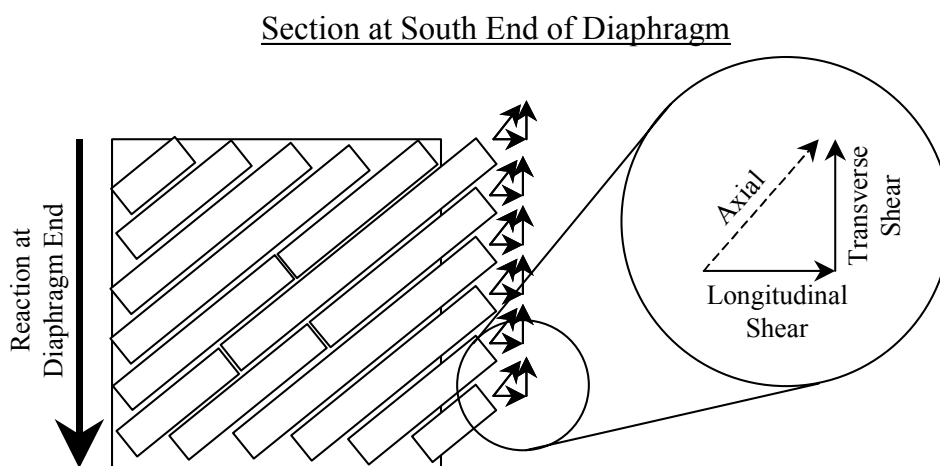


Figure 4.51 Decomposition of measured axial forces in sheathing boards

Figure 4.52 shows that the diaphragm sheathing resisted only a portion of the total applied shear in the diaphragm. Presumably, frictional forces between the test frame and the diaphragm assembly, as well as those within the diaphragm itself, resisted a significant portion of the applied lateral load at low levels of diaphragm drift ratios. Moreover, the figure indicates that the masonry chords and lumber nailers resisted forces by their own out-of-plane stiffnesses. Those

stiffnesses are discernable by the difference in slopes of the hysteretic loops for the instrumented sheathing and applied shear (Figure 4.52).

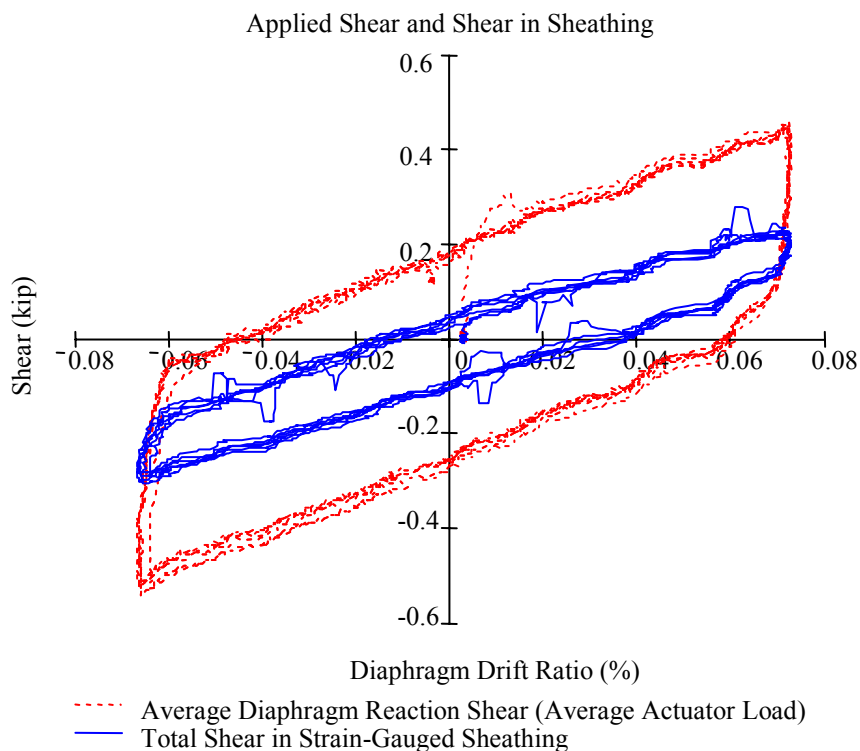


Figure 4.52 Comparison of applied in-plane shear and that resisted by lumber sheathing (Test #1, Diaphragm #1)

Figure 4.53 shows that the diaphragm sheathing resisted a greater portion of the applied shear at higher diaphragm drift ratios. Unlike material resistance, frictional resistance does not change with deformation. Therefore, the proportion of lateral force resisted by friction decreases with increasing deformations. This is consistent with observations drawn from Figure 4.52 and Figure 4.53.

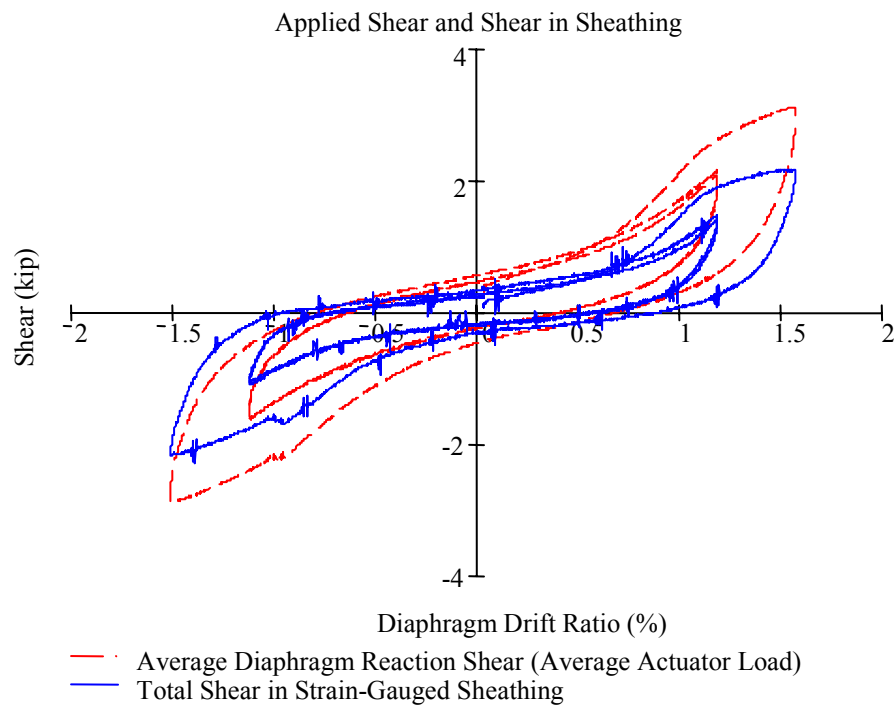


Figure 4.53 Comparison of applied in-plane shear and that resisted by lumber sheathing (Test #8, Diaphragm #1)

Strain data from the sheathing also permitted the determination of force profiles through the transverse cross-section of the diaphragm. The in-plane flexibility of a complex lumber assembly, such as a diaphragm, derives from several mechanisms: flexibility of the sheathing itself; bending flexibility of the nails; bearing flexibility of wood matrix around the nails; out-of-plane flexibility of the masonry chords; and others. As a result, simple rational analysis cannot generally determine the actual distribution of forces in the sheathing across a given cross-section of the diaphragm.

Many researchers have observed, however, that the in-plane flexibility and strength of a lumber sheathed diaphragm chiefly depends on the number and size of the sheathing nails. For that reason, the measured axial force in each sheathing

board was divided by the lesser number of nails that lay to either side of the strain gauge, over the length of that board. For instance, Board 12 (Figure 4.29) had two nails connecting it to the diaphragm south of its strain gauge and three nails connecting it to the diaphragm north of its strain gauge. Thus, the axial force in the board was divided by two (Figure 4.54). This process effectively normalized the force in each board and facilitated comparison with other sheathing boards in the same transverse cross-section of the diaphragm.

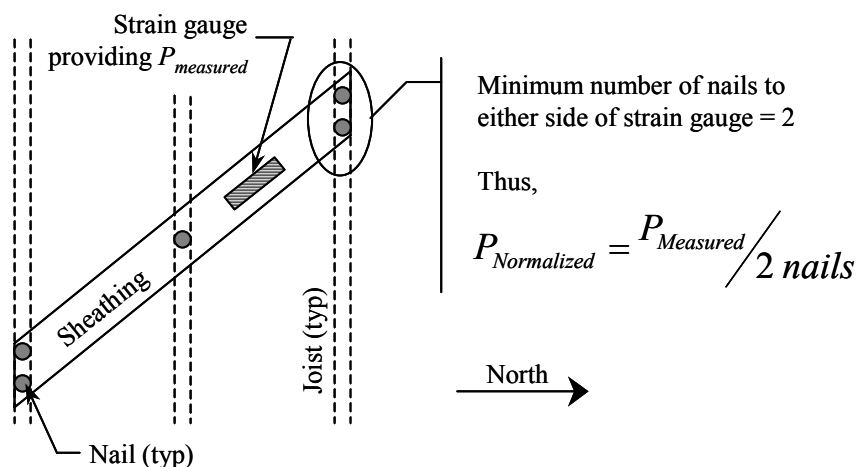


Figure 4.54 Schematic process for normalizing axial forces in sheathing boards

This normalization was only justified, however, when each nail resisted approximately equal forces. At low diaphragm drift ratios (in the elastic range of response) the distribution of force to each nail for a particular sheathing board is complex. At high diaphragm drift ratios, and specifically near the lateral load capacity of the diaphragm, however, the nails of the strain-gauged sheathing boards were observed to behave well into their inelastic range. Thus, each sheathing board likely developed a plastic mechanism, with the lateral resistance of the nails representing the plastic elements. It is thus plausible that the nails of a given sheathing board resisted similar load magnitudes at high diaphragm drift

ratios. For these reasons, the normalized force distribution is only presented for Test #8, at a maximum diaphragm drift ratio of 1.52 % (Figure 4.55). (Extensive damage occurred to the strain-gauged sheathing boards of Diaphragm #1 during Test #9, precluding the use of data from that test for this evaluation.)

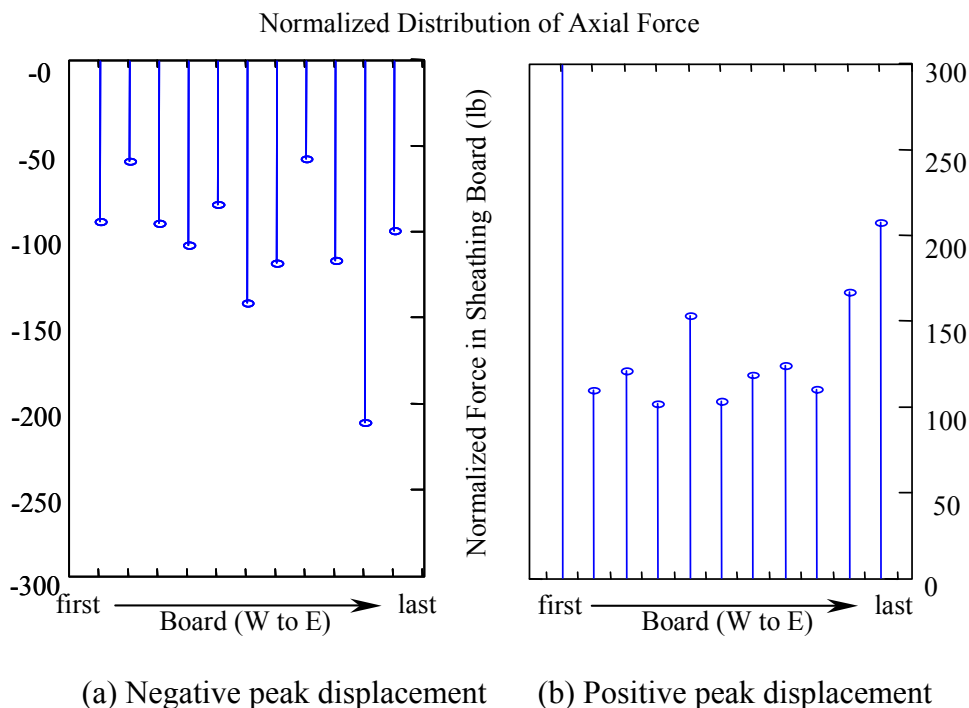


Figure 4.55 Normalized axial force distribution in sheathing boards, for a transverse cross-section in the south-end quarter, at peak diaphragm drift ratios (Diaphragm #1, Test #8)

Figure 4.55 shows that the distribution of normalized axial forces across that particular transverse cross-section of Diaphragm #1 was approximately uniform. This conclusion is true for both the negative peak of Test #8 (Figure 4.55a) and the positive peak of Test #8 (Figure 4.55b). The normalized axial forces are a measure of transverse force per nail, for the nails comprising the lesser group that lay to either side of the strain gauge. The LRFD Reference Lateral Resistance for the nails (4d) used in Diaphragm #1 is about 130 lb (AFPA

1996). Figure 4.55a and Figure 4.55b show average nail forces consistent with that value, respectively of about 100 lb and about 130 lb.

There is some variation in the normalized axial forces, however. Reasonable variation in the normalized axial force, as seen for instance between Boards 11-18, was expected due to the complex nature of a lumber diaphragm and the simplified techniques used here to evaluate it. Boards 10 and 20 in Figure 4.55b, however, resist significantly greater normalized axial forces. Similar is Board 19 in Figure 4.55a. These larger anomalous variations may result from relatively high in-plane or out-of-plane bending of the board, erroneous strain data, erroneous or uncharacteristic elastic moduli, or other sources.

Table 4-4 shows the mean axial forces, standard deviations, and coefficients of variation (COV), for Figure 4.55. COVs of the data are significantly reduced when the anomalous forces are treated as statistical outliers and removed from the calculation. This suggests that the conclusion of uniformly distributed normalized axial forces in that particular cross-section of Diaphragm #1, is reasonably consistent and justified.

Table 4-4 Variation of sheathing axial forces in transverse cross section

Boards included in calculation	Figure 4.55a		Figure 4.55b	
	10 - 20	10 - 18, 20	10 - 20	11 - 19
Mean Axial Force	-108 lb	-97 lb	152 lb	123 lb
Standard Deviation	40 lb	25 lb	70 lb	21 lb
COV	-37 %	-25 %	46 %	17 %

4.6.4 Hysteretic Energy Dissipation

The ability of a structural assembly to resist seismic actions while undergoing large reversed cyclic deformations is generally characterized using the concepts of toughness and inelastic energy dissipation capacity. Toughness qualitatively describes a system's ability maintain its structural integrity at the

maximum anticipated lateral displacement resulting from a seismic ground motion (ACI 1999). Energy dissipation capacity can be quantified using the relative energy dissipation ratio, the ratio of the energy actually dissipated by the lateral-force resisting system to that dissipated by an equivalent linear elastic-perfectly plastic system. The relative energy dissipation ratio is meaningful only when inelastic material response dominates the energy dissipation in the system. Friction (Figure 4.42), however, dissipated a significant amount of energy and therefore, the measured hysteretic energy dissipation shown in Figure 4.43 and Figure 4.44 is the sum of two distinct contributions: hysteretic energy dissipated by frictional forces; and hysteretic energy dissipated by inelastic material response. This concept is shown schematically in Figure 4.56.

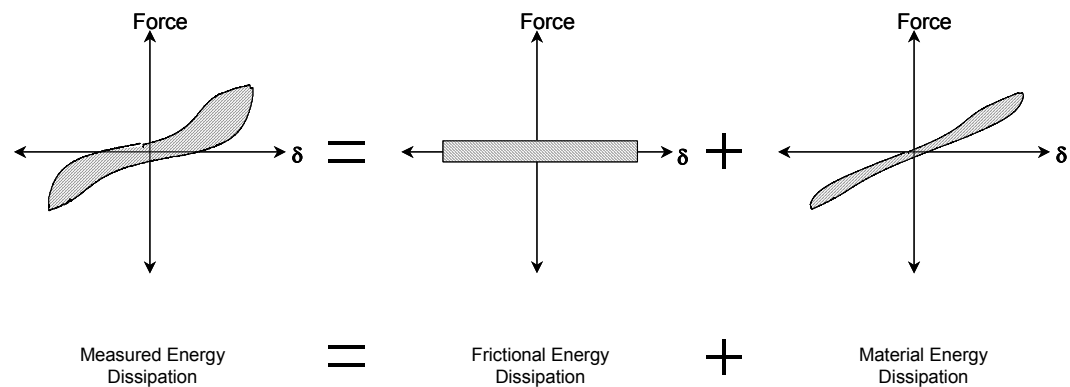


Figure 4.56 Contribution of friction to hysteretic energy dissipation

Evaluation of the test data showed that the total frictional force was about 0.50 kip (Figure 4.41). The measured hysteretic energy dissipation can thus be numerically separated into the two contributions illustrated in Figure 4.56. Figure 4.57 shows the contributions of each energy-dissipation mechanism by comparing the ratios of each contribution to the total measured energy dissipation. That figure shows that energy dissipation was dominated by friction at low diaphragm

drift ratios (Major Cycles #1 - #6), and by material response at high diaphragm drift ratios (Major Cycles #7 - #9). This observation would be expected; frictional forces remain essentially constant during the test, while inelastic energy dissipation increases with increasing damage (diaphragm drift ratios). Figure 4.57 erroneously shows, however, that frictional energy initially dissipated 115 % of the total dissipated energy, and that inelastic material response initially dissipated -15 % of the total dissipated energy. These slight inaccuracies follow from the approximation of total frictional force in the system, and do not affect the qualitative results implied by Figure 4.57.

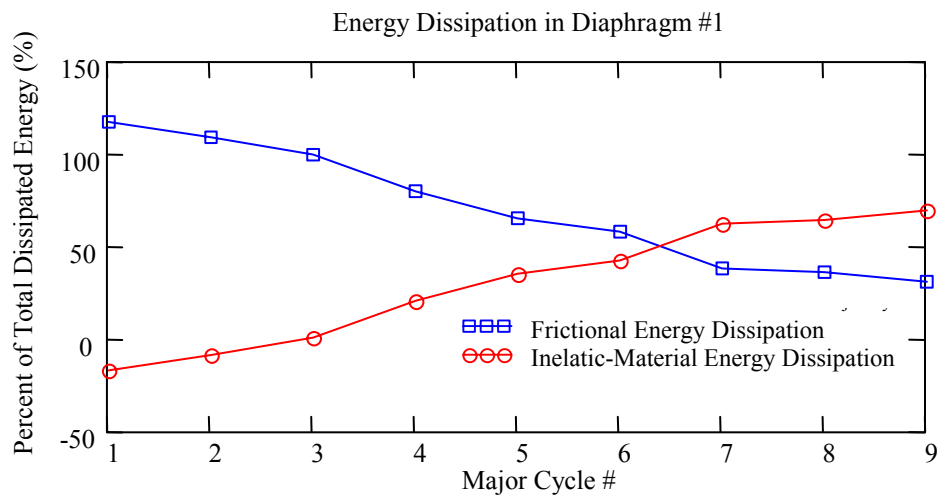


Figure 4.57 Relative contributions of friction and inelastic material response to measured hysteretic energy dissipation in Diaphragm #1

4.7 Evaluation of Test Data for Diaphragm #2 (Metal Deck)

Data from the instrumentation were evaluated for deflections and deformations. Of particular interest were the hysteretic relationships between applied lateral load and diaphragm drift ratio.

4.7.1 Hysteretic Behavior of Diaphragm #2

4.7.1.1 Low Diaphragm Drift Ratios (Test #1 - #5)

For the same reasons discussed earlier, frictional forces in the test setup for Diaphragm #2 resisted a portion of the applied lateral forces and also dissipated energy. This effect is especially pronounced in hysteresis of the diaphragm at very low levels of deflection, when the diaphragm should respond in a linear-elastic manner.

Figure 4.58 shows the hysteretic relationship between the applied load and the DDR for Diaphragm #2 for Tests #1 - #5. The figure shows that frictional forces totaled about 0.42 kip and that Diaphragm #2 had an elastic stiffness (Force/DDR) of about 6.3 kips for each increase of one percentage point in DDR. Or similarly, Diaphragm #2 had an effective elastic shearing rigidity, $A'G$, of about 160 kips.

Figure 4.59, however, shows that the north and south actuators resisted asymmetric frictional forces. It was determined during testing, that the apparent asymmetry in frictional forces was due to small differences in the actuator vertical support systems, and would not affect the results of the test. Figure 4.58 includes both the major and minor cycles of applied lateral force and shows little degradation in stiffness or strength. Diaphragm #2 exhibited stable hysteretic behavior for diaphragm drift ratios less than 0.6 % (Tests #1 - #5).

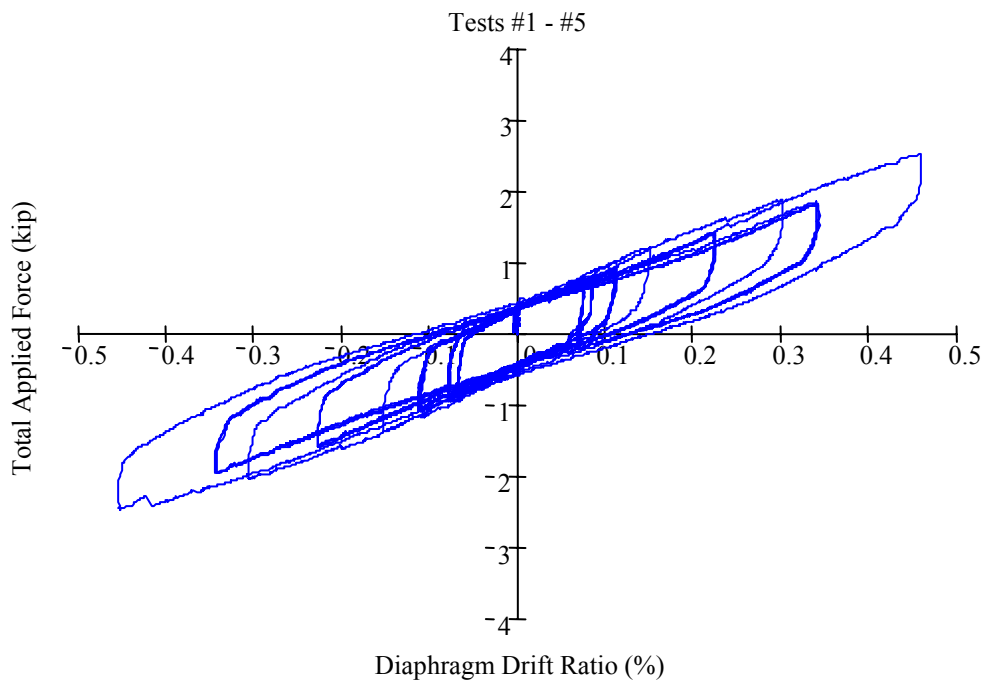


Figure 4.58 Relationship between applied load and diaphragm drift ratio of Diaphragm #2 for low diaphragm drift ratios (DDR < 0.6 %)

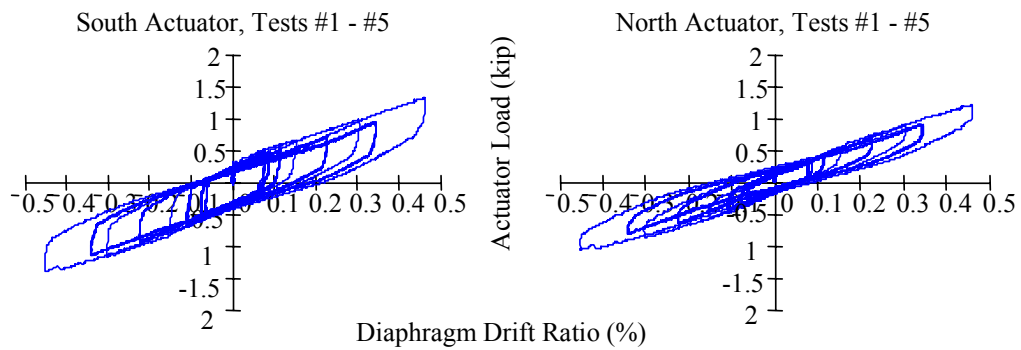


Figure 4.59 Comparison of relationships between applied load and diaphragm drift ratio in the north and south actuators for Diaphragm #2 (DDR < 0.6 %)

4.7.1.2 High Diaphragm Drift Ratios (Test #6 - #9)

Figure 4.60 shows the hysteretic relationship between applied load and diaphragm drift ratio for Diaphragm #2 for Tests #6 through #9. That figure includes both the major and minor cycles of applied lateral load and shows that the diaphragm sustained considerable degradation of stiffness and strength as a result of hysteretic cycling. The figure also shows that the diaphragm maintained a linear elastic relationship of load and DDR between points of significant strength degradation.

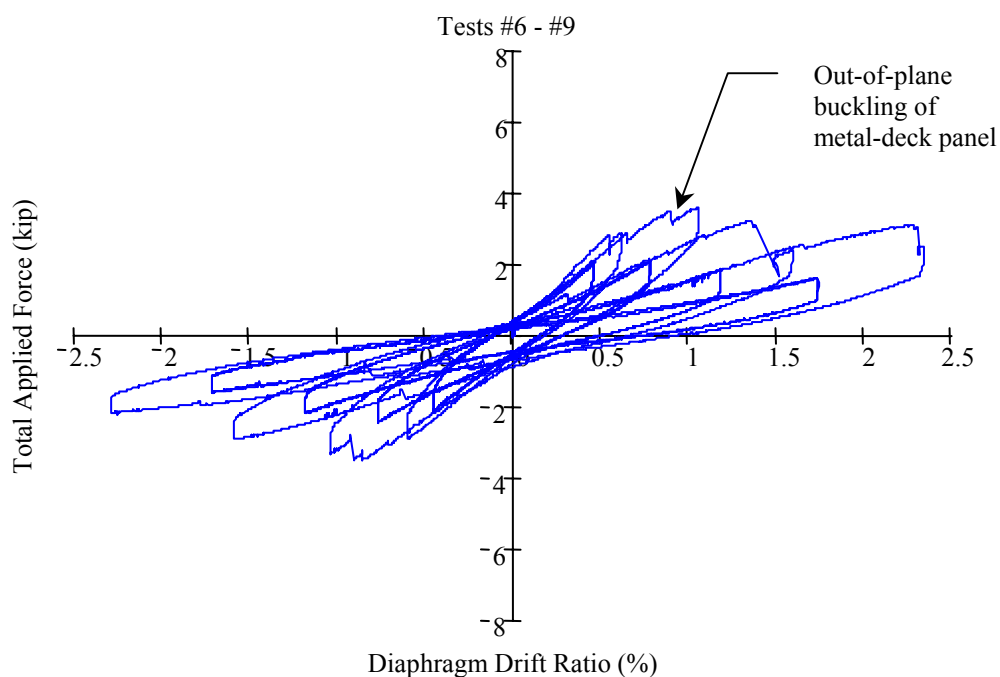


Figure 4.60 Relationship between applied load and diaphragm drift ratio of Diaphragm #2 for high diaphragm drift ratios (DDR > 0.6 %)

Nonlinear behavior in structural systems generally results from constitutive nonlinearities (for example, yielding), kinematical nonlinearities (for example, P- Δ effects), changes in internal distribution of structural actions (for example, fracture), or any combination of the three. Welded metal-deck

diaphragms show constitutive nonlinearities, or damage, by the yielding and tearing of metal deck around welds and side-lap connectors. That damage, as observed during the quasi-static testing of Diaphragm #2, occurs only in regions very local to the welds and side-lap screws and thus does not significantly affect the load-drift relationship of the diaphragm. Welded metal-deck diaphragms show kinematical nonlinearities by out-of-plane buckling of the metal-deck panels. Figure 4.60 provides an example of this effect. It is generally detectable but not significant because metal-deck panels preserve significant in-plane stiffness by maintenance of tension fields oriented along the axes of buckling. Welded metal-deck diaphragms show nonlinearities due to changes in internal distribution of structural actions by the failure of welds and side-lap connectors. This nonlinear behavior significantly decreases the strength and stiffness of Diaphragm #2 and is apparent by comparing the number of failed welds in the diaphragm during each test (Figure 4.35 through Figure 4.38) with the corresponding apparent diaphragm stiffness and maximum load sustained during that test (Figure 4.60)

To investigate the observed behavior more thoroughly, load-drift envelopes of the diaphragm were created; only peak major-cycle envelopes are provided. The diaphragm was displaced symmetrically in the transverse direction at its quarter points. A metal-deck diaphragm is an orthotropic assembly, however, for which symmetric actuator displacements do not necessarily imply symmetric actuator loads. Others have shown, however, that in the linear-elastic range of response, the in-plane stiffness of metal-deck diaphragms is generally independent of the orientation of the decking panels (Ellifrit and Luttrell 1970). Thus not surprisingly, the envelopes of Figure 4.61 and Figure 4.62 show that the

north and south actuators maintained approximately equal loads at approximately equal diaphragm drift ratios for $DDR < 0.6\%$.

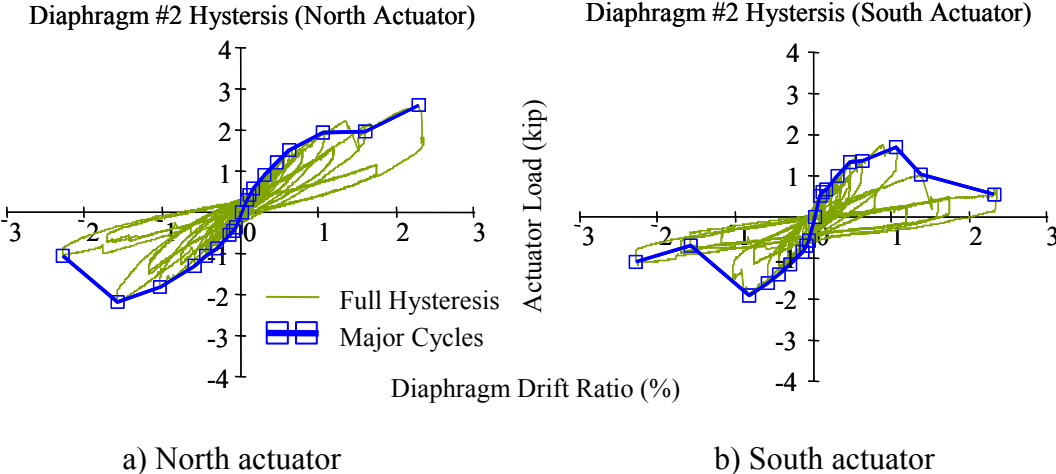


Figure 4.61 Hysteresis peak envelopes for south actuator (Diaphragm #2)

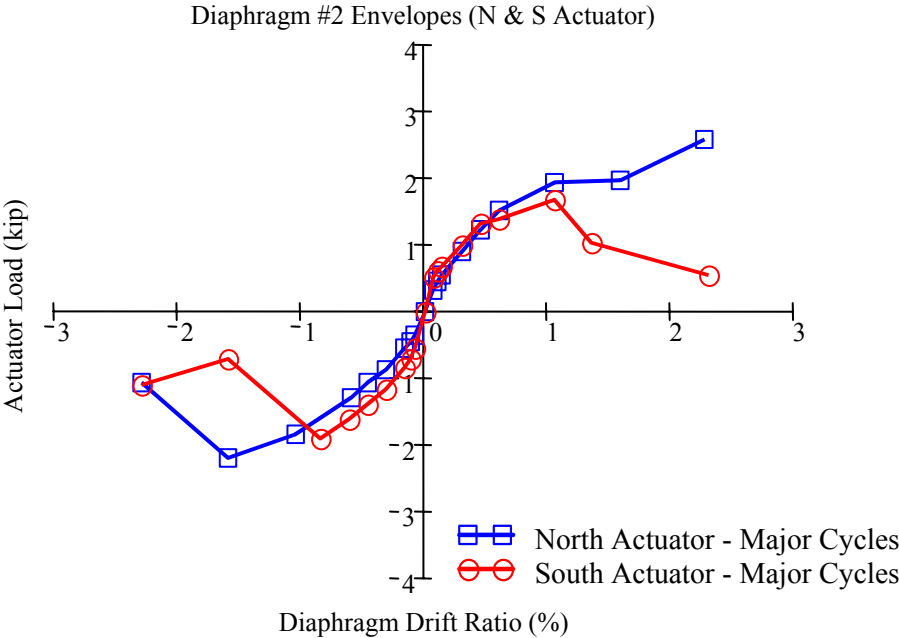


Figure 4.62 Comparison of hysteresis peak envelopes for north and south actuators (Diaphragm #2)

At high diaphragm drift ratios ($DDR > 0.6 \%$), however, the actuators resisted considerably different loads. This result is consistent with the observation that the diaphragm did not sustain transversely symmetric weld failures during the tests (Figure 4.35 through Figure 4.38). For example, Figure 4.37 shows that following Test #7 metal-deck panels in the south-end quarter of the diaphragm were not sufficiently connected to the rest of the specimen to resist in-plane loads. Conversely, that figure also shows that the metal-deck panels in the north-end quarter sustained only one weld failure and thus still provided considerable in-plane shear resistance. The asymmetric weld failures likely resulted from variation in welding quality.

Significant variation in welding quality is unfortunately typical for puddle (arc-spot) welds. Welding quality depends on welding-machine settings and welding technique. Inevitable variation of these prohibits a consistently accurate prediction of weld strength or failure mode (tear-out or cleavage fracture).

The non-symmetric orthotropic assembly of Diaphragm #2 behaved symmetrically with respect to transverse displacements at low diaphragm drift ratios. This implies that in spite of their physical orthotropy, welded metal deck diaphragms can be idealized as isotropic when linear elastic response is expected. When nonlinear response is expected at high diaphragm drift ratios, however, these types of diaphragms are expected to behave asymmetrically, and thus an isotropic assumption is not justified.

The relationships discussed here, between the applied lateral load and the diaphragm drift ratio for Diaphragm #2, demonstrated that at low diaphragm drift ratios, the diaphragm did not degrade in stiffness or strength and exhibited stable overall hysteretic behavior; at high diaphragm drift ratios, the diaphragm exhibited stiffness degradation, strength degradation, and specifically, unstable

nonlinear elastic hysteretic behavior. Furthermore, at low diaphragm drift ratios the diaphragm behaved symmetrically and isotropically, in the context of lateral deflections.

4.8 Summary, Conclusions, and Significance of Quasi-Static Diaphragm Testing

4.8.1 Summary of Results and Conclusions

Following the shaking-table testing of two, low-rise reinforced masonry building specimens, diaphragms and top four courses of attached masonry walls were removed and subjected to in-plane reversed cyclic quasi-static displacements. Two diaphragm-masonry chord assemblies were tested: a diagonally sheathed lumber diaphragm; and a welded metal-deck diaphragm.

Data collected during the tests were evaluated in the context of diaphragm drift ratios and characterized the hysteretic behavior of the two assemblies. At low diaphragm drift ratios (less than 0.6 % for the lumber diaphragm and less than 0.45 % for the metal-deck diaphragm), the diaphragms did not degrade in stiffness or strength. At high diaphragm drift ratios, the lumber diaphragm exhibited stable overall hysteretic behavior (no strength degradation) with stiffness degradation and pinching; the metal-deck diaphragm exhibited stiffness degradation, strength degradation, and specifically, unstable nonlinear elastic hysteretic behavior.

These evaluations demonstrated the usefulness of the diaphragm drift ratio as a measure of overall diaphragm deformation, and hence an index of potential diaphragm damage.

4.8.2 Significance of Quasi-Static Testing

The previous chapter contains a review of results and conclusions from earlier shaking-table testing of two, low-rise reinforced masonry building specimens with flexible diaphragms. Those tests characterized the seismic behavior of the buildings and suggested that the effect of diaphragm flexibility should be accounted for in their seismic analysis, design, evaluation, and rehabilitation. This chapter describes the quasi-static testing of two flexible diaphragms and provides insight to the seismic performance the systems, critical levels of deformation (diaphragm drift ratio), attendant damage mechanisms, and hysteretic characteristics. These insights, as well as those gained from shaking-table tests, are synthesized in the following chapter to develop an analytical tool for the accurate analysis of these types of buildings. The tool is verified in the linear and nonlinear range of response (Chapter 5) and applied to seismic evaluation and rehabilitation methodologies in respectively Chapters 6 and 7. It is applied to four real structures in Chapter 8, and ultimately shown to be effective, simple, and accurate.

5.0 Low-Degree-of-Freedom Idealizations of Low-Rise Reinforced Masonry Buildings with Flexible Diaphragms

As demonstrated by the shaking-table testing discussed in Chapter 3, diaphragm flexibility can significantly affect the seismic response of low-rise reinforced masonry buildings. In contrast to the common design assumption that seismic response is governed by the in-plane response of the shear walls, diaphragms tend to respond independently of supporting shear walls, and the in-plane shear walls tend to respond together, in-phase. To investigate this behavior and the possibility of developing a simplified analysis tool based on it, it is useful to idealize these types of structures systems with only a few degrees of freedom. The development, implementation, and verification of such idealizations are now discussed.

5.1 General Approach and Mathematical Development

Low-rise reinforced masonry buildings with flexible diaphragms were first idealized as two-degree-of-freedom (2DOF) systems. To do this, the generalized coordinates q_1 and q_2 , described in Figure 5.1, were chosen. Because those generalized coordinates were selected so as to be kinematically independent, they are referred to here as degrees of freedom. Degree of Freedom 1 is associated with the in-plane deformation of the transverse shear walls. Degree of Freedom 2 is associated with the in-plane deformation of the diaphragm.

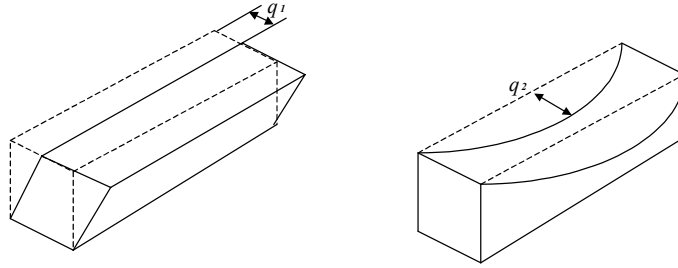


Figure 5.1 Generalized coordinates for 2DOF idealization

5.1.1 First Degree of Freedom, q_1

Relative contribution of shearing and flexural deformations to the deflection of a cantilever shear wall depends on that wall's vertical aspect ratio. This analysis considers both deformation mechanisms. Thus, the chosen shape function $\phi(y)$ has non-uniform first and second derivatives.

$$\phi(y) = 1 - \cos\left(\frac{y\pi}{2H}\right), \quad \text{Equation 5-1}$$

where, H is the height of the building and y is the vertical coordinate. The generalized mass M^*_1 associated with q_1 is

$$M^*_1 = \int_0^H \mu(y) [\phi(y)]^2 dy, \quad \text{Equation 5-2}$$

where, $\mu(y)$, the mass of the building per unit height must include the concentrated mass of the roof diaphragm $M_{diaphragm}$ at $y = H$, but is otherwise a constant μ . Evaluation of the integral gives

$$M^*_1 = \frac{1}{5} \mu H + M_{diaphragm}. \quad \text{Equation 5-3}$$

The generalized stiffnesses K^*_{S1} and K^*_{f1} , representing respectively the shearing stiffness and the flexural stiffness associated with DOF q_1 , are

$$K^*_{s1} = A'G \int_0^H [\phi'(y)]^2 dy \quad \text{and} \quad \text{Equation 5-4}$$

$$K^*_{f1} = EI \int_0^H [\phi''(y)]^2 dy, \quad \text{Equation 5-5}$$

where, G = shearing modulus of the masonry;
 E = elastic modulus of the masonry;
 A' = effective shear area of the transverse walls; and
 I = moment of inertia of the transverse walls.

Evaluation of these integrals gives

$$K^*_{s1} = \frac{A'G \pi^2}{H} \quad \text{and} \quad \text{Equation 5-6}$$

$$K^*_{f1} = \frac{EI \pi^4}{H^3 32}. \quad \text{Equation 5-7}$$

Flexibility is the reciprocal of stiffness. Thus, the total generalized stiffness for the two transverse shear walls is

$$K^*_1 = 2 \cdot \frac{K^*_{s1} K^*_{f1}}{K^*_{s1} + K^*_{f1}}. \quad \text{Equation 5-8}$$

5.1.2 Second Degree of Freedom, q_2

The shape function approximating the deflected shape of the diaphragm during transverse excitation is

$$\phi(x) = \sin\left(\frac{\pi}{L}x\right), \quad \text{Equation 5-9}$$

where, L = longitudinal dimension of building; and
 x = horizontal coordinate.

The expression for the generalized mass M^*_2 associated with the second degree of freedom q_2 is thus

$$M^*_2 = \int_0^L \mu(x) [\phi(x)]^2 dx, \quad \text{Equation 5-10}$$

where $\mu(x)$ is a constant μ , and is approximated here as the mass per unit length of the diaphragm plus one-half the mass per unit length of the longitudinal walls. This factor of one-half accounts for the approximately inverted-triangular distribution of inertial mass for the out-of-plane walls. Evaluation of this integral gives

$$M^*_2 = \frac{1}{2} \mu L. \quad \text{Equation 5-11}$$

The in-plane response of most flexible diaphragms is dominated by shearing deformations. Thus, the generalized stiffness K^*_2 associated with the second degree of freedom q_2 is

$$K^*_2 = A'G \int_0^L [\phi'(x)]^2 dx. \quad \text{Equation 5-12}$$

Evaluation of this integral gives

$$K^*_2 = A'G \frac{\pi^2}{2L}. \quad \text{Equation 5-13}$$

For purposes of this study, K^*_1 is called k_{walls} , K^*_2 is called k_{diaph} , M^*_1 is called m_{walls} , and M^*_2 is called m_{diaph} . These generalized mass and stiffness values fully describe a 2DOF dynamic system.

5.1.3 General Expressions for Response

To arrive at general expressions describing the spectral response of a 2DOF system, it is useful to consider the ratios of the generalized mass and

stiffness values (Equation 5-3, Equation 5-8, Equation 5-11, and Equation 5-13) corresponding to degrees of freedom q_1 and q_2 .

$$\alpha \equiv \frac{K^*_2}{K^*_1} = \frac{k_{diaph}}{k_{walls}}$$

Equation 5-14

$$\beta \equiv \frac{M^*_2}{M^*_1} = \frac{m_{diaph}}{m_{walls}}$$

The governing differential equation of motion for an undamped MDOF system is

$$\mathbf{M} \ddot{\mathbf{u}} + \mathbf{K} \mathbf{u} = \mathbf{0} .$$

Equation 5-15

For the generalized 2DOF system developed here, the stiffness matrix is

$$\mathbf{K} = \begin{Bmatrix} (k_{walls} + k_{diaph}) & -k_{diaph} \\ -k_{diaph} & k_{diaph} \end{Bmatrix} \text{ or,}$$

Equation 5-16

$$\mathbf{K} = \begin{Bmatrix} (1/\alpha + 1) & -1 \\ -1 & 1 \end{Bmatrix} \alpha k_{walls} .$$

Equation 5-17

The mass matrix is

$$\mathbf{M} = \begin{Bmatrix} m_{walls} & 0 \\ 0 & m_{diaph} \end{Bmatrix} \text{ or,}$$

Equation 5-18

$$\mathbf{M} = \begin{Bmatrix} 1 & 0 \\ 0 & \beta \end{Bmatrix} m_{walls} .$$

Equation 5-19

The corresponding modal matrix of the system is

$$\mathbf{\Phi} = \begin{Bmatrix} \phi_1 & \phi_2 \end{Bmatrix} = \begin{Bmatrix} \phi_{11} & \phi_{12} \\ \phi_{21} & \phi_{22} \end{Bmatrix} .$$

Equation 5-20

Dynamic response of these types of buildings is dominated by the fundamental mode (Cohen 2001, Cohen *et al.* 2002a, Jain and Jennings 1984, Tremblay and Steimer 1995). For that reason, this analysis considers only that mode. After

arbitrarily assigning the diaphragm DOF a fundamental modal amplitude of $\phi_{21} = 1$, the corresponding amplitude of the shear-wall DOF can be shown to be

$$\phi_{11} = \frac{\alpha - \gamma^2 \beta}{\alpha} . \quad \text{Equation 5-21}$$

The fundamental mode shape thus becomes

$$\underline{\phi}_1 = \left\{ \begin{array}{c} \left(\frac{\alpha - \gamma^2 \beta}{\alpha} \right) \\ 1 \end{array} \right\} . \quad \text{Equation 5-22}$$

Contribution of the fundamental mode to the total distribution of inertial mass is

$$\underline{s}_1 = \Gamma_1 \mathbf{M} \underline{\phi}_1 , \quad \text{Equation 5-23}$$

where the scalar Γ_1 is

$$\Gamma_1 = \frac{\underline{\phi}_1^T \mathbf{M} \begin{Bmatrix} 1 \\ 1 \end{Bmatrix}}{\underline{\phi}_1^T \mathbf{M} \underline{\phi}_1} . \quad \text{Equation 5-24}$$

Specific contributions of inertial mass to each DOF are

$$\underline{s}_1 = \begin{Bmatrix} s_1 \\ s_2 \end{Bmatrix} = \begin{Bmatrix} s_{walls} \\ s_{diaph} \end{Bmatrix} = m_{walls} \begin{Bmatrix} \phi_{11} \frac{\phi_{11} + \beta}{\phi_{11}^2 + \beta} \\ \beta \frac{\phi_{11} + \beta}{\phi_{11}^2 + \beta} \end{Bmatrix} . \quad \text{Equation 5-25}$$

Similarly, inertial forces are

$$\underline{f}_1 = \begin{Bmatrix} f_1 \\ f_2 \end{Bmatrix} = \begin{Bmatrix} f_{walls} \\ f_{diaph} \end{Bmatrix} = S_a m_{walls} \begin{Bmatrix} \phi_{11} \frac{\phi_{11} + \beta}{\phi_{11}^2 + \beta} \\ \beta \frac{\phi_{11} + \beta}{\phi_{11}^2 + \beta} \end{Bmatrix} , \quad \text{Equation 5-26}$$

where S_a is the spectral acceleration defined at the fundamental frequency ω_1 .

Finally, the spectral displacements \underline{u}_1 are

$$\underline{u}_1 = \Gamma_1 \underline{\phi}_1 S_d = \Gamma_1 \underline{\phi}_1 \frac{S_a}{\omega_1^2} \quad \text{or,} \quad \text{Equation 5-27}$$

$$\underline{u}_1 = \begin{Bmatrix} u_1 \\ u_2 \end{Bmatrix} = \begin{Bmatrix} u_{walls} \\ u_{diaph} \end{Bmatrix} = \frac{S_a}{\omega_1^2} \frac{\phi_{11} + \beta}{\phi_{11}^2 + \beta} \begin{Bmatrix} \phi_{11} \\ 1 \end{Bmatrix}. \quad \text{Equation 5-28}$$

Where, the fundamental frequency is

$$\omega_1 = \gamma \sqrt{\frac{k_{walls}}{m_{walls}}} \quad \text{Equation 5-29}$$

and γ can be shown to be

$$\gamma = \sqrt{\frac{1}{2\beta} \left[\beta + \alpha\beta + \alpha + \left(\beta^2 + 2\alpha\beta^2 - 2\alpha\beta + \alpha^2\beta^2 + 2\alpha^2\beta + \alpha^2 \right)^{1/2} \right]}. \quad \text{Equation 5-30}$$

5.2 Implementation of Two-Degree-of-Freedom Idealization to Low-Rise Reinforced Masonry Buildings with Flexible Diaphragms

Spectral responses depend on the accuracy with which the mass and stiffness associated with degrees of freedom q_1 and q_2 can be approximated. So, to test the accuracy of the 2DOF analysis tool it was useful to examine the sensitivity of the above response expressions to variations in their variables.

5.2.1 Parametric Sensitivity of Response

To examine this, it was useful to express the degree-of-freedom stiffness and mass ratios, α and β , as simple expressions involving the: plan aspect ratio of the building; vertical aspect ratio of the in-plane shear walls; masonry wall mass; diaphragm mass; masonry wall stiffness; and diaphragm stiffness. Equation 5-3

and Equation 5-11 give the degree-of-freedom masses. The ratio of those expressions is

$$\beta = \frac{5(\gamma_{walls} VAR + \gamma_{diaph})}{4\gamma_{walls} \left(\frac{VAR}{PAR} + VAR \right) + 10\gamma_{diaph}}, \quad \text{Equation 5-31}$$

where

VAR = vertical aspect ratio of the in-plane shear walls, H/B ;

PAR = plan aspect ratio of diaphragm, L/B ;

γ_{walls} = mass per square foot of walls attached to diaphragm; and

γ_{diaph} = mass per square foot of diaphragm.

Also, the mass of the wall degree of freedom m_{walls} is

$$m_{walls} = \frac{2}{5}\gamma_{walls}H(B+L) + \gamma_{diaph}BL, \quad \text{Equation 5-32}$$

where

H = vertical dimension of building;

B = transverse dimension of building; and

L = longitudinal dimension of building.

Similarly, Equation 5-8 and Equation 5-13 are the degree-of-freedom stiffnesses.

The ratio of those expressions is

$$\alpha = \frac{G_{diaph} t_{diaph}}{E_{walls} t_{walls}} \frac{VAR}{PAR} \left\{ \frac{96}{\pi^2} VAR^2 + 5 \right\}, \quad \text{Equation 5-33}$$

where

E_{walls} = elastic modulus of masonry walls;

G_{diaph} = effective shear modulus of diaphragm;

t_{walls} = effective thickness of in-plane shear walls; and

t_{diaph} = effective thickness of diaphragm.

It was only meaningful, however, to investigate the response of typical low-rise reinforced masonry buildings. In other words, practical maximum and minimum values, or parametric limits, of Equation 5-31 and Equation 5-33 needed to be identified. To do this, domains of the constituent variables in Equation 5-31 and Equation 5-33 were identified which subsequently identified the practical range, or parametric limits, of the equations themselves.

Typical construction practice explicitly identified some of the domains, and the scope of this work implicitly identified others. For example, typical masonry construction practice explicitly defined maximum and minimum values for the masonry wall mass, γ_{walls} . Conversely, the fact that this work involves low-rise masonry buildings with high plan aspect ratios implicitly specified that the plan aspect ratio, PAR , should be less than five and the vertical aspect ratio, VAR , should be less than two.

A variety of sources provided the necessary data. The *NEHRP Guidelines for the Seismic Rehabilitation of Buildings* (FEMA 273/274) documents provided information regarding wood diaphragm stiffness and masonry stiffness. Although, those guidelines have since been combined and updated as FEMA 356, the former documents were the latest available when this work was done. The Steel Deck Institute *Diaphragm Design Manual* (1981, 1995) provided information regarding metal-deck diaphragm stiffness. *Masonry Structures Behavior and Design* (Drysdale et al. 1999), *The Reinforced Masonry Handbook* (Amrhein 1983), and the Masonry Standards Joint Committee 2000 provisions (MSJC 2000) provided general information on typical masonry construction. Table 5-1 summarizes the results of that assessment.

Table 5-1 Parametric limits of variables affecting response

Parameter	Symbol	Maximum	Minimum
Wall mass	γ_{walls}	210 psf	26 psf
Wall elastic modulus	E_{walls}	2750 ksi	165 ksi
In-plane wall thickness	t_{walls}	11.6 in.	3.4 in.
Diaphragm mass	γ_{diaph}	200 psf	5 psf
Diaphragm shear stiffness	$G_{diaph} t_{diaph}$	450 k/in.	0.40 k/in.
Vertical aspect ratio	VAR	2	1/10
Plan aspect ratio	PAR	5	1

It should be noted, however, that the complex mechanisms contributing to diaphragm flexibility preclude the explicit definition of a diaphragm shear modulus and effective diaphragm thickness. Instead, diaphragm stiffness calculations generally involve the parameter shown in Table 5-1 for “Diaphragm shear stiffness.” The shear rigidity, $A'G$, of a diaphragm is instead characterized by $G'B$, where B is the width of the diaphragm and G' is an effective quantity defined as the effective product of the material shear modulus and diaphragm thickness (Gt).

Evaluation of Equation 5-31 and Equation 5-33 over the range of values in Table 5-1 eventually identified the parametric limits of α and β . To that end, the DOF mass ratio, β , was evaluated as a function of the vertical and plan aspect ratios over four combinations of wall and diaphragm mass:

- high-mass walls and high-mass diaphragms;
- high-mass walls and low-mass diaphragms;
- low-mass walls and high-mass diaphragms; and
- low-mass walls and low-mass diaphragms.

Similarly, the DOF stiffness ratio, α , was evaluated as a function of the vertical and plan aspect ratios over four combinations of maximum and minimum wall and diaphragm stiffness:

- high-stiffness walls and high-stiffness diaphragms;
- high-stiffness walls and low-stiffness diaphragms;
- low-stiffness walls and high-stiffness diaphragms; and
- low-stiffness walls and low-stiffness diaphragm.

Figure 5.2 and Figure 5.3 show results of those evaluations.

Figure 5.2 shows that the degree-of-freedom mass ratio varies from about 0.5 to about 1.0, and is therefore taken here as such. Figure 5.3 shows that the diaphragm DOF may indeed be significantly stiffer than the wall DOF. That implication, however, prohibits classifying the diaphragm as “flexible.” A diaphragm is generally considered flexible if, when subjected to lateral load, its in-plane deflection at mid-span is at least twice that of its supporting in-plane shear walls. This particular criterion imposed an additional parametric limitation on the DOF stiffness ratio, α .

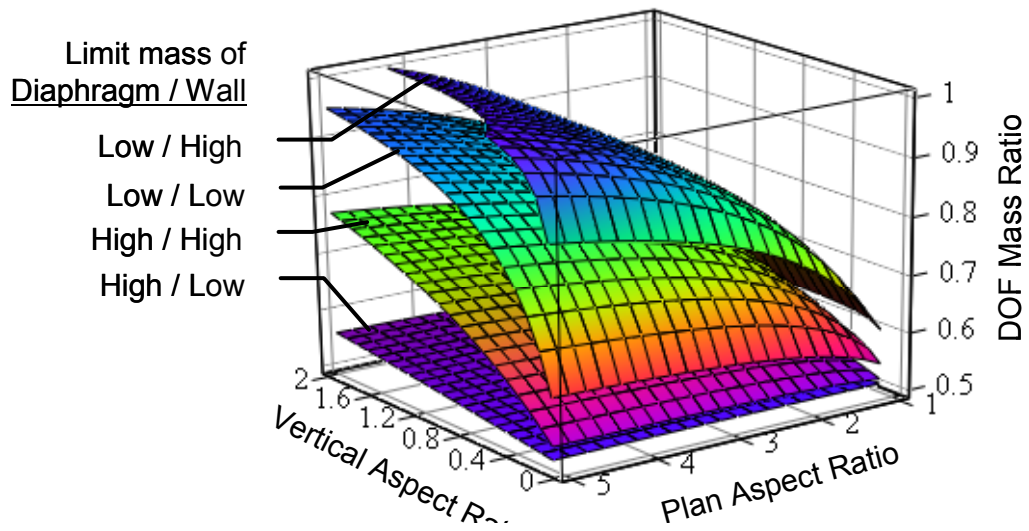


Figure 5.2 Degree-of-freedom mass ratio, β , for four different combinations of maximum and minimum wall mass and diaphragm mass

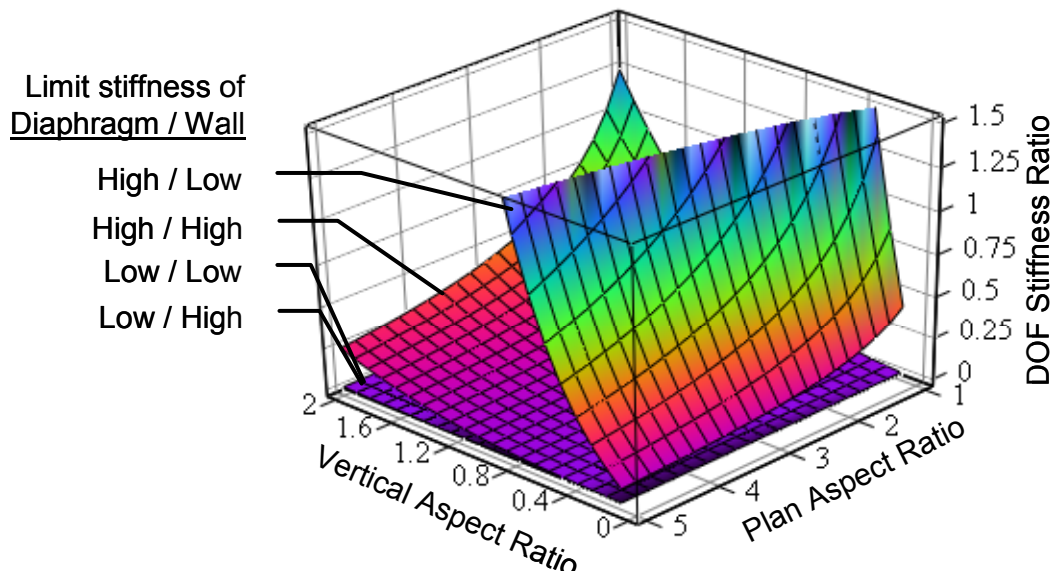


Figure 5.3 Degree-of-freedom stiffness ratio, α , over four different combinations of maximum and minimum wall stiffness and diaphragm stiffness

To examine this further, the general expression for DOF displacements (Equation 5-28) was configured to provide the ratio of the diaphragm DOF displacement to the wall DOF displacement. That expression showed that for the displacement ratio to exceed two, the DOF stiffness ratio α must be less than about 0.5. Therefore, the DOF stiffness ratio, α , is taken here between 0.0 and 0.5.

The spectral responses of a 2DOF system were then examined over $0.0 \leq \alpha \leq 0.5$ and $0.5 \leq \beta \leq 1.0$. Of particular interest were: the fundamental frequency modification factor, γ (Equation 5-30); the effective diaphragm DOF inertia force, f_{diaph} (Equation 5-26); and the diaphragm DOF displacement, u_{diaph} (Equation 5-28).

To study these expressions in the general case, the latter two were redefined as dimensionless parameters. The effective DOF inertia forces were non-dimensionalized by dividing the expression by the spectral acceleration, S_a , and the wall DOF mass, m_{walls} . These dimensionless inertia forces are mass participation factors.

$$\underline{PF}_1 = \begin{Bmatrix} PF_1 \\ PF_2 \end{Bmatrix} = \begin{Bmatrix} PF_{walls} \\ PF_{diaph} \end{Bmatrix} = \begin{Bmatrix} \phi_{11} \frac{\phi_{11} + \beta}{\phi_{11}^2 + \beta} \\ \beta \frac{\phi_{11} + \beta}{\phi_{11}^2 + \beta} \end{Bmatrix}. \quad \text{Equation 5-34}$$

Similarly, the DOF displacements were non-dimensionalized by dividing the expression by the spectral displacement, S_d . These dimensionless displacements are displacement amplification factors;

$$\underline{d}_1 = \begin{Bmatrix} d_1 \\ d_2 \end{Bmatrix} = \begin{Bmatrix} d_{walls} \\ d_{diaph} \end{Bmatrix} = \frac{\phi_{11} + \beta}{\phi_{11}^2 + \beta} \begin{Bmatrix} \phi_{11} \\ 1 \end{Bmatrix}. \quad \text{Equation 5-35}$$

Figure 5.4 through Figure 5.6 show the three non-dimensional response expressions over $0.0 \leq \alpha \leq 0.5$ and $0.5 \leq \beta \leq 1.0$.

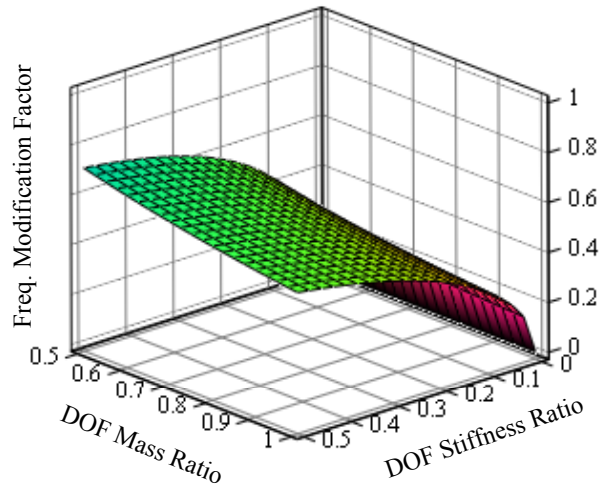


Figure 5.4 Fundamental frequency modification factor, γ

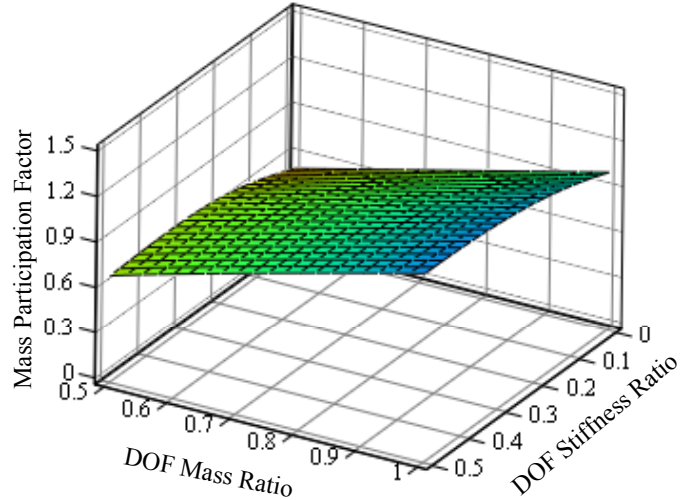


Figure 5.5 Diaphragm degree of freedom mass participation factor, PF

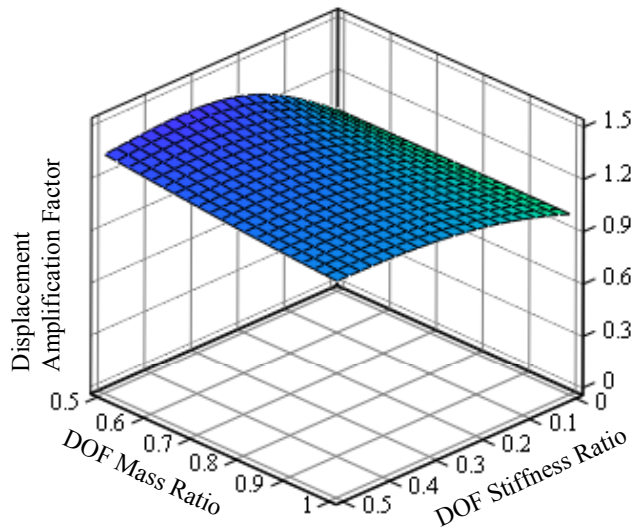
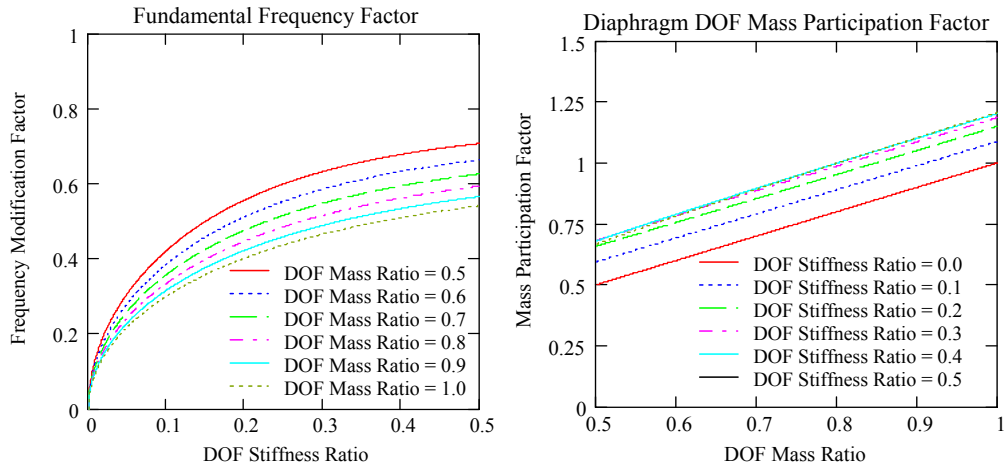
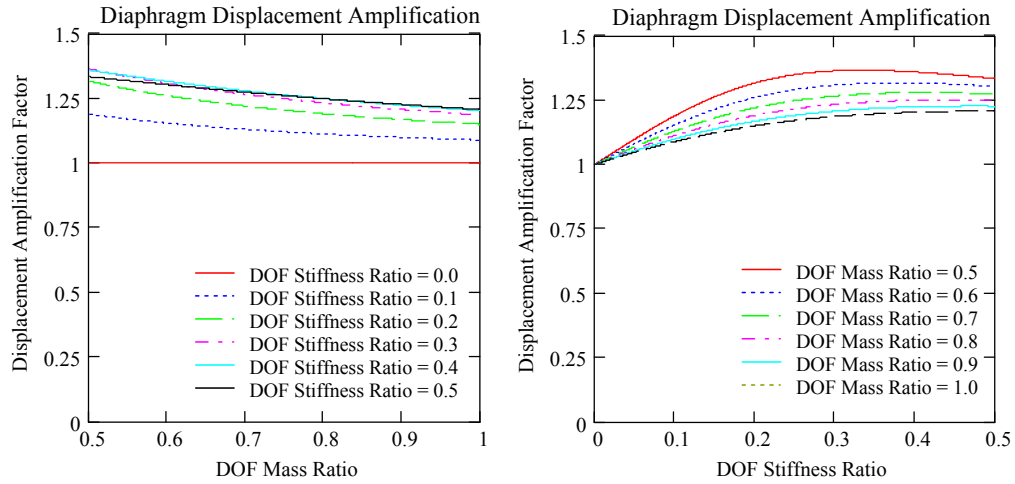


Figure 5.6 Diaphragm spectral displacement amplification factor, d

Figure 5.4 shows that the fundamental frequency modification factor, γ , is chiefly sensitive to change in the DOF stiffness ratio, α . Figure 5.5 shows that the diaphragm DOF mass participation factor, PF_2 , is chiefly sensitive to changes in the DOF mass ratio, β . Figure 5.6 shows that the diaphragm DOF displacement amplification factor, d_2 , is not very sensitive to changes in either the DOF mass or stiffness ratio. These observations are alternatively evident in Figure 5.7.



a) Frequency modification factor b) Diaphragm participation factor



c) Diaphragm displacement amplification factor

Figure 5.7 Two-dimensional slices of Figure 5.4 through Figure 5.6

5.2.2 Implications of Parameter Study

Over the range of probable buildings ($0.0 \leq \alpha \leq 0.5$ and $0.5 \leq \beta \leq 1.0$) Figure 5.5, Figure 5.6, and Figure 5.7 show that the response parameters PF and d do not deviate significantly (less than 35 %) from those of a single-degree-of-

freedom (SDOF) system, when that degree of freedom is associated with in-plane response of the diaphragm.

For a SDOF system, PF_2 and d_2 are unity. That is, the DOF inertia force is exactly the product of spectral acceleration and DOF mass, and DOF displacement is exactly the spectral displacement; there is no modal amplification of response. The former is evident in Figure 5.7b by the observation that the limiting cases of degree-of-freedom stiffness ratios of zero (SDOF system, rigid in-plane shear walls) and 0.5 (maximum modal participation) only differ by 35 %. The latter is similarly evident in Figure 5.7c simply by the observation that no values exceed 1.35.

These observations imply that low-rise reinforced masonry buildings with flexible diaphragms may in fact be accurately idealized as SDOF systems, with those single degrees of freedom associated with response of the diaphragm. This point and how it is useful to design, analysis, evaluation, and rehabilitation are examined further in later sections of this dissertation.

5.3 Verification of Two-Degree-of-Freedom Idealization for Low Levels of Response (Linear Elastic)

Accuracy of the 2DOF and SDOF analysis tools in the linear elastic range of response was verified by applying them to the analysis of the two, half-scale shaking-table specimens and of four, hypothetical prototypical finite-element building models.

5.3.1 Shaking-Table Specimens

The tool was implemented using the two, half-scale shaking-table specimens to verify the accuracy of the 2DOF analysis tool and as part of a previous study. Details of this are discussed by Cohen (2001) and are not

repeated here. As part of this study, however, the two specimens were also idealized as SDOF systems, with that degree of freedom associated with response of the diaphragm. DOF mass and stiffness are given by Equation 5-11 and Equation 5-13. Table 5-2 summarizes results from the analyses and show that both the 2DOF and SDOF idealizations are reasonably accurate; calculated periods, accelerations, and displacements agree well with measured responses.

Table 5-2 Calculated and measured peak responses of Specimens #1 and #2 from 2DOF and SDOF idealizations

Specimen	Model	Fundamental Period, sec	Diaphragm acceleration, g	Diaphragm displacement, in.
1 (lumber)	Measured	0.071 sec	1.6	0.12
	2DOF	0.085 sec	$S_a = 1.5$	0.11
	SDOF	0.082 sec	$S_a = 1.5$	0.10
2 (metal)	Measured	0.083 sec	1.2	0.12
	2DOF	0.095 sec	$S_a = 1.3$	0.12
	SDOF	0.092 sec	$S_a = 1.3$	0.11

5.3.2 Hypothetical Prototypical Finite-Element Building Models

Four, linear elastic finite-element models of hypothetical prototypical low-rise reinforced masonry buildings with flexible diaphragms (Table 5-3) were created using SAP2000 (1999), to further verify the accuracy and usefulness of the 2DOF and SDOF analysis tools. Figure 5.8 and Figure 5.9 respectively show models VM1 Metal and VM2 Metal (similar to VM1 Wood and VM2 Wood), and illustrate that the models also included door and window openings in the reinforced masonry walls.

Table 5-3 Finite-element models for verification of 2DOF and SDOF analysis

General Property	VM1		VM2	
Plan Footprint	187.5 ft x 75 ft		100 ft x 100 ft	
Height*	18 ft		32 ft	
Plan Aspect Ratio	2.5		1	
Masonry Walls	CMU and brick cavity wall		CMU barrier wall	
Weight of Walls	100 psf		74 psf	
Openings	On three sides		On two sides	
Interior Columns	Steel tube shapes		Steel wide-flanges	
Diaphragm surface mass for analysis	20 psf		20 psf	
Specific Property	VM1 Wood	VM1 Metal	VM2 Wood	VM2 Metal
Diaphragm	Straight lumber sheathing with panel overlay	1.5B20 screw-connected	Diagonal lumber sheathing	1.5B22 welded
Roof framing	Glu-lam rafters and girders	Open-web steel joists and girders	Dimension rafters and Glu-lam girders	Open-web steel joists and girders

* Includes 4 ft parapet

The finite-element models, the 2DOF idealizations representing them, and the SDOF idealizations representing them, were arbitrarily analyzed using a uniform 1-g acceleration response spectrum. All predicted similar fundamental frequencies (Table 5-4) and diaphragm displacements. The latter, however, exhibited greater variation as a result of the relationship between spectral acceleration, S_a , and pseudo-spectral displacement, S_d (Equation 5-27). Errors in the approximate natural frequencies manifested themselves as increased errors in the predicted approximate displacements. Nevertheless, these analyses demonstrated the accuracy of the 2DOF, and more important, the SDOF analysis tools.

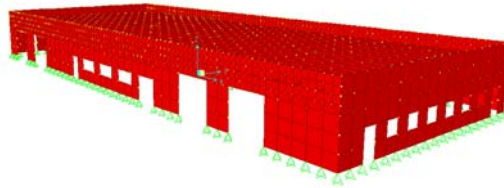


Figure 5.8 Finite-element verification model, VM1 Metal

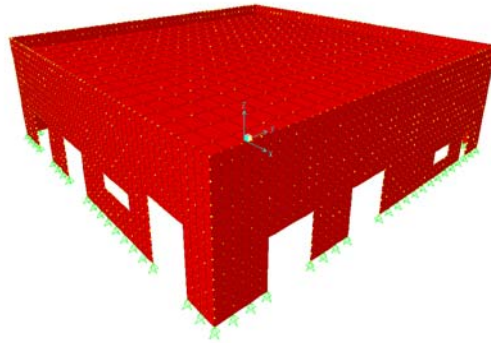


Figure 5.9 Finite-element verification model, VM2 Metal

Table 5-4 Comparison of responses from finite-element modeling, 2DOF modeling, and SDOF modeling

Quantity	Units	Analysis	VM1		VM2	
			Wood	Metal	Wood	Metal
α	-	-	0.0009	0.0014	0.0130	0.0007
β			0.658	0.658	0.561	0.561
T	sec	FEM	0.98	0.86	0.31	0.71
T		2DOF	1.04	0.86	0.21	0.90
T		SDOF	1.04	0.86	0.21	0.89
u_{diaph}	in.	FEM	12.8	9.91	0.51	6.91
u_{diaph}		2DOF	10.6	7.25	0.46	7.90
u_{diaph}		SDOF	10.8	7.26	0.44	7.79

5.3.3 Comparison With an Existing Period Expression (FEMA 356)

The *Prestandard and Commentary for the Seismic Rehabilitation of Buildings* FEMA 356 (2000) provides an approximate period expression for low-rise buildings with flexible diaphragms. That equation (FEMA Equation 3-8) is based on the Raleigh method:

$$T = \sqrt{0.1 \cdot \Delta_w + 0.078 \cdot \Delta_d}, \quad \text{Equation 5-36}$$

where, from that document,

T = fundamental period of building in direction under consideration;

Δ_w = deflection of in-plane shear walls, in inches, resulting from a lateral load, in the direction under consideration, equal to the weight tributary to the diaphragm; and

Δ_d = deflection of diaphragm relative to tops of in-plane shear walls, in inches, resulting from a lateral load, in the direction under consideration, equal to the weight tributary to the diaphragm.

Commentary to FEMA 356 provides a complete discussion of the equation and specific definitions of its variables. As a comparison, the FEMA equation, here listed as Equation 5-36, was evaluated in the context of a 2DOF idealization representing the finite-element models VM1 and VM2. The independent variables of the equation, Δ_w and Δ_d , were evaluated as follows:

1. A weight tributary to the diaphragm was assumed and applied as a lateral force;
2. the wall and diaphragm deflections were calculated using the equations for degree-of-freedom stiffnesses, Equation 5-8 and Equation 5-13; and
3. the building period was calculated using Equation 5-36.

The FEMA document, however, does not provide guidance for the calculation of the “weight tributary to the diaphragm” (Step 1). That value was therefore calculated using two techniques. The first technique assumed that the entire weight of the diaphragm and one-half the weight of the supporting longitudinal walls were tributary to the diaphragm. The second technique assumed that one-half the weight of the diaphragm and one-quarter the weight of the longitudinal walls were tributary to the diaphragm. This second technique provides a value of mass that is mathematically identical value to that of the diaphragm degree of freedom (Equation 5-11).

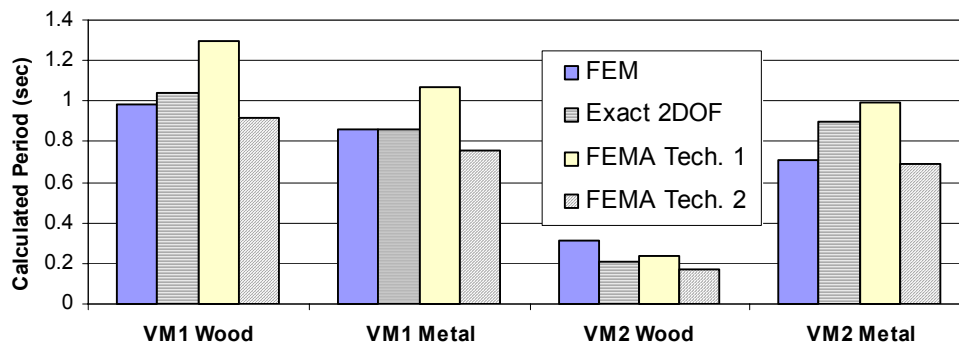


Figure 5.10 Calculated periods of hypothetical prototypical building models

Figure 5.10 compares the periods calculated by finite-element modeling, two-degree-of-freedom analysis, and FEMA 356 Equation 3-8. The table shows that the FEMA expression for the fundamental period of a low-rise building with a flexible diaphragm is reasonably accurate.

5.4 Verification of Two-Degree-of-Freedom Idealization for High Levels of Response (Nonlinear)

Nonlinear lumped-parameter models were created and tested using the program CANNY (1999) to verify that nonlinear responses of low-rise buildings could be reasonable approximated using a 2DOF idealization.

5.4.1 General Approach and Model Development

The program CANNY has a suite of analysis elements and hysteresis models. From that suite, four-noded eight-degree-of-freedom panel elements were selected for analysis. Those elements have four available deformation mechanisms (Figure 5.11), each governed by an appropriate hysteresis model. The shaking-table specimens were idealized using two elements; one representing the wall degree of freedom, and one representing the diaphragm degree of freedom (Figure 5.1 and Figure 5.11).

Spring stiffnesses for the wall elements used the measured elastic moduli of the specimen masonry and, to be consistent with experimental observations (Cohen 2001 and Cohen *et al.* 2002a), linear elastic hysteresis models. Axial and flexural spring stiffnesses for the diaphragm elements were assigned high values to specifically characterize the observation that flexible diaphragms deform primarily in shear. This effectively reduced the number of active degrees of freedoms to two, one associated with in-plane response of the walls and one associated with in-plane response of the diaphragm.

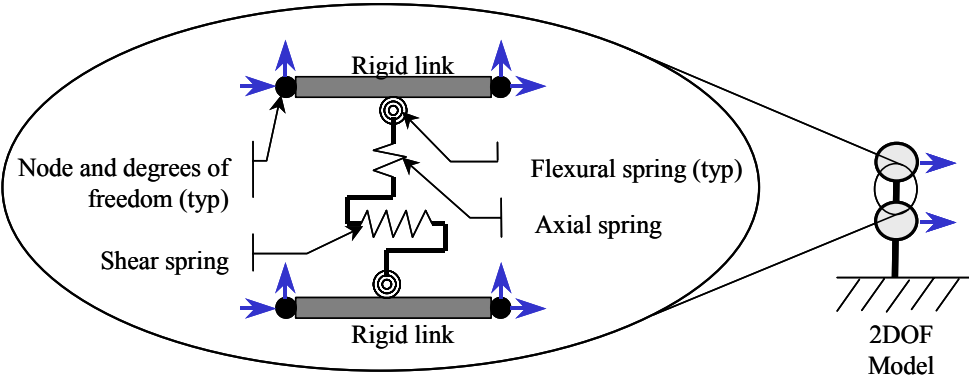


Figure 5.11 Schematic of lumped-parameter panel element and 2DOF model

Hysteretic models governing the diaphragm shear springs were based on measured responses of the two shaking-table specimens. Those models, as well

as how test-to-test accumulation of damage was accounted for, were different in the models representing Specimen #1 and Specimen #2, and are now discussed.

5.4.2 Modeling of Shaking-Table Specimen #1 (Lumber)

Damage in lumber assemblies increases only with increasing maximum levels of deformation; damage does not typically increase with cyclic constant-level deformations. Although visibly damaged pieces of sheathing and roof joist were removed, replicated, and replaced prior to quasi-static testing, the diaphragm still embodied some damage and therefore also a degraded stiffness. This explains why stiffness degradation was not observed during quasi-static testing until the diaphragm-masonry chord assembly was deformed to DDRs roughly equal to those sustained during seismic testing – in this case, 0.7 %. Since the nonlinear modeling discussed in this study intended to investigate specimen behavior at deformation levels consistent with those observed during seismic tests, it was useful to evaluate the lateral stiffness of Specimen #1's roof diaphragm during the seismic tests themselves.

That evaluation used measured acceleration and displacement values at the roof diaphragm level as well as the diaphragm degree-of-freedom mass (Equation 5-11), to arrive at diaphragm reaction shear-DDR hysteresis loops. Diaphragm reaction shear is defined, in this study, as one-half the total effective inertial shear on the diaphragm (product of the diaphragm degree-of-freedom mass and diaphragm acceleration). Figure 5.12 shows hysteresis and backbone stiffnesses for the transverse seismic testing of Specimen #1. The relative scale of abscissa to ordinate in Figure 5.12 was deliberately maintained to clarify the degradation in lateral stiffness.

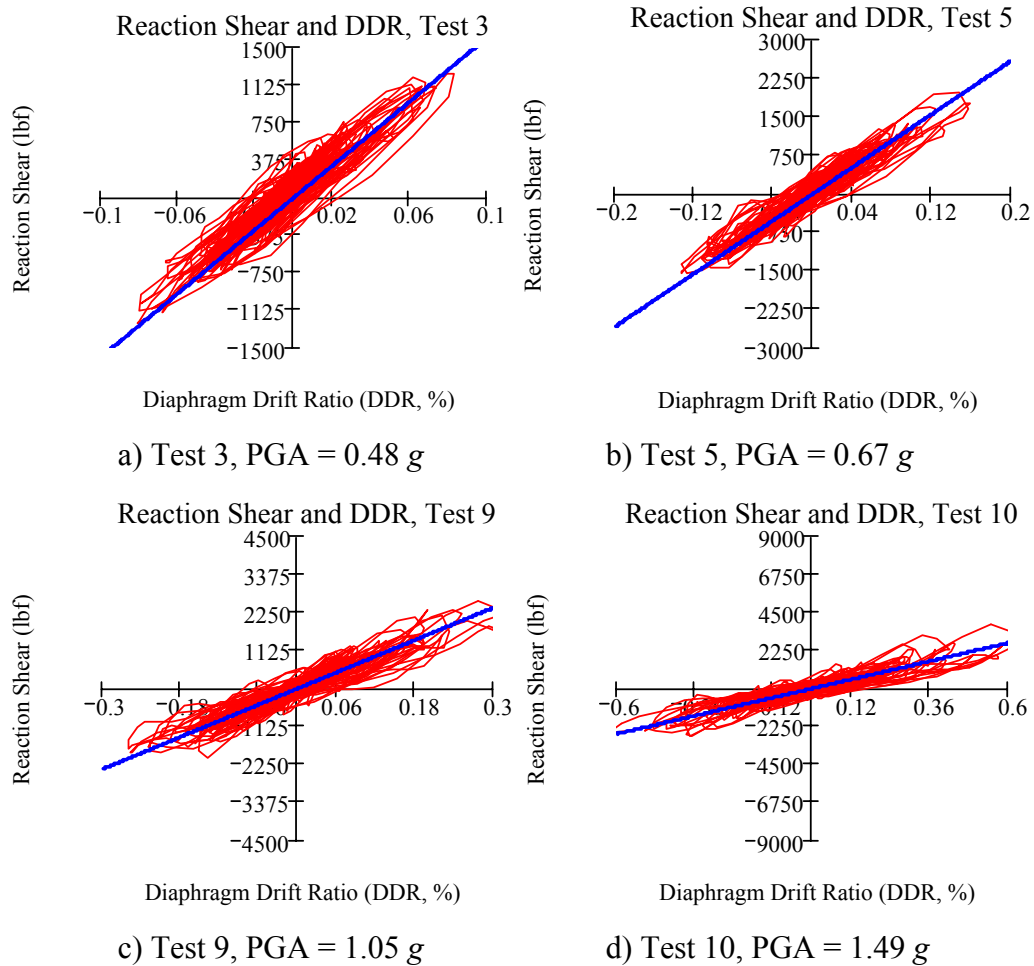


Figure 5.12 Hysteresis and backbone stiffness of Specimen #1; Seismic Tests 3, 5, 9 and 10

Figure 5.12 shows that the seismic behavior of Specimen #1 could be characterized as degrading linear elastic with Coulomb damping (friction). Coulomb damping was observed during quasi-static testing of the lumber diaphragm as well as during seismic testing. The latter is exemplified, for example, in the hysteresis of peak response for Seismic Test 9 (Figure 5.13).

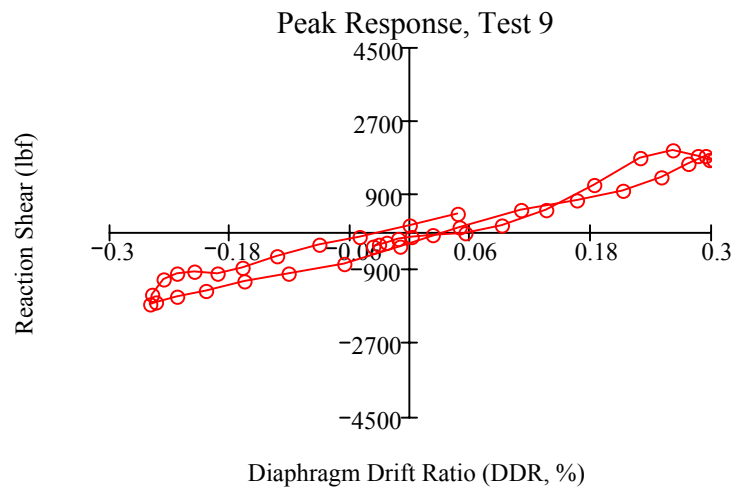
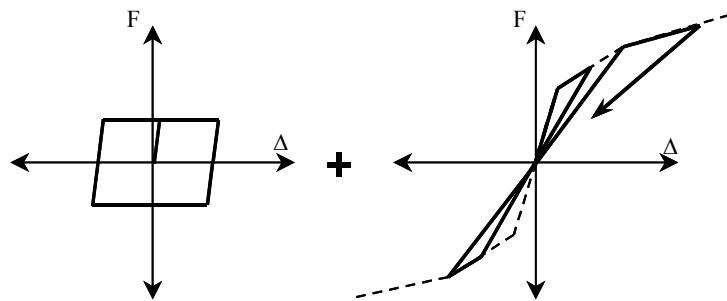


Figure 5.13 Hysteresis of peak response of Specimen #1; Test 9

The diaphragm was modeled using two elements, in parallel. Coulomb damping was modeled using an elastic-perfectly plastic element designed so that plasticity occurred at very small deformations (Figure 5.14a); therefore, the additional stiffness contributed by this element did not alter the overall frequency response of the model. Lateral stiffness and stiffness degradation was modeled using an origin-oriented degrading linear elastic element designed such that the secant stiffness of the element was defined by the previous point of maximum deformation on a tri-linear envelope curve (Figure 5.14b).



a) Coulomb damping elastic-plastic element b) Origin-oriented linear elastic element

Figure 5.14 Schematic of element hysteresis rules used to model lumber diaphragm

Modeling also accounted for test-to-test accumulation of damage. At the beginning of each analysis, the model was subjected to an artificial pulse acceleration designed to deform the model to a level consistent with the peak deformation sustained during the prior seismic test. For example, if a seismic test, say Test 1, deformed the specimen to a certain DDR then a pulse acceleration, that would deform the specimen to that same DDR, was included at the beginning of the analysis simulating Test 2. The software package used for this modeling, CANNY, would not allow each test to be run sequentially; which would have automatically accounted for the accumulation of damage.

All modeling used a Coulomb damping magnitude of 115 lb. and no equivalent viscous damping. Figure 5.15 through Figure 5.18 show results of the nonlinear modeling of Specimen #1. Note that the ordinate scales of those figures are different.

Figure 5.15 (Test 3) shows that calculated and measured displacements agree reasonably well over the majority of the time history but deviate somewhat during peak response (11 sec to 12.5 sec). Figure 5.16 and Figure 5.17 (Tests 5 and 9) show that calculated and measured displacements agree reasonably well. Figure 5.18, however, shows unsatisfactory agreement between calculated and measured displacements.

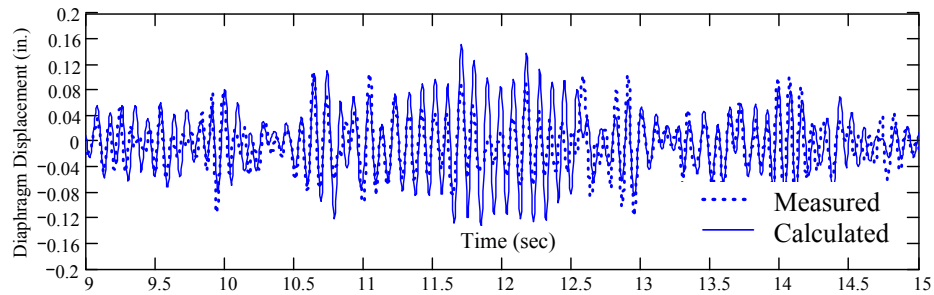


Figure 5.15 Results of nonlinear modeling of Specimen #1; Test 3

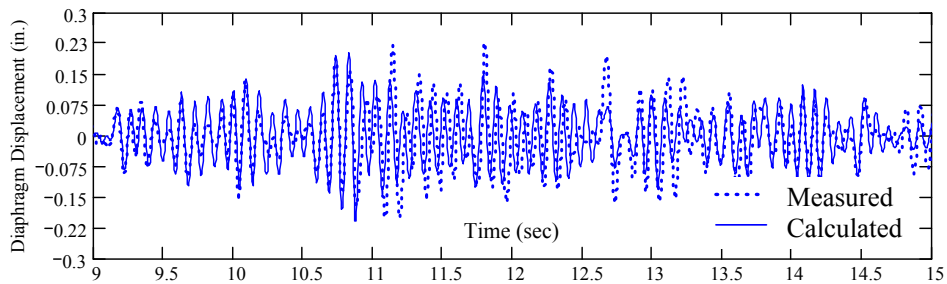


Figure 5.16 Results of nonlinear modeling of Specimen #1; Test 5

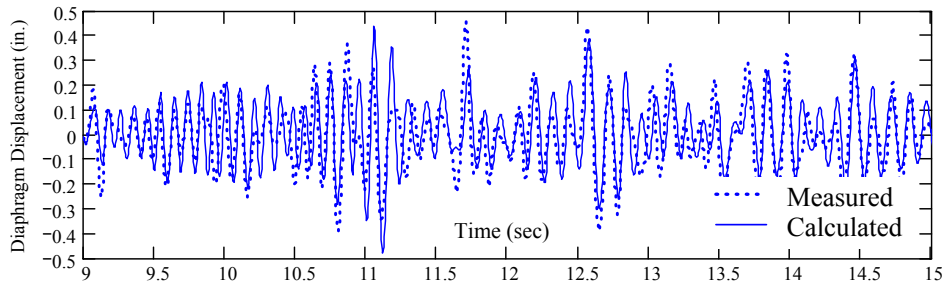


Figure 5.17 Results of nonlinear modeling of Specimen #1; Test 9

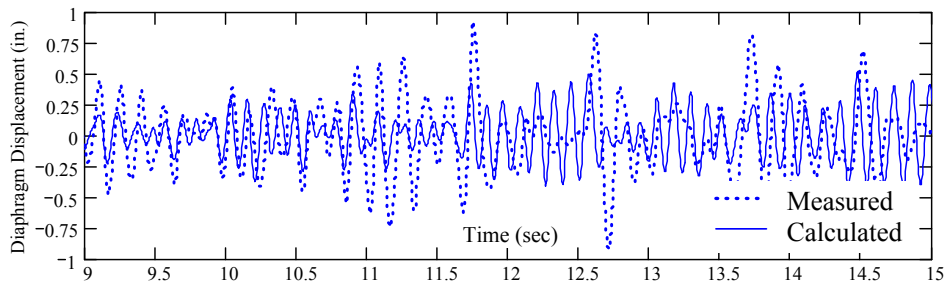


Figure 5.18 Results of nonlinear modeling of Specimen #1; Test 10

The transverse shear walls of Specimen #1 rocked during very high-level seismic testing (Cohen 2001 and Cohen *et al.* 2002a). The modeling described here used linear elastic wall elements, and did not account for such behavior, however. The observed wall rocking in Specimen #1 therefore likely explains the disagreement between calculated and measured response during Test 10 (Figure 5.18). For typical low-rise reinforced masonry buildings, like those addressed here, wall rocking does not appear to have an important contribution to response. In the case of Specimen #1, wall rocking was primarily an artifact of the specimen configuration and did not characterize typical behavior for low-rise reinforced masonry buildings. Furthermore, vertical aspect ratios of transverse walls in typical low-rise reinforced masonry buildings generally preclude wall rocking.

5.4.3 Modeling of Shaking-Table Specimen #2 (Metal-Deck)

Damage in welded metal-deck assemblies generally manifests itself as sudden failure of puddle welds and associated abrupt decreases in in-plane stiffness and strength. It also manifests itself as bearing deformation of side-lap screws into metal deck, but this is generally not detectable in lightly connected metal-deck assemblies such as that discussed here.

Specimen #2 did not sustain puddle-weld fractures as a result of transverse seismic testing (Cohen 2001 and Cohen *et al.* 2002a). The sequence of seismic tests for Specimen #2 comprised several low-level transverse tests; followed by several longitudinal tests of increasing excitation; followed by several transverse tests of increasing excitation. Rather surprisingly, the specimen sustained puddle-weld fractures as a result of strong longitudinal testing and therefore only degraded in lateral stiffness during that sequence of tests.

For that reason, the strength degrading and stiffness degrading behavior observed during quasi-static testing was not modeled. Modeling instead accounted for the observed stiffness degradation during seismic testing by using two different diaphragm stiffnesses: that before the sequence of longitudinal tests (not yet degraded in stiffness); and that after the sequence of longitudinal tests (degraded in stiffness). In the same way as discussed for Specimen #1, Figure 5.19 shows hysteresis and backbone stiffnesses for transverse seismic testing of Specimen #2. The relative scales of abscissa to ordinate in Figure 5.19 were deliberately maintained to clarify the degradation in lateral stiffness.

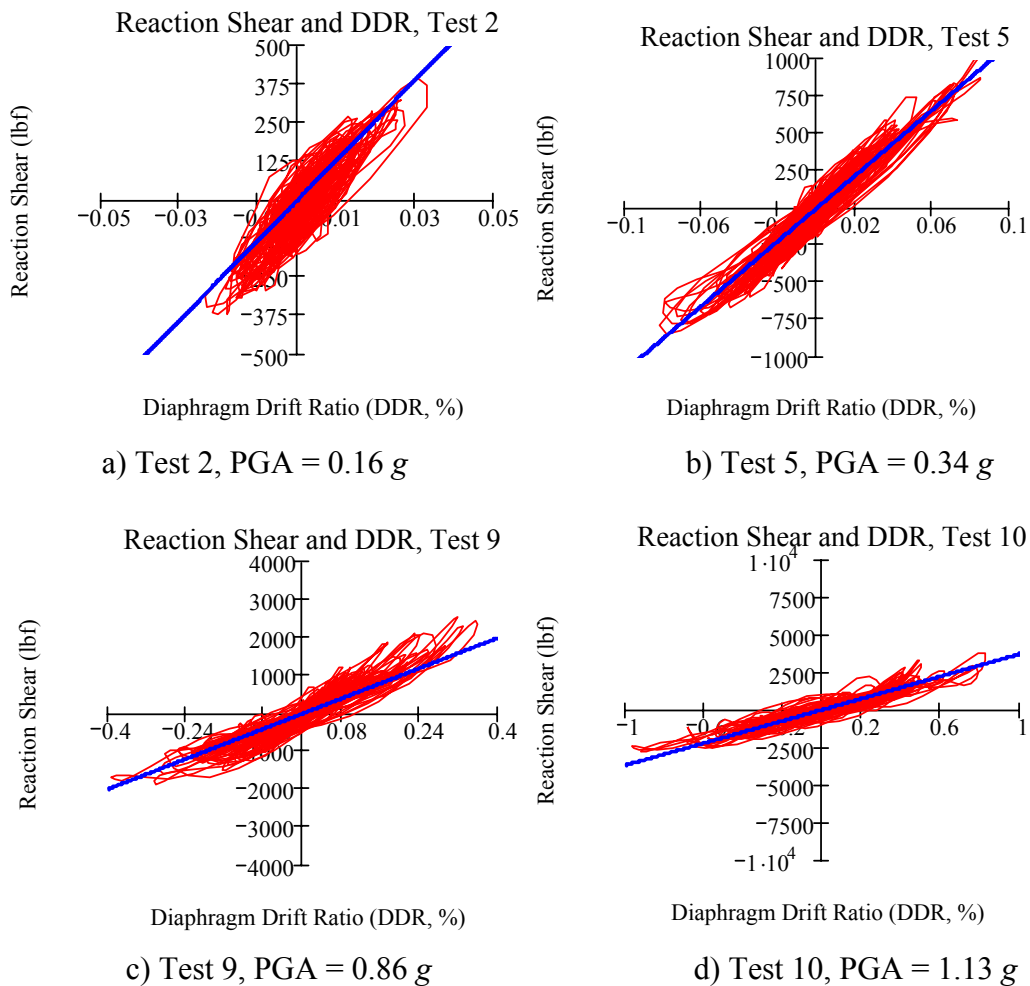


Figure 5.19 Hysteresis and backbone stiffness of Specimen #2; Tests 2, 5, 9, 10

The hysteresis of Figure 5.19a through Figure 5.19d show that the seismic behavior of Specimen #2 could be characterized as linear and elastic and, unlike that of Specimen #1, without Coulomb damping. The latter is exemplified by the individual hysteresis loop for peak response of Test 9 (Figure 5.20). For these reasons, the diaphragm of Specimen #2 was modeled as linear elastic. Analyses of Tests 5, 9, and 10 used 1.5 % equivalent viscous damping; analysis of Test 3

used 5 % equivalent viscous damping. Figure 5.21 through Figure 5.24 show results of modeling. Note that the ordinate scales of those figures are different.

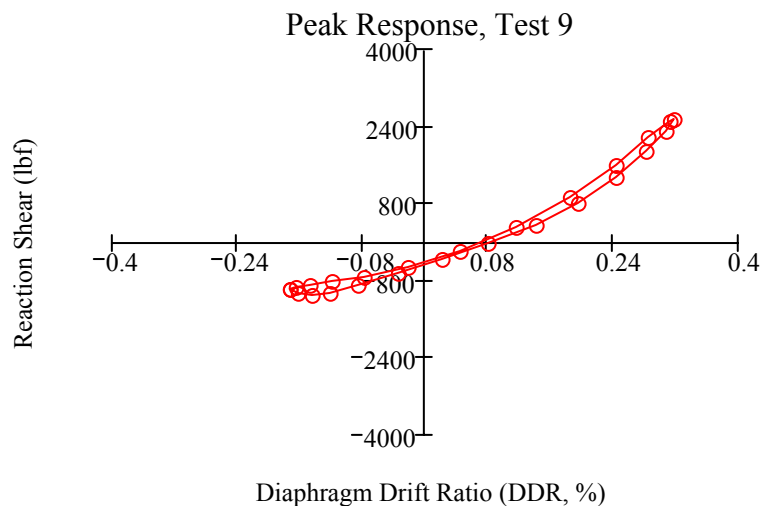


Figure 5.20 Hysteresis for peak response of Specimen #2; Test 9

Figure 5.21 (Test 2) and Figure 5.22 (Test 5) and shows that calculated and measured displacements agree reasonably well over the majority of the time history, but deviate in certain regions. Figure 5.23 (Test 9) shows significant deviation between calculated and measured displacements for the majority of the time history but shows better agreement following peak response (time greater than about 7.5 sec). Figure 5.24 (Test 10) shows that calculated and measured displacements agree reasonably well over the time history with particularly good agreement during peak response (4 sec to 6 sec).

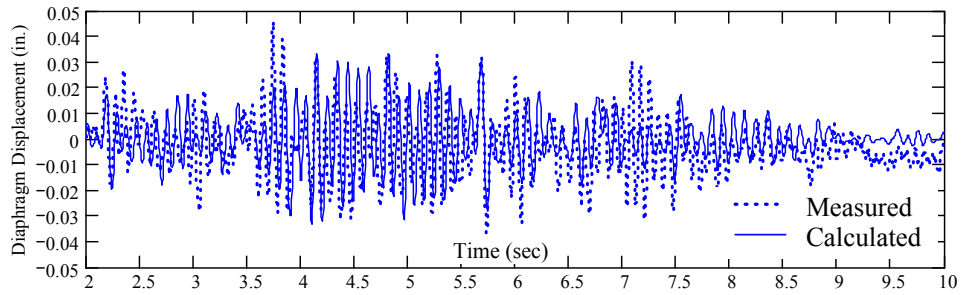


Figure 5.21 Results of nonlinear modeling of Specimen #2; Test 3

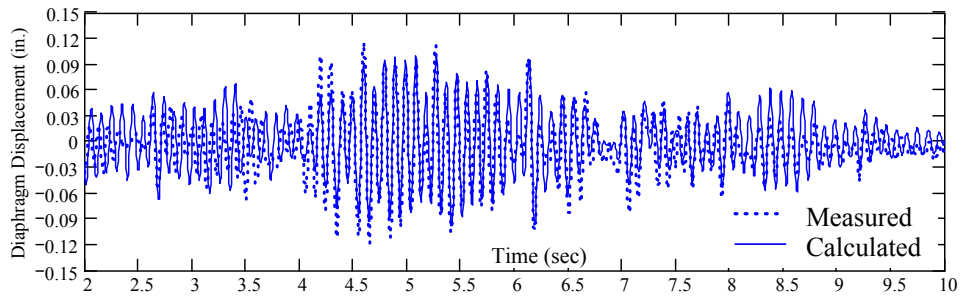


Figure 5.22 Results of nonlinear modeling of Specimen #2; Test 5

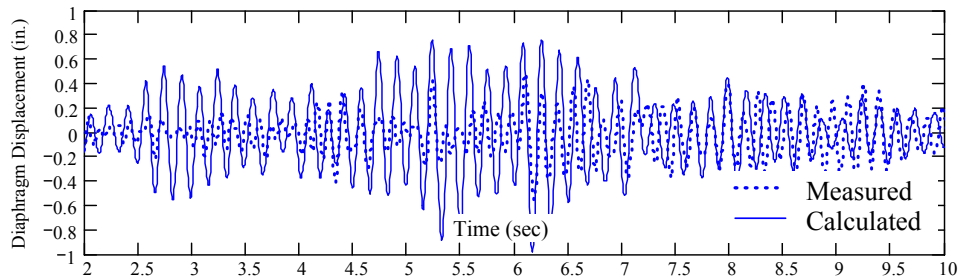


Figure 5.23 Results of nonlinear modeling of Specimen #2; Test 9

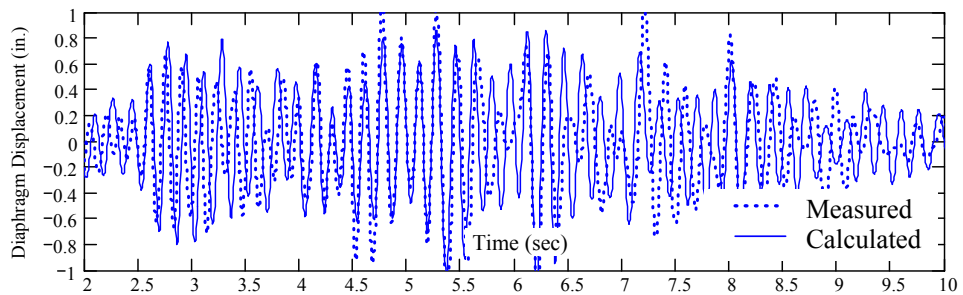


Figure 5.24 Results of nonlinear modeling of Specimen #2; Test 10

Figure 5.23 (Test 9) initially suggested that the nonlinear model of Specimen #2 was not accurate, at least for simulation of that seismic test. Recall, however, that during seismic testing of Specimen #2 the specimen was subjected to low-level transverse tests, then high-level longitudinal tests, and finally high-level transverse tests; the first of which was Seismic Test 9. Because of this, the longitudinal walls of Specimen #2 were essentially undamaged prior to Seismic Test 9. During that test, those walls sustained significant cracking consistent with their out-of-plane response and the effective lateral stiffness of the diaphragm was consequently decreased. This is not evident in Figure 5.19 because that figure shows a backbone stiffness based only on peak responses.

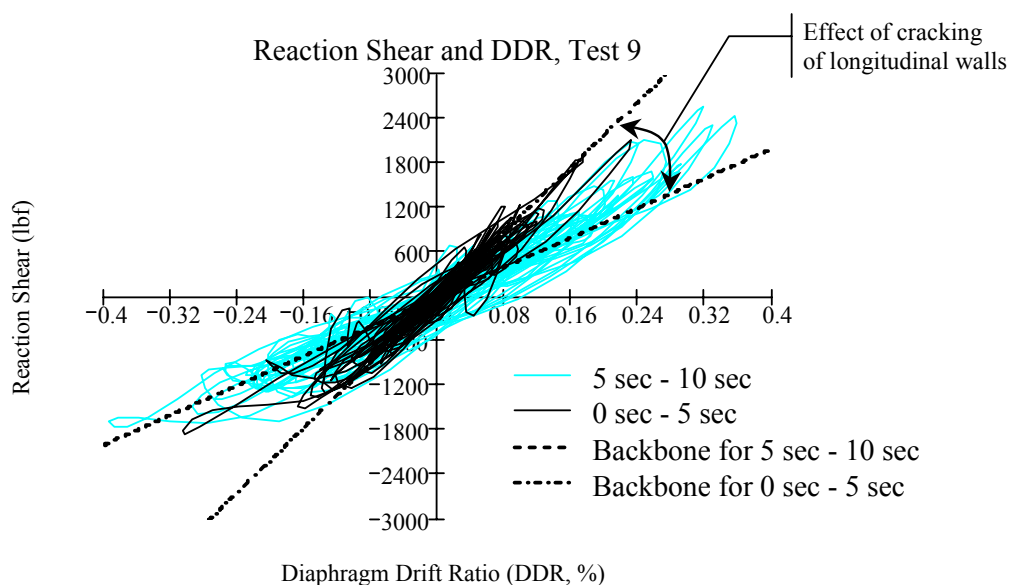


Figure 5.25 Hysteresis for Test 9 of Specimen #2

Figure 5.25, however, shows hysteresis and backbone stiffnesses for two portions of the time history of Seismic Test 9: that for 0 sec to 5 sec, and that for 5 sec to 10 sec. The difference in backbone stiffnesses of the two portions shows the effect of cracking in the longitudinal walls during the test. This potentially

explains the differences between calculated and measured responses shown in Figure 5.23. Specifically, the analytical model used a diaphragm stiffness that was consistent only with the stiffness of the specimen after the longitudinal walls had cracked (Figure 5.19).

5.5 Summary of Results, Conclusions, and Significance of Idealizations

5.5.1 Summary of Results and Conclusions

Observations from shaking-table and quasi-static testing were synthesized into a simplified two-degree-of-freedom analysis tool. Using parameter studies, the sensitivity of the tool to changes in its constituent variables was investigated. Practical upper and lower bounds were established for those variables, and the idealization was applied to the particular case of low-rise reinforced masonry buildings with flexible diaphragms. Those studies suggested that the tool could be further simplified into a single-degree-of-freedom tool, without losing significant accuracy. This hypothesis was corroborated through the analyses of the two, half-scale shaking-table specimens and four, prototypical hypothetical analytical building models. Both the two-degree-of-freedom and single-degree-of-freedom idealizations were shown to accurately calculate periods and responses. Nonlinear lumped-parameter modeling validated the accuracy of the tool at high levels of excitation.

These studies demonstrated that the single-degree-of-freedom analysis tool is simple and justified for the seismic analysis of low-rise reinforced masonry buildings with flexible diaphragms. The tool is accurate in its calculation of response, robust with respect to required analysis parameters, and provides a logical method for the expedient calculation of global building response.

5.5.2 Significance of Idealizations

Results and conclusions from shaking-table testing and quasi-static testing, presented in Chapters 3 and 4, were synthesized into an analysis tool designed to account for the effect of diaphragm flexibility on the response of low-rise reinforced masonry buildings. That tool, the two-degree-of-freedom idealization and further-simplified single-degree-of-freedom idealization, was presented and verified in this chapter. It is used in combination with conclusions from additional physical testing, performed by others, to develop and implement seismic evaluation and rehabilitation methodologies in respectively Chapters 6 and 7. The tool is applied to four real structures in Chapter 8, and is ultimately shown to be effective, simple, and accurate.

6.0 Seismic Evaluation of Low-Rise Reinforced Masonry Buildings with Flexible Diaphragms

The seismic response of these types of buildings was first characterized using experimental testing, and then used to develop simple analysis tools. This chapter shows that the tool can be used to accurately identify seismic deficiencies in buildings, such as insufficient diaphragm strength, stiffness, or both. In this chapter, the integration of the tool into an existing seismic evaluation methodology, to enhance its treatment of these types of buildings, is discussed.

6.1 FEMA 310: Handbook for the Seismic Evaluation of Buildings – A Prestandard

Low-rise reinforced masonry buildings with flexible diaphragms may have many different seismic deficiencies: general structural redundancy; strength of in-plane or out-plane masonry walls; strength or stiffness of horizontal diaphragms; strength of diaphragm anchorage; or general detailing such as diaphragm cross ties, prescriptive masonry reinforcement, or reinforcement around diaphragm openings; and others. Chapter 4 of FEMA 310, *Evaluation Phase (Tier 2)*, and Chapter 10 of FEMA 356, *Simplified Rehabilitation*, describe typical seismic deficiencies in these types of buildings as well as typical rehabilitation techniques used to mitigate those deficiencies.

As discussed in Chapter 2 of this dissertation, the seismic evaluation provisions of FEMA 310 comprise tiered evaluation criteria of incrementally increasing rigor: the Screening phase (Tier 1); the Evaluation phase (Tier 2); and the Detailed Evaluation phase (Tier 3). The Screening phase primarily uses limited analyses and checklists to quickly identify probable seismic deficiencies. The checklist items are chiefly based on correlations between observed seismic

damage and specific building configurations or characteristics. Specific items related to this study, for low-rise reinforced masonry buildings with flexible diaphragms (FEMA Building Type RM1), are reproduced here:

FEMA 310 Checklist 3.7.13:

Connections

Wall Anchorage: Exterior concrete or masonry walls shall be anchored for out-of-plane forces at each diaphragm level with steel anchors or straps that are developed into the diaphragm.

Transfer to Shear Walls: Diaphragms shall be reinforced and connected for transfer of loads to the shear walls for Life Safety and the connections shall be able to develop the shear strength of the walls for Immediate Occupancy.

FEMA 310 Checklist 3.7.13S:

Diaphragms

Cross Ties: There shall be continuous cross ties between diaphragm chords.

Plan Irregularities: There shall be tensile capacity to develop the strength of the diaphragm at re-entrant corners or other locations of plan irregularities. This statement shall apply to Immediate Occupancy Performance Level only.

Straight Sheathing: All straight-sheathed diaphragms shall have an aspect ratio less than 2 to 1 for Life Safety and 1 to 1 for Immediate Occupancy in the direction being considered.

Spans: All wood diaphragms with spans greater than 24 ft for Life Safety and 12 ft for Immediate Occupancy shall consist of wood structural panels or diagonal sheathing. Wood commercial and industrial buildings may have rod-braced systems.

Unblocked Diaphragms: All unblocked wood structural panel diaphragms shall have horizontal spans less than 40 ft for Life Safety and 25 ft for Immediate Occupancy and shall have aspect ratios less than or equal to 4 to 1 for Life Safety and 3 to 1 for Immediate Occupancy.

Non-Concrete Diaphragms: Untopped metal deck diaphragms or metal deck diaphragms with fill other than concrete shall consist of horizontal spans of less than 40 ft and shall have aspect ratios less than 4 to 1. This statement shall apply to the Immediate Occupancy Performance Level only.

If deficiencies are identified in the Screening phase, the evaluating engineer can choose to perform the Evaluation phase (Tier 2) or can directly recommend rehabilitation.

The Evaluation phase (Tier 2) involves more rigorous evaluations on either a deficiency-specific or a building-wide basis. In the former and more-common case, only deficiencies identified by the Screening phase are reevaluated; in the latter, the entire structure is reevaluated. In the deficiency-specific case,

each checklist item from the Screening phase corresponds to a complementary procedure in the Evaluation phase. If deficiencies are still identified by the Evaluation phase, the evaluating engineer can choose to perform the final Detailed Evaluation phase (Tier 3), or can directly recommend rehabilitation. The Detailed Evaluation phase basically comprises a rigorous analysis of the deficient structure or its deficient components, according to accepted methodologies for seismic rehabilitation or for new construction, such as respectively FEMA 356 and the International Building Code (IBC).

6.2 United States Army Corps Technical Instructions

The United States Army Corps of Engineers publishes Document TI 809-05 (1999) *Seismic Evaluation and Rehabilitation for Buildings*. That document is in general organizational and technical accordance with FEMA Documents 310, 273/274, and 302/303. This study, presented in the context of the FEMA documents, is therefore directly applicable to Document TI 809-05 as well.

6.3 Potential Gaps in FEMA 310 Methodology

FEMA 310 was revisited to identify and propose refinements for potential gaps in its methodology. In this process, potential deficiencies were critically compared with the existing evaluation criteria intended to identify them. A gap was presumed to exist if a potential deficiency did not appear to be sufficiently identified. The Screening phase was revisited first, followed by the Evaluation phase.

Checklists of the Screening phase (Tier 1) do not explicitly require the comparison of diaphragm shear demand and capacity, or of diaphragm deformation demand and capacity. These are the most significant potential gaps in the methodology. In some cases, these potential limit states are checked qualitatively. For example: diaphragm shear forces are implicitly checked by the

requirement that straight-sheathed lumber diaphragms have aspect ratios less than or equal to 2:1 (for Life Safety performance objectives); diaphragm deflections are implicitly checked by the requirement that wood diaphragms with spans greater than 24 ft. be constructed of diagonal sheathing or structural paneling (for Life Safety performance objectives); and other checklist items are similar. While these checklist items and others like them are effective for some buildings, they do not categorically identify diaphragm force and deformation limit states. The Screening phase of FEMA 310 does not sufficiently characterize the performance of diaphragms.

Interestingly, procedures of the Evaluation phase (Tier 2) directly address diaphragm capacity, and indirectly address diaphragm deformation capacity (through the use of component-specific force-reduction factors (m factors)); this is discussed in following sections of the dissertation. These procedures are activated, however, only if the diaphragm is first found to be deficient in the Screening phase. It is principally this gap (the disconnect between the Screening and Evaluation phases) that this study is intended to address. For that purpose, a supplementary methodology is now developed to systematically identify potential diaphragm deficiencies.

6.4 Development of Proposed Supplementary Methodology

Fundamental to the proposed supplementary methodology is the development of a basic index of probable diaphragm performance, and a method of including that index in the evaluation procedure. To characterize diaphragm performance, test data from previous diaphragm tests, performed by others, were reevaluated in the context of performance-based engineering. Data from previous studies initially designed to identify strength and initial stiffness of diaphragms have been reevaluated to correlate deformation, strength, and damage.

6.4.1 Previous Diaphragm Tests

Chapter 2 of this dissertation catalogs previous research applicable to this study; those specifically involving the testing of flexible diaphragm systems are detailed here. Several research efforts have involved the in-plane testing of flexible wood diaphragms. Atherton *et al.* (1951) tested three series of five diagonally sheathed quarter-scale 5 ft x 15 ft diaphragm specimens, using four equally spaced non-reversed cyclic quasi-static loads. The five specimens of each series used different nailing and sheathing layups. The three series used different chord and side members. The first of those series, Series 1 used unrealistically small chord and side members and thus was excluded from this study. Stillinger *et al.* (1952) tested full-scale 20 ft x 60 ft mockup specimens of the Atherton (1951) tests. Johnson (1954) tested a number of full-scale lumber diaphragms with different aspect ratios using non-reversed cyclic quasi-static loads. The diaphragms measured 20 ft x 20 ft, 20 ft x 40 ft, 20 ft x 60 ft, and 12 ft x 60 ft. Johnson (1955a,b) tested two additional diaphragms: a 12 ft x 60 ft diaphragm replicated from his 1954 tests, and a 20 ft x 80 ft diaphragm.

Nilson (1960) was the first of several researchers to test a large number of metal-deck diaphragms. Racking tests on 46 diaphragms were used to characterize behavior and to determine the effects of different parameters such as welding, deck thickness, and configuration. During that research effort, the now-widely used puddle weld (arc-spot) was developed. Luttrell (1967) and Ellifrit and Luttrell (1970) followed that study with 160 diaphragm tests designed to calibrate expressions predicting the strength and stiffness of metal-deck diaphragms. The First Edition (1981) and Second Edition (1995) of the Steel Deck Institute *Diaphragm Design Manual* are entirely based on that work.

6.4.2 Interpretation of Diaphragm Test Data

Not all diaphragms tested in those studies were configured and loaded in the same way. Some were loaded using two or four equally spaced loads; others were single panels racked by a concentrated load at one end; and still others, such as in this study, were tested as components in dynamically loaded building specimens. To consistently and logically relate the diaphragm deformations, applied loads, and observed damage states from those different tests, it was necessary to identify and properly account for the effects of test setup and loading.

Flexible diaphragms deform primarily in shear; damage therefore occurs through the dissipation of strain energy associated with shearing deformation. Thus, the total strain energy of shearing deformation in a diaphragm can be interpreted as an index of potential diaphragm damage. To illustrate how this hypothesis can be used to relate the performances of diaphragms under different load distributions and configurations, consider a diaphragm under uniformly distributed lateral load, f_o (Figure 6.1):

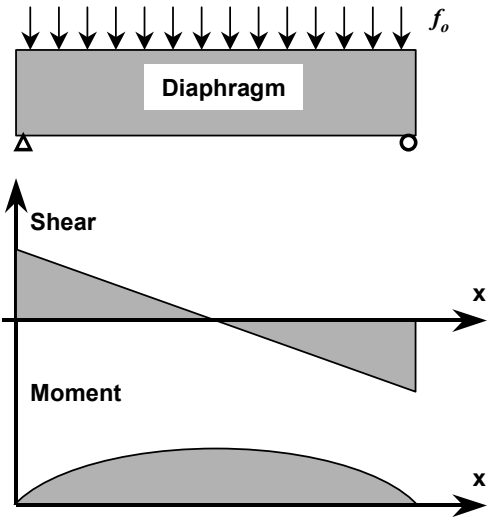


Figure 6.1 Diaphragm under uniformly distributed load

1. Establish the total strain energy of shearing deformation at a given displacement Δ and total applied load V_{total} (Column 4, Table 6-1).

$$\begin{aligned}
 U_{dist} &= \frac{1}{2} \int_0^L f_o \Delta(x) dx \\
 &= \frac{1}{2} \int_0^L f_o \frac{1}{2} f_o \frac{1}{A'G} (xL - x^2) dx \\
 &= \frac{f_o^2}{4A'G} \left[\frac{x^2}{2} L - \frac{x^3}{3} \right]_0^L \\
 &= \frac{f_o^2 L^3}{24A'G} \\
 U_{dist} &= \frac{V_{tot}^2 L}{24A'G}
 \end{aligned}
 \tag{Equation 6-1}$$

where,

$$V_{total} = f_o L. \tag{Equation 6-2}$$

2. The strain energy of shearing deformation associated with seismic loading of the same diaphragm (Column 4, Table 6-1) provides a common basis for comparison. Similar to Step 1,

$$U_{seismic} = \frac{1}{2} \int_0^L f(x) \Delta(x) dx, \tag{Equation 6-3}$$

where $f(x)$ is proportional to the deformed shape of the diaphragm. For a pure shear beam, that shape is known to be sinusoidal, and it can be approximated as such even for this more complex case,

$$f(x) = f_o \sin\left(\frac{\pi x}{L}\right). \tag{Equation 6-4}$$

If $\Delta(x)$ is approximated as,

$$\begin{aligned}
 \Delta(x) &= \frac{1}{A'G} \int V(x) dx \\
 &= \frac{1}{A'G} \iint f(\zeta) d\zeta dx \\
 &= \frac{1}{A'G} \iint f_o \sin\left(\frac{\pi\zeta}{L}\right) d\zeta dx \\
 &= \frac{1}{A'G} \int f_o \frac{L}{\pi} \cos\left(\frac{\pi x}{L}\right) dx \\
 \Delta(x) &= \frac{f_o}{A'G} \left(\frac{L}{\pi}\right)^2 \sin\left(\frac{\pi x}{L}\right)
 \end{aligned}
 \tag{Equation 6-5}$$

then,

$$\begin{aligned}
 U_{seismic} &= \frac{1}{2} \int_0^L f_o \sin\left(\frac{\pi x}{L}\right) \frac{f_o}{A'G} \left(\frac{L}{\pi}\right)^2 \sin\left(\frac{\pi x}{L}\right) dx \\
 &= \frac{f_o^2 L^3}{4\pi^2 A'G} \\
 U_{seismic} &= \frac{V_{total}^2 L}{16A'G}
 \end{aligned}
 \tag{Equation 6-6}$$

where,

$$V_{total} = \int_0^L f(x) dx = f_o L \frac{2}{\pi} .
 \tag{Equation 6-7}$$

3. The two energies are then equated (Column 2, Table 6-1) using a factor C to account for the effect of load distribution,

$$\frac{V_{total}^2 L}{A'G 16} = C \frac{V_{total}^2 L}{A'G 24} .
 \tag{Equation 6-8}$$

4. Imposing the requirement that the total applied load V_{total} for both cases be equal,

$$C = 3/2 .
 \tag{Equation 6-9}$$

5. That constant is then used to calculate effective diaphragm drift ratios, for a displacement Δ (Column 6, Table 6-1).

$$DDR = C \frac{2\Delta}{L} = \frac{3\Delta}{L} \quad \text{Equation 6-10}$$

This result, Equation 6-10, makes sense. In the example above, the total strain energy of shearing deformation for the uniformly loaded diaphragm was only two-thirds that of the same seismically loaded diaphragm, under equal magnitudes of displacement and total load (Equation 6-8). This implied that damage in the uniformly loaded diaphragm was also only two-thirds that in the seismically loaded diaphragm, under equal magnitudes of displacement and total load. Therefore, for a specific magnitude of total load, the diaphragm drift ratio must be effectively calculated as 1.5 times that of the equivalent seismically loaded system, to consistently use the diaphragm drift ratio as an index of diaphragm damage (Figure 6.2). Such is the case in Step 5 above.

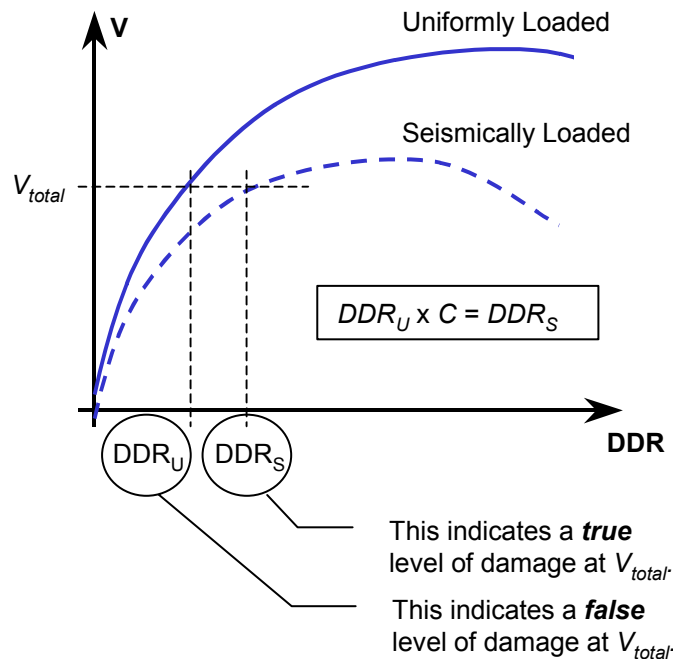
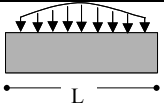
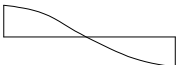
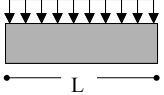
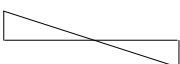
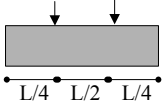
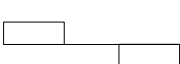
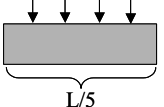

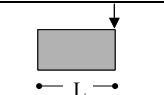
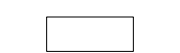


Figure 6.2 Effective calculation of diaphragm drift ratio for different test configurations

This general process, the results of which are summarized in Table 6-1, provided a rational basis for comparison for diaphragm tests of different load distributions and configurations. Using those results, data from different diaphragm load distributions and configurations could be rationally compared in the context of diaphragm drift ratios, if the ratios were calculated appropriately (Table 6-1).

Table 6-1 Relationships between diaphragm load distribution and diaphragm performance

Loading	Sketch	Shear Diagram	Strain Energy	Load Distribution Factor, C	DDR
Sinusoidal			$\frac{V_{total}^2 L}{A'G 16}$	1	$\frac{2\Delta}{L}$
Distributed			$\frac{V_{total}^2 L}{A'G 24}$	3/2	$\frac{3\Delta}{L}$
Quarter-Point Bending			$\frac{V_{total}^2 L}{A'G 16}$	1	$\frac{2\Delta}{L}$
Sixth-Point Bending			$\frac{V_{total}^2 L}{A'G 16}$	1	$\frac{2\Delta}{L}$
Racking			$\frac{V_{total}^2 L}{A'G 8}$	1/4	$\frac{\Delta}{2L}$

6.4.3 Reevaluation of Diaphragm Test Data

Two key parameters were extracted from the test data: diaphragm drift ratios; and the measure of diaphragm rigidity, G' . The latter is related to shear rigidity, $A'G$,

$$G'B = A'G, \quad \text{Equation 6-11}$$

where B is the diaphragm width in the direction of loading, A' is the effective shear area of the diaphragm, and G is the shear modulus of the diaphragm. The complex nature of flexible diaphragms, whether constructed of wood or metal deck, precludes the explicit definition of either a diaphragm shear modulus or effective area. For that reason, G' is widely used and represents an effective quantity describing the shear rigidity of the diaphragm per unit width.

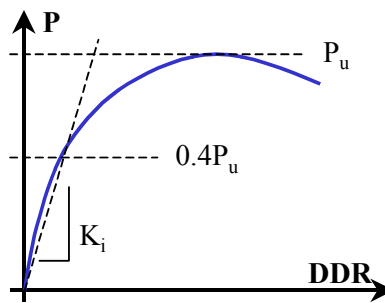


Figure 6.3 Relationship of applied load and deformation of a metal-deck diaphragm

In the case of metal-deck diaphragms, diaphragm drift ratios and stiffnesses were extracted at 40 % of the ultimate capacity of the diaphragm. That value is generally accepted as the load level at which metal-deck diaphragms begin to sustain measurable damage, and to exhibit incipient nonlinearity in their load-displacement responses (Luttrell 1967, Figure 6.3). The studies outlined in Section 6.4.1 showed that lumber diaphragms exhibit similar behavior at roughly 50 % of their ultimate capacity. Stiffness and drift ratio quantities were therefore extracted at that load level, for those diaphragms. Diaphragm drift ratios at these percentages of ultimate load (40 % and 50 %) therefore represent critical levels of deformation consistent with the onset of measurable diaphragm damage.

Figure 6.4 shows that, for metal-deck diaphragms, there is an inverse relationship between G' and the diaphragm drift ratio at 40 % of the ultimate load. The dotted curve in that figure is,

$$DDR_{40\%Pu} = \frac{2}{G'} \quad \text{Equation 6-12}$$

where G' is in units of kips per inch and $DDR_{40\% Pu}$ is in units of percent. For wood diaphragms, Figure 6.5 shows a similar inverse relationship,

$$DDR_{50\%Pu} = \frac{1}{G'} \quad \text{Equation 6-13}$$

Equation 6-12 and Equation 6-13 describe an important interrelationship between an intrinsic characteristic of a diaphragm (G') and its seismic performance (DDR at 40% and 50% of ultimate capacity). This implies that the level of deformation in a diaphragm at the onset of damage (yielding) is not purely kinematical, but it also depends on its stiffness. In an elastic-plastic steel-plate diaphragm, in contrast, yielding (damage) is purely kinematical, occurring at the same deformation (DDR) regardless of the stiffness of the diaphragm.

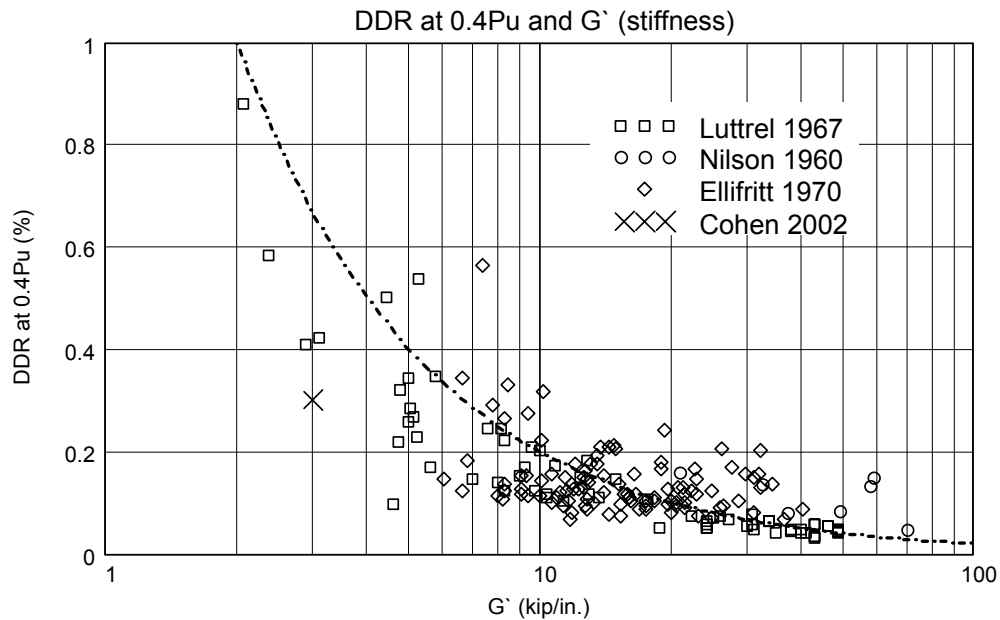


Figure 6.4 Relationship between a measure of diaphragm shear stiffness G' and diaphragm drift ratio, at onset of damage, for metal-deck diaphragms

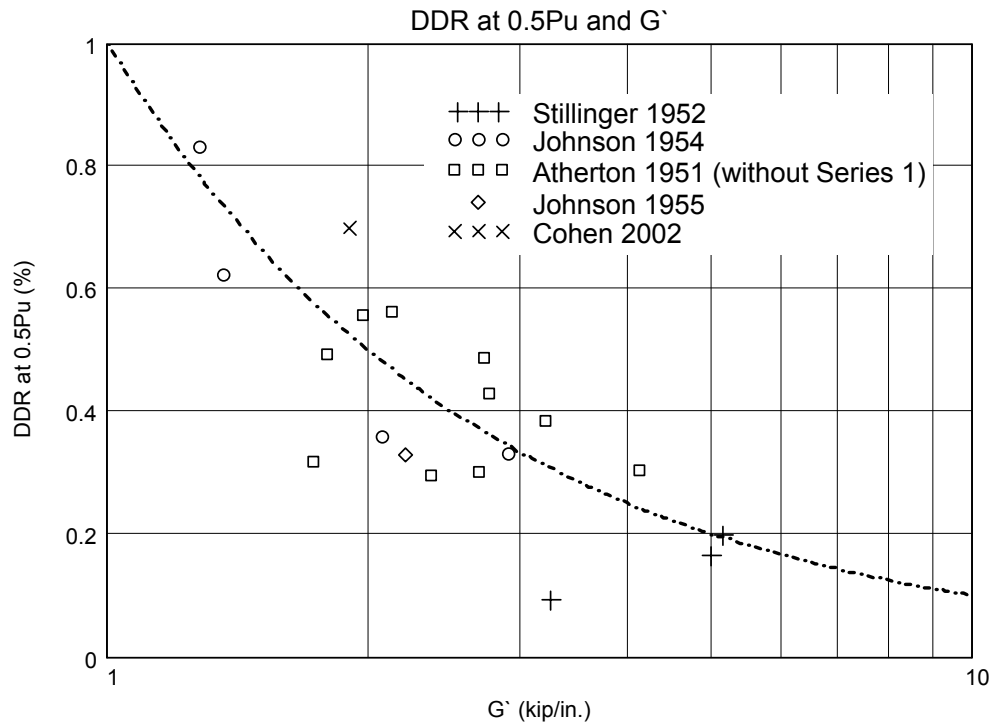


Figure 6.5 Relationship between a measure of diaphragm shear stiffness G' and diaphragm drift ratio, at onset of damage, for lumber sheathed diaphragms

The relationships of Equation 6-12 and Equation 6-13 make physical sense as well. The in-plane stiffness of these types of diaphragms depends on complex mechanisms that, for lumber diaphragms, chiefly derive from nailing patterns, nail sizes, and lumber sizes. For metal-deck diaphragms, they chiefly derive from welding patterns, weld sizes, deck thickness, side-lap fastener patterns, and deck profile. These same elements also contribute to diaphragm strength. For instance, the more nails in a lumber diaphragm or welds in a metal-deck diaphragm, the greater its strength.

6.4.4 Significance of Reevaluations and Observed Relationships

As described in Chapter 2 of this dissertation, the FEMA documents define three seismic performance levels: Immediate Occupancy (IO), Life Safety

(LS), and Collapse Prevention (CP). A design earthquake would cause little to no damage for IO; some damage but no immediate threat to human life for LS; and large amounts of damage but continued overall structural stability for CP. The relationships of Equation 6-12 and Equation 6-13 roughly define boundaries between these performance levels (Figure 6.6); deformation levels at or below those described by the equations are consistent with IO, and levels above them are consistent with LS and CP.

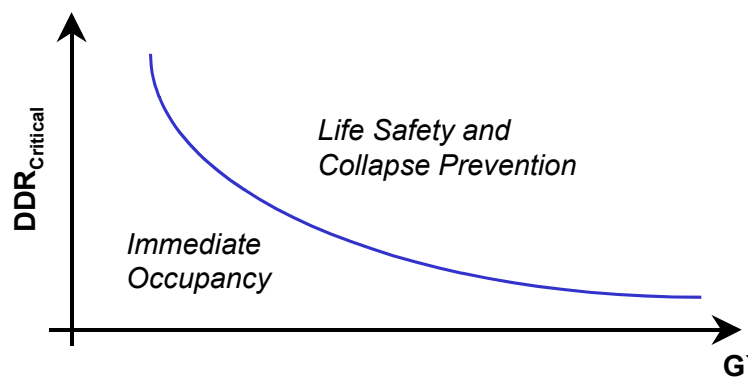


Figure 6.6 Link between FEMA Performance Levels and proposed methodology

This is also consistent with the definitions provided in FEMA 356 for the structural performance of wood and metal-deck diaphragms. Table C1-4 of that document states:

Element	Structural Performance Level		
	CP	LS	IO
Metal-Deck Diaphragms	Large distortions with buckling of some units and tearing of many welds and seam attachments.	Some localized failure of welded connections of deck to framing and between panels. Minor local buckling of deck.	Connections between deck units and framing intact. Minor distortions.
Wood Diaphragms	Large permanent distortion with partial withdrawal of nails and extensive splitting of elements.	Some splitting at connections. Loosening of sheathing. Observable withdrawal of fasteners. Splitting of framing and sheathing.	No observable loosening or withdrawal of fasteners. No splitting of sheathing or framing.

These damage states are similar to the damage-deformation relationships observed during quasi-static testing described in Chapter 4, as well as those described by Luttrell (1967) for the definition of the critical load level of 40% of ultimate for metal-deck diaphragms. It will be demonstrated that these relationships can be used to evaluate flexible diaphragm systems, and to identify deficiencies that current FEMA 310 evaluation procedures do not address.

6.5 Proposed Supplementary Methodology for FEMA 310

The methodology proposed next and outlined in Figure 6.7 is intended to supplement the existing FEMA 310 provisions, and to demonstrate the use of the SDOF analysis tool and the relationships of Equation 6-12 and Equation 6-13.

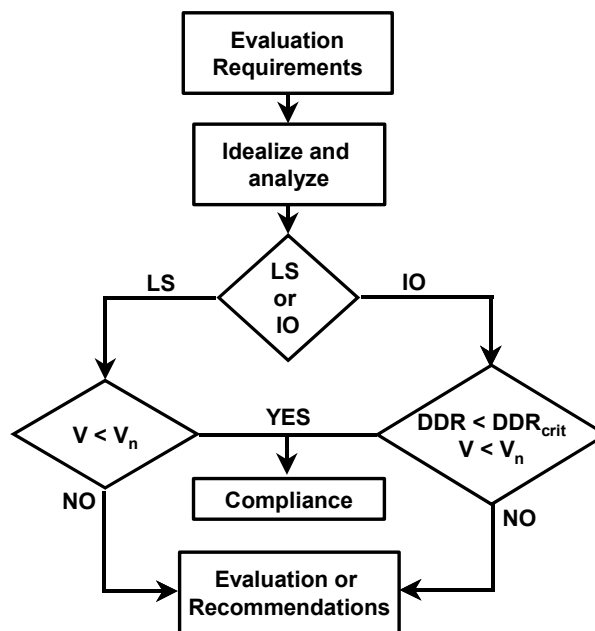


Figure 6.7 Basic organization of proposed supplementary evaluation methodology for FEMA 310

The methodology is presented step-wise using the example building configuration of Figure 6.8a.

1. **Define diaphragm systems.** Buildings with multiple flexible diaphragms should be described as a set of individual diaphragm systems. For example, a building with the plan of Figure 6.8a could be described as the collection of diaphragm systems in Figure 6.8b.
2. **Couple mass and assign stiffness to diaphragm degree of freedom.** Using the methods developed in this study, appropriate mass and stiffness values should be assigned to each diaphragm system. The mass coupled with each diaphragm system is one-half the total mass of the diaphragm itself, plus one-half the mass of any out-of-plane walls associated with response of the diaphragm. This is illustrated by the darkly shaded areas in Figure 6.8c. The deformed shapes of the diaphragm systems are approximated as sinusoids (Figure 6.8d). The in-plane stiffness consistent with this is,

$$k = \frac{BG' \pi^2}{L} \frac{1}{2}, \quad \text{Equation 6-14}$$

where B is the diaphragm width and L is the diaphragm length.

3. **Calculate period of each diaphragm.** Treating each diaphragm system as an independent single-degree-of-freedom system, calculate a period for each diaphragm system (Figure 6.8e).
4. **Calculate response of each diaphragm.** Using appropriate loading criteria (for example, a response spectrum) calculate in-plane forces and diaphragm drift ratios for each diaphragm system (Figure 6.8e).
5. **Compare calculated responses with capacities.** For each diaphragm system, compare applied loads to known capacities. For Immediate

Occupancy performance levels, also compare calculated diaphragm drift ratios to critical values (Equation 6-12 and Equation 6-13).

6. **Recommend further evaluation or rehabilitation.** Based on results of Step 5, proceed with evaluation as outlined in FEMA 310.

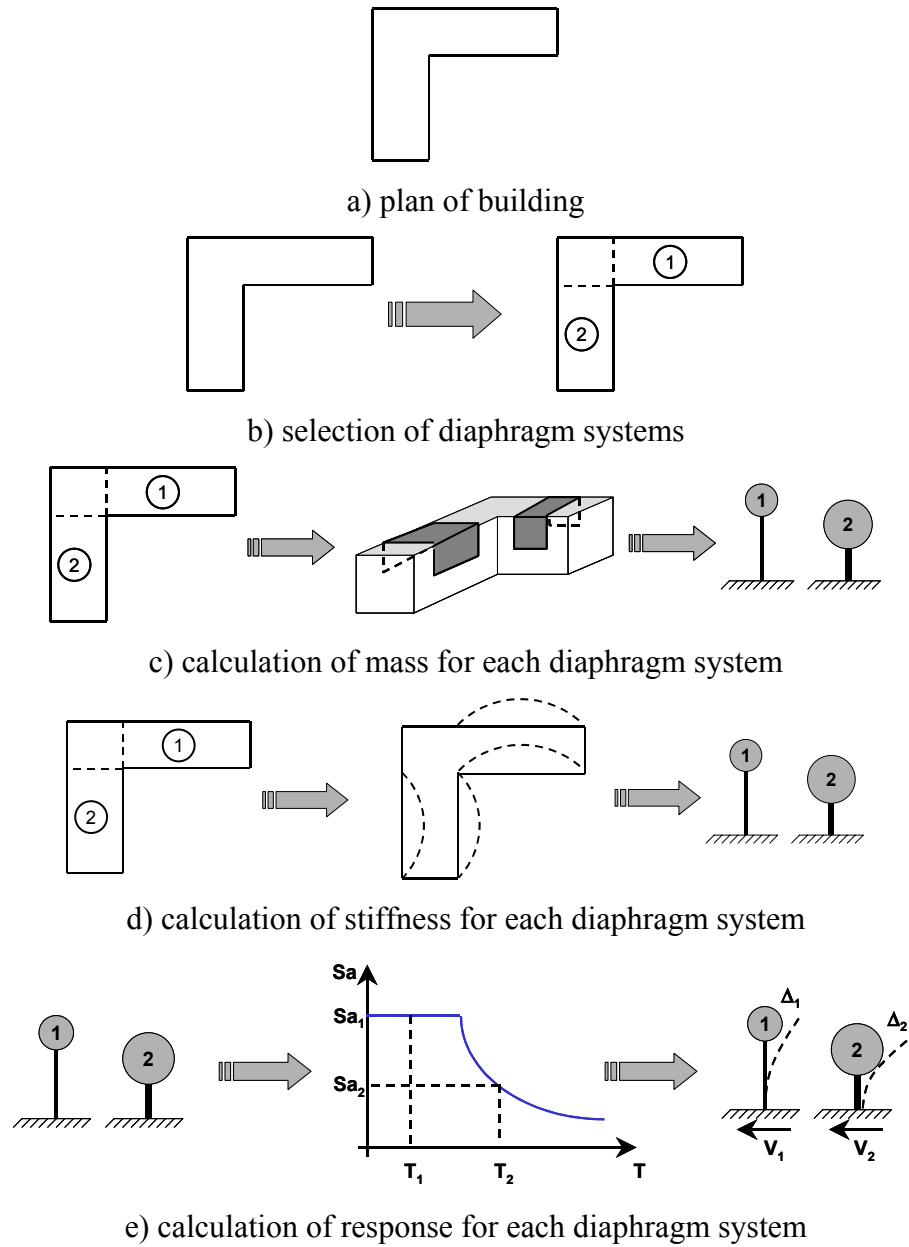


Figure 6.8 Proposed Supplementary Methodology for FEMA 310

6.6 Summary of Results, Conclusions, and Significance of Proposed Supplementary Methodology

6.6.1 Summary of Results and Conclusions

As part of the final phase of this study, a supplementary seismic evaluation methodology for low-rise reinforced masonry buildings with flexible diaphragms was developed. First, a critical review of the existing FEMA 310 document identified potential gaps in that methodology and suggested that it did not sufficiently assess the seismic performance of flexible diaphragm systems. To address this, data from previous diaphragm testing programs were reevaluated in the context of performance-based engineering, and combined with the SDOF analysis tool developed in Chapter 5 into a supplementary seismic evaluation methodology.

6.6.2 Significance of Proposed Supplementary Methodology

Results and conclusions from shaking-table testing and quasi-static testing, presented in Chapters 3 and 4, were synthesized into an analysis tool designed to account for the effect of diaphragm flexibility on seismic response. That tool was presented and verified in Chapter 5. In this chapter data from several previous physical testing programs (critical levels of deformation and attendant damage mechanisms) were reevaluated and integrated with the analysis tool into a supplementary seismic evaluation methodology designed to fill gaps in the FEMA 310 methodology. In Chapter 7, knowledge from this study integrates into the rehabilitation methodology of FEMA 356. The supplementary evaluation methodology is applied to four real structures in Chapter 8, and ultimately shown to be effective, simple, and accurate.

7.0 Seismic Rehabilitation of Low-Rise Reinforced Masonry Buildings with Flexible Diaphragms

The seismic behavior of low-rise reinforced masonry buildings with flexible diaphragms was characterized using experimental testing and results of that testing were implemented to the development of a simple analysis tool. In the previous chapter the potential of that tool for the identification of seismic deficiencies in buildings was demonstrated. This chapter shows that the state-of-the-art methodology for seismic rehabilitation of buildings is in basic overall accord with the conclusions of this study, although some enhancements are possible.

7.1 FEMA 356: Prestandard and Commentary for the Seismic Rehabilitation of Buildings

To mitigate seismic deficiencies in buildings and meet prescribed seismic performance objectives, rehabilitation schemes are designed and implemented. FEMA 356 is the most widely accepted framework for such design. That methodology systematically addresses identified structural deficiencies, and characterizes the effectiveness of rehabilitation measures intended to counter them.

7.1.1 General Methodology

The following steps qualitatively outline the methodology of FEMA 356; many details are eliminated for brevity. Figure C1-1 *Rehabilitation Process* in FEMA 356 outlines the methodology in detail.

1. Recommendations for Rehabilitation.

Following seismic evaluation, recommendations for rehabilitation are drafted. Although FEMA 356 emphasizes the use of FEMA 310, and is generally organized for use with that document, it allows any accepted methodology to be used for seismic evaluation.

2. Building Analysis.

Following recommendations for rehabilitation (Step 1), applicable analytical building models and analysis procedures are selected, implemented, and analyzed for component forces and deformations. Unlike the component-specific analyses of FEMA 310 (for example, only a column or a diaphragm is analyzed), forces and deformations are calculated on a building-wide basis.

Analysis procedures of FEMA 356 are generally more rigorous and accurate than those of FEMA 310. The specific applicability and rigor of the different procedures are based on, among other items, structural regularity and component seismic demand-to-capacity ratios. Buildings with greater irregularity and higher DCRs are analyzed using more complex and rigorous analysis procedure. Listed in order of increasing complexity and rigor, and in the nomenclature of FEMA 356, the analysis procedures are Linear Static, Linear Dynamic, Nonlinear Static, and Nonlinear Dynamic. Briefly describing each, the Linear Static procedure is linear elastic static analysis; the Linear Dynamic procedure is linear elastic modal or time-history analysis; the Nonlinear Static procedure is nonlinear static “push-over” analysis, where lateral loads are incrementally increased up to the lateral-limit load (collapse) of the building model; Nonlinear Dynamic procedure is nonlinear dynamic time-history analysis. Low-rise reinforced masonry buildings are most often analyzed using the Linear Static procedure.

3. Rehabilitation Design.

Based on deficiencies identified in the evaluation phase (FEMA 310) and the analysis of Step 2 in the rehabilitation phase, preliminary rehabilitation schemes are designed. Changes are incorporated into the analytical model of the building, which is then reanalyzed for component forces and deformations.

4. Verification of Rehabilitation and Acceptability.

Based on the design and analysis of Step 3, the seismic performance of the building, as a whole, and of the individual components it comprises, are checked for acceptability. That is, global building response is compared with drift limitations and component responses are compared with strength and deformation capacities. Steps 3 and 4 are iterated until performances of the building, as a whole, and of the individual components it comprises are found to meet the assigned performance objective.

7.1.2 General Provisions and Commentary

Elements of the FEMA 356 methodology that specifically relate to this study are summarized in the following:

Chapter 2: General Requirements

2.6 General Design Requirements

2.6.6 Diaphragms

Sections 2.6.6.1, 2.6.6.2, and 2.6.6.3 respectively discuss force and configuration requirements for diaphragm chords, diaphragm collectors, and diaphragm cross ties.

2.6.7 Walls

Sections 2.6.7.1 and 2.6.7.2 respectively prescribe minimum requirements for out-of-plane wall-to-diaphragm anchorage and out-of-plane wall strength.

Chapter 3: Analysis Procedures

3.2 General Analysis Requirements

3.2.4 Diaphragms

Sections 3.2.4.1 through 3.2.4.3 respectively define “flexible,” “stiff,” and “rigid” diaphragms. Commentary C3.2.4 describes plausible force distributions in flexible diaphragm systems (similar to the sinusoidal approximation used in Chapter 5 of this dissertation) and comments that diaphragm demand calculations should be based on such distributions.

3.3 Analysis Procedures

3.3.1 Linear Static Procedure

This section outlines the analysis procedure, Linear Static, most often used for the analysis of low-rise reinforced masonry buildings with flexible diaphragms. Section 3.3.1.2 introduces FEMA Equation 3-8 for the period calculation of one-story buildings with flexible diaphragms. This equation was shown, in Chapter 5 of this dissertation, to calculate periods with reasonably accuracy. Section 3.3.1.3 provides the calculation of pseudo lateral loads and lateral-load distributions. The modifier “pseudo” is included because lateral loads in this methodology are designed so that when applied to an analysis model they impose displacement amplitudes that approximate those expected during inelastic response. This is consistent with the general philosophy of performance-based engineering that displacements and deformations better indicate the potential for structural damage (performance) than do forces.

3.4 Acceptance Criteria

This section outlines general procedures for the acceptance or rejection of rehabilitation designs, in the context of element demands versus element capacities. Section 3.4.2.2 specifically outlines acceptance procedures for the Linear Static Procedures of Section 3.3.1.

Chapter 5: Steel

5.9 Diaphragms

5.9.1 Bare Metal Deck Diaphragms

This section outlines the strength and stiffness of metal-deck diaphragms. Although some discussion of deformation-controlled (ductile) metal-deck diaphragms is included, these are very rare and metal-deck diaphragms are chiefly force-controlled (brittle) elements. Numerical acceptance criteria are listed (FEMA Table 5-5), although that data only applies to the rare cases of ductile metal-deck diaphragms. A limited discussion of rehabilitation measures for these types of diaphragm is also included.

Chapter 8: Wood and Light Metal Framing

8.6 Wood Diaphragms

This section outlines the calculation of strength, stiffness, and in-plane deflections of wood diaphragms. Different types of diaphragms (single straight-sheathed, panel overlay, diagonally sheathed, and several others) are afforded individual treatments and discussions. Numerical acceptance criteria are listed (FEMA Table 8-3). A limited discussion on rehabilitation measures for these types of diaphragms is also included.

7.2 United States Army Corps Technical Instructions

The United States Army Corps of Engineers publishes Document TI 809-05 (1999) *Seismic Evaluation and Rehabilitation for Buildings*. That document is in general organizational and technical accordance with FEMA Documents 310, 273/274 (356), and 302/303. Rehabilitation measures outlined in the document are based on FEMA 172 as well as general engineering practice. This study, presented in the context of the FEMA documents, is therefore directly applicable to Document TI 809-05.

7.3 Potential Gaps in FEMA 356 Methodology

FEMA 356 was revisited to identify and propose refinements for potential gaps in its methodology. To do this, three main elements of the methodology were critically reviewed and compared with information and conclusions from this study. They regard analysis procedures, diaphragm modeling, and acceptance criteria. A potential gap was presumed to exist if an aspect of the FEMA 356 methodology was not in general accordance with this study.

7.3.1 Analysis Procedures

Low-rise reinforced masonry buildings with flexible diaphragms are most often analyzed using the Linear Static procedure of FEMA 356 (linear elastic static analysis). The procedure comprises two key steps: period determination, and determination of forces and deformations.

7.3.1.1 Analysis of Building Period

As discussed in Section 7.1.2 of this dissertation, FEMA 356 uses, as enumerated in that document, FEMA Equation 3-8 for the calculation of fundamental period of one-story buildings with flexible diaphragms. The

equation was shown, in Chapter 5 of this dissertation, to calculate those periods with reasonable accuracy.

7.3.1.2 Analysis of Building Forces

The Linear Static procedure of FEMA 356 defines the pseudo lateral load (base shear) on a system using FEMA Equation 3-10,

$$V = C_1 C_2 C_3 C_m S_a W, \quad \text{Equation 7-1}$$

where,

- C_1 = factor intended to relate maximum expected inelastic displacements to displacements calculated from elastic analysis;
- C_2 = factor intended to account for pinched hysteresis response, stiffness degradation, and strength degradation; 1.0 for linear elastic analysis;
- C_3 = factor intended to account for P- Δ effects (geometric nonlinearity);
- C_m = factor intended to account for effect of participation of higher dynamic modes to response;
- S_a = spectral acceleration at fundamental period of building; and
- W = effective seismic weight of building; this quantity is basically the dead load of building and applicable portions of the live load, defined in FEMA 356 Section 3.3.1.3.1.

The pseudo lateral load is distributed vertically to the floor levels according to the distribution of building weight, the height from base, and, in the case of longer-period structures, expected participation of higher dynamic modes. The document notes that seismic loads applied a flexible diaphragm should be distributed in proportion to its displaced shape. This latter fact is discussed in detail in Section 7.3.2.1 of this dissertation.

FEMA 356 Section 3.3.1.3.5 outlines a sub-methodology for the analysis of unreinforced masonry buildings with flexible diaphragms:

1. For each span of the building at each level, calculate period from Equation 3-9.
2. Using Equation 3-10, calculate pseudo lateral load for each span.
3. Apply lateral loads calculated for each span and calculate forces in vertical seismic-resisting elements using tributary loads.
4. Diaphragm forces for evaluation of diaphragms shall be determined from the results of Step 3 above and distributed along the diaphragm span considering its deflected shape.
5. Diaphragm deflections shall not exceed 6 in. for this method of distribution of pseudo lateral loads to be applicable.

FEMA Equation 3-9 is an adapted form of FEMA period Equation 3-8, and FEMA Equation 3-10 is previously defined.

This sub-methodology generally emulates the proposed supplementary evaluation methodology outlined in Chapter 6 of this dissertation. The chief similarity between the two is the calculation of distinct periods and pseudo lateral loads for each diaphragm. Furthermore, as in this study, diaphragm lateral loads are distributed in proportion to the displaced shapes of the diaphragms. The proposed methodology of Chapter 6 does not, however, impose a categorical limit of 6 in. on diaphragm deflections, such as in Step 5 above. Diaphragm deflections in that methodology are limited only in the case of Immediate Occupancy performance level, where the relationships of Equations 6-12 and 6-13 provide such limits.

7.3.2 Diaphragm Modeling

FEMA 356 provides guidance for the modeling of diaphragm strength, stiffness, and in the case of wood diaphragms, in-plane deflections.

7.3.2.1 Modeling of Lateral Force Distributions

Commentary to FEMA 356 suggests that lateral forces in a flexible diaphragm be distributed in proportion to the deflected shape of the diaphragm and to the distribution of its participating mass (Figure 7.1). Specific functional distributions provided in the document are consistent with the sinusoidal approximation used for the development of the 2DOF and SDOF analysis tools in Chapter 5.

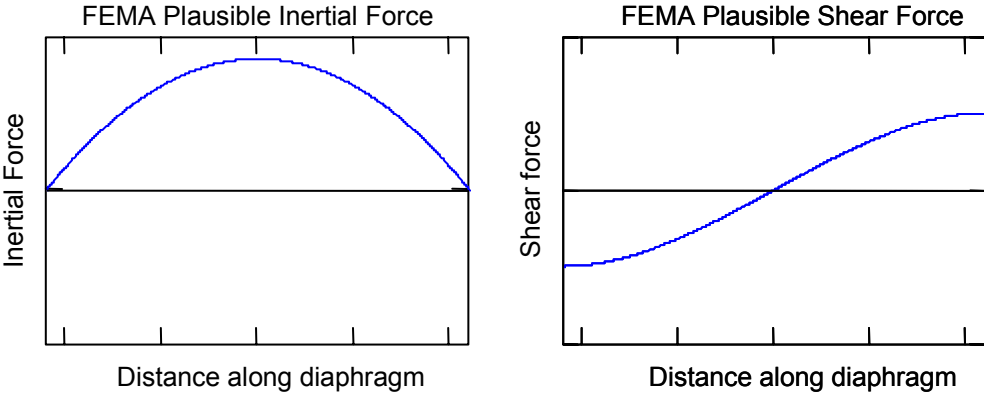


Figure 7.1 FEMA 356 plausible distribution of lateral and shear forces in a flexible diaphragm

7.3.2.2 Modeling of Lumber Diaphragms

The document provides strength and stiffness values for 22 different types of wood diaphragms and appropriately recognizes that complex nailed wood assemblies, such as diaphragms, can exhibit significant variations in strength or stiffness. Specific characterization of strength and stiffness of lumber diaphragms

is beyond the scope of this study and the accuracy of such values listed in FEMA 356 is not examined further.

To calculate the in-plane deflection at yield of a lumber diaphragm, FEMA 356 provides, as enumerate in that document, FEMA Equation 8-3,

$$\Delta_y = \frac{v_y L}{2G_d}, \quad \text{Equation 7-2}$$

where,

v_y = in-plane yield shear force in units of force/length;

L = length of diaphragm perpendicular to direction of load; and

G_d = measure of in-plane stiffness, provided in FEMA Table 8-2.

It can be shown that the expression describes the in-plane deflection of a diaphragm subjected to a concentrated lateral load, of magnitude $v_y L$, applied at mid-span. The in-plane deflection of a diaphragm subjected to a more-accurate sinusoidal lateral load distribution, similar to that shown in Figure 7.1, can be shown to be,

$$\Delta_y = \frac{v_y L}{\pi G_d}. \quad \text{Equation 7-3}$$

This expression predicts diaphragm deflections that are only 64% ($2/\pi$) those calculated by FEMA Equation 8-3 (Equation 7-2). In this respect, the FEMA 356 procedure is conservative.

7.3.2.3 Modeling of Metal-Deck Diaphragms

FEMA 356 suggests that accepted industry procedures, such as those provided in the *Diaphragm Design Manual* 1st and 2nd Edition (SDI 1981 and 1995) and proprietary manuals supplied by steel-deck manufacturers, be used to characterize strengths and stiffnesses of metal-deck diaphragms. The document offers no alternative values or procedures. Modeling efforts based on such an

approach have been shown to be reasonably accurate (for example, Cohen 2001 and Cohen *et al.* 2002a). The specific characterization of strength and stiffness of metal-deck diaphragms is beyond the scope of this study and is not examined further.

7.3.3 Acceptance Criteria

The acceptability of a rehabilitation scheme is explicitly based on assigned seismic performance levels and ratios of component force demands to component capacities; deformation demands are only checked implicitly.

As discussed in Section 7.1.2, linear elastic analysis procedures of the methodology (Linear Static and Linear Dynamic) are designed to impose expected levels of displacement on a structure, as opposed to expected levels of force. This is accomplished in FEMA 356 through the use of various amplification factors that depend on expected building period and building configuration, and intend to account for the general observations that in the “constant-acceleration” region of response spectra, inelastic systems tend to respond at greater maximum displacements than their elastic counterparts, and in the “constant-velocity” or “constant-displacement” regions of response spectra, inelastic systems and their elastic counterparts tend to respond at roughly equal maximum displacements.

These analyses are elastic and thus component forces are directly proportional to component deformations. Actual building responses are likely inelastic, however, and no such proportionality is maintained. To implicitly account for this, forces in ductile components are divided by force-reduction factors (m-factors) during the acceptability check of the rehabilitation process. These are analogous to the base shear-reduction factors (R factors) of the FEMA

302/303 documents and of the IBC. In basic terms, m-factors are component-specific R-factors (Figure 7.2).

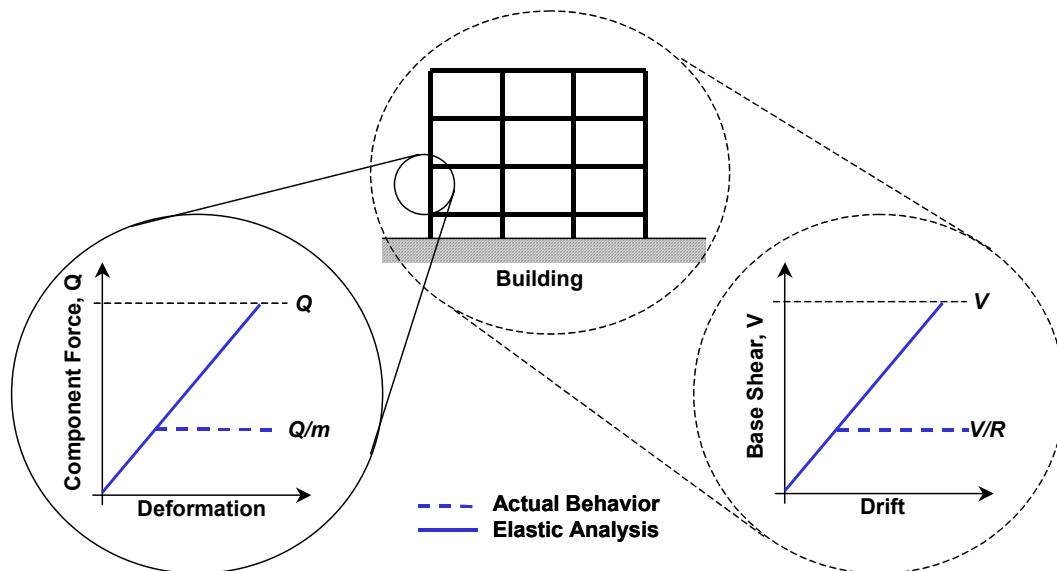


Figure 7.2 Comparison of FEMA 356 component-specific force-reduction m-factors and FEMA 302/303 and IBC base shear-reduction R-factors

M-factors are selected for each component based on three classifications: the performance objective of the building, and two component-specific classifications. Components are classified as “primary” (critical) or “secondary” (not critical), based on the criticality of the component to the lateral capacity of the building, and as “deformation-controlled” (ductile) or “force-controlled” (not ductile), based on the available ductility of the component. Once selected, individual m-factors are applied to the calculated forces of each component. Rehabilitation is acceptable for deformation-controlled components if,

$$m \kappa Q_{CE} \geq Q_{UD} \quad \text{or} \quad Q_{CE} \geq \frac{Q_{UD}}{m \kappa}, \quad \text{Equation 7-4}$$

where,

Q_{CE} = (from FEMA 356) expected strength of the component or element at the deformation level under consideration for deformation-controlled actions;

Q_{UD} = combined earthquake and gravity force in component, calculated using applicable analysis procedure;

m = (from FEMA 356) component or element demand modifier to account for expected ductility associated with this action at the selected Structural Performance Level; and

κ = “knowledge” factor intended to account for accuracy and level of knowledge regarding as-built and current conditions of building.

For example, the m-factors for a single straight-sheathed chorded diaphragm are:

IO	Primary		Secondary	
	LS	CP	LS	CP
1.0	2.0	2.5	2.4	3.1

Less critical components and more lenient performance objectives permit greater levels of inelastic response to be assigned to the component. In the above table, for example, a primary diaphragm under a Life Safety performance objective is assigned an m-factor of 2.0, while a secondary diaphragm under a Collapse Prevention performance objective is assigned an m-factor of 3.1. Basically, the former is allowed a maximum deformation of 2.0 times the yield deformation; the latter is allowed a maximum deformation of 3.1 times the yield deformation.

Only forces in deformation-controlled components are permitted to be reduced by m-factors. Force-controlled components must remain elastic during expected response. Rehabilitation is acceptable for force-controlled components if,

$$\kappa Q_{CL} \geq Q_{UF} \quad , \quad \text{Equation 7-5}$$

where,

Q_{CL} = (from FEMA 356) lower-bound strength of component or element at the deformation levels under consideration for force-controlled actions; and

Q_{UF} = combined earthquake and gravity force in component, calculated using applicable analysis procedure.

Fundamental to this study was the development of a basic index of probable diaphragm performance (diaphragm drift ratio), and the incorporation of that index into the existing FEMA 310 evaluation procedures. In Chapter 6, simple relationships were identified (Equations 6-12 and 6-13) that describe the level of diaphragm drift ratio at which a diaphragm, described by the intrinsic measure of in-plane stiffness G' , begins to sustain measurable damage (Figure 7.3). It was shown in Chapter 6 that the relationships describe the boundary between Immediate Occupancy and Life Safety/Collapse Prevention performance levels for wood and metal-deck diaphragms (Figure 7.3).

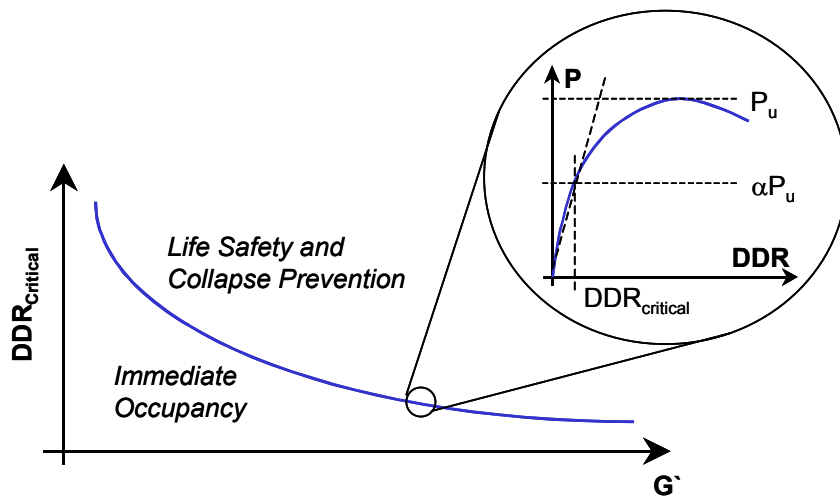


Figure 7.3 Relationship between reevaluated diaphragm data and performance levels

M-factors and attendant acceptability procedures (Equation 7-4 and Equation 7-5) are critical to the rehabilitation process and hence must be consistent with conclusions drawn from this study.

7.3.3.1 Acceptance Criteria for Lumber Diaphragms

Lumber diaphragms are considered deformation-controlled elements in FEMA 356 and are thus afforded the use of force-reducing m-factors. The document catalogs yield strengths of wood diaphragms, as opposed to ultimate strengths, for use in Equation 7-4. The construction of Figure 7.3, with each data point indicating incipient yield, implies that the m-factor for lumber diaphragms at the IO performance level should approximately equal 1.0; load in the diaphragm should not exceed its yield strength. FEMA 356 lists m-factors for 22 different types of wood diaphragms with 10 lumber-sheathed diaphragms and 12 panel-sheathed diaphragms. Indeed, the average m-factor for lumber-sheathed diaphragms is 1.2, nearly the expected value of 1.0.

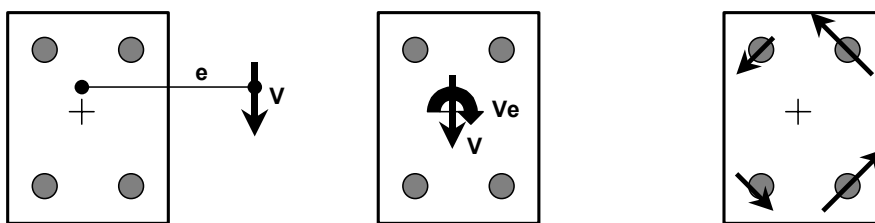
7.3.3.2 Acceptance Criteria for Metal-Deck Diaphragms

Metal-deck diaphragms are considered force-controlled components in FEMA 356 and are not afforded the use of force-reducing m-factors. FEMA 356 Table C1-4 defines the IO performance level for metal-deck diaphragms as: “Connections between deck units and framing intact. Minor distortions.” Similarly, the LS performance level is defined as: “Some localized failure of welded connections of deck to framing and between panels. Minor local buckling of deck.” Although otherwise suggested by the existence of this language, the framework of FEMA 356 does not afford the distinction of performance level for force-controlled components. The document categorically requires that force-controlled components remain elastic. The categorical acceptance criterion for

metal-deck diaphragms of Equation 7-5 may not accurately identify elastic response, however.

Lower-bound strength (approximate elastic limit) of a metal-deck diaphragm, used in Equation 7-5, is governed by the strength of the connections. This was demonstrated by the quasi-static testing described in Chapter 4 of this dissertation and is corroborated by the provisions and commentary of FEMA 356 Section 5.9.1.3 for welded metal deck: “Lower-bound strengths, Q_{CL} , of welded connectors shall be as specified in the Welding Code for Sheet Steel, *AWS D1.3*, or other approved standard.” Evaluation of Equation 7-5 for these types of diaphragms therefore involves the determination of individual weld strength, such as in *AWS D1.3*, and the distribution of individual weld forces.

The latter is not trivial, however. Many studies have shown (Chapter 2) that the distribution of weld forces is complex; some welds may carry significantly higher loads than others. A somewhat analogous situation is the distribution of bolt shear forces in a structural steel connection, in an eccentrically loaded bolt group (Figure 7.4). The combination of shear and torsion result in some bolts resisting significantly higher loads than others.



Eccentrically Loaded Group = Combination of Shear and Torsion = Unequal Forces in Group

Figure 7.4 Effect of shear eccentricity on resultant connector forces

In the case of metal-deck diaphragms, the differences in weld forces result from a similar mechanical circumstance. In-plane shear forces in a metal-deck panel are not applied through the center of resistance of that panel. They are

applied eccentrically. This does not preclude the calculation of the lower-bound strength of an individual weld; it rather precludes the simple and accurate calculation of the lower-bound strength of a diaphragm, as a whole, and hence its disposition for acceptance.

7.4 Proposed Supplementary Methodology

The critical review of FEMA 356, presented in Sections 7.3.1 through 7.3.3, suggests that the FEMA methodology is generally consistent with the conclusions of this study. Two refinements to that methodology are possible, however:

1. the FEMA 356 Section 3.3.1.3.5 sub-methodology for the analysis of unreinforced masonry buildings should be adapted to include the analysis of low-rise reinforced masonry buildings with flexible diaphragms; and
2. the FEMA 356 acceptance criterion for force-controlled metal-deck diaphragms should be modified to give a more accurate calculation of diaphragm lower-bound strength.

These proposed refinements are now detailed.

FEMA 356 includes a sub-methodology outlining the analysis of unreinforced masonry buildings with flexible diaphragms. The sub-methodology is similar to that presented in Chapter 6 of this dissertation for low-rise reinforced masonry buildings with flexible diaphragms, and should be adapted to include the analysis of such buildings. Adaptation would require the incorporation of a qualified diaphragm deformation limit for Immediate Occupancy performance levels, such as Equations 6-12 and 6-13.

FEMA 356 insufficiently characterizes the performance of metal-deck diaphragms. The acceptance criterion of Equation 7-5 compares the elastic

performance (lower-bound strength) of a metal-deck diaphragm with the applied seismic load. As discussed, the complex distribution of weld forces precludes the accurate identification of such a lower-bound strength. It has been shown in this dissertation and elsewhere (Luttrel 1967), however, that a metal-deck diaphragm begins to sustain damage, such as weld failure, at approximately 40 % of its ultimate strength, and that level of load generally corresponds to a distinct level of diaphragm drift ratio (Equation 6-12). Therefore, the lower-bound strength of a metal-deck diaphragm is approximately 40 % of ultimate strength.

This simplifies the calculation of acceptance for a metal-deck diaphragm. The evaluating engineer could avoid the difficult determination of strengths and forces of individual welds, and could instead use a lower-bound strength of 40 % of ultimate strength, or the relationship of Equation 6-12 as a limit on the diaphragm drift ratio.

7.5 Summary of Results, Conclusions, and Significance of Critical Review and Supplementary Methodology

7.5.1 Summary of Results and Conclusions

Three main components of the FEMA 356 methodology were critically reviewed: analysis, diaphragm modeling, and acceptability criteria. The review suggested that, although it did not exhibit apparent gaps, the Linear Static analysis procedure of FEMA 356 could be enhanced by adapting the existing sub-methodology for the analysis of unreinforced masonry buildings to incorporate the class of buildings addressed by this study. The review also suggested that the acceptability criterion for metal-deck diaphragms was potentially erroneous. Results from this research provide a solution to that potential error, however. Other aspects of the existing methodology did not exhibit any apparent

methodological gaps and was consistent with the knowledge and conclusions of this study.

7.5.2 Significance of Critical Review

Results and conclusions from shaking-table testing and quasi-static testing, presented in Chapters 3 and 4, were synthesized into an analysis tool designed to account for the effect of diaphragm flexibility on response of low-rise buildings. The tool was presented and verified in Chapter 5, and further enhanced in Chapter 6. In that chapter, the tool was integrated with the existing seismic evaluation methodology of FEMA 310 to fill gaps in that methodology. In this chapter the seismic rehabilitation methodology of FEMA 356 was critically reviewed to identify potential gaps in the treatment of low-rise reinforced masonry buildings with flexible diaphragms. It was shown that this study can enhance some aspects of the methodology. The supplementary evaluation methodology of Chapter 6 is applied to four real structures in the next chapter, and is ultimately shown to be effective, simple, and accurate.

8.0 Application of Proposed Supplementary Seismic Evaluation Methodology

As the final phase of this study, four existing military-owned low-rise reinforced masonry buildings with flexible diaphragms were evaluated for seismic deficiencies. The buildings were evaluated using two methodologies: the existing methodology of the FEMA 310 document; and the supplementary methodology proposed in Chapter 6. Results of the evaluations were compared with each other, and with the results from existing seismic evaluations of the same buildings performed by URS Greiner Inc. (San Francisco, CA) in the mid-1990s. The evaluations qualitatively and quantitatively assessed the proposed supplementary methodology. Example evaluations, using FEMA 310 and the supplementary methodology proposed in Chapter 6, are provided in Appendix C of this dissertation.

8.1 Selection of Buildings for Evaluation

In the mid-1990s, as a result of Executive Order 12941, the US Army contracted URS Greiner to screen their existing building inventory in Ft. Lewis, Washington, for seismic deficiencies (URS Greiner 1997). Those screenings were used in this study to identify candidate buildings for evaluation using the supplementary methodology proposed in Chapter 6.

8.1.1 URS Greiner Inc. Hierarchy of Structural Classifications for Ft. Lewis

URS Greiner performed a facility-wide seismic evaluation of over 4000 structures in Ft. Lewis, Washington. To simplify the evaluation of such a large number of structures, URS Greiner and CERL developed the hierarchical inventory-classification system outlined in Figure 8.1.

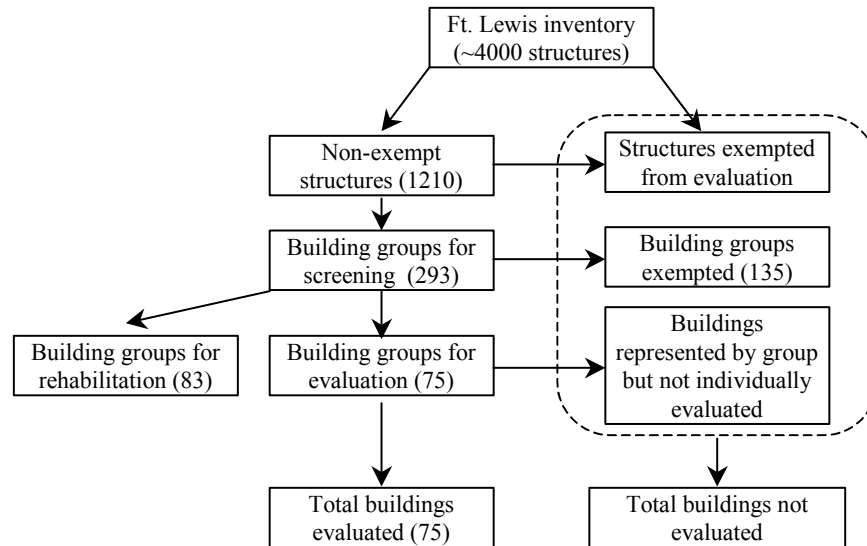


Figure 8.1 Hierarchy of building classification used by URS Greiner for Ft. Lewis, WA

Ft. Lewis comprises an inventory of over 4000 structures. Of those more than 4000 structures, 1210 were classified as “non-exempt” and were considered for seismic evaluation. Structures classified as “exempt” were deemed to pose no significant threat to human life, and were not considered for seismic evaluation. Based on criteria established by CERL, the remaining inventory of 1210 buildings was further divided into 293 “building groups.” Each building group comprised a subset of the non-exempt inventory that shared key structural characteristics such as year of construction, primary structural system, and number of stories. One representative building from each building group was then selected for evaluation, and group-wide dispositions were based on that single evaluation. The number of buildings comprising each group ranged from only one to over 80.

Preliminary screening of the 293 building groups by URS Greiner Inc. determined that 135 building groups were exempted from further evaluation, 83 building groups were classified in need of rehabilitation without further

evaluation, and 75 building groups were classified in need of further evaluation before assignment of disposition.

In this dissertation, buildings are arbitrarily assigned numerical identifications.

8.1.2 CERL Screening of Ft. Lewis Inventory

CERL reviewed the results of the URS Greiner screening and, of those, identified buildings belonging to the general family of low-rise reinforced masonry buildings with flexible diaphragms. Out of those, six particular buildings, selected by CERL, were reviewed and compared with a set of selection criteria to determine their applicability to this study. Presented in the form of questions, those are:

- A. Are the diaphragms flexible?
- B. Are the plan aspect ratios of diaphragms greater than one?
- C. Are the walls constructed of reinforced masonry?
- D. Are the general plan and vertical layouts of the building regular?
- E. Are structural drawings available?
- F. Is the building located near other potential candidate buildings?

This set was not strictly hierarchical, however. That is, for example, a building that embodies some irregularities in configuration (Criterion D) may still be selected for further evaluation, however, because a complete set of structural drawings is available (Criterion E) and it is located near other candidate buildings (Criterion F). To handle such cases, the overall compliance of each building with the criteria set was assessed numerically. Numerical scores of zero, one, or two representing, respectively, increasing levels of compliance, were assigned to each criterion for each building. Then, overall compliance scores were calculated for each building. Table 8-1 summarizes results of that assessment.

Based on this, the four highest-scoring buildings were selected for possible further evaluation and are described in Table 8-2. Assessments of Buildings 1 and 2 resulted in low overall compliance scores primarily because Building 1 has multiple reentrant corners and multiple reinforced masonry cross walls, and Building 2 has multiple reentrant corners, an inclined roof diaphragm, a discontinuous roof diaphragm due to vertical offsets in the plane of the diaphragm, and is located in Ft. Irwin, CA (rather than Ft. Lewis, WA).

Table 8-1 Numerical assessment of candidate buildings selected by CERL

Building	Criterion						Total score (Sum of A to F)
	A	B	C	D	E	F	
1	1	0	2	0	2	2	8
2	2	1	2	0	2	0	7
3	2	2	2	1	2	2	11
4	1	2	2	1	1	2	9
5	2	2	2	1	2	2	11
6	2	2	2	1	2	2	11

Table 8-2 Buildings selected for possible additional seismic evaluation

Building	Location	Construction of walls	Construction of diaphragm	Structural drawings
3	Ft. Lewis, Washington	Reinforced concrete-masonry barrier wall	Welded metal-deck on steel framing	Available
4		Reinforced masonry cavity wall	T&G** sheathing on dimension lumber framing	Partial set
5		Reinforced concrete-masonry barrier wall	Welded metal-deck on steel framing	Available
6		Reinforced concrete-masonry barrier wall	Welded metal-deck on OWJ	Available

**Tongue and Groove

8.1.3 Additional Screening of Ft. Lewis Inventory

The entire non-exempt Ft. Lewis building inventory was also screened to identify possible additional candidate buildings. The inventory was specifically screened for the subset of one-story reinforced masonry buildings with flexible diaphragms. The non-exempt inventory was evaluated using several simple criteria. Presented in the form of questions, those are:

- A. Is the building one-storied?
- B. Was the building built between the years 1950 and 1980?
- C. Was the building already evaluated by URS Greiner Inc.?
- D. Is the structure a low-rise masonry building with a flexible wood or metal-deck diaphragm (FEMA 310 Type RM1)?

Of the 1210 non-exempt buildings in Ft. Lewis, 186 buildings complied with Criterion A; 97 buildings complied with Criteria A and B; 17 buildings complied

with Criteria A, B, and C; and 7 buildings complied with all the criteria. Of those 7 buildings, 3 had been previously identified in the earlier CERL selection process (Section 8.1.2), and one was immediately eliminated from the selection process because of extreme plan and vertical geometric irregularities. Therefore, Buildings 7, 8, and 9 were additionally identified as possible candidate buildings for seismic evaluation.

Buildings 7, 8, and 9 were then compared with the same set of selection criteria in listed in Section 8.1.2. Similarly, numerical scores of zero, one, or two (representing increasing levels of compliance) were assigned to each criterion for each building. Those scores were then summed over all criteria to obtain an overall compliance score for each building.

8.1.4 Buildings for Evaluation

Table 8-3 summarizes results of the assessments for the buildings of Table 8-2 and Buildings 7, 8, and 9. Based on the results, Buildings 8, 9, 6, and 3 were selected for seismic evaluation, are described in Table 8-4 and shown in Figure 8.2 through Figure 8.5

Table 8-3 Numerical assessment of candidate buildings for compliance with criteria

Building number	Criterion						Total score (Sum of A to F)
	A	B	C	D	E	F	
3	2	2	2	1	2	2	11
4	1	2	2	1	1	2	9
5	2	2	2	1	2	2	11
6	2	2	2	2	2	2	12
7	2	2	2	2	2	2	12
8	2	2	2	2	2	2	12
9	2	2	2	1	2	2	11

Although they had the same compliance scores and the two buildings are very similar in construction, use, and configuration, Building 8 was selected

rather than Building 7 because Building 8 has a larger diaphragm plan aspect ratio. Similarly, although it had the same compliance score as other buildings (for example, Buildings 9 and 3), Building 5 was not selected because it is two-storied.

Table 8-4 Buildings selected for additional seismic evaluation

Building	Construction of walls	Construction of diaphragm	Structural drawings set number
8	Reinforced CMU barrier wall	Welded metal-deck on open-web joists	AS-BLT 222-25-102
9		Welded metal-deck on open-web joists	22s/33-26-07
6		Welded metal-deck on open-web joists	AS-BLT 22s/30-05-03
3		Welded metal deck on steel framing	AS-BLT 22s/33-01-02



Figure 8.2 Building 8



Figure 8.3 Building 9



Figure 8.4 Building 6



Figure 8.5 Building 3

8.2 Application of Current Seismic Evaluation Methodology

A total of twenty-eight seismic evaluations of the four buildings in Table 8-4 are reported in this dissertation. The buildings were evaluated using two methodologies: FEMA 310, and the methodology proposed as part of this study. URS Greiner performed four evaluations using site-specific seismicity consistent with Ft. Lewis, WA. The four buildings were evaluated in this study three times using procedures of FEMA 310: once using seismicity consistent with Ft. Lewis, WA and diaphragm stiffnesses consistent with as-built conditions; again using seismicity consistent with Ft. Lewis, WA but with hypothetically reduced diaphragm stiffnesses, and finally using seismicity consistent with San Francisco, CA and diaphragm stiffnesses consistent with as-built conditions.

Following development of the proposed supplementary evaluation methodology (Chapter 6), the four buildings were evaluated three times using the proposed methodology: once using seismicity consistent with Ft. Lewis, WA and

diaphragm stiffnesses consistent with as-built conditions; again using seismicity consistent with Ft. Lewis, WA and hypothetically reduced diaphragm stiffnesses; and finally using seismicity consistent with San Francisco, CA and diaphragm stiffnesses consistent with as-built conditions. Specific discussions of each set of evaluations (cataloged in Figure 8.6) follow.

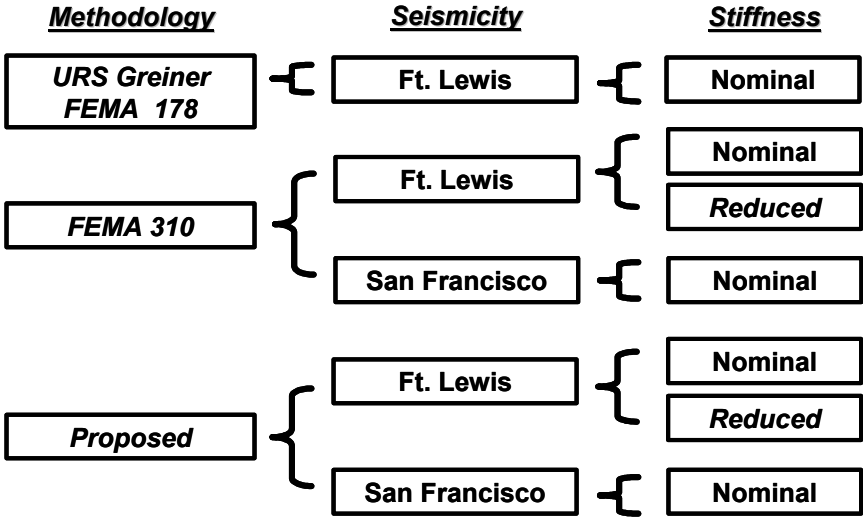


Figure 8.6 Catalog of building evaluations

8.2.1 URS Greiner Evaluations

The URS Greiner evaluations were based on the US Army *Screening and Evaluation Procedures for Existing Military Buildings* (US Army Corps of Engineers 1995), which is based on FEMA 178. Results of those evaluations for the four selected buildings are summarized in Table 8-5.

Table 8-5 URS Greiner dispositions of selected buildings, evaluated in Ft. Lewis, WA

Building	Disposition	Identified Deficiency
8	Compliant	-
9	Non-compliant	shear transfer from diaphragm to wall
6	Compliant	-
3	Compliant	-

It is important to note that the dispositions and deficiencies listed in Table 8-5 are not entirely consistent. Three buildings (9, 6, 3) used similar joist-to-wall details (Figure 8.7) as the only mechanism to transfer shear forces from diaphragm to walls. The engineers who evaluated Buildings 6 and 3 considered this detail to be sufficient for shear transfer. The engineer who evaluated Building 9 considered it otherwise. Of the two engineers who considered the condition sufficient, one considered it so based on judgment without justification; the other considered it so only following further analysis of the connection detail. Therefore, the dispositions of “compliant” and “non-compliant,” as shown in Table 8-5, were not consistently assigned throughout the evaluation process.

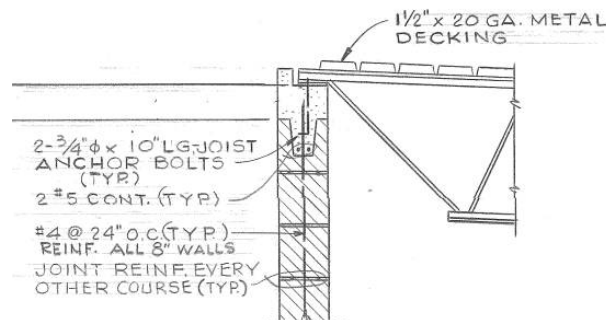


Figure 8.7 Typical joist-to-wall connection in Buildings 9, 6, 3

8.2.2 FEMA 310 Evaluations

The goal of these evaluations was to verify suspected gaps in the FEMA 310 methodology, discussed in Chapter 6, and to provide a comparison to both the URS Greiner methodology and the supplementary methodology proposed in this study. The four buildings of Table 8-4 were evaluated twice using FEMA 310: once using seismicity consistent with Ft. Lewis, WA; and again using seismicity consistent with San Francisco, CA. In both evaluations, the buildings were assumed to be founded on soil corresponding to Site Class D (stiff soil). The buildings were evaluated at the Life Safety performance level.

Screening (Tier 1) indicated deficient diaphragm-to-wall shear-transfer mechanisms in three of the four buildings (Buildings 9, 6, and 3, Table 8-6 and Figure 8.7). As discussed earlier, in most cases the metal-deck diaphragm itself was connected to the shear walls only through the joist-to-wall connections (Figure 8.7). That condition was considered deficient in these evaluations. Modern construction of metal-deck diaphragms requires that the metal deck itself be continuously connected to all shear walls along the diaphragm perimeter. This is generally accomplished using continuous structural angles anchored along the tops of perimeter shear walls, and intermittently welded or otherwise connected to the metal deck.

Further deficiency-specific Evaluation (Tier 2) of the deficient joist-to-wall connections, in the three non-compliant buildings, indicated that the connections were actually sufficient to transfer the diaphragm shear (Table 8-6).

To test the sensitivity of the methodology to the level of seismicity, the four buildings were then evaluated using seismicity consistent with San Francisco, CA. Connections in two of the three buildings (6 and 3) were found to be deficient when subjected to the higher level of seismicity (Table 8-6). The

deficiencies were due to insufficient shear capacities of anchor bolts connecting the roof framing to the masonry walls (Figure 8.7).

Table 8-6 Dispositions of selected buildings, evaluated using FEMA 310

Building	Screening (Tier 1)		Evaluation (Tier 2)
	Disposition	Deficiency	Disposition
Ft. Lewis, Washington ($S_s = 1.2g$, $S_1 = 0.4g$)			
8	Compliant	-	-
9	Non-compliant	shear transfer from diaphragm to wall	Compliant
6	Non-compliant	shear transfer from diaphragm to wall	Compliant
3	Non-compliant	shear transfer from diaphragm to wall	Compliant
San Francisco, California ($S_s = 2.0g$, $S_1 = 0.9g$)			
8	Compliant	-	-
9	Non-compliant	shear transfer from diaphragm to wall	Compliant
6	Non-compliant	shear transfer from diaphragm to wall	Non-compliant
3	Non-compliant	shear transfer from diaphragm to wall	Compliant

8.3 Application of Proposed Supplementary Seismic Evaluation Methodology

The four buildings of Table 8-4 were evaluated for Life Safety using the methodology proposed in Steps 1 through 6, in Chapter 6. The methodology emphasized three items not currently addressed by the Screening phase of FEMA 310:

1. accurate calculation of diaphragm period;
2. calculation of diaphragm shear force demand and capacity; and
3. in the case of Immediate Occupancy performance, calculation of diaphragm deformation demand and capacity.

The diaphragms in the four buildings have unusually large in-plane stiffnesses compared to other typical metal-deck diaphragms. As an example, these diaphragms (20 gage, 36/7 puddle welding, button-punched @ 18in. o/c; $G' = 60$ kip/in.) are more than 10 times stiffer in-plane than those constructed using another typical configuration (for example, 22 gage, 36/3 puddle welding, button-punched @ 18in. o/c; $G' = 5$ kip/in.).

Table 8-7 Fundamental periods calculating using FEMA 310 Screening (Tier 1) provisions and proposed supplementary methodology

Building	Fundamental Period, <i>sec</i>	
	FEMA	Proposed supplementary methodology
Nominal diaphragm stiffness (20 gage, 36/7 puddle welds, button-punched at 18in. o/c)		
8	0.17	0.13
9	0.12	0.13
6	0.13	0.22
3	0.14	0.14
Reduced diaphragm stiffness (22 gage, 36/3 puddle welds, button-punched at 18in. o/c)		
8	0.17	0.47
9	0.12	0.47
6	0.13	0.77
3	0.14	0.50

The evaluations presented here are intended to demonstrate gaps in the existing FEMA 310 methodology, rather than identify specific deficiencies in specific buildings. The four buildings were thus evaluated twice using seismicity consistent with Ft. Lewis, WA: once, using the nominal diaphragm stiffnesses ($G' = 60$ kip/in.); and again using hypothetically decreased, but still typical, diaphragm stiffnesses ($G' = 5$ kip/in.). Table 8-7 and Table 8-8 summarize results of the eight evaluations.

Table 8-7 shows that fundamental periods calculated by the FEMA 310 Screening Phase (Tier 1) provisions are generally significantly shorter than those calculated by the proposed supplementary methodology. The FEMA 310 Evaluation Phase (Tier 2) includes a period expression developed specifically for low-rise buildings with flexible diaphragms (FEMA 310 Equation 4-1, FEMA 356 Equation 3-8). That equation is reasonably accurate for flexible diaphragm systems (Chapter 5) and would calculate periods similar to those calculated by the proposed supplementary methodology.

Table 8-8 Dispositions of buildings, evaluated using proposed supplementary methodology

Building	Diaphragm Shear, plf (Demand/Capacity)	DDR, % (Demand/Capacity)	Disposition
Ft. Lewis, WA			
Nominal diaphragm stiffness (20 gage, 36/7 puddle welds, button-punched at 18in. o/c)			
8	915 / 780	0.05 / 0.03	Non-compliant
9	473 / 780	0.05 / 0.03	Compliant
6	769 / 780	0.09 / 0.03	Compliant
	528 / 780	0.06 / 0.03	
3	462 / 780	0.05 / 0.03	Compliant
	397 / 780	0.04 / 0.03	
Ft. Lewis WA			
Reduced diaphragm stiffness (22 gage, 36/3 puddle welds, button-punched at 18in. o/c)			
8	915 / 391	0.66 / 0.40	Non-compliant
9	473 / 391	0.66 / 0.40	Non-compliant
6	486 / 391	0.68 / 0.40	Non-compliant
	478 / 391	0.67 / 0.40	
3	447 / 391	0.65 / 0.40	Compliant
	386 / 391	0.54 / 0.40	
San Francisco, CA			
Nominal diaphragm stiffness (20 gage, 36/7 puddle welds, button-punched at 18in. o/c)			
8	1386 / 780	0.08 / 0.03	Non-compliant
9	716 / 780	0.08 / 0.03	Compliant
6	1166 / 780	0.13 / 0.03	Non-compliant
	799 / 780	0.09 / 0.03	
3	699 / 780	0.08 / 0.03	Compliant
	601 / 780	0.07 / 0.03	

Table 8-8 shows that the proposed supplementary methodology found six of the twelve evaluated buildings to be non-compliant with a Life Safety performance objective (Column 4). Each pair of diaphragm demand and capacity values listed in the table (Columns 2 and 3) represents the response of one of the diaphragm systems used to idealize the building (Step 1 in the Proposed Supplementary Methodology). Table 8-8 also shows, however, that *DDR* demands were greater than *DDR* capacities in many cases. This requirement, according to the proposed supplementary methodology, applies to Immediate Occupancy performance levels only, and is hence not considered further. All buildings were evaluated for Life Safety.

Table 8-9 Dispositions of selected buildings from evaluations

Building	URS Greiner	FEMA 310			Proposed Supplementary Methodology		
		Ft. Lewis	Ft. Lewis reduced stiffness	San Francisco	Ft. Lewis	Ft. Lewis reduced stiffness	San Francisco
8	C	C	C	C	NC	NC	NC
9	NC	C	C	C	C	NC	C
6	C	C	C	NC	C	NC	NC
3	C	C	C	C	C	C	C

C: Compliant
 NC: Non-compliant

Table 8-9 compares results from all the evaluations presented in this chapter, and shows that the proposed supplementary methodology found a significantly greater number of buildings to be deficient, at the Life Safety performance level, than either the FEMA 310 or URS Greiner methodologies. (It is recognized that the URS Greiner methodology was based on the FEMA 178 document; an outdated version of FEMA 310.) In the deficient (non-compliant) cases, diaphragm shear demands exceeded diaphragm shear capacities. As demonstrated in Chapters 4 and 6, metal-deck diaphragms exhibit stiffness degradation and sustain significant damage at load levels greater than about 40 %

of ultimate capacity; they exhibit instability, and stiffness and strength degradation at load levels greater than ultimate capacity. Responses calculated using the proposed supplementary methodology therefore imply that, during an earthquake with spectral ordinates consistent with those of the appropriate FEMA 310 response spectrum, diaphragms of the deficient buildings would at least sustain significant damage, probably lose significant strength and stiffness, and possibly lose overall diaphragm action.

This conclusion indicates that a significant gap indeed exists in the FEMA 310 Screening Phase (Tier 1) assessment of low-rise reinforced masonry buildings with flexible diaphragms. The supplementary methodology proposed in this dissertation is intended to fill that gap.

8.4 Summary of Results, Conclusions, and Significance of Evaluations

8.4.1 Summary of Results and Conclusions

To assess the proposed supplementary seismic evaluation methodology developed in Chapter 6, four military-owned low-rise reinforced masonry buildings with flexible diaphragms were evaluated for seismic deficiencies. The four buildings were evaluated using three methodologies: first, by URS Greiner in 1997 using the US Army *Screening and Evaluation Procedures for Existing Military Buildings* (US Army Corp of Engineers 1995); second, as part of this study using the current FEMA 310 methodology; and third, using the proposed supplementary methodology.

The evaluations substantiated the hypothesis that the existing FEMA 310 methodology, while complete in many ways, does not sufficiently identify potential deficiencies in low-rise masonry buildings with flexible diaphragms. As shown, the proposed supplementary methodology can correct this gap and provide

a logical bridge between the Screening (Tier 1) and Evaluation (Tier 2) Phases of FEMA 310, where more rigorous evaluation procedures can sufficiently characterize the seismic performance of flexible diaphragms.

8.4.2 Significance of Evaluations

Results and conclusions from shaking-table testing and quasi-static testing, presented in Chapters 3 and 4, were synthesized, in Chapter 5 into a analysis tool designed to account for the effect of diaphragm flexibility on the response of these types of buildings. The tool was integrated with conclusions from previous testing programs to propose supplementary seismic evaluation and rehabilitation methodologies in Chapters 6 and 7, respectively. As the final phase of this study, the methodology was applied, in this chapter, to four real structures. Evaluations using the proposed supplementary methodology were compared to evaluations performed using existing methodologies (FEMA 310 and URS Greiner). The proposed supplementary methodology was shown to be needed, effective, and accurate.

9.0 Summary of Results and Conclusions, Synthesis of Study, and Recommendations

This dissertation reports a multi-phased research study performed jointly by The University of Texas at Austin and the United States Army Corp of Engineers, Construction Engineering Research Laboratory, Engineer Research and Development Center, from September 1999 to May 2004. The study integrates experimental testing, analytical modeling, and application-oriented research to the development of supplementary seismic evaluation and rehabilitation methodologies for low-rise reinforced masonry buildings with flexible diaphragms.

9.1 Summary of Results and Conclusions from Study Phases

The study was completed in four distinct phases: behavior, analysis, evaluation and rehabilitation, and application and verification. In the following summaries, the latter two (evaluation and rehabilitation, and application and verification) are discussed together.

9.1.1 *Summary of Results and Conclusions from Behavior Phase*

The seismic behavior (response and performance) of low-rise reinforced masonry buildings with flexible diaphragms was characterized using seismic and quasi-static testing.

First, two half-scale low-rise reinforced masonry building specimens with flexible diaphragms were tested on the United States Army Tri-axial Earthquake and Shock Simulator at CERL. The two shaking-table specimens, one with a diagonally sheathed diaphragm and one with a welded metal-deck diaphragm, were designed and constructed based on identified prototypical building

configurations. The specimens were then subjected to sequences of uni- and bi-axial earthquake ground motions at incrementally increasing levels of excitation.

The tests provided significant insights into, and data regarding, the seismic response of these types of buildings, and validated the widely held belief that diaphragm flexibility may significantly affect seismic response. These types of buildings rarely behave as single-degree-of-freedom systems, governed by the in-plane response of the shear walls; rather, they essentially behave as single-degree-of-freedom systems, governed by the in-plane response of the diaphragm. This result implied the need for an analysis tool that specifically models this behavior; indeed one that explicitly accounts for diaphragm flexibility and more accurately describes seismic response.

To augment results from shaking-table testing and complete the characterization of seismic behavior, the diaphragms and top four courses of attached masonry walls were removed from the shaking-table specimens and subjected to in-plane reversed cyclic quasi-static displacements. Data collected from these tests were evaluated in the context of diaphragm drift ratios and were used to characterize the hysteretic behaviors of the two assemblies. At low diaphragm drift ratios (less than about 0.6 % for the lumber diaphragm and less than about 0.5 % for the metal-deck diaphragm), the diaphragms did not degrade in stiffness or strength. At high diaphragm drift ratios, the lumber diaphragm exhibited stable overall hysteretic behavior (no strength degradation) with stiffness degradation and pinching, and the metal-deck diaphragm exhibited stiffness degradation, strength degradation, and specifically, unstable nonlinear elastic hysteretic behavior.

These tests, in combination with results from the shaking-table tests, also demonstrated the usefulness of the diaphragm drift ratio as a measure of overall diaphragm deformation, and as an index of potential diaphragm damage.

Completion of the shaking-table and quasi-static tests marked the end of the behavior phase of the study.

9.1.2 Summary of Results and Conclusions from Analysis Phase

Shaking-table and quasi-static testing demonstrated the effect of diaphragm flexibility on building behavior and also the need for an analysis tool to characterize that behavior.

To meet this need, a simple two-degree-of-freedom (2DOF) idealization of low-rise buildings with flexible diaphragms was developed. Linear elastic 2DOF analyses of the two shaking-table specimens and four prototypical hypothetical finite-element building models established the accuracy of the idealization for low levels of response. Calculated responses were very comparable to measured responses, in the case of the shaking-table specimens, and to responses from finite-element modeling, in both the cases of the shaking-table specimens and the prototypical hypothetical building models. Nonlinear lumped-parameter modeling of the two shaking-table specimens established the accuracy of the idealization for high levels of excitation.

Using parameter studies, the sensitivity of the idealization to changes in its constituent variables was investigated. Practical upper and lower bounds were established for those variables, and the idealization was applied to the particular case of low-rise reinforced masonry buildings with flexible diaphragms. Results of those studies suggested that the tool could be further simplified into a single-degree-of-freedom (SDOF) analysis tool, with that degree-of-freedom associated with the in-plane response of the diaphragm.

It was also shown that such a simplification would not significantly affect the accuracy of the tool. The two shaking-table specimens and the four prototypical hypothetical building models were analyzed as SDOF systems and

calculated responses from these analyses agreed well with those calculated by 2DOF analysis.

These studies demonstrated that the single-degree-of-freedom analysis tool is simple, justified, and accurate for the seismic analysis of low-rise reinforced masonry buildings with flexible diaphragms. The tool is accurate, robust with respect to required analysis parameters, and provides a logical method for the expedient calculation of global building response. Completion of these analyses marked the end of the analysis phase of the study

9.1.3 Summary of Results and Conclusions from Evaluation and Rehabilitation, and Application and Verification Phases

As discussed, a simple SDOF analysis tool was developed and verified for the analysis of these types of buildings. To realize the end objectives of this study, the tool was further enhanced and then integrated into existing evaluation and rehabilitation methodologies, to improve their treatment of low-rise reinforced masonry buildings with flexible diaphragms.

Critical reviews of existing evaluation (FEMA 310) and rehabilitation (FEMA 356) documents identified potential gaps in those methodologies. Review of FEMA 310 suggested that it did not sufficiently characterize or assess the seismic performance of these types of buildings. Deficient buildings might indeed be found sufficient.

To fill potential gaps in the FEMA 310 evaluation procedures, a supplementary seismic evaluation methodology was developed and integrated into the existing methodology. First, data from several previous flexible-diaphragm testing programs, performed by others, were reevaluated in the context of performance-based engineering. Data from the tests were reevaluated for critical levels of deformation and damage and then qualitatively related to specific

seismic performance levels described in the FEMA documents. The reevaluations demonstrated that simple describable relationships exist between an intrinsic measure of diaphragm stiffness and critical levels of diaphragm deformation (diaphragm drift ratio). These relationships, in combination with the SDOF analysis tool, comprise the proposed supplementary seismic evaluation methodology.

Potential gaps in the FEMA 356 rehabilitation procedures were less significant than that found in FEMA 310. It was suggested that adapting the existing FEMA 356 sub-methodology for unreinforced masonry buildings could enhance the analysis procedure most often used for these types of buildings. The acceptance criterion for metal-deck diaphragms was also enhanced using conclusions drawn from this study. These two items comprise the proposed supplementary seismic rehabilitation methodology.

To assess and validate the usefulness of the proposed supplementary evaluation methodology, four military-owned low-rise reinforced masonry buildings with flexible diaphragms were evaluated for seismic deficiencies. The four buildings were evaluated 28 times using different combinations of three methodologies, two levels of seismicity, and two hypothetical diaphragm stiffnesses. The three methodologies were: that used by URS Greiner in 1997; the current FEMA 310 methodology; and the supplementary methodology proposed in this study. The two levels of seismicity were those consistent with Ft. Lewis, Washington and with San Francisco, California.

The evaluations substantiated the hypothesis that the existing FEMA 310 methodology, while complete in many ways, does not sufficiently identify potential diaphragm deficiencies in low-rise reinforced masonry buildings with flexible diaphragms. It was shown that out of 16 buildings evaluated using the existing methodologies (URS Greiner and FEMA 310) only 2 were found to be

non-compliant/deficient. Contrastingly, out of 12 buildings evaluated using the the proposed supplementary methodology, 6 were found to be non-compliant/deficient. The proposed supplementary methodology was therefore ultimately shown to be needed, effective, and simple.

Completion of these evaluations marked the ends of the evaluation and rehabilitation phase and the application and verification phase, as well as the end of the study.

9.2 Synthesis of Study Elements to Meet Study Objectives

As discussed, the four phases of study were synthesized and the basic study objective was realized. Methodologies for the seismic evaluation and rehabilitation of these types of buildings were critically assessed and consequently enhanced. Auxiliary to this and equally significant, was the development a consistent overall approach for the characterization of seismic performance of these types of buildings (Figure 9.1). In that figure, data from shaking-table testing are integrated with dynamic analysis to form a simple analysis tool, used to characterize seismic behavior. Data from quasi-static testing and from previous testing programs are integrated with the diaphragm drift ratio concept to form a simple performance tool, used to relate seismic behavior with seismic performance. Together, the analysis and performance tools form a methodology for the consistent and accurate seismic evaluation and rehabilitation of these types of buildings. It is important to note that the methodology uses the same basic set of tools and criteria for modeling, analysis, and evaluation and rehabilitation, regardless of the low-rise reinforced masonry building with flexible diaphragm being considered. Use of such a methodology by the structural engineering technical community will help emphasize consistency and reliability in the evaluation and rehabilitation of these types of buildings.

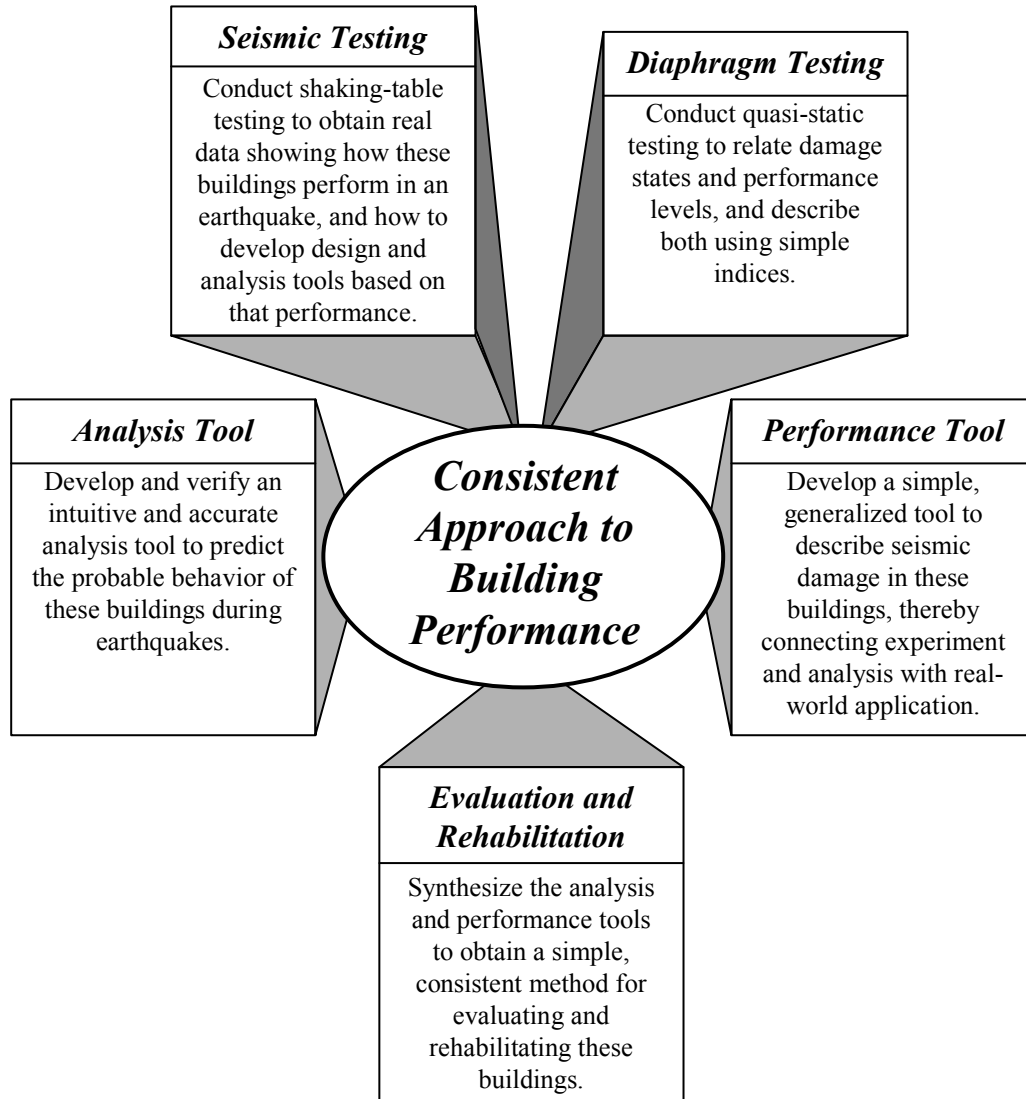


Figure 9.1 Synthesis of study elements into a consistent approach performance of low-rise reinforced masonry buildings with flexible diaphragms

9.3 Recommendations

Roof and floor diaphragm flexibility can significantly affect the seismic response of buildings, and in particular the response of low-rise reinforced

masonry buildings. The abundance of these types of buildings in the United States inventory impresses the need for seismic evaluation and rehabilitation methodologies that accurately assess the performance of such systems.

The FEMA 310 *Handbook for the Seismic Evaluation of Buildings – A Prestandard* methodology currently exhibits gaps in its treatment of these types of buildings. The Screening Phase (Tier 1) of the document does not sufficiently characterize flexible diaphragm performance and hence does not generally trigger the more rigorous and accurate Evaluation Phase (Tier 2), where diaphragm deficiencies might be identified. The methodology should be refined to fill this demonstrated gap.

Such a refinement is presented in Chapter 6 of this dissertation, and is demonstrated in Chapter 8. The single-degree-of-freedom analysis tool and attendant diaphragm-performance relationships comprise a coherent and useful supplementary seismic evaluation methodology for these types of buildings. The methodology identifies flexible diaphragm deficiencies not otherwise identified by the current FEMA 310 methodology.

Similarly, the FEMA 356 *Prestandard and Commentary for the Seismic Rehabilitation of Buildings* methodology currently exhibits a gap in its characterization of metal-deck performance. The acceptance criterion for such a diaphragm cannot be correctly assessed using common analysis methods. The methodology should be refined to fill this potential gap.

Such a refinement is presented in Chapter 7 of this dissertation. Relationships developed in this study relate diaphragm force and deformation, with distinct levels of damage. These relationships can be used to identify the lower-bound strength of a diaphragm, and consequently to determine its disposition of acceptability.

The analysis procedures of FEMA 356 may also be enhanced. The document includes a sub-methodology for the analysis of unreinforced masonry buildings with flexible diaphragms that is similar to the supplementary evaluation methodology developed in this study. The sub-methodology should be adapted to include the analysis of similar low-rise reinforced masonry buildings. Such an adaptation would require the incorporation of a qualified diaphragm force or deformation limit for Immediate Occupancy performance levels, such as those presented in this dissertation.

The two items, refinement of lower-bound strength calculation for metal-deck diaphragms and enhancement of the analysis procedures, comprise the proposed supplementary rehabilitation methodology.

These proposed supplementary seismic evaluation and rehabilitation methodologies represent the realization of the overall study objectives; to enhance the accuracy and efficiency of seismic hazard assessment and mitigation for low-rise reinforced masonry buildings with flexible diaphragms.

Appendix A: Instrumentation of Diaphragm Specimens

A.1 Instrumentation of Diaphragm #1 (Lumber Sheathing)

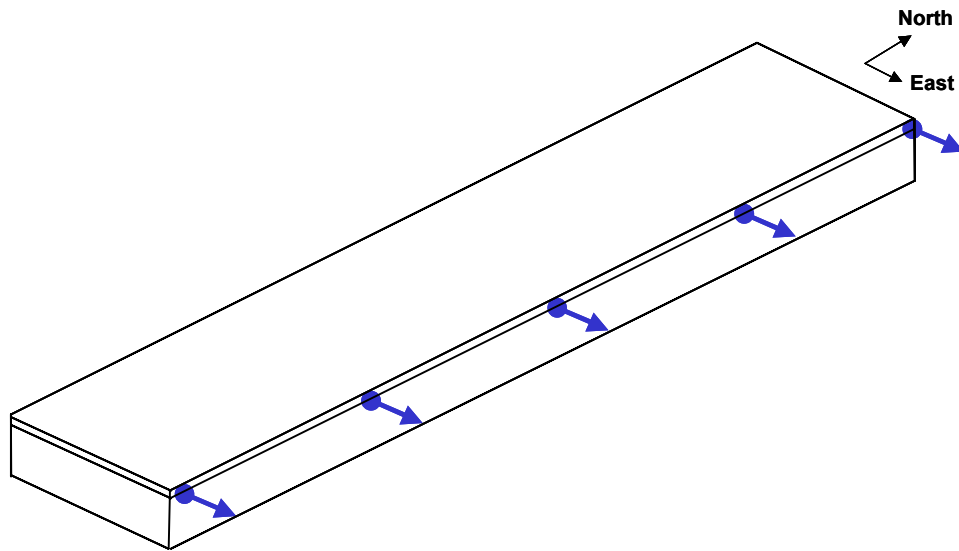


Figure A.1 Instrumentation measuring transverse in-plane deflections

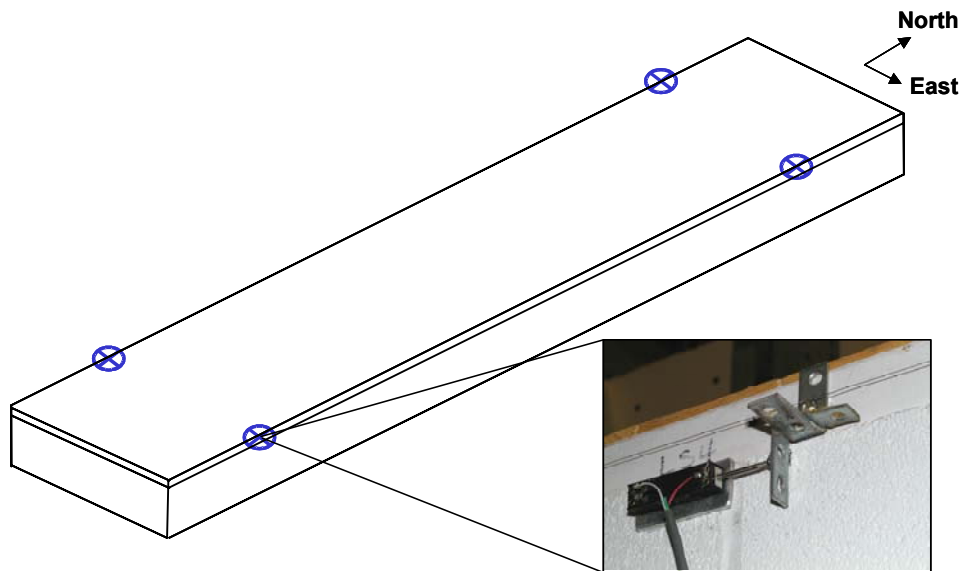


Figure A.2 Instrumentation measuring relative slip between masonry chords and nailer

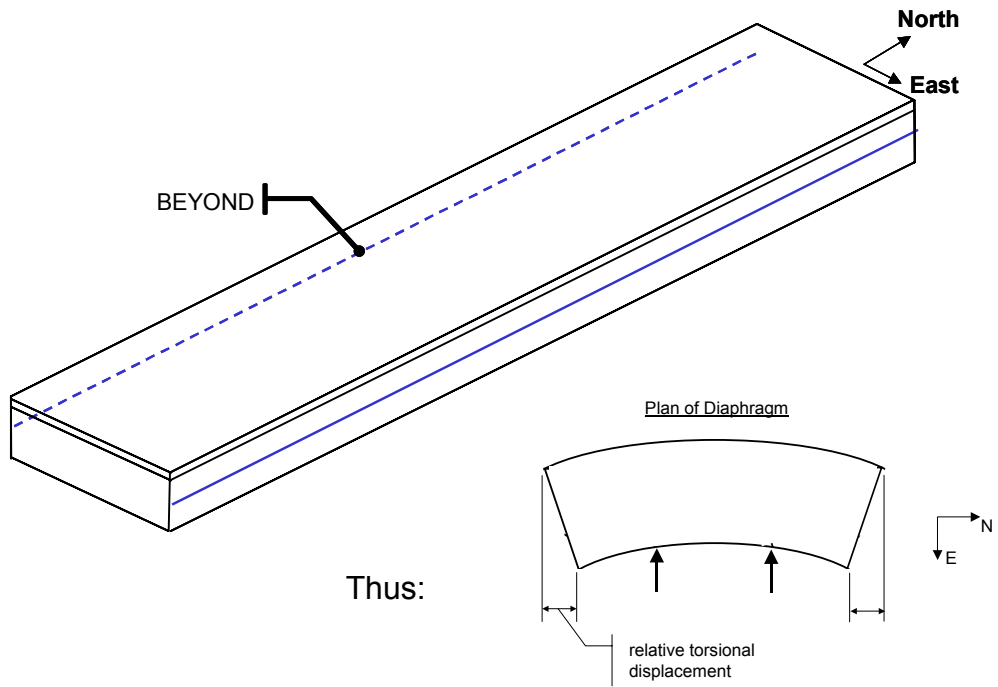


Figure A.3 Instrumentation measuring relative torsional displacement of end columns

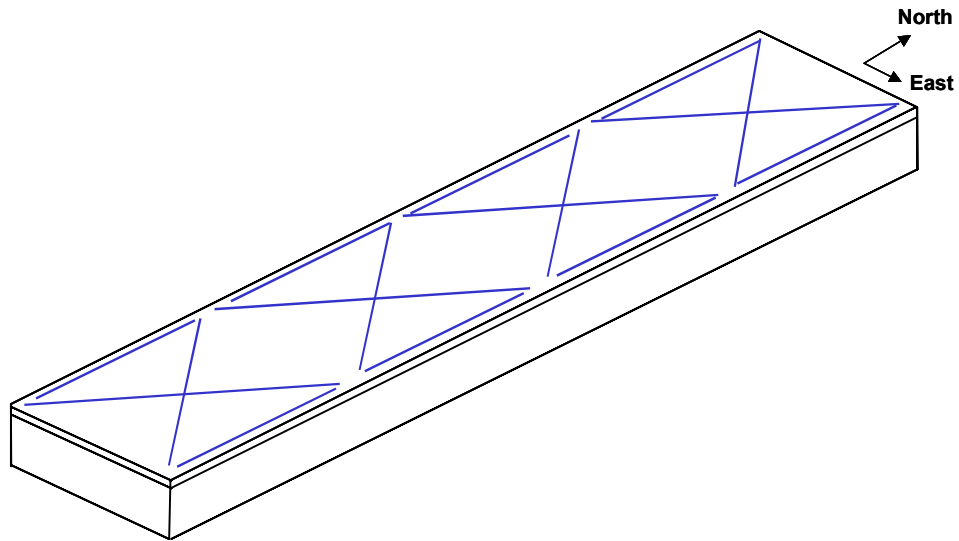


Figure A.4 Instrumentation measuring relative in-plane deformations

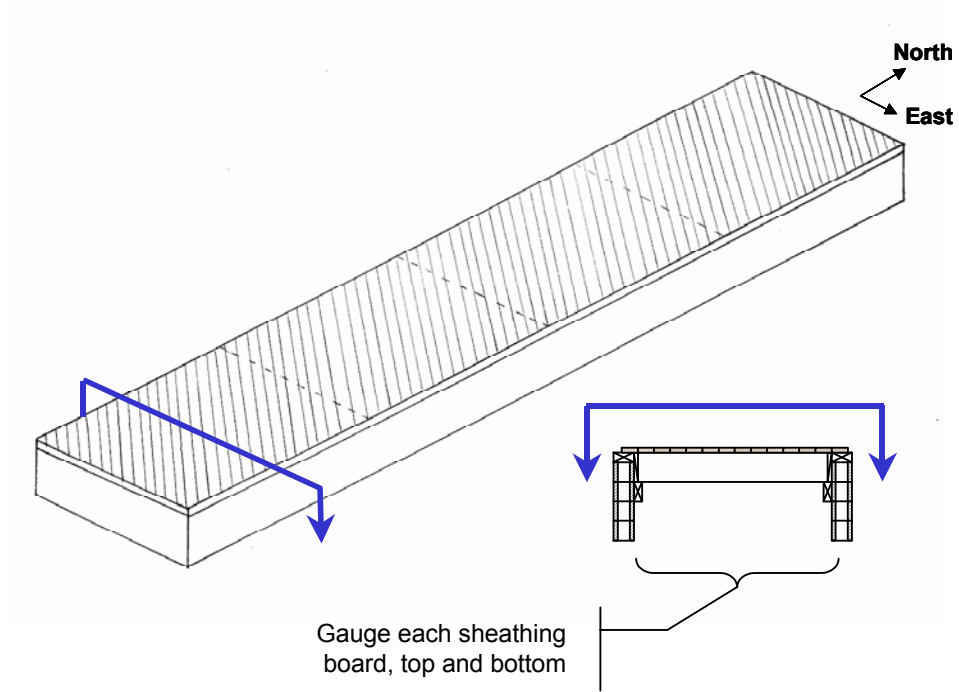


Figure A.5 Instrumentation measuring in-plane shear strains

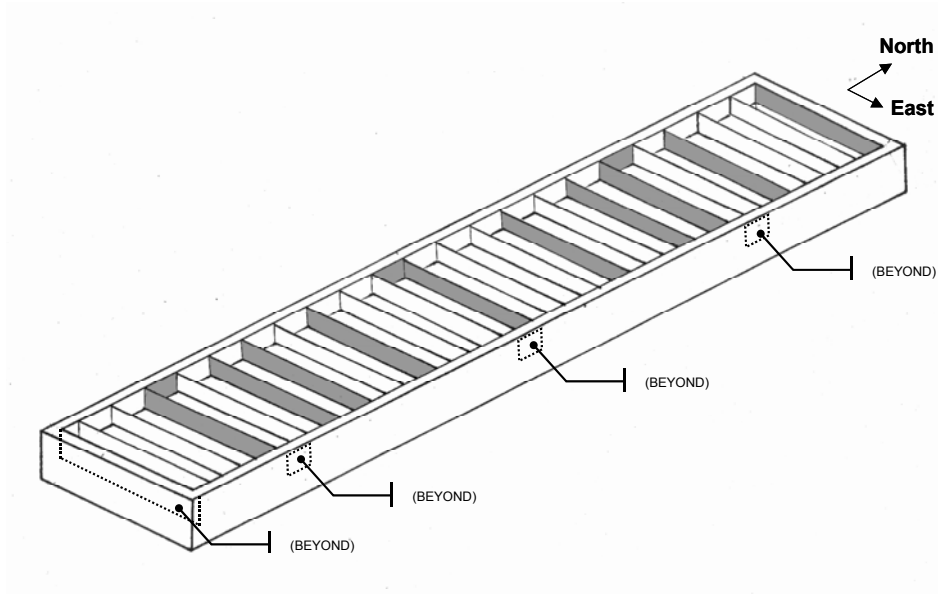


Figure A.6 Instrumentation measuring strains in diaphragm rafters and blocking; shaded members are strain-gauged

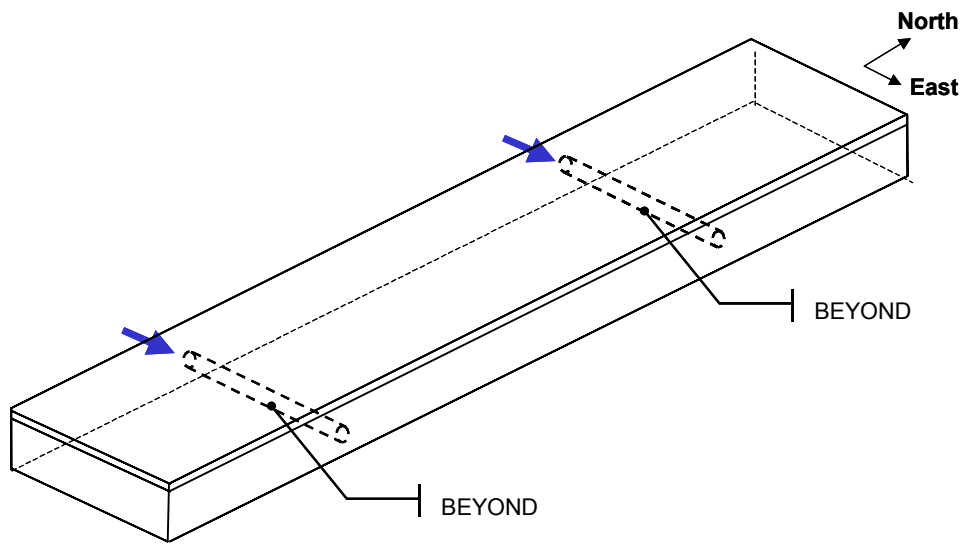


Figure A.7 Instrumentation measuring axial forces in load struts; struts are strain-gauged

A.2 Instrumentation of Diaphragm #2 (Metal-Deck)

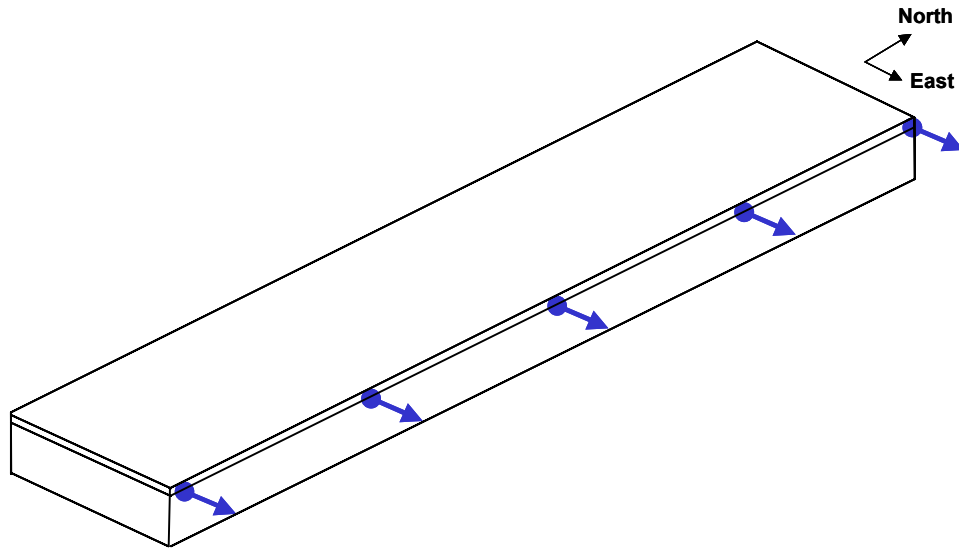


Figure A.8 Instrumentation measuring transverse in-plane deflections

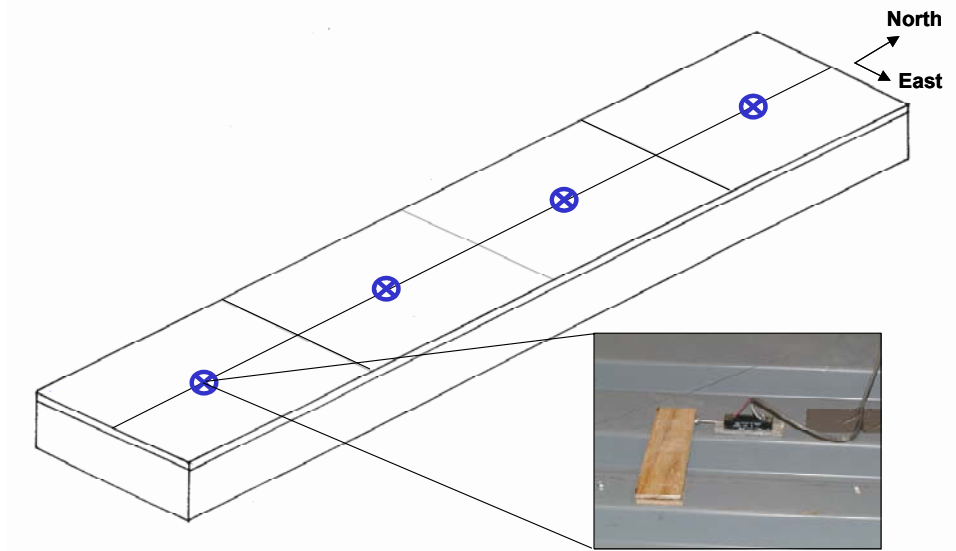


Figure A.9 Instrumentation measuring relative side-lap slip between adjacent panels

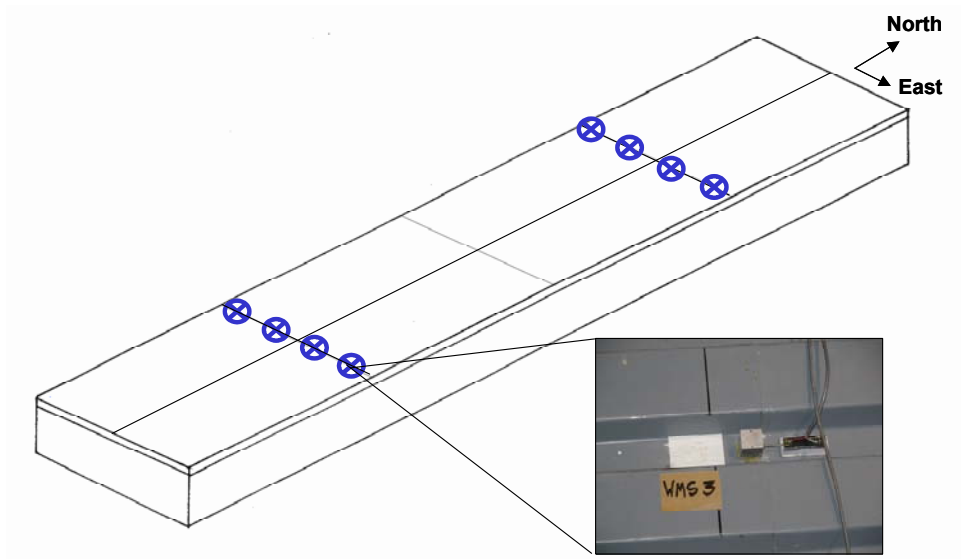


Figure A.10 Instrumentation for measuring end-lap slip at puddle welds

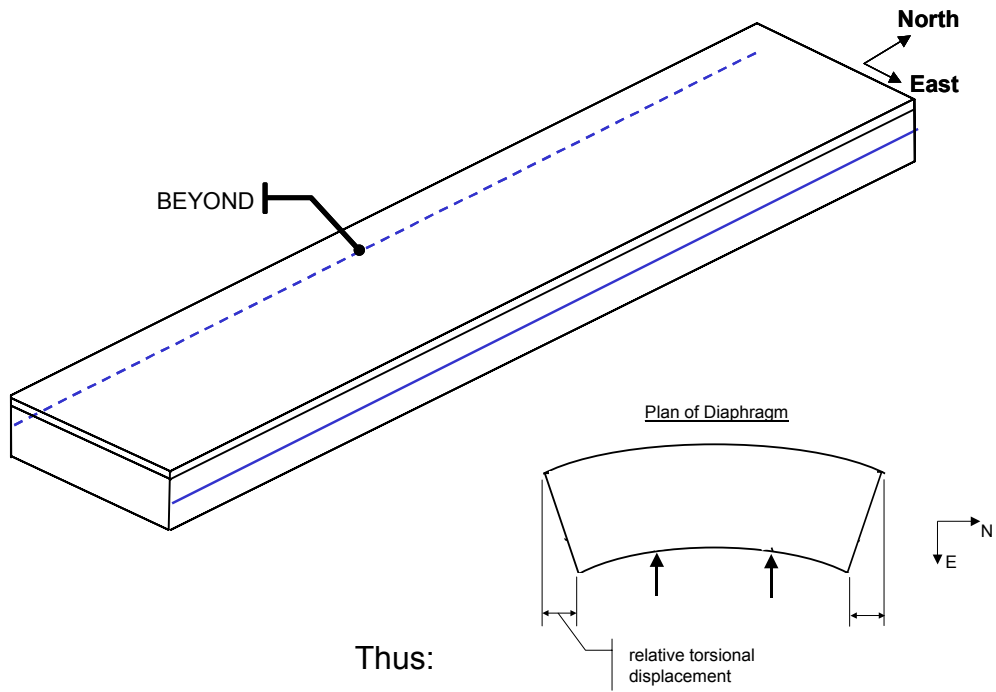


Figure A.11 Instrumentation measuring relative torsional displacement of end columns

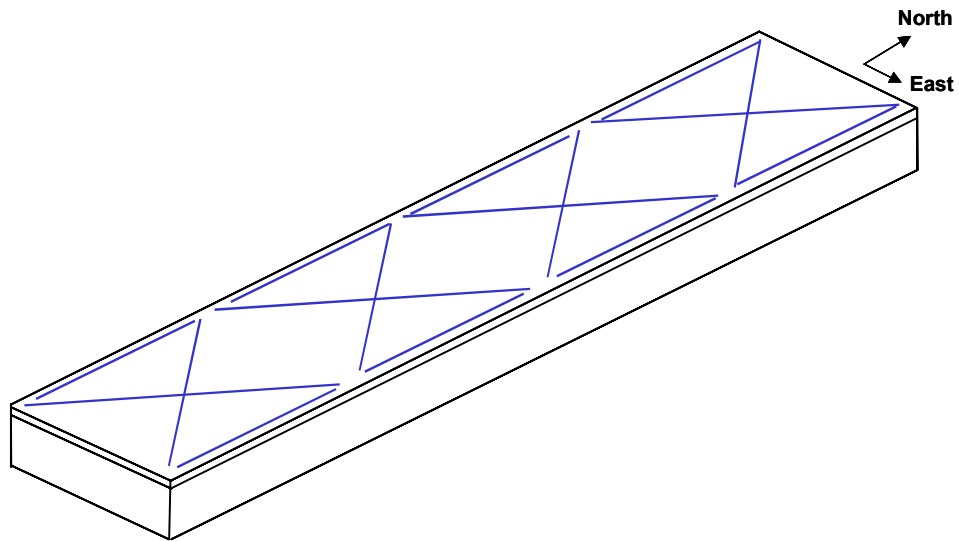


Figure A.12 Instrumentation measuring relative in-plane deformations

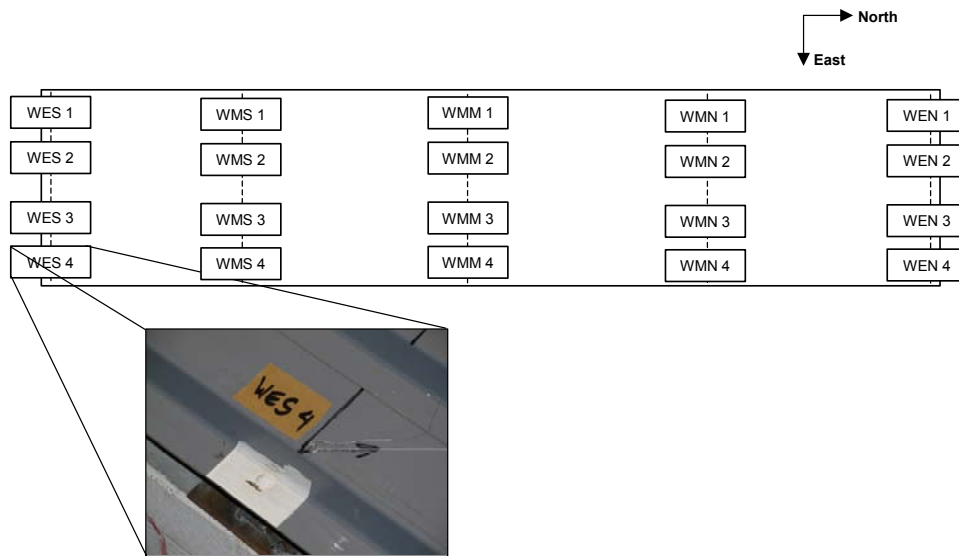


Figure A.13 Locations and labels of welds with thin Hydrostone® coatings

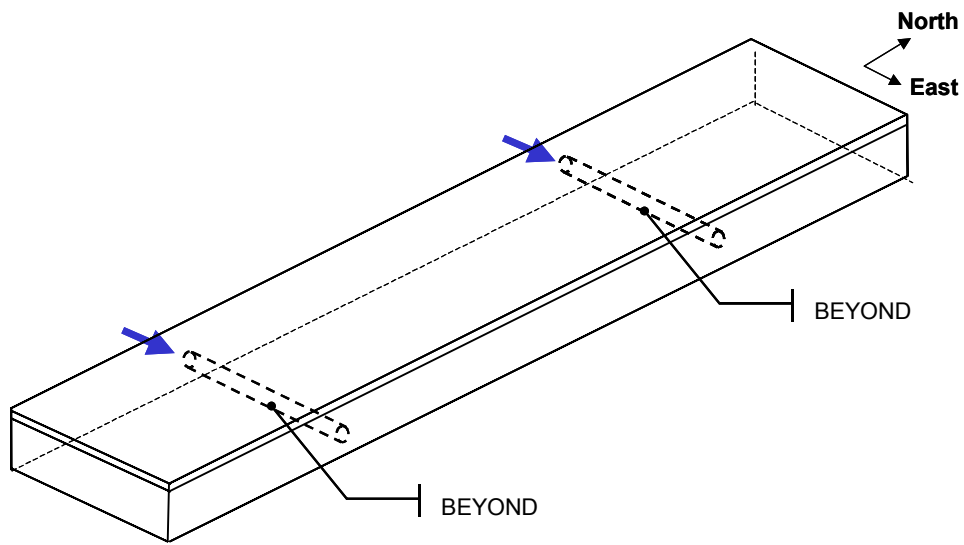


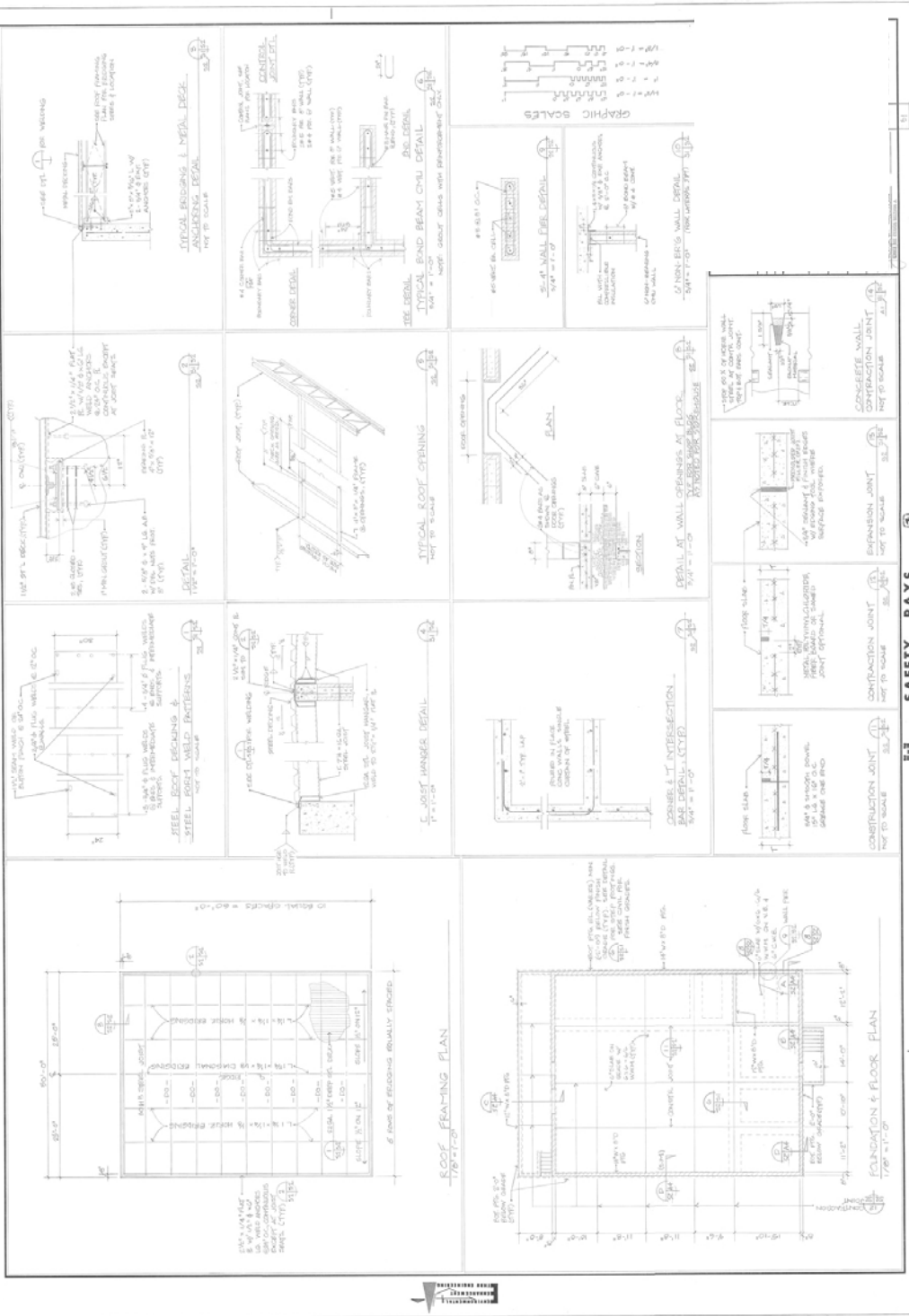
Figure A.14 Instrumentation measuring axial forces in load struts; struts are strain-gauged

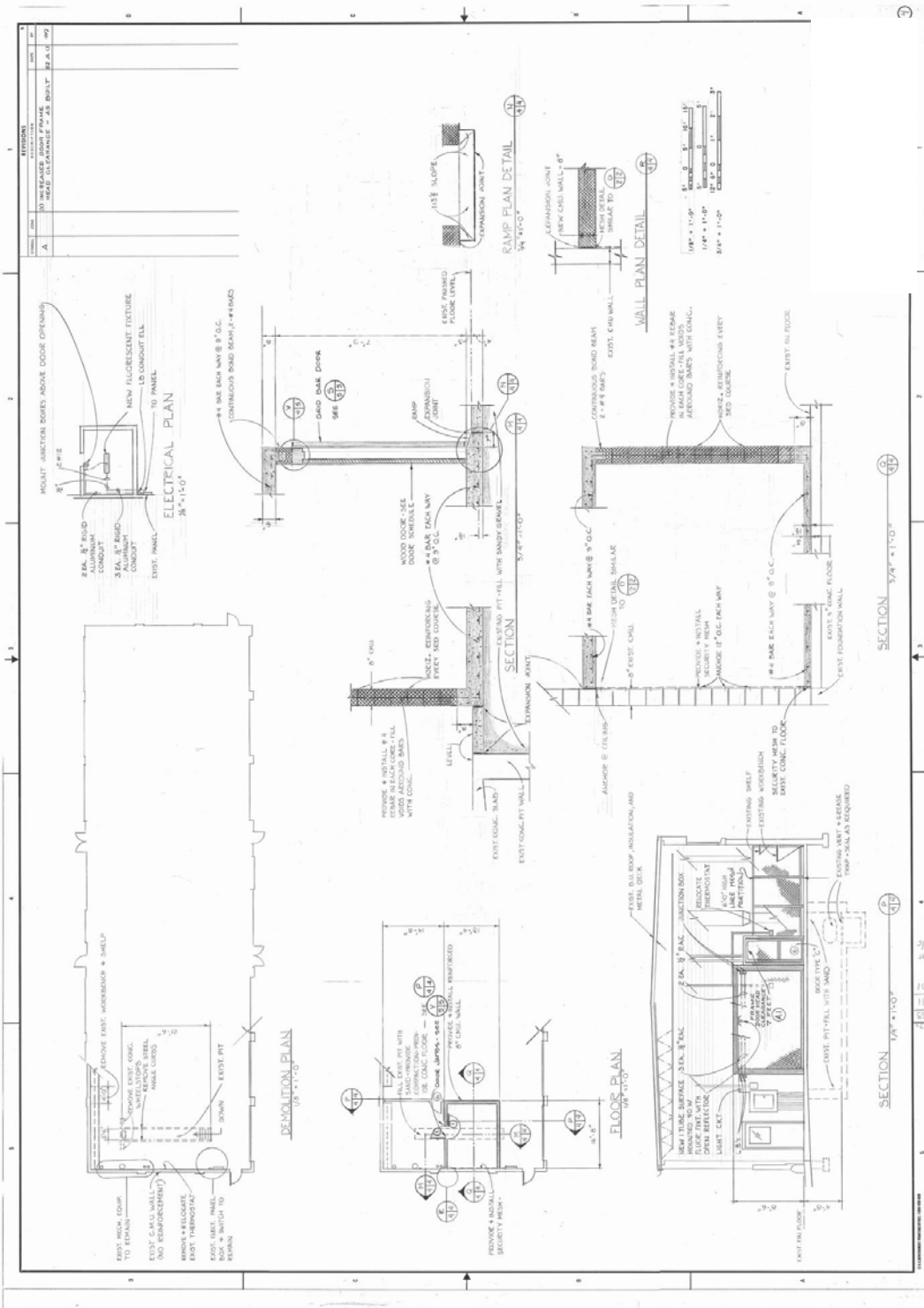
Appendix B: Structural and Architectural Drawings

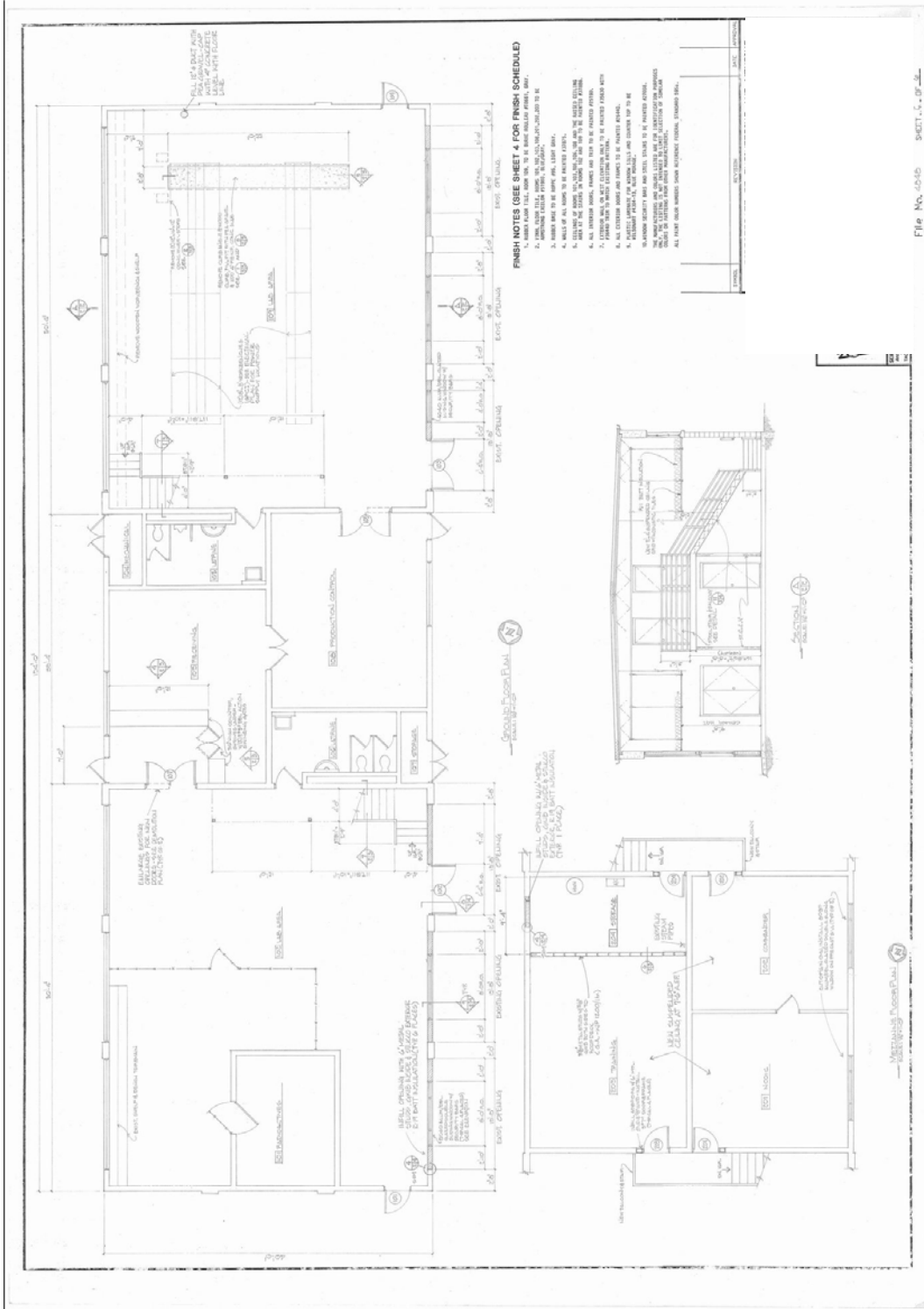
B.1 Building 8

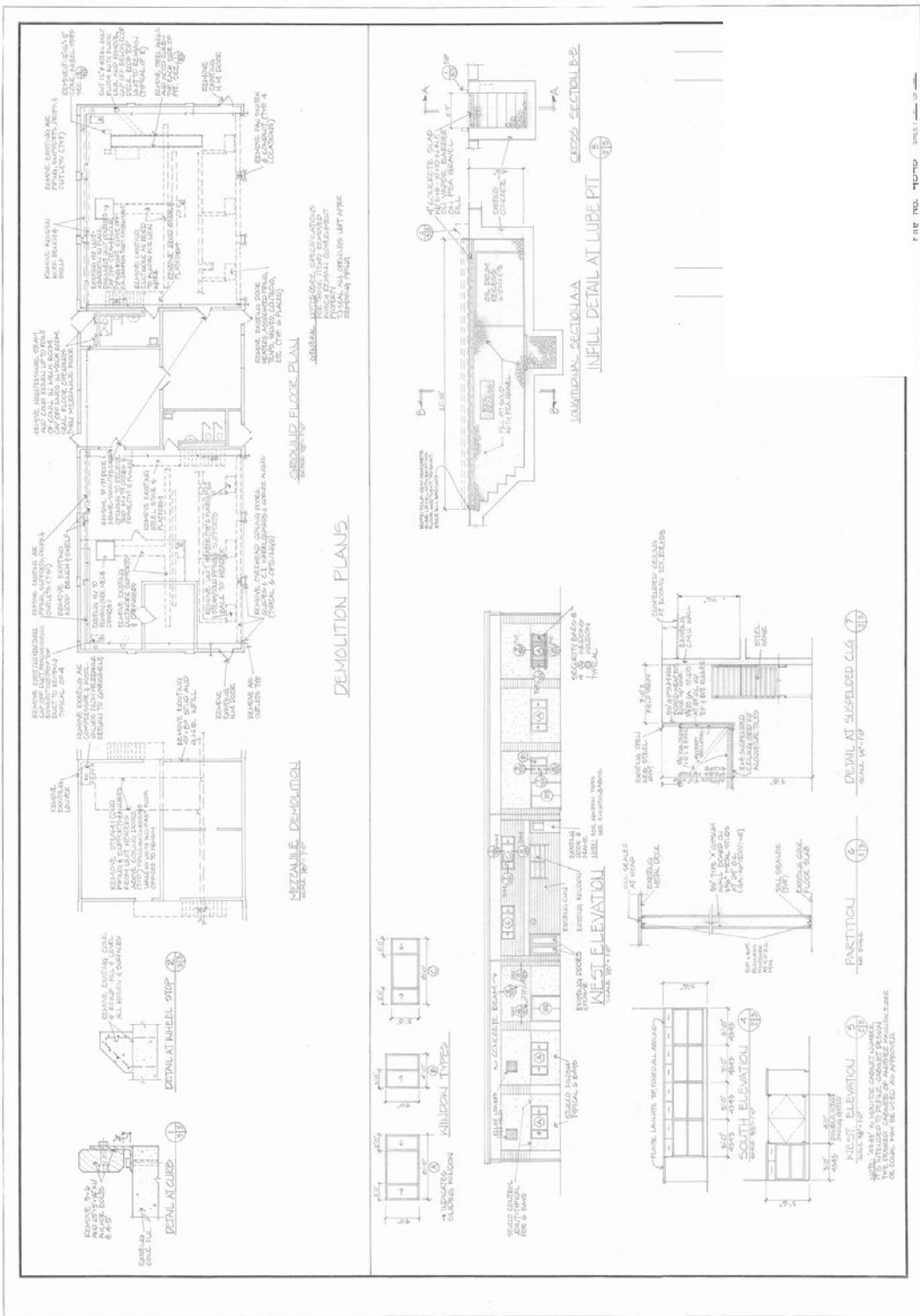
Full-size electronic copies (*.jpg format) of the following structural and architectural plans are available from the author of this dissertation.

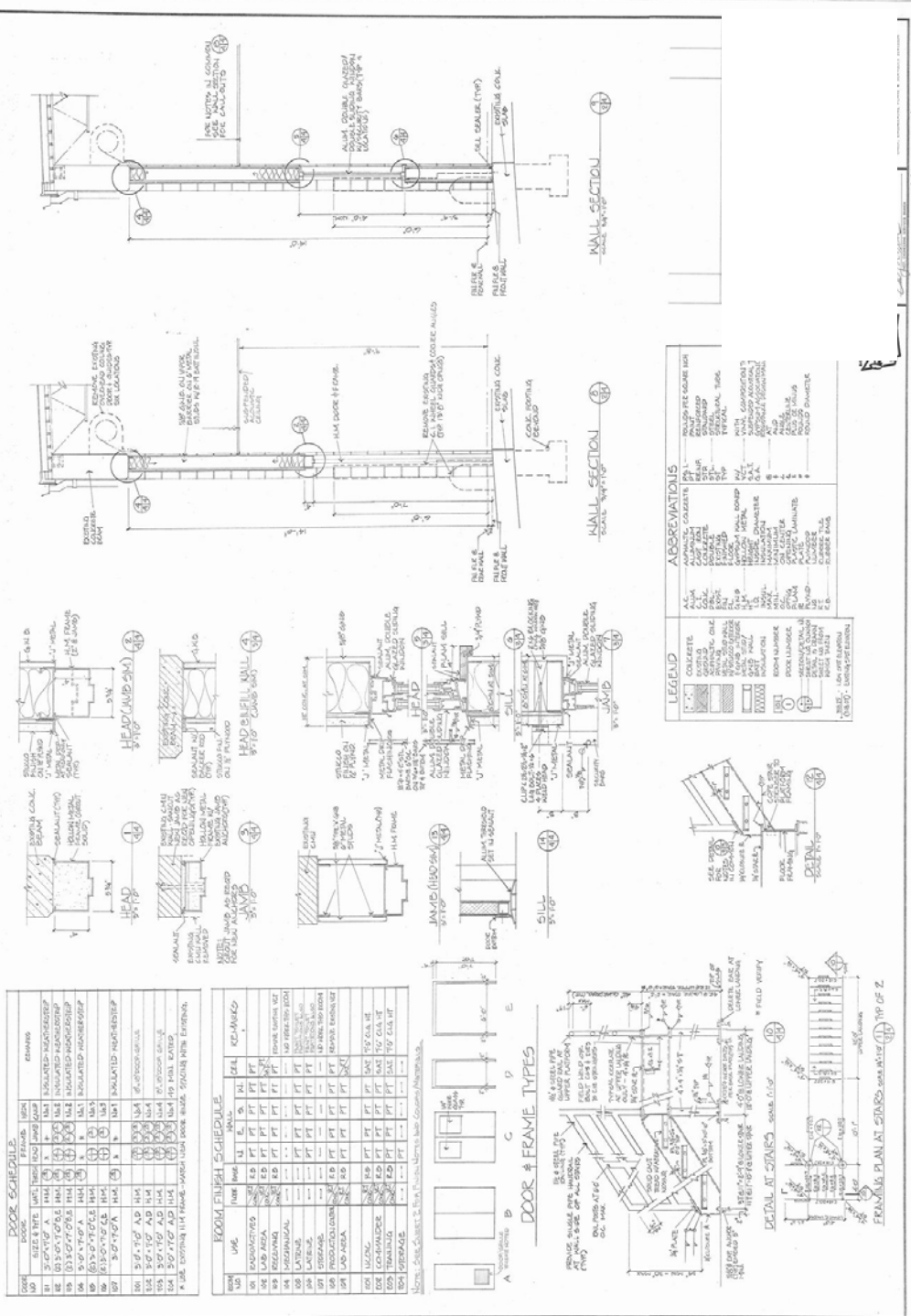
VALUE ENGINEERING PAYS









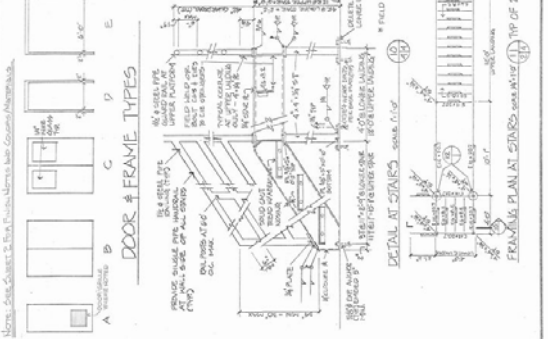


DOOR SCHEDULE

DOOR	TYPE	FINISH	MARK
101	3'0" x 7'0" AD	1H4	101
102	3'0" x 7'0" AD	1H4	102
103	3'0" x 7'0" AD	1H4	103
104	3'0" x 7'0" AD	1H4	104
105	3'0" x 7'0" AD	1H4	105
106	3'0" x 7'0" AD	1H4	106
107	3'0" x 7'0" AD	1H4	107
108	3'0" x 7'0" AD	1H4	108
109	3'0" x 7'0" AD	1H4	109
110	3'0" x 7'0" AD	1H4	110
111	3'0" x 7'0" AD	1H4	111
112	3'0" x 7'0" AD	1H4	112
113	3'0" x 7'0" AD	1H4	113
114	3'0" x 7'0" AD	1H4	114
115	3'0" x 7'0" AD	1H4	115
116	3'0" x 7'0" AD	1H4	116
117	3'0" x 7'0" AD	1H4	117
118	3'0" x 7'0" AD	1H4	118
119	3'0" x 7'0" AD	1H4	119
120	3'0" x 7'0" AD	1H4	120

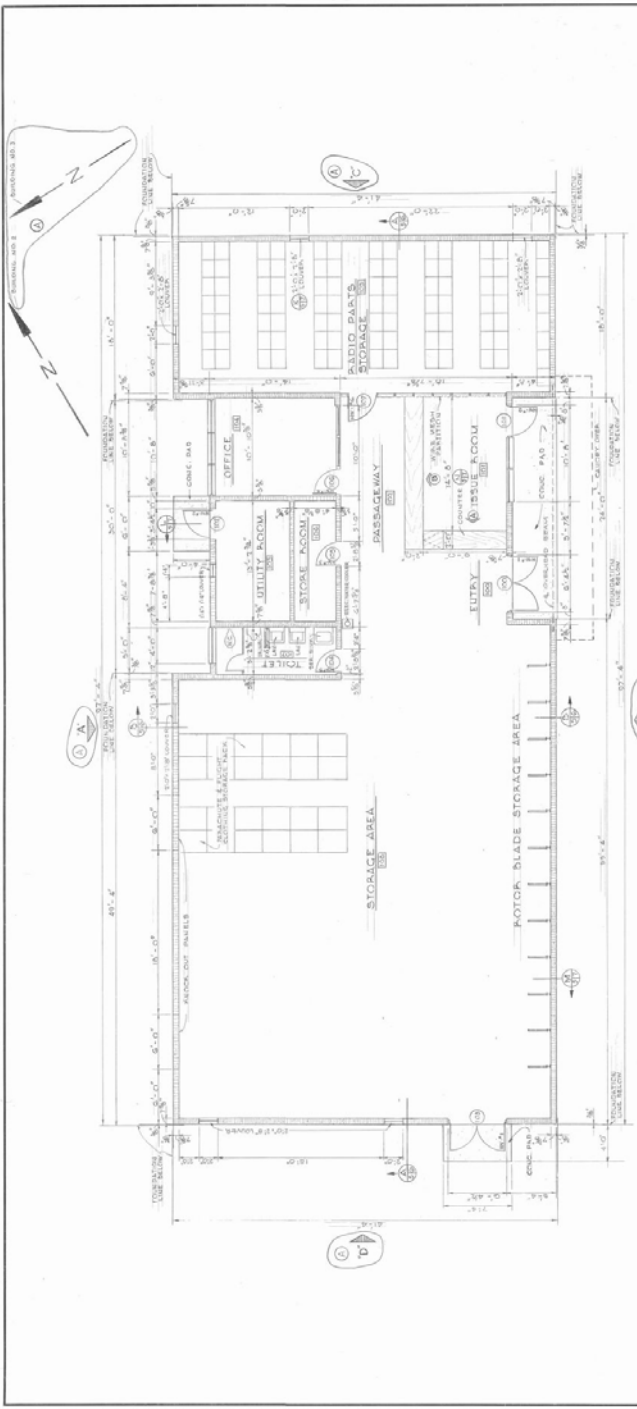
WINDOW SCHEDULE

WINDOW	TYPE	FINISH	MARK
201	3'0" x 7'0" AD	1H4	201
202	3'0" x 7'0" AD	1H4	202
203	3'0" x 7'0" AD	1H4	203
204	3'0" x 7'0" AD	1H4	204
205	3'0" x 7'0" AD	1H4	205
206	3'0" x 7'0" AD	1H4	206
207	3'0" x 7'0" AD	1H4	207
208	3'0" x 7'0" AD	1H4	208
209	3'0" x 7'0" AD	1H4	209
210	3'0" x 7'0" AD	1H4	210
211	3'0" x 7'0" AD	1H4	211
212	3'0" x 7'0" AD	1H4	212
213	3'0" x 7'0" AD	1H4	213
214	3'0" x 7'0" AD	1H4	214
215	3'0" x 7'0" AD	1H4	215
216	3'0" x 7'0" AD	1H4	216
217	3'0" x 7'0" AD	1H4	217
218	3'0" x 7'0" AD	1H4	218
219	3'0" x 7'0" AD	1H4	219
220	3'0" x 7'0" AD	1H4	220



B.2 Building 9

Full-size electronic copies (*.jpg format) of the following structural and architectural plans are available from the author of this dissertation.

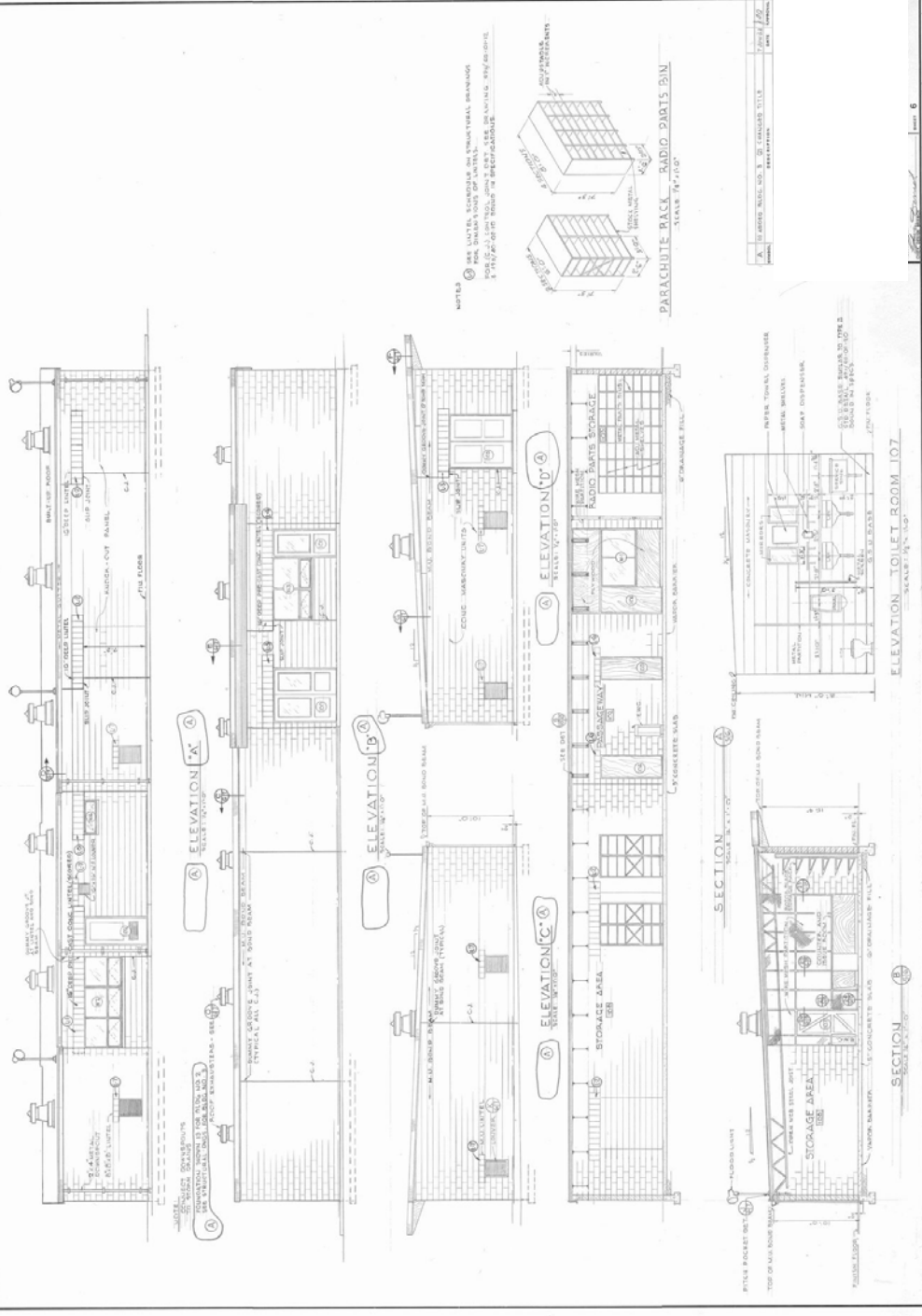


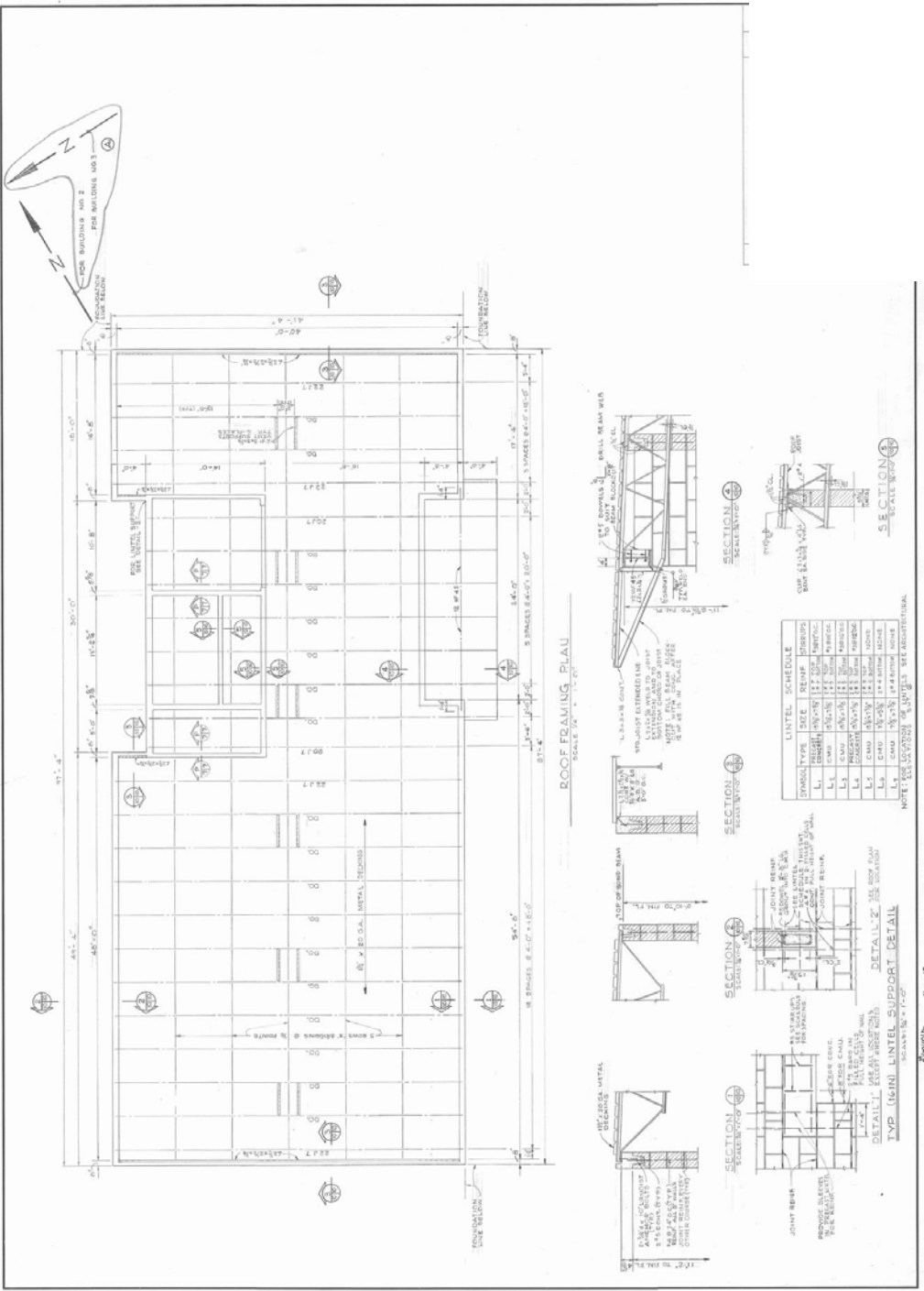
FLOOR PLAN
SCALE 3/4" = 1'-0"

FINISH NOTES
 1. SURFACE FINISH TO BE AS SHOWN ON DRAWING.
 2. ALL SURFACE FINISH TO BE DONE BY THE CONTRACTOR.
 3. ALL SURFACE FINISH TO BE DONE BY THE CONTRACTOR.
 4. ALL SURFACE FINISH TO BE DONE BY THE CONTRACTOR.

ABBREVIATION
 1. WALL
 2. CEILING
 3. FLOOR
 4. DOOR
 5. WINDOW
 6. PARTITION
 7. STAIR

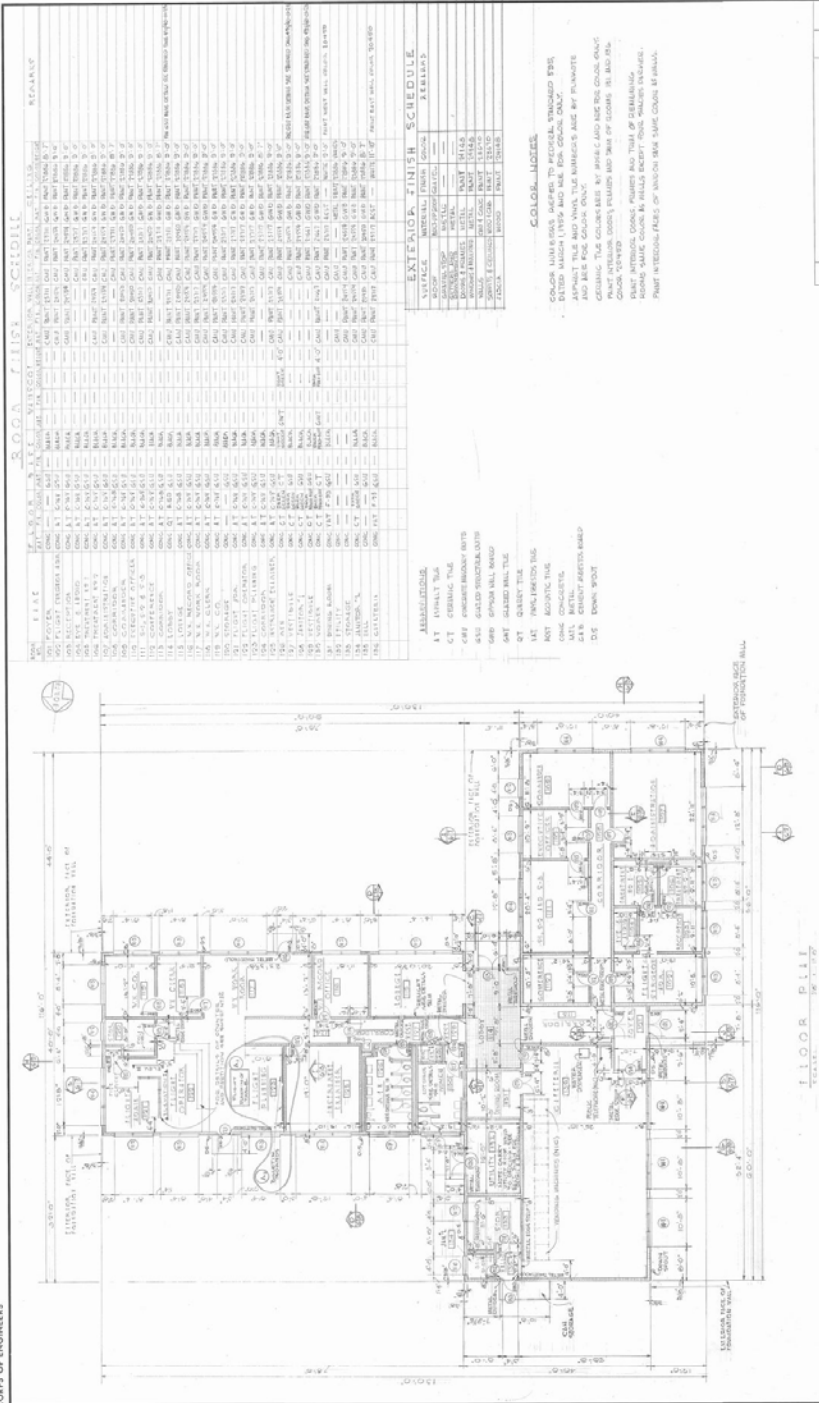
NO.	ROOM	FINISH SCHEDULE		DOOR SCHEDULE	
		NO.	DESCRIPTION	NO.	DESCRIPTION
100	ENTRY	100	EXP. PAINT (100)	100	EXP. PAINT (100)
101	OFFICE	101	EXP. PAINT (101)	101	EXP. PAINT (101)
102	UTILITY ROOM	102	EXP. PAINT (102)	102	EXP. PAINT (102)
103	STORAGE ROOM	103	EXP. PAINT (103)	103	EXP. PAINT (103)
104	RADIO PARTS STORAGE	104	EXP. PAINT (104)	104	EXP. PAINT (104)
105	MOTOR BLADE STORAGE AREA	105	EXP. PAINT (105)	105	EXP. PAINT (105)
106	STORAGE AREA	106	EXP. PAINT (106)	106	EXP. PAINT (106)
107	ENTRY	107	EXP. PAINT (107)	107	EXP. PAINT (107)
108	RESTROOM	108	EXP. PAINT (108)	108	EXP. PAINT (108)





B.3 Building 6

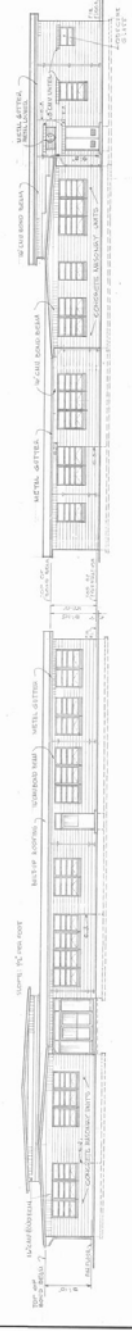
Full-size electronic copies (*.jpg format) of the following structural and architectural plans are available from the author of this dissertation.





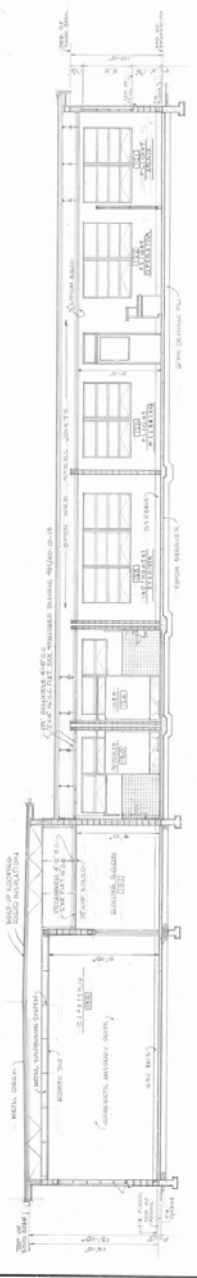
WEST ELEVATION
ELEVATION

EAST ELEVATION
ELEVATION

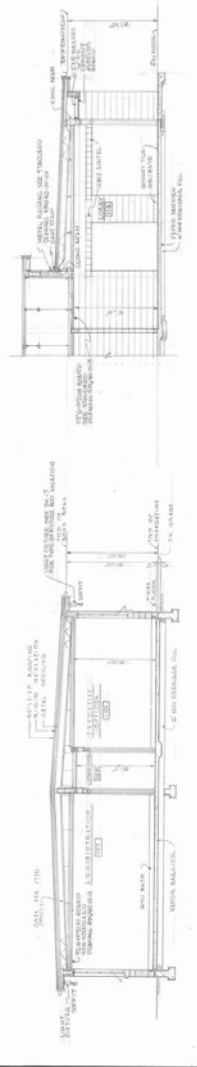


EAST ELEVATION
ELEVATION

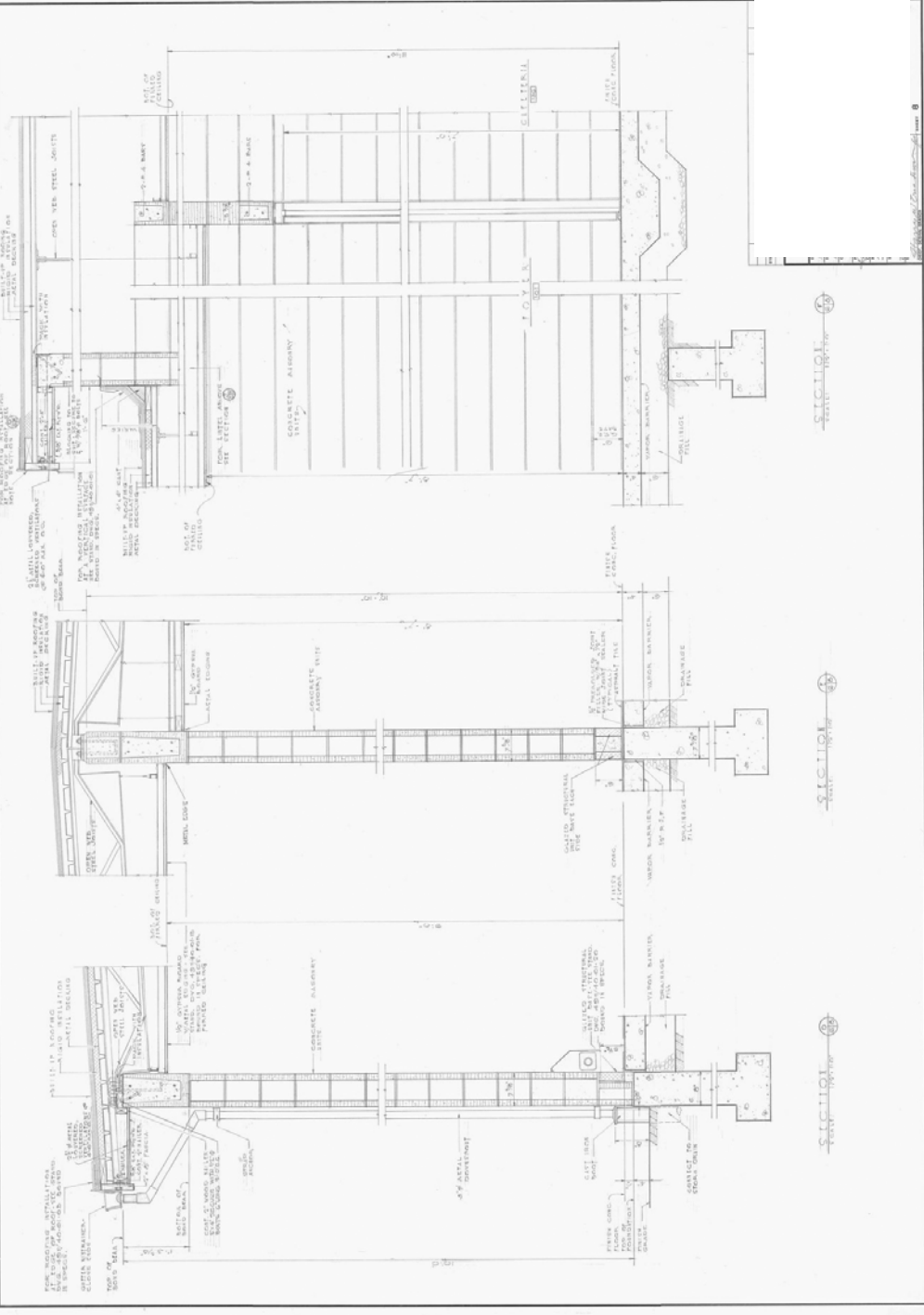
SECTION
SECTION

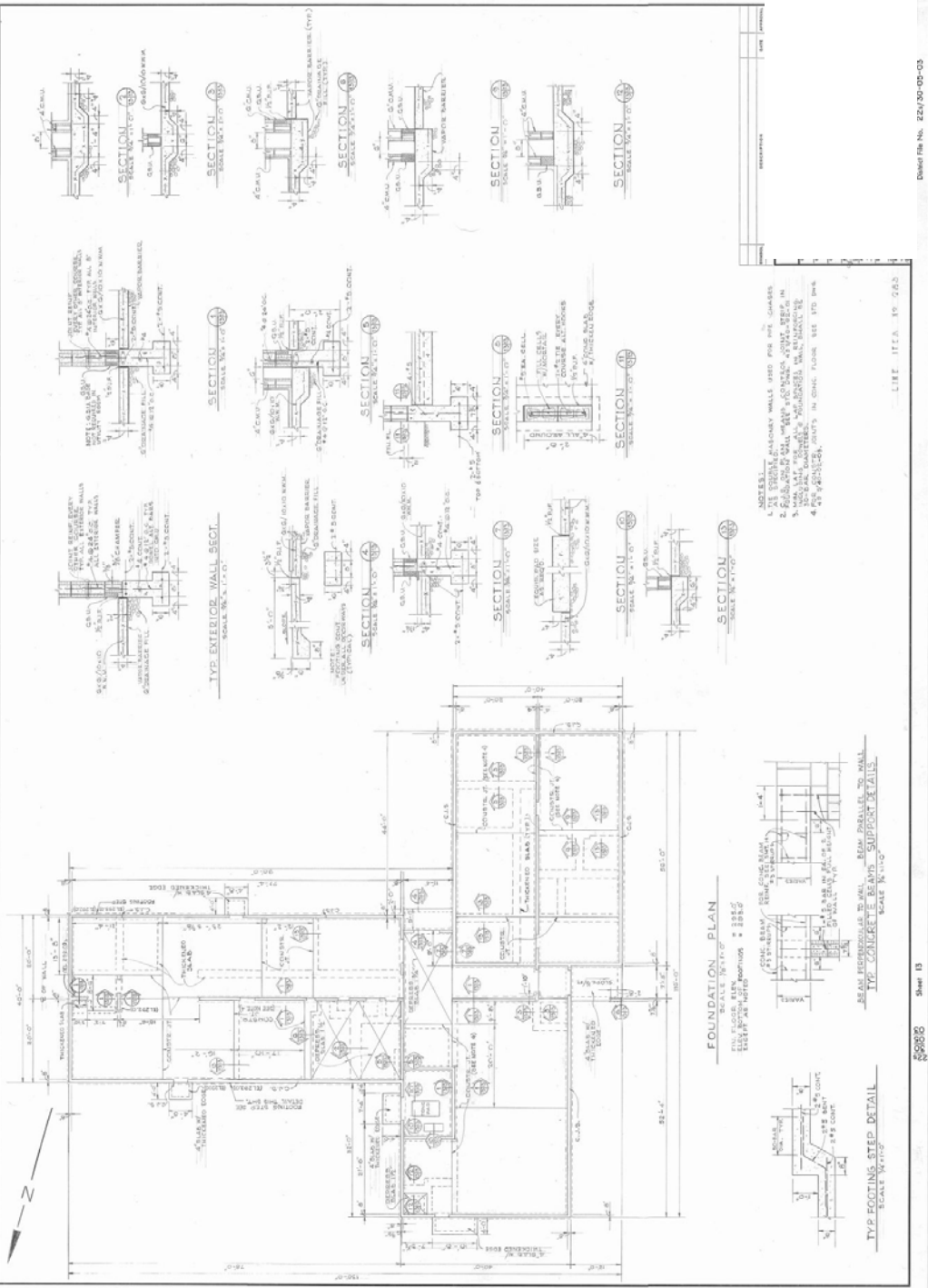


SECTION
SECTION



SECTION
SECTION





- NOTES:
1. USE PRECAST CONCRETE WALLS USED FOR THE CHAMBER.
 2. REINFORCEMENT SHALL BE AS SHOWN AND SHALL BE PLACED IN ACCORDANCE WITH THE REINFORCEMENT SCHEDULE.
 3. ALL REINFORCEMENT SHALL BE WELDED TO THE WALLS.
 4. FOR REINFORCEMENT JOINTS IN CONC. FLOOR SEE STD. DWG.

FOUNDATION PLAN
SCALE 1/4" = 1'-0"



TYP. CONCRETE BEAM SUPPORT DETAILS
SCALE 1/4" = 1'-0"

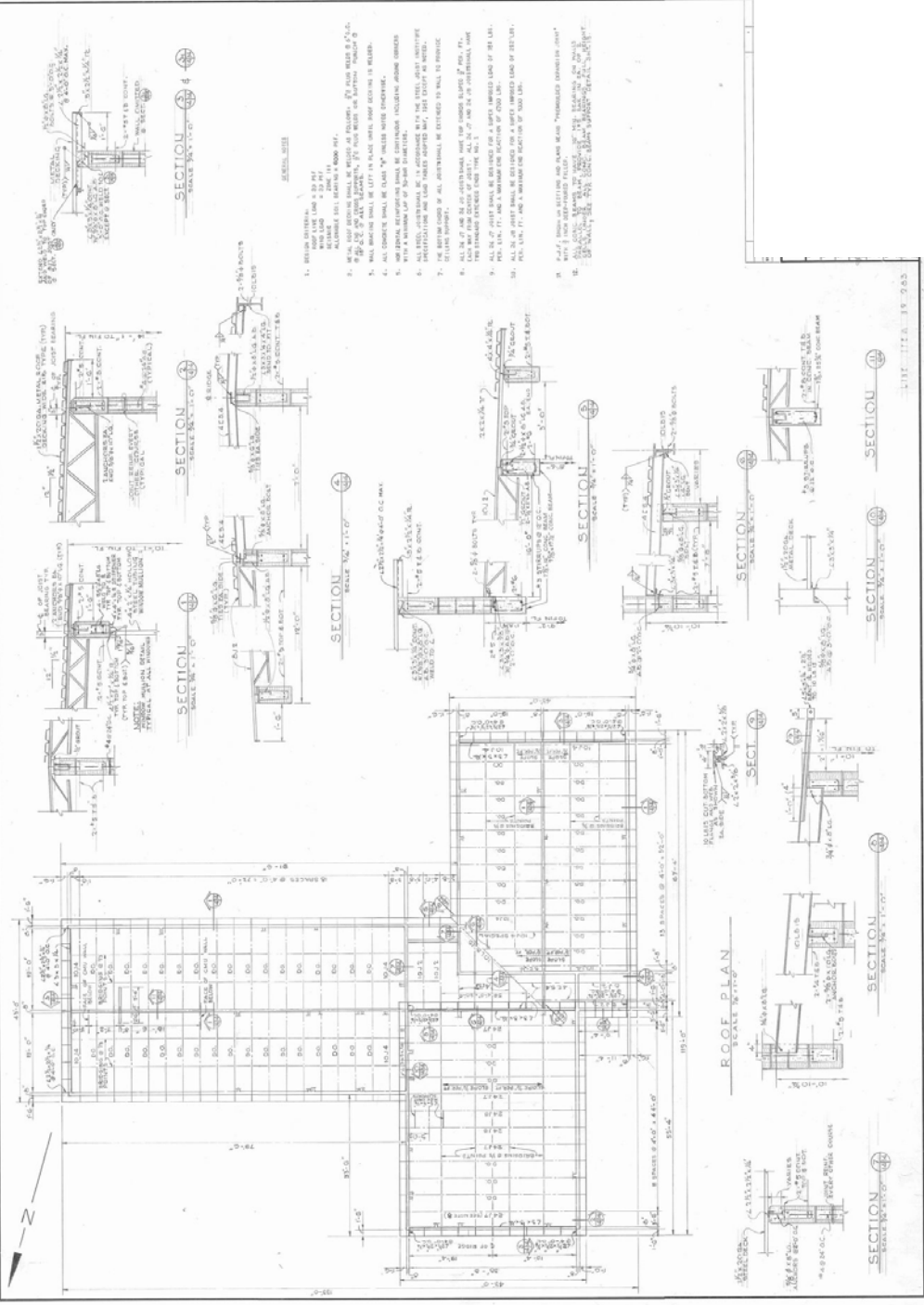


TYP. FOOTING STEP DETAIL
SCALE 1/4" = 1'-0"

LINE ITEM 19-085

Sheet 13

59082



1. THE ROOF SHALL BE CONSTRUCTED AS SHOWN ON THE DRAWINGS.
2. THE ROOF SHALL BE CONSTRUCTED AS SHOWN ON THE DRAWINGS.
3. THE ROOF SHALL BE CONSTRUCTED AS SHOWN ON THE DRAWINGS.
4. ALL JOINTS SHALL BE MADE AS SHOWN ON THE DRAWINGS.
5. THE ROOF SHALL BE CONSTRUCTED AS SHOWN ON THE DRAWINGS.
6. THE ROOF SHALL BE CONSTRUCTED AS SHOWN ON THE DRAWINGS.
7. THE ROOF SHALL BE CONSTRUCTED AS SHOWN ON THE DRAWINGS.
8. THE ROOF SHALL BE CONSTRUCTED AS SHOWN ON THE DRAWINGS.
9. THE ROOF SHALL BE CONSTRUCTED AS SHOWN ON THE DRAWINGS.
10. THE ROOF SHALL BE CONSTRUCTED AS SHOWN ON THE DRAWINGS.
11. THE ROOF SHALL BE CONSTRUCTED AS SHOWN ON THE DRAWINGS.
12. THE ROOF SHALL BE CONSTRUCTED AS SHOWN ON THE DRAWINGS.
13. THE ROOF SHALL BE CONSTRUCTED AS SHOWN ON THE DRAWINGS.
14. THE ROOF SHALL BE CONSTRUCTED AS SHOWN ON THE DRAWINGS.
15. THE ROOF SHALL BE CONSTRUCTED AS SHOWN ON THE DRAWINGS.
16. THE ROOF SHALL BE CONSTRUCTED AS SHOWN ON THE DRAWINGS.
17. THE ROOF SHALL BE CONSTRUCTED AS SHOWN ON THE DRAWINGS.
18. THE ROOF SHALL BE CONSTRUCTED AS SHOWN ON THE DRAWINGS.
19. THE ROOF SHALL BE CONSTRUCTED AS SHOWN ON THE DRAWINGS.
20. THE ROOF SHALL BE CONSTRUCTED AS SHOWN ON THE DRAWINGS.

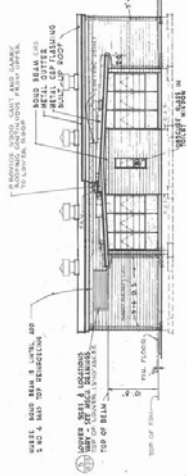
1111-1111-1111-1111

Sheet 14

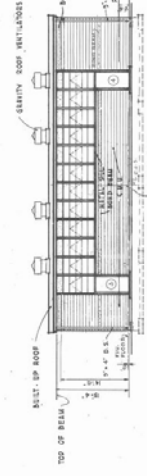
5988

B.4 Building 3

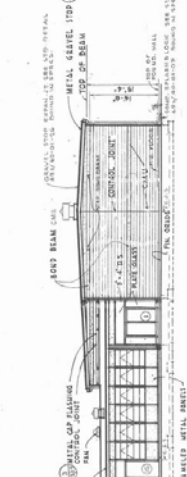
Full-size electronic copies (*.jpg format) of the following structural and architectural plans are available from the author of this dissertation.



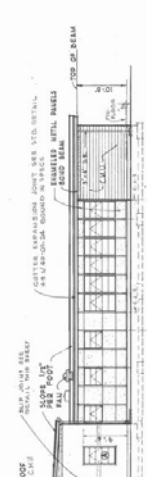
WEST ELEVATION
SCALE: 1" = 5'



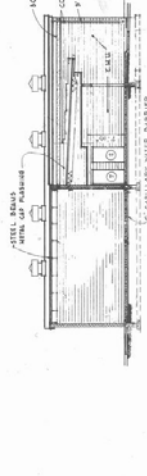
EAST ELEVATION
SCALE: 1" = 5'



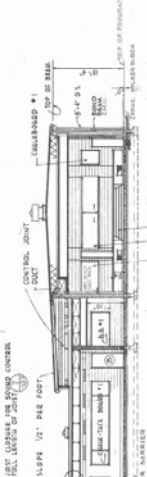
SOUTH ELEVATION
SCALE: 1" = 5'



NORTH ELEVATION
SCALE: 1" = 5'



SECTION
SCALE: 1" = 5'



SECTION
SCALE: 1" = 5'



SECTION
SCALE: 1" = 5'

GRAPHIC SCALE

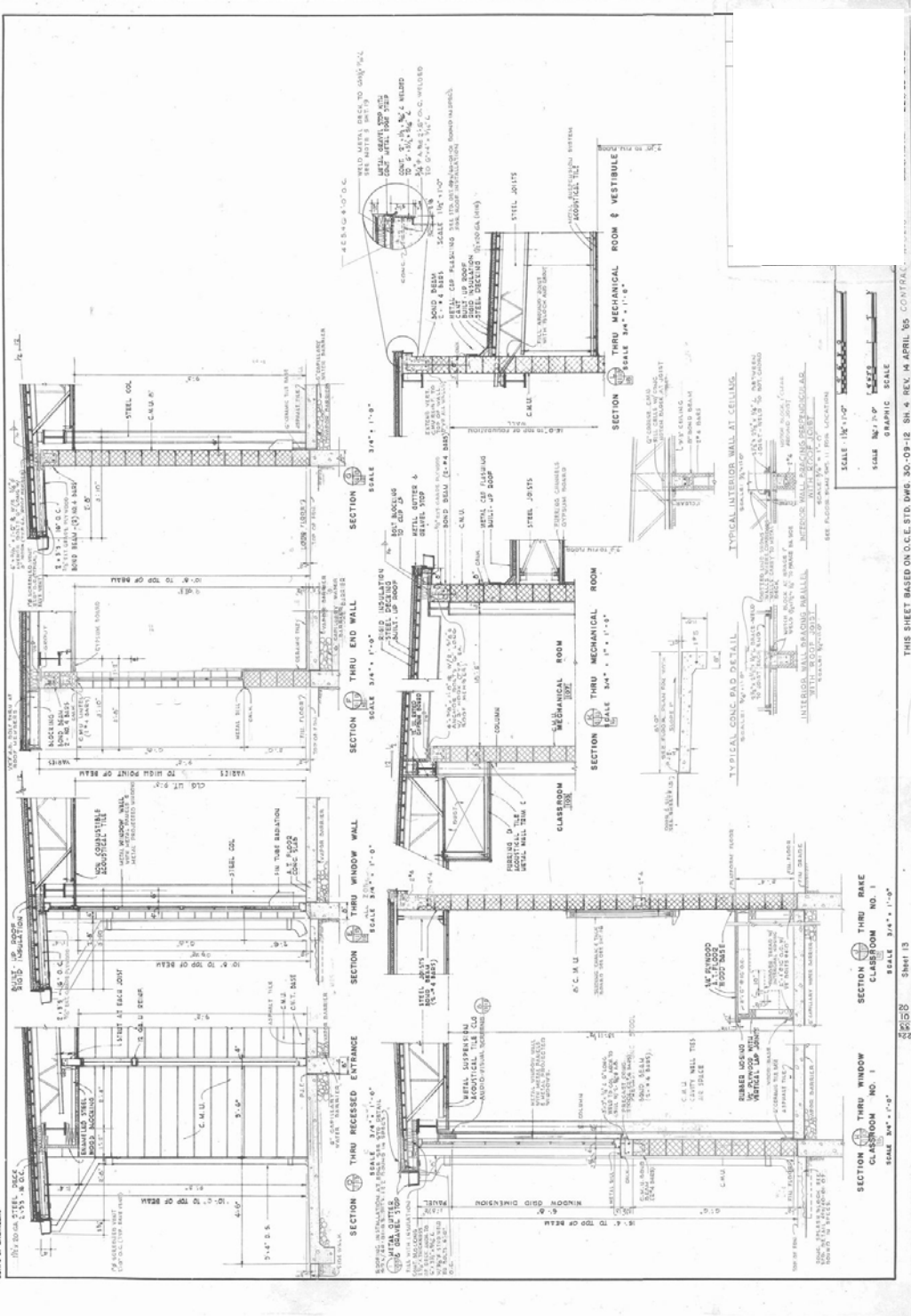
SCALE 1/8" = 1'-0"

SCALE 1/4" = 1'-0"

SCALE 1/2" = 1'-0"

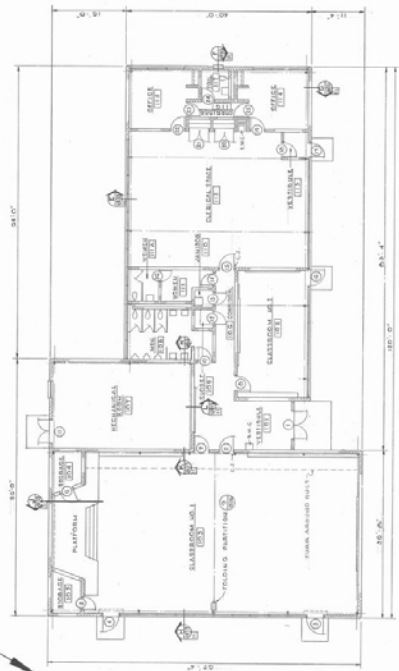
SCALE 3/4" = 1'-0"

SCALE 1" = 1'-0"



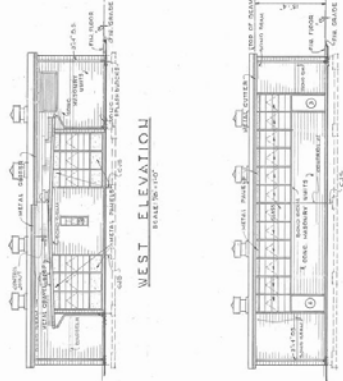
THIS SHEET BASED ON O.C.E. STD. DWG. 30-09-12 SH. 4 REV. 14 APRIL '65 CONTRAL.

Sheet 13



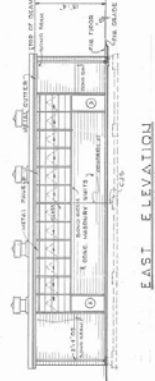
FLOOR PLAN

SCALE: 1/8" = 1'-0"
BUILDING AREA 9,111 SQUARE FEET.



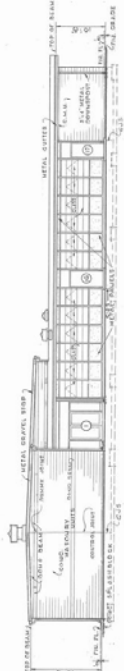
WEST ELEVATION

SCALE: 1/8" = 1'-0"



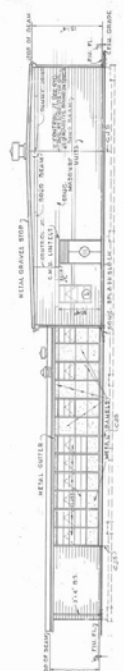
EAST ELEVATION

SCALE: 1/8" = 1'-0"



NORTH ELEVATION

SCALE: 1/8" = 1'-0"



SOUTH ELEVATION

SCALE: 1/8" = 1'-0"

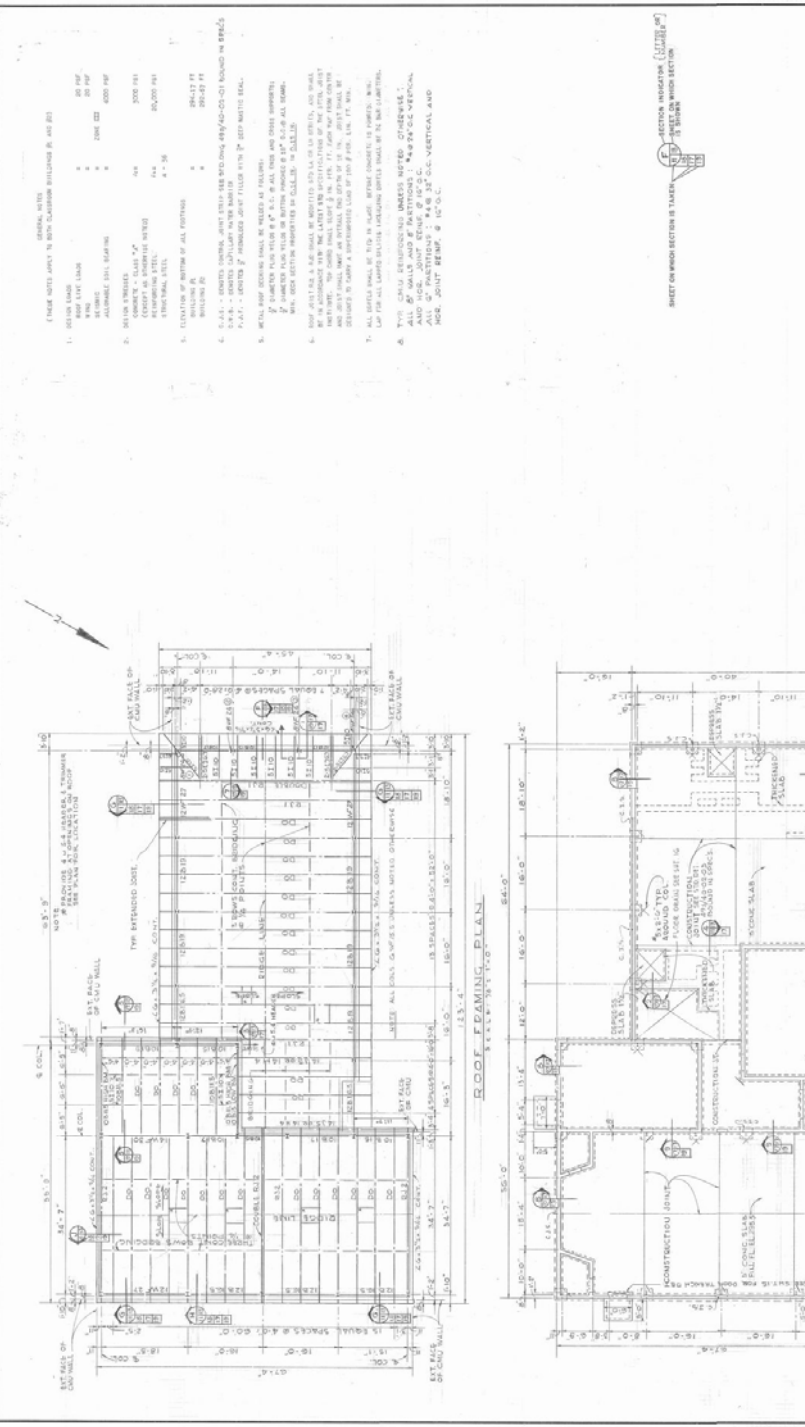


ROOF PLAN

SCALE: 1/8" = 1'-0"

STANDARD SYMBOLS FOR ARCHITECTURAL DRAWINGS





THIS SHEET BASED ON OCE DWG. 30-012-2M 11 DATED 23 OCT 61 CONTRACT # 818

Sheet 19

Drawn File No. 24/330102

Appendix C: Example Seismic Evaluation

C.1 Evaluation Using FEMA 310 Methodology

Evaluation checklists are provided following these calculations.

Seismic Evaluation of Ft. Lewis, Building 8

- Building Information
- Tier 1 Screening Phase: Summary of results and calculations
- Final recommendations

Building Information:

Building Number: 8

Year Built: 1976

Plans Date: 1976

Location: Ft. Lewis, WA

Tier 1 Screening Phase: Summary of Results and Calculations

The following evaluation follows procedures outlined in FEMA 310: *Handbook for the Seismic Evaluation of Existing Buildings*. Relevant sections are referenced.

2.3 Site Visit

Site visit was performed on June 11, 2003.

2.4 Level of Performance

Building is evaluated at Life Safety (LS) performance level.

2.5 Region of Seismicity

Region of "high" seismicity (Table 2-1)

2.6 Building Type

Building is FEMA 310 Type RM1: Reinforced Masonry Building with Flexible Diaphragms (Table 2-2)

3.2 Benchmark Building

Building was not designed under the Benchmark Model Code of Table 3-1 for Building Type RM1 (in this case, UBC 1997).

3.3 Selection and Use of Checklists

Evaluation requires Basic Structural and Supplemental Structural Checklists 3.7.13 and 3.17.13S (Figure C.1 through Figure C.4)

3.5 Tier 1 Analysis

$$\text{kip} \equiv 1000\text{lbf} \quad \text{psi} \equiv \frac{\text{lbf}}{\text{in}^2}$$

$$C \equiv 1.0 \quad (\text{Table 3-4})$$

Constants depend on region and soil type. Values from FEMA 310 and NEHRP 2000 seismicity maps:

$$F_a := 1.1 \quad F_v := 1.6 \quad S_1 := 0.4 \quad S_s := 1.20$$

$$S_{D1} := \frac{2}{3} \cdot F_v \cdot S_1 \quad S_{DS} := \frac{2}{3} \cdot F_a \cdot S_s$$

Pseudo-spectral ordinates are,

$$S_a(x) := \text{if} \left(\frac{S_{D1}}{x} \leq S_{DS}, \frac{S_{D1}}{x}, S_{DS} \right) \quad \text{where "x" is period in seconds.}$$

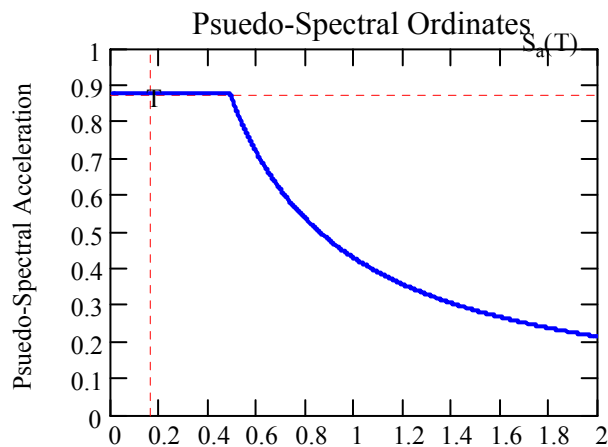
Estimate period of building in seconds (FEMA 310 method),

$$T := 0.020 \cdot h^{\frac{3}{4}} \quad \text{where h is average height of building in feet, } h \equiv 17$$

$$T = 0.167$$

Pseudo-spectral acceleration (in units of g):

$$S_a(T) = 0.88$$



Pseudo-lateral load is:

$$V := S_a(T) \cdot W \cdot C \quad \text{where "W" is seismic weight of building.}$$

$$W \equiv 566 \text{ kip}$$

$$V = 498 \text{ kip}$$

Shear stress in shear walls,

$$v_{\text{avg}} := \frac{1}{m} \cdot \frac{V}{A_w}$$

where "m" is the force-reduction factor.

$$m \equiv 3.0 \quad (\text{Table 3-7})$$

" A_w " is net area of shear walls in direction under consideration. In this case, from the building plans, the minimum of the transverse and longitudinal directions is,

$$A_w \equiv (40.67 \cdot 2) \cdot 12 \text{ in} \cdot 7.625 \text{ in}$$

So,

$$v_{\text{avg}} = 22 \text{ psi} \quad \text{-OK-}$$

Walls are reinforced vertically w/ #4 @ 24 in. o/c and horizontally w/ 2-#5 @ 48 in. o/c. Reinforcement ratios are:

$$\rho_v := \frac{0.2}{7.6 \cdot 24} \quad \rho_v = 0.0011 \quad \text{-OK-}$$

$$\rho_h := \frac{0.31 \cdot 2}{7.6 \cdot 48} \quad \rho_h = 0.0017 \quad \text{-OK-}$$

$$\rho_{\text{total}} := \rho_v + \rho_h \quad \rho_{\text{total}} = 0.0028 \quad \text{-OK-}$$

Final Recommendations Using FEMA 310

3.7 Structural Checklists 3.7.13 and 3.7.13S

Building is fully compliant with Basic Structural Checklist 3.7.13 and Supplemental Structural Checklist 3.7.13S. No additional (Tier 2) evaluations are necessary.

3.7.13 Basic Structural Checklist For Building Type RM1: Reinforced Masonry Bearing Wall Buildings With Flexible Diaphragms

This Basic Structural Checklist shall be completed when required by Table 3-2.

Each of the evaluation statements on this checklist shall be marked compliant (C), non-compliant (NC), or not applicable (N/A) for a Tier 1 Evaluation. Compliant statements identify issues that are acceptable according to the criteria of this Handbook, while non-compliant statements identify issues that require further investigation. Certain statements may not apply to the buildings being evaluated. For non-compliant evaluation statements, the design professional may choose to conduct further investigation using the corresponding Tier 2 evaluation procedure; the section numbers in parentheses following each evaluation statement correspond to Tier 2 evaluation procedures.

Commentary:

These buildings have bearing walls that consist of reinforced brick or concrete block masonry. Wood floor and roof framing consists of wood joists, glulam beams and wood posts or small steel columns. Steel floor and roof framing consists of steel beams or open web joists, steel girders and steel columns. Lateral forces are resisted by the reinforced brick or concrete block masonry shear walls. Diaphragms consist of straight or diagonal wood sheathing, plywood, or untopped metal deck, and are flexible relative to the walls. Foundations consist of brick or concrete spread footings.

Building System

- | | | | |
|---|----|-----|--|
| C | NC | N/A | LOAD PATH: The structure shall contain one complete load path for Life Safety and Immediate Occupancy for seismic force effects from any horizontal direction that serves to transfer the inertial forces from the mass to the foundation. (Tier 2: Sec. 4.3.1.1) |
| C | NC | N/A | ADJACENT BUILDINGS: An adjacent building shall not be located next to the structure being evaluated closer than 4% of the height for Life Safety and Immediate Occupancy. (Tier 2: Sec. 4.3.1.2) |
| C | NC | N/A | MEZZANINES: Interior mezzanine levels shall be braced independently from the main structure, or shall be anchored to the lateral-force-resisting elements of the main structure. (Tier 2: Sec. 4.3.1.3) |
| C | NC | N/A | WEAK STORY: The strength of the lateral-force-resisting system in any story shall not be less than 80% of the strength in an adjacent story above or below for Life-Safety and Immediate Occupancy. (Tier 2: Sec. 4.3.2.1) |
| C | NC | N/A | SOFT STORY: The stiffness of the lateral-force-resisting system in any story shall not be less than 70% of the stiffness in an adjacent story above or below or less than 80% of the average stiffness of the three stories above or below for Life-Safety and Immediate Occupancy. (Tier 2: Sec. 4.3.2.2) |
| C | NC | N/A | GEOMETRY: There shall be no changes in horizontal dimension of the lateral-force-resisting system of more than 30% in a story relative to adjacent stories for Life Safety and Immediate Occupancy, excluding one-story penthouses. (Tier 2: Sec. 4.3.2.3) |
| C | NC | N/A | VERTICAL DISCONTINUITIES: All vertical elements in the lateral-force-resisting system shall be continuous to the foundation. (Tier 2: Sec. 4.3.2.4) |

Figure C.1 FEMA 310 Basic Structural Checklist 3.7.13 (page 1 of 2)

C	NC	N/A	MASS: There shall be no change in effective mass more than 50% from one story to the next for Life Safety and Immediate Occupancy. (Tier 2: Sec. 4.3.2.5)
C	NC	N/A	DETERIORATION OF WOOD: There shall be no signs of decay, shrinkage, splitting, fire damage, or sagging in any of the wood members and none of the metal accessories shall be deteriorated, broken, or loose. (Tier 2: Sec. 4.3.3.1)
C	NC	N/A	MASONRY UNITS: There shall be no visible deterioration of masonry units. (Tier 2: Sec. 4.3.3.7)
C	NC	N/A	MASONRY JOINTS: The mortar shall not be easily scraped away from the joints by hand with a metal tool, and there shall be no areas of eroded mortar. (Tier 2: Sec. 4.3.3.8)
C	NC	N/A	REINFORCED MASONRY WALL CRACKS: All existing diagonal cracks in wall elements shall be less than 1/8" for Life Safety and 1/16" for Immediate Occupancy; shall not be concentrated in one location, and shall not form an X pattern. (Tier 2: Sec. 4.3.3.10)
Lateral Force Resisting System			
C	NC	N/A	REDUNDANCY: The number of lines of shear walls in each principal direction shall be greater than or equal to 2 for Life Safety and Immediate Occupancy. (Tier 2: Sec. 4.4.2.1.1)
C	NC	N/A	SHEAR STRESS CHECK: The shear stress in the reinforced masonry shear walls, calculated using the Quick Check procedure of Section 3.5.3.3, shall be less than 50 psi for Life Safety and Immediate Occupancy. (Tier 2: Sec. 4.4.2.4.1) $v = 22 \text{ psi}$
C	NC	N/A	REINFORCING STEEL: The total vertical and horizontal reinforcing steel ratio in reinforced masonry walls shall be greater than 0.002 for Life Safety and 0.003 for Immediate Occupancy of the wall with the minimum of 0.0007 for Life Safety and 0.001 for Immediate Occupancy in either of the two directions; the spacing of reinforcing steel shall be less than 48" for Life Safety and 24" for Immediate Occupancy; and all vertical bars shall extend to the top of the walls. (Tier 2: Sec. 4.4.2.4.2) $\rho_v = 0.0011$ $\rho_h = 0.0017$ $\rho_t = 0.0028$
Connections			
C	NC	N/A	WALL ANCHORAGE: Exterior concrete or masonry walls shall be anchored for out-of-plane forces at each diaphragm level with steel anchors or straps that are developed into the diaphragm. (Tier 2: Sec. 4.6.1.1) OPEN-WEB JOISTS
C	NC	N/A	TRANSFER TO SHEAR WALLS: Diaphragms shall be reinforced and connected for transfer of loads to the shear walls for Life Safety and the connections shall be able to develop the shear strength of the walls for Immediate Occupancy. (Tier 2: Sec. 4.6.2.1)
C	NC	N/A	WALL REINFORCING: Walls shall be doweled into the foundation for Life Safety and the dowels shall be able to develop the strength of the walls for Immediate Occupancy. (Tier 2: Sec. 4.6.3.5)
C	NC	N/A	GIRDER/COLUMN CONNECTION: There shall be a positive connection between the girder and the column support. (Tier 2: Sec. 4.6.4.1)

Figure C.2 FEMA 310 Basic Structural Checklist 3.7.13 (page 2 of 2)

3.7.13S Supplemental Structural Checklist For Building Type RM1: Reinforced Masonry Bearing Wall Buildings With Flexible Diaphragms

This Supplemental Structural Checklist shall be completed when required by Table 3-2. The Basic Structural Checklist shall be completed prior to completing this Supplemental Structural Checklist.

Lateral Force Resisting System

- C NC (N/A) REINFORCING AT OPENINGS: All wall openings that interrupt rebar shall have trim reinforcing on all sides. This statement shall apply to the Immediate Occupancy Performance Level only. (Tier 2: Sec. 4.4.2.4.3)
- C NC (N/A) PROPORTIONS: The height-to-thickness ratio of the shear walls at each story shall be less than 30. This statement shall apply to the Immediate Occupancy Performance Level only. (Tier 2: Sec. 4.4.2.4.4)

Diaphragms

- (C) NC N/A CROSS TIES: There shall be continuous cross ties between diaphragm chords. (Tier 2: Sec. 4.5.1.2)
OPEN-WEB JOISTS ARE TIES
- C NC (N/A) OPENINGS AT SHEAR WALLS: Diaphragm openings immediately adjacent to the shear walls shall be less than 25% of the wall length for Life Safety and 15% of the wall length for Immediate Occupancy. (Tier 2: Sec. 4.5.1.4)
- C NC (N/A) OPENINGS AT EXTERIOR MASONRY SHEAR WALLS: Diaphragm openings immediately adjacent to exterior masonry shear walls shall not be greater than 8 feet long for Life Safety and 4 ft. long for Immediate Occupancy. (Tier 2: Sec. 4.5.1.6)
- C NC (N/A) PLAN IRREGULARITIES: There shall be tensile capacity to develop the strength of the diaphragm at re-entrant corners or other locations of plan irregularities. This statement shall apply to the Immediate Occupancy Performance Level only. (Tier 2: Sec. 4.5.1.7)
- C NC (N/A) DIAPHRAGM REINFORCEMENT AT OPENINGS: There shall be reinforcing around all diaphragm openings larger than 50% of the building width in either major plan dimension. This statement shall apply to the Immediate Occupancy Performance Level only. (Tier 2: Sec. 4.5.1.8)
- C NC (N/A) STRAIGHT SHEATHING: All straight sheathed diaphragms shall have aspect ratios less than 2 to 1 for Life Safety and 1 to 1 for Immediate Occupancy in the direction being considered. (Tier 2: Sec. 4.5.2.1)
- C NC (N/A) SPANS: All wood diaphragms with spans greater than 24 ft. for Life Safety and 12 ft. for Immediate Occupancy shall consist of wood structural panels or diagonal sheathing. Wood commercial and industrial buildings may have rod-braced systems. (Tier 2: Sec. 4.5.2.2)
- C NC (N/A) UNBLOCKED DIAPHRAGMS: All unblocked wood structural panel diaphragms shall have horizontal spans less than 40 ft. for Life Safety and 25 ft. for Immediate Occupancy and shall have aspect ratios less than or equal to 4 to 1 for Life Safety and 3 to 1 for Immediate Occupancy. (Tier 2: Sec. 4.5.2.3)
- (C) NC N/A NON-CONCRETE DIAPHRAGMS: Untopped metal deck diaphragms or metal deck diaphragms with fill other than concrete shall consist of horizontal spans of less than 40 ft. and shall have aspect ratios less than 4 to 1. This statement shall apply to the Immediate Occupancy Performance Level only. (Tier 2: Sec. 4.5.3.1)

Figure C.3 FEMA 310 Supplemental Structural Checklist 3.7.13S (page 1 of 2)

C	NC	N/A	OTHER DIAPHRAGMS: The diaphragm shall not consist of a system other than those described in Section 4.5. (Tier 2: Sec. 4.5.7.1)
Connections			
C	NC	N/A	WOOD LEDGERS: The connection between the wall panels and the diaphragm shall not induce cross-grain bending or tension in the wood ledgers. (Tier 2: Sec. 4.6.1.2)
C	NC	N/A	ANCHOR SPACING: Exterior masonry walls shall be anchored to the floor and roof systems at a spacing of 4 ft. or less for Life Safety and 3 ft. or less for Immediate Occupancy. (Tier 2: Sec. 4.6.1.3)
C	NC	N/A	STIFFNESS OF WALL ANCHORS: Anchors of concrete or masonry walls to wood structural elements shall be installed taut and shall be stiff enough to prevent movement between the wall and the diaphragm. If bolts are present, the size of the bolt holes in both the connector and framing shall be a maximum of 1/16" larger than the bolt diameter. This statement shall apply to the Immediate Occupancy Performance Level only. (Tier 2: Sec. 4.6.1.5)
<p style="margin-left: 100px;">METAL DECK WELDED TO TOP PLATE, TOP PLATE ANCHORED TO R/C RING BEAM @ 24 in. o/c</p>			

Figure C.4 FEMA 310 Supplemental Structural Checklist 3.7.13S (page 2 of 2)

C.2 Evaluation Using Proposed Supplementary Methodology

Seismic Evaluation of Ft. Lewis, Building 8

- Building Information
- Period Calculation and diaphragm response

Building Information:

Building Number: 8

Year Built: 1976

Plans Date: 1976

Location: Ft Lewis, WA

Period Calculation and Diaphragm Response: Summary of Results and Calculations

Response Spectrum: The spectrum used in this analysis is the same as that used in the FEMA 310 evaluations.

$$\text{kip} \equiv 1000\text{lbf} \quad \text{psi} \equiv \frac{\text{lbf}}{\text{in}^2}$$

$$C \equiv 1.0 \quad (\text{Table 3-4})$$

Constants depend on region and soil type. Values from FEMA 310 and NEHRP 2000 seismicity maps,

$$\boxed{F_a := 1.1} \quad \boxed{F_v := 1.6} \quad \boxed{S_1 := 0.4} \quad \boxed{S_s := 1.20}$$

$$S_{D1} := \frac{2}{3} \cdot F_v \cdot S_1 \quad S_{DS} := \frac{2}{3} \cdot F_a \cdot S_s$$

Pseudo-spectral ordinates are:

$$S_a(x) := \text{if} \left(\frac{S_{D1}}{x} \leq S_{DS}, \frac{S_{D1}}{x}, S_{DS} \right) \quad \text{where "x" is period in seconds.}$$

According to procedures developed in Chapters 5 and 6, the mass of diaphragm DOF is,

$$M_{\text{diaph}} := \frac{43\text{kip}}{32.2 \frac{\text{ft}}{\text{s}^2}}$$

In-plane shear rigidity of diaphragm is calculated using Vulcraft Co. Technical Manual. 20 gage, 36/7 Welding (6in. o/c w/ sidelap fast. @ 18in. o/c, 3 SL fast/span)

$$G' := \frac{K_2}{3.78 + \frac{0.3 \cdot D_B}{\text{Span}} + 3 \cdot K_1 \cdot \text{Span}} \cdot \frac{\text{kip}}{\text{in}} \quad \begin{array}{l} K_2 \equiv 1056 \quad K_1 \equiv 0.537 \\ \text{Span} \equiv 4 \quad D_B \equiv 97 \end{array}$$

$$G' = 60 \frac{\text{kip}}{\text{in}}$$

According to the procedures developed in Chapter 5 and 6, the stiffness of the diaphragm DOF is,

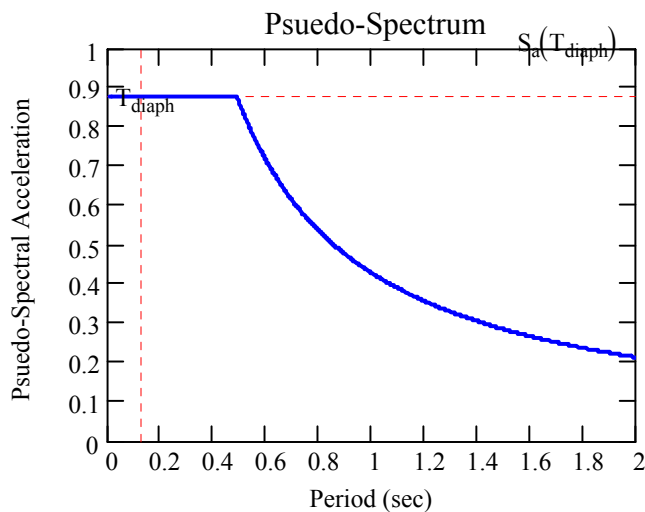
$$K_{\text{diaph}} := B \cdot G' \cdot \frac{\pi^2}{2L} \quad \text{where} \quad B \equiv 40\text{ft} \quad L \equiv 48\text{ft} \quad K_{\text{diaph}} = 248 \frac{\text{kip}}{\text{in}}$$

The period of the system is therefore,

$$T_{\text{diaph}} := 2 \cdot \pi \cdot \sqrt{\frac{M_{\text{diaph}}}{K_{\text{diaph}}}} \quad T_{\text{diaph}} = 0.13 \text{ sec}$$

Pseudo-spectral acceleration (in units of g):

$$S_a \left(\frac{T_{\text{diaph}}}{s} \right) = 0.88$$



Pseudo-lateral load is:

$$V := S_a \left(\frac{T_{\text{diaph}}}{s} \right) \cdot M_{\text{diaph}} \cdot g$$

$$V = 38 \text{ kip}$$

Deflection of the diaphragm DOF is:

$$d := \frac{V}{K_{\text{diaph}}} \quad d = 0.15 \text{ in} \quad \text{DDR} := \frac{2 \cdot d}{L} \quad \text{DDR} = 0.05\%$$

Shear force per foot of width is:

$$v := \frac{V}{41.33 \text{ ft}} \quad \boxed{v = 0.915 \frac{\text{kip}}{\text{ft}}}$$

Allowable shear force per foot of width is calculated using the Vulcraft Co. Technical Manual (assumed 5/8 in. puddle welds),

$$v_{\text{all}} := 0.377 \frac{\text{kip}}{\text{ft}} \cdot \frac{2.75}{1.33} \quad \boxed{v_{\text{all}} = 0.780 \frac{\text{kip}}{\text{ft}}} \quad \text{-NG-}$$

Final Recommendations Using Proposed Supplementary Methodology

Building 8 is deficient at the Life Safety performance level. Expected force in the diaphragm is greater than the expected strength. The building requires further evaluation or rehabilitation.

References

ABK, A Joint Venture (1981), "Methodology for Mitigation of Seismic Hazards in Existing Unreinforced Masonry Buildings: Categorization of Buildings," *Topical Report ABK-TR-01*, El Segundo, CA.

ABK, A Joint Venture (1981), "Methodology for Mitigation of Seismic Hazards in Existing Unreinforced Masonry Buildings: Diaphragm Testing," *Topical Report ABK-TR-02*, El Segundo, CA.

ABK, A Joint Venture (1981), "Methodology for Mitigation of Seismic Hazards in Existing Unreinforced Masonry Buildings: Wall Testing, Out-of-plane," *Topical Report ABK-TR-03*, El Segundo, CA.

American Concrete Institute (1999), "Acceptance Criteria for Moment Frames Based on Structural Testing," *ACI Provisional Standard*, Innovation Task Group 1, Farmington Hills, MI.

American Forest and Paper Association (1996), "Manual for Engineered Wood Construction, Load and Resistance Factor Design," American Wood Council, Washington, D. C.

American Iron and Steel Institute (1967), "Design of Light Gage Steel Diaphragms," *First Edition*, New York, NY.

American Society for Testing and Materials (1999), “Standard Test Methods of Static Tests of Lumber in Structural Sizes,” *ASTM D198-99*, West Conshohocken, PA.

American Welding Society (1998), “Structural Welding Code – Sheet Steel,” *ANSI/AWS D1.3-98*, Miami, FL.

Amrhein, J. E. (1983), “Reinforced Masonry Engineering Handbook, Clay and Concrete Masonry,” *Fourth Edition*, Masonry Institute of America, Los Angeles, CA.

Applied Technology Council (1981), “Guidelines for the Design of Horizontal Wood Diaphragms,” *Publication ATC-7*, Berkeley, CA.

Atherton, G. H., Johnson, J. W. (1951), “Diagonally Sheathed Wood Diaphragms,” *Proceedings*, Annual Meeting of the Structural Engineer Association of California, Yosemite, CA.

Breyer, D. E. (1980), “Design of Wood Structures,” *First Edition*, McGraw-Hill, Inc.

Bryan, E. R., El-Dakhakhni, W. M. (1968), “Shear Flexibility and Strength of Corrugated Decks,” *Journal of the Structural Division*, V. 94, No. 11, 2549-2580.

CANNY 99 (1996), CANNY Structural Analysis, *Version 1.0*, Vancouver, BC, Canada.

- Cohen, G. L. (2001), "Seismic Response of Low-rise Masonry Buildings with Flexible Roof Diaphragms," *MS Thesis*, The University of Texas at Austin.
- Cohen, G. L., Klingner, R. E., Hayes, J. R. Jr., Sweeney, S. C. (2002a), "Seismic Response of Low-Rise Masonry Buildings with Flexible Roof Diaphragms," United States Army Construction Engineering Research Laboratory, Engineer Research and Development Center, *ERDC/CERL SR-01-19*, Champaign, IL.
- Cohen, G. L., Klingner, R. E. (2002b), "Seismic Behavior and Evaluation of Flexible Roof Diaphragms," United States Army Construction Engineering Research Laboratory, Engineer Research and Development Center, Champaign, IL, (Accepted).
- Cohen, G. L., Klingner, R. E., Hayes, J. R. Jr., Sweeney, S. C. (2002c), "Seismic Response of Low-rise Masonry Buildings with Flexible Roof Diaphragms," *Proceedings*, Seventh National Conference on Earthquake Engineering, Boston, MA.
- Cohen, G. L., Klingner, R. E., Hayes, J. R. Jr., Sweeney, S. C. (2003a), "Seismic Response of Low-rise Masonry Buildings with Flexible Roof Diaphragms: Seismic Testing, Quasi-Static Testing, and Analytical Modeling," *Proceedings*, Ninth North American Masonry Conference, Clemson, NC.

- Cohen, G. L., Klingner, R. E., Hayes, J. R. Jr., Sweeney, S. C. (200Xa), "Seismic Response of Low-rise Masonry Buildings with Flexible Roof Diaphragms Part I: Seismic and Quasi-Static Testing," *Earthquake Spectra*, (Accepted).
- Cohen, G. L., Klingner, R. E., Hayes, J. R. Jr., Sweeney, S. C. (200Xb), "Seismic Response of Low-rise Masonry Buildings with Flexible Roof Diaphragms Part II: Analytical Modeling," *Earthquake Spectra*, (Accepted).
- Davies, M. J. (1976), "Calculation of Steel Diaphragm Behavior," *Journal of the Structural Division*, V. 101, No. 7, 1410-1430.
- Davies, M. J. (1977), "Simplified Diaphragm Analysis," *Journal of the Structural Division*, V. 103, No. 11, 2092-2108.
- Easley, J. T. (1977), "Strength and Stiffness of Corrugated Metal Shear Diaphragms," *Journal of Structural Engineering*, V. 103, No. ST1, 169-180.
- Easley, J. T. (1975), "Buckling Formulas for Corrugated Metal Shear Diaphragms," *Journal of the Structural Division*, V. 101, No. 7, 1402-1416.
- Easley, J. T., McFarland, D. E. (1969), "Buckling of Light-Gage Corrugated Metal Shear Diaphragms," *Journal of the Structural Division*, V. 95 No.7, 1497-1516.

Ellifritt, D. S., Luttrell, L. D. (1970), "Strength and Stiffness of Steel Deck Subjected to In-plane Loading," *Final Report*, Steel Deck Institute, West Virginia University Department of Civil Engineering Report No. 2011, Morgantown, WV.

English, M. J., Knowlton, K. C. (1955), "Load Test of a Diagonally Sheathed Timber Building," *Proceedings of the Structural Division*, V. 81, Paper No. 830.

Federal Emergency Management Agency (1988), "Rapid Visual Screening of Buildings for Seismic Hazards; A Handbook," *Document 154*, Washington D.C.

Federal Emergency Management Agency (1991), "Recommended Provisions for the Seismic Regulations of New Buildings and Other Structures, Part 1: Provisions" *Document 222*, Washington D.C.

Federal Emergency Management Agency (1991), "Recommended Provisions for the Seismic Regulations of New Buildings and Other Structures, Part 2: Commentary" *Document 223*, Washington D.C.

Federal Emergency Management Agency (1992), "Handbook for the Seismic Evaluation of Existing Buildings," *Document 178*, Washington D.C.

Federal Emergency Management Agency (1992), "NEHRP Handbook for the Seismic Rehabilitation of Existing Buildings," *Document 172*, Washington D.C.

Federal Emergency Management Agency (1994), “Recommended Provisions for the Seismic Regulations of New Buildings and Other Structures, Part 1: Provisions” *Document 222a*, Washington D.C.

Federal Emergency Management Agency (1994), “Recommended Provisions for the Seismic Regulations of New Buildings and Other Structures, Part 2: Commentary” *Document 223a*, Washington D.C.

Federal Emergency Management Agency (1997), “NEHRP Guidelines for the Seismic Rehabilitation of Buildings,” *Document 273*, Washington D.C.

Federal Emergency Management Agency (1997), “NEHRP Commentary on the Guidelines for the Seismic Rehabilitation of Buildings,” *Document 274*, Washington D.C.

Federal Emergency Management Agency (1997), “Recommended Provisions for the Seismic Regulations of New Buildings and Other Structures, Part 1: Provisions” *Document 302*, Washington D.C.

Federal Emergency Management Agency (1997), “Recommended Provisions for the Seismic Regulations of New Buildings and Other Structures, Part 2: Commentary” *Document 303*, Washington D.C.

Federal Emergency Management Agency (1998), “Evaluation of Earthquake Damaged Concrete and Masonry Wall Buildings,” *Document 306*, Washington D.C.

Federal Emergency Management Agency (1998), "Handbook for the Seismic Evaluation of Buildings – A Prestandard," *Document 310*, Washington D.C.

Federal Emergency Management Agency (2000), "Prestandard and Commentary for the Seismic Rehabilitation of Buildings," *Document 356*, Washington D.C.

Federal Emergency Management Agency (2000), "Recommended Provisions for the Seismic Regulations of New Buildings and Other Structures, Part 1: Provisions" *Document 368*, Washington D.C.

Federal Emergency Management Agency (2000), "Recommended Provisions for the Seismic Regulations of New Buildings and Other Structures, Part 2: Commentary" *Document 369*, Washington D.C.

Foschi, R. O, (1977), "Analysis of wood diaphragms and trusses. Part I: Diaphragms," *Canadian Journal of Civil Engineering*, V. 4, 345-352.

Fonseca, F. S., Wood S. L., Hawkins, N.M. (1996), "Measured Response of Roof Diaphragms and Wall Panels in Tilt-up Systems Subjected to Cyclic Loading," *Earthquake Spectra*, V. 12, No. 4, 783-802.

Drysdale, R. G., Hamid, A. A., Baker, L. R. (1999), "Masonry Structures Behavior and Design," *Second Edition*, The Masonry Society, Boulder, CO.

- Harris, H. G., Sabnis, G. M., (1999), "Structural Modeling and Experimental Techniques", *Second Edition*, CRC Press, Boca Raton, FL.
- Holmes, W. T., Somers, P., Editors (1996), "Northridge Earthquake Reconnaissance Report," *Earthquake Spectra*, Supplement C, Vol. 2, 11, Earthquake Engineering Research Institute, Oakland, CA.
- International Conference of Building Officials (1927-1997), "Uniform Building Code," Los Angeles, CA.
- International Code Council (2000), "International Building Code," Los Angeles, CA.
- Jain, J. K., Jennings, P. C. (1985), "Analytical Models of Low-Rise Buildings with Flexible Floor Diaphragms," *Earthquake Engineering and Structural Dynamics*, V. 13, 225-241.
- Jennings, P. C., Editor (1971), "Engineering Features of the San Fernando Earthquake February 9 1971," *EERL 71-02*, Earthquake Engineering Research Laboratory California Institute of Technology, Pasadena, CA.
- Johnson, J. W. (1954), "Lateral Tests on Full-scale Lumber-sheathed Roof Diaphragms of Various Length-width Ratios," *Report No. T-9*, Oregon Forest Products Laboratory.

- Johnson, J. W. (1955), "Lateral Tests on a 12- by 60-foot Plywood-sheathed Roof Diaphragm," *Report No. T-11*, Oregon Forest Products Laboratory.
- Johnson, J. W. (1955), "Lateral Tests on a 12- by 60-foot and 20- by 80-foot Lumber-sheathed Roof Diaphragms," *Report No. T-12*, Oregon Forest Products Laboratory.
- Kariotis, J., El-Mustapha, A., Ewing, R. (1988), "Dynamic Response of Building Systems with Reinforced Masonry Shear Walls," *Proceedings*, Eighth International Brick and Block Masonry Conference, Trinity College, Dublin, Ireland, September 1988, V II, 740-751.
- Kariotis, J., El-Mustapha, A., Ewing, R. (1988), "A Nonlinear Dynamic Lumped Parameter Model for Reinforced Masonry Structures," *Proceedings*, Eighth International Brick and Block Masonry Conference, Trinity College, Dublin, Ireland, September 1988, V II, 728-739.
- Kariotis, J. (1995), "Seismic Response of Unreinforced Masonry Buildings with Flexible Diaphragms," *Proceedings*, Structures Congress of the American Society of Civil Engineers, 1995, 1817-1820.
- Kihn, H. H., El-Hakim, N., Fazio, P. (1979), "Refined Calculations for the Strength and Stiffness of Cold-Formed Steel Diaphragms," *Canadian Journal of Civil Engineering*, V. 6, No. 2, 268-275.
- Krawinkler, H., Parisi, F., Ibarra, L., Medina, R. (2000), "Development of a Testing Protocol for Wood Framed Structures," *Engineering Report*,

Department of Civil and Environmental Engineering, Stanford University,
Stanford, CA.

Luttrell, L. D. (1967), "Strength and Behavior of Light-Gage Steel Shear Diaphragms," *Engineering Research Bulletin 67-1*, Cornell University, Ithaca, NY.

The Masonry Society (2003), "Masonry Designer's Guide," *Fourth Edition*, Boulder, CO.

Masonry Standards Joint Committee (2000), "Building Code Requirements for Masonry Structures, Specification for Masonry Structures," Working Draft.

Medearis, K., Young, D. H. (1964), "Energy Absorption of Structures Under Cyclic Loading," *Journal of the Structural Division*, V. 90, No.1.

Murphy, L. M. (1973), "San Fernando California Earthquake February 9 1971," United States Department of Commerce National Oceanic and Atmospheric Administration, Washington, D.C.

Nilson, A. H. (1960), "Shear Diaphragms of Light Gage Steel," *Journal of the Structural Division*, V. 86, No. 11, 111-139.

Nilson, A. H. (1969), "Buckling of Light-Gage Corrugated Metal Deck Shear Diaphragms," *Journal of the Structural Division*, V. 95, No.12, 3004-3006.

Nilson, A. H., Ammar, A. R. (1974), "Finite Element Analysis of Metal Deck Shear Diaphragms," *Journal of the Structural Division*, V. 100, No. 4, 711-726.

SAP2000 Non-Linear (1999), Computers and Structures, Inc., *Version 7.10*, Berkeley, CA.

Steel Deck Institute (1981), "Diaphragm Design Manual," *First Edition*, St. Louis, MO.

Steel Deck Institute (1995), "Diaphragm Design Manual," *Second Edition*, St. Louis, MO

Steel Deck Institute (1992), "SDI Manual of Construction With Steel Deck," Fox River Grove, IL.

Soltis, L. A., Mtenga, V. A. (1985), "Strength of Nailed Wood Joints Subjected to Dynamic Load," *Forest Products Journal*, V. 35, No. 11/12, 14-18.

Stillinger, J. R., Johnson, J. W. (1952), "Lateral Tests on Full-Scale Lumber Sheathed Diaphragms," *Report No. T-3*, Oregon Forest Products Laboratory.

Stillinger, J. R., Johnson, J. W. (1954), "Racking Tests on Quarter-scale Diagonally Sheathed Wall Panels," *Report No. T-1*, Oregon Forest Products Laboratory.

- Structural Engineers Association of California (1995), "Vision 2000 - A Framework for Performance Based Design, Volumes I, II, III," Vision 2000 Committee, Sacramento, CA.
- Tena-Colunga, A., Abrams, D. (1995), "Simplified 3-D Dynamic Analysis of Structures with Flexible Diaphragms," *Earthquake Engineering and Structural Dynamics*, V.24, 221-232.
- Tena-Colunga, A., Abrams, D. (1996), "Seismic Behavior of Structures with Flexible Diaphragms," *Journal of Structural Engineering*, V.122, No. 4, 439-445.
- Tremblay, R., Stiemer, S. (1996), "Seismic Behavior of Single-Storey Steel Structures with Flexible Roof Diaphragm," *Canadian Journal of Civil Engineering*, V. 23, 49-62.
- United States Army Corps of Engineers (1999), "Seismic Evaluation and Rehabilitation for Buildings," *Document TI 809-05*, Washington, D.C.
- URS Greiner, Inc. (1997), "Seismic Evaluation of Existing Buildings, Fort Lewis Washington, Final Evaluation Report," *Final Report to US Army Corp of Engineers*, San Francisco, CA.
- Wen, Y.K. and Wu, C.L. (1999), "Generation of Ground Motions for Mid-America Cities," *Projects RR-1 and RR-2 of the Mid-America Earthquake Center*, University of Illinois at Urbana-Champaign.

Western Wood Products Association (1973), "Western Woods Use Book,"
Portland, OR.

VITA

Gregory Linwood Cohen was born in Boston, Massachusetts on August 29, 1977, to Gary and Joy Cohen. After graduating in May of 1995 from Bedford High School in Bedford, Massachusetts, he entered The University of Connecticut at Storrs. From that university, he earned the degree of Bachelor of Science in Civil Engineering in May of 1999. He entered the graduate school of The University of Texas at Austin in September of 1999, earned his Masters of Science in Civil Engineering in May of 2001, and received his Doctorate of Philosophy in Civil Engineering in May of 2004.

Permanent address:

101 River Road, Eliot, ME 03903-1302

This dissertation was typed by the author.